Applications of toric Calabi-Yau singularities to Cosmological model building in String Theory

Memoria de Tesis Doctoral realizada por

Ander Retolaza

presentada ante el Departamento de Física Teórica
de la Universidad Autónoma de Madrid
para optar al Título de Doctor en Física Teórica

Tesis Doctoral dirigida por **Dr. D. Ángel M. Uranga**,
Profesor de Investigación del Instituto de Física Teórica

Departamento de Física Teórica
Universidad Autónoma de Madrid

Instituto de Física Teórica UAM/CSIC

Mayo de 2016

Abstract

String Theory is nowadays the best candidate to describe gravity at the quantum level together with the other interactions and matter fields. Therefore, it should be able to describe physics at the most fundamental level.

In order to describe many phenomena consistently it is often necessary to provide some mechanism creating hierarchies between the different scales in the physical system. These kind of hierarchies admit a natural explanation in terms of warping on the internal space, which leads to suppression factors on the 4 dimensional field theories. In String Theory these warp suppressions can be obtained by the use of the so-called warped throats. In this thesis I will use toric Calabi-Yau singularities in order to build up warped throats where different physical phenomena happen. Most phenomena I focus on are related to dark energy, the source of accelerate expansion of the Universe on its very early stages and nowadays. I also present some new techniques in order to guess which throats admit orientifold actions, and use them to describe UV completions of stringy instantons in terms of gauge instantons in such geometries.

Resumen

Teoría de Cuerdas es a día de hoy la mejor candidata para describir la gravedad a nivel cuántico junto con el resto de interacciones y partículas elementales. Por lo tanto, debería ser capaz de describir cualquier proceso físico al nivel más funamental posible.

En muchos procesos físicos resulta muchas veces necesario hacer uso de algún mecanismo que de lugar a jerarquías entre las diferentes escalas presentes en el sistema físico. Este tipo de jerarquías admiten una explicación natural en términos de un factor de deformación del espacio interno, que da lugar a factores de supresión en la teoría de campos efectiva describiendo la física 4 dimensional. En Teoría de Cuerdas esta supresión mediante factores de deformación en el espacio interno puede obtenerse mediante el uso de las denominadas gargantas deformadas. En esta tesis haré uso de singularidades cónicas 6 dimensionales que sean tóricas y Calabi-Yau para construir gargantas de este tipo donde se puedan describir diferentes fenómenos físicos. La mayoría de fenómenos en los que me centro están relacionados con energía oscura, la fuente de crecimiento acelerado del Universo tanto en sus primeros instantes como a día de hoy. También presento una serie de técnicas que permiten decir qué gargantas son compatibles con acciones de orientifold, y hago uso de estas ideas para describir compleciones al ultravioleta de configuraciones con instantones exóticos, que admiten una descripción en términos de instantones gauge.

Esta tesis doctoral está basada en los siguiente artículos:

1. "*Bifid Throats for Axion Monodromy Inflation*"
   Ander Retolaza, Angel M. Uranga y Alexander Westphal.
   Publicado en JHEP 1507 (2015) 099 ; arXiv e-Print: 1504.02103 [hep-th].

2. "*Axion Monodromy Inflation on Warped Throats*"
   Sebastián Franco, Daniele Galloni, Ander Retolaza y Angel Uranga.
   Publicado en JHEP 1502 (2015) 086 ; arXiv e-Print: 1405.7044 [hep-th].

3. "*Orientifolds of Warped Throats from Toric Calabi-Yau Singularities*"
   Ander Retolaza y Angel Uranga.
   ArXiv e-Print: 1605.01732 [hep-th].

4. "*De Sitter Uplift with Dynamical Susy Breaking*"
   Ander Retolaza y Angel Uranga.
   Publicado en JHEP 1604 (2016) 137 ; arXiv e-Print: 15012.06363 [hep-th].

5. "*D-brane Instantons as Gauge Instantons in Orientifolds of Chiral Quiver Theories*"
   Sebastián Franco, Ander Retolaza y Angel Uranga.
   Publicado en JHEP 1511 (2015) 165 ; arXiv e-Print: 1507.05330 [hep-th].

Agradecimientos

No son poc@s l@s que han ayudado a que al fin este momento haya llegado y merecen que les de las gracias por su ayuda y apoyo a lo largo de estos años.

Hay alguien que por encima del resto ha hecho que esto sea posible, y eso merece una mención especial. No puede ser otro que Ángel. Mil gracias. Primero por haberme dado la oportunidad de ver algo más de ese gran iceberg que es la Teoría de Cuerdas, del cual sólo había visto la punta antes de llegar al IFT. Gracias también por las mil y una lecciones y explicaciones de física a lo largo del doctorado, y sobre todo por tener paciencia con mi cabezonería cuando no conseguía visualizar conceptos (que no han sido pocas). Estoy seguro de que no podía haber tenido mejor director de tesis. Ha sido un verdadero placer embarcarse en el mundo de las cuerdas y la investigación de tu mano, has sido todo un ejemplo a seguir.

Además de Ángel, son much@s los que me han ayudado a lo largo de estos años a entender los entresijos de las cuerdas y desarrollar nuevas ideas en los proyectos en los que he participado. Seba y Daniele, os debo muchísimos conociemientos en lo que rodean los dimers y las singus tóricas, además de estaros muy agradecido por lo a gusto que estuve cuando fui a Durham. Alexander, a ti te debo muchas ideas sobre inflación, y vendrán más cosas en cuanto vaya a Hamburgo. Y a Miguel y Mikel, sin vosotros no sabría hacer scattering de dimensiones, disfruté como un niño *jugando* con las supercríticas. A todos vosotros, mil gracias por todo.

Y no me puedo olvidar del resto del grupo cuerdoso del IFT, que tantas veces me ha ayudado a aclarar mis dudas y que sin duda me han ayudado a aprender gran parte de la física que ahora sé. Y aquí quiero dar las gracias especialmente a Luis y Fernando por un lado, pero sobre todo a Irene, Gianluca y Miguel, a los que he robado muchísimos minutos. Muchísimas gracias por estar siempre dispuestos a aclararme las ideas. Sin vosotros esto no habría sido posible.

Tampoco me puedo olvidar de aquellos a los que también he robado minutos y me han ayudado a entender muchos otros conceptos, tanto cuerdosos como otros más generales. Gracias Aitor, Diego, Juanmi, Mario, Víctor, Wieland y Xabi.

Y por supuesto, esto no habría sido posible sin la ayuda de de toda la gente que se ha encargado de papeleos y de mil gestiones, tanto en el IFT como en el departamento. Gracias Chaveli, Javier, Milvia, María, Mónica Encinas, Mónica Vergel y Tiina. Y sobre todo, muchas gracias Isa por lo profesional y sobre todo porque nos has cuidado como una madre.

Además, son muchos los momentos compartidos con los tres cuerdosos de mi quinta en congresos y sobre todo después de éstos (sobre todo con Irene, que has sido la compañera de fatigas). Ha sido una gozada poder ir a comer pizzas, adentrarnos en cuevas y ríos subterráneos, darnos baños en el Adriático, ponerse a -20°C al lado del Mont Blanc, hacer el gamba con raquetas por la nieve, juntarse con Maldacena en un templo Hindú o ir a ver elefantes. Me llevo mil recuerdos y espero que sigamos aprovechando este tipo de ocasiones para hacer otros mil planes de este tipo.

Y es que no todo lo relacionado con el IFT ha sido física estos cuatro años. Quedan en la memoria unas cuantas fiestas, bastantes chistes muy malos, apuestas de lo más absurdo, comidas y cenas, excursiones al monte, a la Warner, al Sagardotegi, partidas de la pocha, partidillos de fútbol sala, tonterías en el despacho... Aitor, Ana, Antonio, Carlos, Claudia, Edu, Gianluca, Ginevra, Irene, Javi (Abajo), Javi (Quilis), Josu, Juanjo, Leyre, Miguel, Óscar, Pablo, Pedro, Santi, Xabi, Víctor; habéis hecho que estos años hayan tenido muchos momentos que hay que guardar.

Y cómo no, estáis todos aquellos de fuera del IFT.

Primero, los brothers de *Euskal Etxea*, que sin duda habéis contribuido ayudándome a matar unas cuantas neuronas. No sé qué habría hecho sin dar patadas al balón (que no jugar a fútbol), echar birras y sucedáneos de comida en *El Rubio*, las cenitas en el *Sukalde* y las juergas que nos hemos cascado. Sois muy, muy grandes y muy brothers. Gracias por estos años keñeeee!

La gente de la *kuadrila* también habéis hecho vestra contribución en matar neuronas. Eskerrik asko txabales por las juergas en Eibar y en las excursiones para ver partidos del Eibar, por las vueltillas por el monte, por los poteos, o simplemente por los momentos en Argatxa. Siempre viene bien escapar al pueblo y desconectar de todo, y más con los txabales. KGG!

También Carlos. No han sido pocas las juergas, cervecillas y conversaciones trascendentales estos años. Has sido una referencia durante este tiempo. Gracias chaval!

Además, quiero dar las gracias a much@s otr@s que también han puesto su granito de arena en hacer que estos años hayan sido tan buenos. Gracias al spanish ghetto y el resto de gente de Leiden, y sobre todo a Cabesa, Guillem, Jordi, Xabi, Pei... A l@s compañer@s de piso; sobre todo a Miren ¡qué pena que te fueses tan pronto a Chile! Y a Maialen y el resto de la tropa que me acogió en Durham.

Hay dos últimos agradecimientos que son muy especiales. A los de casa: aita, ama y Markel, eskerrik asko por todo el apoyo durante estos años. Por los ánimos en los buenos tiempos y por hacerme creer en mí en los momentos de bajón, por hacerme recapacitar en muchas ocasiones y por estar siempre ahí para lo que hiciese falta. Eskerrik asko familia!

Y cómo no, Alba. Para ti no tengo palabras. En este par de años hemos compartido mil momentos que no cambio por nada del mundo: desde viajes maravillosos hasta noches en las que simplemente picábamos algo y veíamos una serie. Gracias por cada uno de ellos y por hacer que hayan sido años increíbles. También te ha tocado aguantar mis momentos de cansancio, frustración o cabreo... muchas gracias también por la paciencia que has tenido en esos momentos y por ayudarme a superarlo con tus consejos.

A tod@s vosotr@s, muchísimas gracias!

Contents

1 Introduction

Since ancient times the curiosity of human beings to understand the world around us has led to questions whose answers always led to new and more fundamental questions. This evolution of knowledge has taken us to understand nature at a level that could not even be thought of some centuries (or even decades) ago. The current borders of knowledge lie on "objects" whose sizes are far from the ones we are used to: these are elementary particles and the Universe as a whole; the smallest and the largest "objects" one may think of. And as happened in other times, the open questions related to both of them are not a few. Nowadays, high energy theoretical physicist try to find an answer to these questions, providing models with new ideas that may give an answer to these question. These models lie on two pillars that sustain the fundamental physics of the 20^{th} and the 21^{st} centuries: quantum mechanics, describing the behaviour of matter at atomic or subatomic scales, and General Relativity (GR), describing the structure of spacetime and its answer to the inclusion of matter and other types of energy in the long distance range.

The current knowledge on elementary particles can be well described by the Standard Model (SM) of particle physics and some of its extensions. This model describes the different matter particles, quarks and leptons, as well as the electromagnetic, strong and weak interactions. Moreover, it also includes the recently discovered Higgs boson, which is necessary in order to explain electro-weak symmetry breaking and the origin of mass. The theory is compatible with quantum mechanics, since it provides a description of both the matter particles and the interactions in terms of a field theory which is quantized. The model was developed together with experimental results from colliders, and thus it fits experimental data with an enormous degree of accuracy.

Nonetheless, the SM is not without problems. It is certain that it needs to be extended to explain phenomena such as neutrino oscillations, which are nowadays well understood in terms of neutrino masses, but it has deeper open questions which do not have well known and accepted answers yet. One of them is explaining the smallness of the Higgs boson mass, that gets quantum corrections that are quadratic on the cutoff scale of the model. This can be explained by a huge bare mass of the boson with a fine tuned value such that the physical mass is way smaller than the bare mass and the cutoff scale. Another possibility is to make quantum corrections small due to an extension or ultraviolet completion of the SM. The fine tuning required for the first option led many people to believe in the second option in the past years, which is a priori more natural, but the recent lack of experimental results in this direction is weakening the naturalness argument. Still, many other facts push in favour of the existence of a completion, such as dark matter or right handed neutrinos (if they exist), which may eventually result in an explanation for the smallness of the mass of the boson.

Going to the other border of knowledge on fundamental physics, the standard model describing the Universe is known as ΛCDM, where Λ stands for dark energy, and CDM stands for cold dark matter. According to this model, the Universe is approximately homogeneous and isotropic, and it evolves according to its matter and energy content following the field equations of GR. Nowadays, approximately 70% of this content is the so-called dark energy, which is responsible for the current accelerated expansion of the Universe and whose origin constitutes one of the biggest questions in physics. Then, out of the other 30% left, almost one sixth goes to matter we know, and the rest is the so-called dark matter, which nowadays remains a mystery. Moreover, the model needs of an almost exponential growth of the Universe on its very early stages lasting for around a second in order to solve e.g. the horizon problem. This period is known as the Cosmic Inflationary period or just *Inflation*. Its existence was predicted years ago and it is widely accepted by the community. Recently the experimental results by the BICEP2 and Planck observations, as well as their combined analysis confirmed the existence of polarization B-modes on the Cosmic Microwave Background (CMB). Part of these B-modes could be sourced by the interaction of the CMB with Primordial Gravitational Waves, which would provide observational evidence of the existence of an inflationary epoch.

Since Inflation lasts for a finite amount of time, the mechanism triggering this almost exponential growth of the Universe was suggested to be described by a scalar field that slowly rolls down its potential effectively giving rise to a positive cosmological constant until it reaches its minimum. The effective field theory description of this phenomenon contains several Planck suppressed operators, which need to be under control for the slow roll conditions to be fulfilled if inflation requires transplanckian field excursion. In order to obtain such a controlled situation it is necessary to find a UV completion of this effective field theory, by embedding inflation in a theory of Quantum Gravity.

Finding a theory of Quantum Gravity has proven not to be an easy task. Applying standard field theoretical approaches to quantize GR one finds that a straight forwardly quantized version of GR has many divergences, so new ideas are necessary in order to find a well behaved theory of quantum gravity.

Nowadays, String Theory (ST) is the most promising candidate for a quantum description of gravity as well as the other interactions and matter particles. The underlying idea of the theory is a rather simple one: fundamental particles are not point-like objects but rather have an extension, such that they are really one dimensional (actually 1+1 dimensional) objects. The size of strings, also known as the string scale l_s is very small, which explains why we effectively observe that particles are point-like and thus can be well described in terms of quantum field theory. Starting from this simple principle, one finds that the different particles correspond to different vibrating modes of strings. There is a particularly interesting vibrating mode for the closed string that corresponds to a massless spin 2 particle, whose effective field theory is described by GR. This is why strings describe gravity at the quantum level. Moreover, ST can provide the UV completion of the SM and its possible extensions, since it contains all the ingredients to describe gauge groups and matter fields.

It is important to mention at this point the existence of five different Super String Theories depending on their matter content on the worldsheet. These are the $SO(32)$ and $E_8 \times E_8$ heterotic, type I, type IIB and type IIA. These five theories share some common features such as the requirement of spacetime having 10 dimensions, but also have quite a lot of differences. Still, there exists a series of relations between them, known as dualities,

which relate certain ST in a limit to another ST in another limit. This series of dualities led to the conclusion that all these ST's are actually different manifestations at certain limits of a underlying more fundamental theory which is known as M-Theory. M-theory (and thus ST) is expected to be the theory that can describe every physical process at the most fundamental level, and is thus thought to be a theory of everything. Currently a complete non-perturbative formulation of neither M-theory nor ST is known, and therefore most of the developments in ST are limited to its perturbative region. The duality web and other types of progress (such as F-Theory) are slowly providing a better comprehension of the non-perturbative aspects of ST's but there is still a long way to go in this direction. Let me mention here that in this thesis I will focus mostly on perturbative type IIB ST configurations, with some comments on certain type IIA configurations.

The dualities found due to ST not only relate different ST's between themselves but also relate ST configurations to Quantum Field Theories. This point will be of special relevance in this thesis, where the Gauge/Gravity correspondence will be an invaluable tool. This duality has proven to be very useful not only for high energy physicists but also for e.g. condensed matter physicists.

Despite of the enormous amount of work on ST, we are still far from being able to provide a description of the fundamental laws of nature in this framework. The reason is precisely that as quantum field theory, ST is nothing else but a framework, and thus there exist a huge amount of ST configurations or vacua which lead to different effective field theories at low energies. The set of all possible configurations get the name of the String Landscape. The existence of the landscape makes it complicated to formulate generic statements about ST, and usually it is convenient to focus on the properties of some set of vacua in order to look for the concrete ST configuration (if any) describes the laws of nature in our Universe. This strategy allows to improve our knowledge on new aspects of the theory that may eventually result in the discovery of our vacuum.

Nonetheless, the existence of the Landscape is not the only problem we have to test the theory. Another restriction comes from the current technological developments, that do not allow us to create experiments achieving the required energies to study matter at small enough scales. The required energy scales are of the order of the string scale l_s, whose value still remains an open question and could in principle get values from a few TeV to being close to the Planck scale. The option of having a string scale on the TeV range looks very interesting from a phenomenological point of view since it would imply that collider experiments on the near future would allow us to test the theory. Unfortunately, these type of models often have problems such as risky operators that are not suppressed enough due to the low UV cutoff scale and lead to phenomena such as proton decay. These kind of problems make it quite conventional to set the string scale at energies much higher than the ones we will be able to explore on the short term. Fortunately, there might exist a source of information about processes at energy scales way higher than the ones currently available at colliders. The process sourcing this type of information is nothing else but Inflation, whose imprints on the current Universe can be used in order to extract information about high energy processes and may provide the only test of ST on the short term.

Luckily for us, the first accurate measures in this direction started short ago, which opens up an epoch of excitement for high energy physicists. These started with the original claim by BICEP2 of the detection of B-mode polarization on the CMB and consequent tensor to scalar ratio. These news resulted in a lot of researchers focusing on this direc-

tion, including string phenomenologists, which found the best chance so far of testing the theory. The eventual realization that the B-modes are consistent with cosmic dust led the combined analysis by BICEP2 and Planck, which resulted in a bound of the tensor to scalar ratio of $r \lesssim 0.12$, which is still compatible with large field inflation and thus can be one of the main sources of information about quantum gravity and thus ST.

This thesis addresses some of the issues arising when describing large field Inflation and also the origin of the current accelerated expansion of the Universe from a ST perspective. In particular, one finds that in order to provide a microscopic origin of these phenomena by embedding them on ST it is usually necessary to create hierarchies for a satisfactory description. An example of this type can be found when embedding inflation in ST, since in order to have single field inflation one needs to separate the moduli stabilization scale form the scale of inflation. In order to create these hierarchies I will exploit a ingredient that is well known in ST embeddings of particle physics models: warped throats. In particular, the focus will go on warped throats from deformed toric CY singularities, which provide a specially tractable scenario to engineer manifolds with certain desired properties. Throughout the thesis I will also address other topics that are non-related to Cosmology but are related to these kind of warped throats.

1.1. Plan of the thesis

This thesis contains several chapters that are slightly independent from each other. The binding line between all of them is the use of warped throats from toric CY singularities in type IIB ST, which I review in chapter 2. These type of manifolds have some properties that allow to easily engineer singularities with some desired properties. Moreover, ST configurations of probe D3-branes on such singularities provide a holographic gauge theory description which can be encoded in terms of the so-called dimer diagrams. Many of the properties of these diagrams will be given in this chapter since they will be one of the key tools in the following analysis.

The next two chapters are devoted to embedding inflation in ST. As I will explain, large field models of string inflation require a monodromic structure for the inflaton potential, and this monodromy can be achieved either by 5-branes or by fluxes. In chapter 3 I will provide a geometry where to embed models of the first type and study the back-reaction of the necessary 5-brane-antibrane pair, which was argued to be dangerous, to conclude that the configuration is indeed under control. Then, in chapter 4 I will describe a mechanism to separate the moduli stabilization scale from the scale of inflation. This time the analysis is carried out on the fluxed axion monodromy scenario. Among other things, in this chapter I will provide a holographic description of monodromy, as well as an analysis of the possibility of inflation being spoiled via bubble nucleation.

The purpose of chapter 5 is different from the previous ones: this chapter studies orientifolds of warped throats, providing a series of new tools that will be used on the following chapters. Concretely, it contains criteria to tell which toric singularities are compatible with orientifolds, and for those accepting them, which type(s) of orientifolds they admit. Finally, these ideas are mixed with the criterion to have a warped throat from a complex deformation of the singularity. It is a chapter devoted to the development of new techniques and thus has no further phenomenology-oriented analysis.

Then, in chapter 6 I embed in ST a sector with Dynamical Supersymmetry Breaking (DSB) which uplifts the Cosmological constant. This sector with DSB lies on a D3-brane on an orientifold of a warped throat, and thus makes use of the previous technology.

Chapter 7 changes the direction again: here I study D-brane instantons on the bottom orientifolds of warped throats giving rise to superpotential terms for quiral quiver theories. The embedding of the instantons into a throat provides a UV completion of the effects of the exotic instanton in terms of a gauge instanton. Moreover, the considered setups include for the first time non-perturbative contributions involving flavours.

Finally, chapter 8 contains the conclusions and summary of the main results found in the thesis.

2

Warped throats from toric Calabi-Yau singularities and dimer technology

One of the most characteristic properties of superstring theories is that they require spacetime to be ten dimensional as compared to the four dimensional one we are used to. Therefore, if string theory is the theory that completes on the UV our current theories to describe nature at the most fundamental level, the six extra dimensions need to be compact. This leads to a generalization of the Kaluza-Klein idea where the four dimensional physics is completely related to the geometry and topology of the extra dimensions, also known as the internal space.

Among many other things, the ingredients on the internal manifold can lead to many phenomena on the 4 dimensional effective field theory, such as generating hierarchies. The idea of creating hierarchies in four dimensions using extra dimensions was first introduced by Randall and Sundrum [1]. The key to create such hierarchies was warping the extra directions, such that modes located at different points of the internal manifold are affected by this warping in a different amount. This idea was first brought to string theory in [2], where the warping of the internal manifold came from space-filling D3-branes. This setup was still not appropriate for realistic compactifications due to the existence of several massless moduli, which made the warping moduli dependent and thus required the introduction of fluxes for an stable warp factor. It turns out that compactifications with fluxes leading to warping of the internal space and 4 dimensional supersymmetry were already available in the market [3], but had not been used for these purposes. The first applications of these type of flux compactifications were presented in [4]. Moreover, the authors of [4] analysed the local structure required in a region with large warping. They noticed that by turning on fluxes it was possible to have stable and warped solutions, following the ideas in the Klebanov and Strassler (KS) solution [5]. The KS solution is a smooth solution of type IIB supergravity based on the deformed conifold with fluxes and it is the first example of a warped throat. Warped throats in general are non-compact conical manifolds with a warp factor depending on the radial direction of the cone leading to hierarchies on the four dimensional effective field theory.

In this thesis I will focus on warped throats arising from toric CY singularities. These singularities are particularly interesting: the CY condition leads to 4 dimensional supersymmetric field theories and the toric condition provides an extra structure that enables a holographic description of the warped throat in terms of the so-called dimer diagrams [6]. Moreover, the toric diagram characterizing these type of singularities turns out to be extremely useful in order to engineer geometries where to describe e.g. some cosmology-related phenomena from the string theory perspective.

In this chapter I provide some general background on warped throats. I will begin with the KS solution and some of its properties in section 2.1, then I will give some insights on more general throats in section 2.2 and then move to the more tractable scenario of warped throats from toric CY singularities in section 2.3 . Once these singularities are introduced, I will review some of their properties, with special focus on the holographic dual description in terms of dimer diagrams and the general properties of these diagrams.

2.1. Review of the Klebanov-Strassler throat

Since the discovery of the gauge/gravity duality by Maldacena [7], there has been an enormous amount of work on finding other pairs of dual theories and using them for different purposes: from AdS/CMT to dualities motivated by high energy physics. This thesis focuses on the latter, in particular, in the ideas proposed by Klebanov and Witten in [8] and subsequent work on that direction. Their proposal was to generalize the duality by considering type IIB ST in a setup with a stack of N D3-branes on a singularity instead of flat space. More concretely, they focused on putting them on the tip of a conifold [9], which is a six dimensional cone over a 5 dimensional compact manifold with $\mathbb{S}^3 \times \mathbb{S}^2$ topology, and found out that the dual gauge theory in this particular case is a 4 dimensional $\mathcal{N} = 1$ superconformal gauge theory with gauge group $SU(N) \times SU(N)$ and chiral superfields A_i in the representation ($\square$, $\overline{\square}$) of the gauge group and B_i in the ($\overline{\square}$, $\square$) with a superpotential of the form

$$W = A_1 B_1 A_2 B_2 - A_1 B_2 A_2 B_1 \ . \tag{2.1}$$

This research line was further developed by Klebanov and collaborators in the following years [10–12], where they found out that placing $M \ll N$ fractional branes it is possible to slightly break conformal invariance. On the gauge theory picture fractional branes correspond to an increase of the rank of one of the gauge factors to $SU(N) \times SU(N+M)$. The gauge theory then is no longer conformal, so RG equations are non-trivial and lead to strong coupling of the gauge factor of higher rank. At certain point this theory is better understood in terms of the Seiberg dual of this gauge factor [13]. Seiberg duality is a strong-weak duality between two different UV gauge theories that flow to the same IR theory. The Seiberg dual IR theory for this case is similar to the UV one but with gauge group $SU(N) \times SU(N-M)$. As the energy scale decreases, the other gauge factor goes to strong coupling and once again it is convenient to describe its dynamics in terms of its Seiberg dual. This series of dualities is periodically repeated throughout the RG flow, effectively reducing the rank of both gauge factors logarithmically with the energy scale, and it is known as the *RG cascade*, *duality cascade* or the Klebanov-Tseytlin throat [12]. On the gravitational side fractional branes are D5-branes wrapped on the collapsed 2-cycle of the internal manifold. They carry D3-brane charge, and so the fluxes induced by M fractional branes are

$$\int_A F_3 = 4\pi^2 \alpha' M \quad ; \quad \int_B H_3 = -4\pi^2 \alpha' K(r) \ , \tag{2.2}$$

A being the 3-cycle surrounding the D5-brane, so transverse to the 2-cycle where it is wrapped and the radial direction on the conifold, and B the dual 3-cycle precisely composed by the product of this 2-cycle and the radial direction. $K(r)$ depends on the radial

value where the throat is cut, and its profile was shown to scale with $1/r$, so the NSNS 2-form B_2 depends logarithmically on the radius [12]. The D3-brane charge then increases as one moves away from the tip of the cone because of these fluxes

$$N(r) = \frac{1}{(4\pi^2\alpha')^2}\int_{X_5}\tilde{F}_5 = \frac{1}{(4\pi^2\alpha')^2}\int_{X_5} B_2\wedge F_3 = \frac{3}{2\pi}g_s M^2\log(r/\varepsilon), \tag{2.3}$$

in agreement with the decrease of the ranks on the gauge theory. ε is a length scale that I will shortly explain. This non-trivial profile of $\tilde{F}_5$ was shown to give rise to a non-trivial warp factor on the internal space [12]

$$ds^2 = e^{2A(r)}\eta_{\mu\nu}dx^\mu dx^\nu + e^{-2A(r)}\left(dr^2 + r^2 ds^2_{X_5}\right) \quad ; \quad e^{-4A(r)} = \frac{15\pi^4}{32}\alpha'^2 g_s^2 M^2\frac{4\log(r/\varepsilon)+1}{r^4}. \tag{2.4}$$

The culminating work in this direction resulted in the Klebanov-Strassler (KS) throat [5]. In this paper they addressed the problems arising close to the tip of the conifold, or equivalently the deep IR of the gauge theory, where the previous analysis was found to have divergences [12]. The claim of the paper was that once the fractional branes are included, the conifold is no longer singular but is rather on a deformed phase, i.e. the $\mathbb{S}^3$ on the base of the cone is kept at finite size on the tip because the fluxes stabilize the modulus (via the flux superpotential in [14]) and redshift scales by a warp factor as follows

$$\varepsilon \sim \exp\Big(-\frac{2\pi K}{M g_s}\Big). \tag{2.5}$$

The radial direction of a throat is holographically interpreted as the energy scale in the dual gauge theory. For this reason, I will often use the common terminology of UV and IR to refer to the large and small radius regions, respectively. The main lesson is that the dynamics down the throat is exponentially suppressed with respect to the UV scale in the bulk of the compactification.

This growth of the $\mathbb{S}^3$ on the bottom of the throat has a nice description on the holographic dual, where the deformation corresponds to a quantum deformation of the moduli space. Being more concrete, at certain point on the IR the ranks of gauge factors are of order M and the one with the higher rank has equal number of colors and flavors $N_c = N_f$, which leads it to confine. The field theory is thus described in terms of its mesons $M_{ij} = A_i B_j$ and baryons. Due to the strong dynamics of the factor the moduli space of the gauge theory is modified, as can be seen by probing the geometry with a stack of D3-branes, or equivalently by exploring the mesonic branch of the moduli space defined by

$$M_{11}M_{22} - M_{12}M_{21} = \Lambda^{2M}, \tag{2.6}$$

which is precisely the equation of the deformed conifold [9].[1] In this equation Λ is the dynamically generated SQCD scale and it is related to the deformation parameter on the gravitational side, which is precisely the length scale ε where the previous work [12] broke down. The IR theory after the deformation can be seen to be $\mathcal{N}=4$ $SU(M)$ SYM theory dual to placing D3-branes on flat space.

[1] More general cases are also possible, where $N_c > N_f$. In these cases the gauge factor also confines and develops a non-perturbative Affleck-Dine-Seiberg superpotential [15]. The outcome is also a deformation of the moduli space of the same type, but its realization in terms of the F-terms is not as straight forward as that with $N_c = N_f$.

The KS throat is the prototypical example of a warped throat. The deformed conifold is a local CY manifold that can describe the physics on the surrounding of a conifold point where the warping is large in a global compactification. This warping allows to effectively cut the region from the rest of the compact CY manifold and describe the physics locally. In the holographic dual, this means that one can decouple the IR physics, happening deep on the throat, from the UV physics, happening on the bulk of the CY. This matches nicely with the Randall-Sundrum (RS) idea [1], where the warping on the extra dimensions was used to create hierarchies in the 4 dimensional effective field theory. In fact, when the string theory generalization of RS was studied by Giddings, Kachru and Polchinski [4], they found that the KS solution fulfilles the requisites to be part of a global embedding with warping and Lorentz invariance in 4 dimensions. These requisites are a non-trivial profile for the D3-brane charge sourcing the warp factor, an imaginary self dual 3-form flux $*G_3 = iG_3$, where $G_3 = F_3 + ig_s H_3$ and some constrains on the local sources, which allow for example objects with D3-brane charge but no anti D3-brane charge. In fact, there is a stronger constrain than the 3-form flux being imaginary self dual, since this allows it to have a (2,1) component as well as a (0,3) one. In order to preserve supersymmetry, it is necessary that the latter vanishes and the former is a primitive harmonic form [16]. This is indeed the case for the KS throat.

A final remark on the KS solution goes on a particularly visual description in terms of a T-dual type IIA Hanany-Witten (HW) [17] brane configuration [18, 19]. The T-dual of a stack of D3-branes on the tip of the conifold along the circle parametrized by α in

$$xy - zw = 0 \quad ; \quad x \to e^{i\alpha} x \ , y \to e^{-i\alpha} y \tag{2.7}$$

looks as follows. The singular loci $z = 0$ and $w = 0$ are T-dual [20] to two NS5 branes spanning the Minkowski directions (throughout the thesis I will refer to directions 0123 as the Minkowski directions) as well as the complex w and z planes respectively (so one spans e.g. the 012345 directions, and the other one 012389, I will call them NS and NS' brane in what follows). The stack of N D3-branes becomes a stack of N D4-branes spanning the compact dualized direction, say x^6. The outcome is a setup with a NS brane and a NS' brane which cut the D4-branes in the x^6 direction. The relative position of the NS and NS' brane depend on the B_2 field on the type IIB setup. The effective field theory arising from the D4-branes that wrap a $\mathbb{S}^1$ is precisely the gauge theory described above, as expected from T-duality. When studying the non-conformal case with fractional branes, these are mapped to D4-branes spanning the compact x^6 direction, but unlike the regular D3-branes, fractional branes only span one interval between the NS branes, not the whole $\mathbb{S}^1$. This is illustrated in figure 2.1(a). The logarithmic profile of B_2 in this picture then translates to the relative motion of the NS and NS' branes as the energy scale of the 4-dimensional effective field theory changes. This relative motion changes the gauge coupling of both gauge factors, which scales as $1/d$, d being the distance between the NS branes. When the two NS-branes get very close to each other, the gauge group on the D4-branes between them becomes very large, so the gauge theory is better understood in terms of the weakly coupled Seiberg dual theory which arises from crossing both branes [21]. The amount of D4-branes on the interval decreases after the crossing of NS branes due to the Hanany-Witten effect [17], in agreement with the decrease of the ranks in the holographic theory, see figure 2.1(b). The relative motion of these branes follows describing the RG cascade in this picture, until one reaches the point where the amount of regular D4-branes N is of the same order as that of fractional branes M, figure 2.1(c). At this point, the deformation recombines the NS and NS' branes, as in figure 2.1(d).

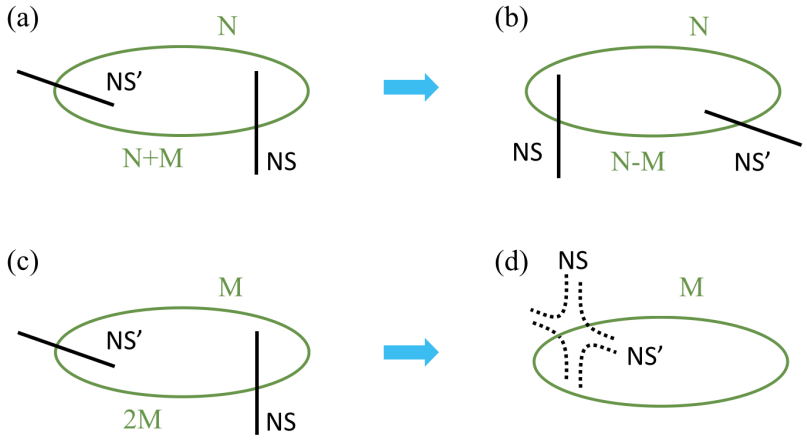

Figure 2.1: (a) HW brane configuration T-dual to the conifold with N regular branes and M fractional branes. Fractional branes increase the amount of D4-branes along one segment in the compact direction, which is bound by a NS and a NS' brane. (b) When the gauge group of higher rank goes to strong coupling, its description is better understood in terms of the Seiberg dual gauge theory. On the HW picture, this corresponds to crossing the NS and NS' branes, which due to Hanany-Witten effect decreases the number of D4-branes in the corresponding interval. (c) After many Seiberg dualities, the amount of regular branes N gets as small as that of fractional branes $N = M$ leaving this HW setup. At this point, the gauge group with rank $2M$ confines. (d) The confinement process on the HW-brane picture implies the recombination of the NS and NS'-branes. As shown in the picture, one is left with M D4-branes wrapped on a circle, whose worldvolume theory is precisely $\mathcal{N} = 4$ $SU(N)$ SYM.

2.2. More general warped throats

The above analysis can be extended to more general type IIB setups describing local warped regions close to singularities which share some of the properties of the deformed conifold. In this section I review what the requisites to construct such scenarios are.

The first constrains arise because the throats of interest have 4d supersymmetry. This imposes that the singularity is CY and the G_3 flux is a primitive harmonic (2,1)-form [16]. For the throat to be stable it is necessary to include fluxes. These must lead to a non-trivial profile of the D3-brane charge in order to have warping on the internal manifold. It was argued above that warping required G_3 to be imaginary self-dual [4], but this is already fulfilled if it is a harmonic (2,1)-form. The non-trivial profile of D3-brane charge of interest comes from fractional branes. In a general setup these are D5-branes wrapping collapsed 2-cycles of the internal space and also spanning the Minkowski directions. After collapsing the 2-cycle they lead to non-trivial fluxes. For singularities more involved than the KS throat one finds that fractional branes not always lead to complex deformations, but can also lead to other phenomena. A classification of fractional branes depending on their consequences was presented in [22]. The so-called deformation fractional branes, that behave as the ones in the KS solution, lead to the non-trivial fluxes holding one or more 3-cycles at finite size in the conifold case. The possibility of having deformation fractional branes then is constrained by the possibility of performing *geometric transitions* that change the Hodge numbers of the internal space while preserving the CY condition.[2]

[2]Recent developments in [23] show that throats transverse to O3-planes can give rise to throats with

When these kind of fractional branes leading to one or more finite size 3-cycles A_I are possible the fluxes induced by them generalize (2.2) to

$$\int_{A^I} F_3 = 4\pi^2\alpha' M_I \quad ; \quad \int_{B^I} H_3 = -4\pi^2\alpha' K_I(r) \ , \tag{2.8}$$

where I is the amount of complex deformations that can be performed on the conical singularity. These fluxes lead to a D3-brane charge

$$N(r) = \frac{1}{(4\pi^2\alpha')^2}\int_{X_5}\tilde{F}_5 = \frac{1}{(4\pi^2\alpha')^2}\int_{X_5} B_2\wedge F_3 \sim \sum_I g_s M_I^2 \log(r/\varepsilon_I), \tag{2.9}$$

and warp factor

$$e^{-4A(r)} \sim \alpha'^2 g_s^2 \sum_I M_I^2 \frac{4\log(r/\varepsilon_I)+1}{r^4} \ . \tag{2.10}$$

It is worth pointing out at this point that a complex deformation due to fractional branes can be located at finite radius along the radial direction of the conical manifold. In fact, this happens e.g. on the setup in chapter 3. When this happens, the complex deformation changes the base of the cone for radii much larger or much smaller than the one where the deformation happens. This process can happen more than once in the same throat when there are different sets of deformation fractional branes.

On the holographic dual picture, a stack of D3-branes on a generic CY singularity is a superconformal quiver gauge theory. In general it consists of several gauge factors and chiral superfields transforming in bifundamental and adjoint representations of these gauge factors depending on the isometry group of the singularity. For certain singularities, it is possible to also find a superpotential, a requisite to completely define the theory if it has $\mathcal{N}=1$ supersymmetry (for those with $\mathcal{N}=2$ it is enough to have the gauge group an matter content for the theory to be completely defined). As in the conifold case, adding fractional branes corresponds to increasing the rank of some gauge factors.[3] These break conformal invariance and trigger a *duality cascade*, generalizing the KS cascade, that effectively reduces the rank of all gauge factors periodically while preserving the amount of fractional branes as the theory flows to the IR. This cascade dualizes to the non-trivial D3-brane charge profile. For deformation fractional branes (from here on I will refer to deformation fractional branes simply as fractional branes, unless otherwise stated), at certain point the gauge factors with fractional branes of type M_I confine and their dynamics is better described in terms of their mesons (and sometimes baryons). These are subject to quantum constrains of the kind (2.6), forcing the mesons to acquire non-trivial *vev*s that higgs the gauge factors under which the mesons transform to their diagonal combinations, reducing the amount of gauge groups and matter fields in the resulting gauge theory. The confinement process corresponds to reaching the radial value where one set of fractional branes is holding the 3-cycle A_I at finite size, such that for smaller radii the base of the cone X_5 has changed in agreement with the fact of having a different quiver theory on the IR. In agreement with the supergravity description, it is possible that after a complex deformation the quiver gauge theory goes through another *duality cascade*

fluxes holding 3-cycles at finite size similar to the KS ones, but do not accept resolutions and thus geometric transitions. This behaviour was found to be a consequence of the O3-planes.

[3] The RR tadpole cancellation condition on the gravitational picture translates to the cancellation condition of non-abelian gauge anomalies [24].

triggered by another set of fractional branes M_J until another group confines. These ideas will be further developed in section 2.3.4.

For a complete supergravity analysis of the above setups knowing the metric of the deformed manifold is necessary. Finding a metric for a singularity is not always possible, but if one knows the holographic theory completely, this provides a way out of this problem: it is enough with finding the ranks of gauge groups triggering a *duality cascade* that decreases the ranks of all gauge groups while preserving the fractional branes and lead to confinement of one or more gauge groups. Since this process dualizes to the complex deformation on the gravitational side, being able to describe it on the gauge theory side is enough to prove the existence of the deformation and non-trivial fluxes. This idea will be used several times along the thesis.

One of the main difficulties to carry out the previous analysis for a generic singularity is to find the quiver gauge theory and superpotential corresponding to a given CY singularity. This is why from here on I will focus on the more tractable set of CY singularities that are also toric, which allow to easily read out the dual gauge theory and whose geometric transitions can be described in a diagramatic way.

2.3. Toric Calabi-Yau singularities

The discovery of the AdS/CFT [7] correspondence quickly motivated people to look for generalizations. The first gauge theory duals other than the conifold case were obtained by quotients of $\mathbb{C}^3$ [25,26]. These included abelian ones $\mathbb{C}^3/\mathbb{Z}_n$ as well as non-abelian ones $\mathbb{C}^3/\mathbb{Z}_n \times \mathbb{Z}_m$ which gave superconformal theories with $\mathcal{N} = 2$ and $\mathcal{N} = 1$ respectively in 4 dimensions. Soon afterwards it was noted that partially resolving the latter it was possible to obtain many more singularities with $\mathcal{N} = 1$ supersymmetry in 4 dimensions [27]. On the holographic picture the resolution was described as a Higgs mechanism which broke certain gauge factors of the quiver theory to their diagonals. These ideas easily allowed to build up many singularities by performing a large enough orbifold and then blowing up 2-cycles to end up with precisely the desired singularity [28] . Finding the holographic dual of these singularities is thus a mechanical task, which requires to follow the same series of steps on the quiver theory instead of the geometry. The conifold theory was found to be an example of the singularities one could build up this way. Moreover, it was already noted that these type of CY singularities could be described in terms of Gauged Linear Sigma Models (GLSMs), and thus were toric singularities . These ideas were exploited in [29–31] to develop an algorithm, known as the *inverse algorithm*, which completely defined the $\mathcal{N} = 1$ supersymmetric gauge theory (its gauge group, matter content and superpotential) from the toric data. It is important to mention at this point that for certain singularities, it was found that a unique singularity can give rise to different gauge theories. These gauge theories are known as different phases and their meaning will be cleared shortly.

Toric CY singularities can be characterized in many ways, one of them being the *toric diagram* (for a general review of toric geometry see e.g. [32]). This is a convex integer sublattice $Q \subset \mathbb{Z}^2$ that will be used below, see figure 2.2(a) for an example. The graph-dual diagram to the *toric diagram* is known as the *web diagram*, this graph-duality is explained with an example in figures 2.2(a) and (b). The web diagram is a series of lines which represent the complex space where the singularity is embedded together with a series of D-terms which describe the toric action that leave the singularity after taking

the quotient of the embedding space by the toric action. The equation(s) defining the singularity are described in terms of relations between gauge invariant operators of the GLSM.

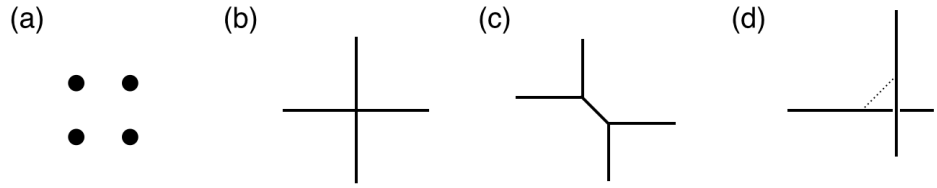

Figure 2.2: (a) Toric diagram for the conifold singularity. (b) Web diagram for the conifold on the singular limit. This diagram is graph-dual to the toric diagram since there is a one to one correspondence between lines on the web and intervals between points on the toric diagram. (c) Web diagram for the conifold on the resolved phase. The growth of the 2-sphere is depicted as the growth of the internal line, corresponding to a non-zero Fayet-Iliopoulos term on the D-term defining the CY. (d) The deformation of the conifold described in terms of the web diagram. It corresponds to taking the geometry to the singular limit and substracting a subweb in equilibrium form the web diagram. The separation between webs represents the growth of the 3-cycle.

Web diagrams are useful not only to define the toric singularity but also because they allow to describe the possible resolutions and complex deformations of the singularity. Partial resolutions of the singularity correspond to turning on Fayet-Iliopoulos terms, which in the diagram are represented by growing internal lines, as done in figure 2.2(c) for the conifold. In order to describe complex deformations, it is necessary to define the (p, q) *web* of the singularity. This is the set of external legs of the web diagram, and it will be very important for many purposes throughout the thesis. The name (p, q) web comes from the fact that each external leg has an associated vector (p, q) that tells to which direction the external leg is pointing at. An important property of these webs is that the sum of all (p, q)'s of a given singularity sum up to zero. Using this web, complex deformations were shown in [33] to be described as a separation of the (p, q) web into into subwebs in equilibrium, i.e. the total (p, q) of the removed subweb must be zero, as shown in figure 2.2(d) for the conifold case. The simplicity in the description of these two operations makes web diagrams the perfect tool to find out the possible geometric transitions a singularity can go through. This gives the first reason why toric CY singularities are specially interesting to build up warped throats: using web diagrams one can easily engineer a throat allowing geometric transitions and thus fractional branes, together with other desired topologic properties.

2.3.1. Dimer diagrams

Another interesting feature of toric singularities is that they are closely related to *dimer diagrams*. These were introduced in the mathematics literature in [34], and first used for other string theory related purposes in [35, 36], but it was not until [6] that they got related to the gauge/gravity community and until [37] that the community realized about their actual usefulness.

Dimer diagrams are two dimensional graphs describing tilings of $\mathbb{T}^2$. The vertices/nodes on the tiling are colored in black and white and each edge is bound by one black and one white vertex, so all tiles/faces are bound by an even number of edges and

vertices. The usefulness of dimers relies on the fact that they provide with a diagramatic description of the whole $\mathcal{N} = 1$ gauge theories as follows: faces of the dimer represent gauge factors of the holographic theory, edges have an orientation (e.g. one can put an arrow on top of them such that they leave a black node on their right and a white one on the left) and represent chiral fields transforming on the fundamental representation of the face on the back of the arrow and the antifundamental representation of the other face they bound, and finally, vertices are superpotential terms involving the ordered product of matter fields they bound with an opposite sign for white and black nodes, such that every field in the theory shows up twice in the superpotential, once in a term with plus sign and once in another one with minus sign. This interpretation of dimers was first given in [37]. Their relation to toric singularities was known since [34], but the developments in [38] made the relation between them more simple. This relation is shortly explored in section 2.3.2. In figure 2.3 I show the the dimer of the conifold.

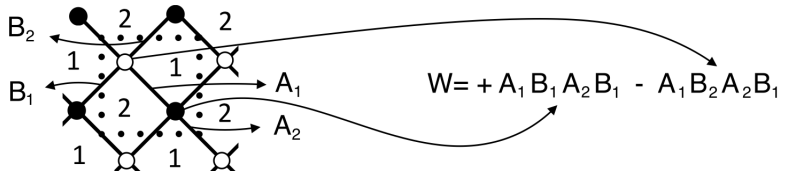

Figure 2.3: Dimer describing the conifold theory. Faces with labels 1 and 2 represent the two gauge factors $SU(n_1)$ and $SU(n_2)$, edges A_i are chiral fields transforming in the $(\mathbf{n}_1, \bar{\mathbf{n}}_2)$ representation of the gauge group whereas edges B_i transform in the $(\bar{\mathbf{n}}_1, \mathbf{n}_2)$. Finally, vertices/nodes are superpotential terms involving the fields touching the node. I will take the convention that black nodes have plus sign in the superpotential and involve a product of the fields ordered in a clockwise direction, and white nodes have negative sign and involve a product of the fields ordered in a counter-clockwise direction.

The usefulness of dimers relies on their powerful encoding of field theory phenomena into diagram combinatorics. One of the most interesting of them is Seiberg Duality [13]. This duality can be easily described in terms of dimer diagrams [37] and is the reason why a unique singularity accepts different dimers, or equivalently different toric phases: all the phases are related by a series of Seiberg dualities [31, 39]. Moreover, these phases are important because the RG flow of dimer theories in the presence of deformation fractional branes is described by a periodic series of Seiberg dualities, that make the dimer of a given singularity go through its different toric phases.

Another important phenomenon that can be easily described in terms of dimers are complex deformations generalizing the KS [5] smoothing of the conifold. Since this changes the gauge theory by reducing the amount of gauge factors due to confinement of certain group(s) and the following higgsings, the amount of faces on the dimer gets reduced when a complex deformation happens. These ideas were developed in [40] in the gauge theory language and translated to the dimer language in [41]. The key point is that the complex deformation corresponds to a removal of a subweb in equilibrium from the web diagram, or equivalently certain zig-zag paths from the dimer. These paths bound some faces on the dimer, corresponding to the gauge groups with fractional branes that confine. Several examples of this kind will be provided throughout the thesis.

The last useful property of dimers that is interesting to mention at this point is that they allow a diagramatic representation of the effect of orientifolds on the supergravity

side. The orientifold action translates to an orientifold action on the dimer diagram as described in [42]. Further details about this will be provided in section 2.3.5.

2.3.2. Zig-zag paths

The objects relating the dimer with the toric data were dubbed *zig-zag paths* (in what follows I will also refer to them as simply zig-zags). These are oriented paths on the dimer that cross the edges on the middle and turn e.g. maximally to the left when they encounter a black node and to the right with a white node, see figure 2.4(a) for an example. The paths cross each other, but the bipartite nature of the dimer prevents any zig-zag to cross itself. A crucial fact of zig-zags is that each path defines a homologically non-trivial 1-cycle on the dimer torus; once the unit cell of the dimer is fixed, each zig-zag has some associated winding numbers (p, q). As the notation suggest, these (p, q)'s are precisely the ones showing up on the (p, q) web, i.e. they are in one to one correspondence with the external legs of the web diagram [38], these are shown for the conifold case in figures 2.4(b) and (c). Retaking the possibility of having multiple gauge theories for a given singularity, on the dimer language this fact translates to different dimers being compatible with the same singularity. Zig-zag paths encode the information about the singularity and thus do not depend on the particular dimer or *toric phase* describing the gauge theory, the resulting (p, q) web is the same for all toric phases of a given singularity. A final comment on this direction goes to modular invariance of the unit cell where the dimer is defined, since winding numbers of zig-zag paths do depend on the unit-cell choice. This implies that the (p, q) web, and thus the web and toric diagrams are defined modulo $SL(2, \mathbb{Z})$ transformations from the different possibilities for the unit cell.

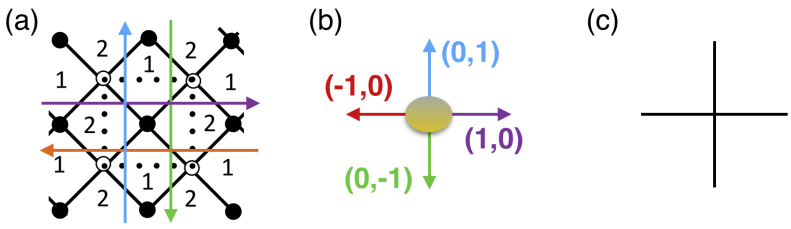

Figure 2.4: (a) The unit cell of the conifold together with its zig-zag paths. (b) The (p, q)'s of the zig-zag paths of the conifold as the external legs of its web diagram. (c) Web diagram of the conifold.

If one is interested in building up the dimer diagram from the toric data, zig-zag paths also provide a nice recipe to do so, which was dubbed the *fast inverse algorith* in [38]. This algorithm consists of undoing the process carried out in figure 2.4, where zig-zag paths translated information of the dimer to the toric data. Note that black nodes on the dimer are surrounded by zig-zags pointing on the clockwise direction, whereas they point counter-clockwise for white nodes. This requires of some structure on the possible ordering of zig-zag paths on the unit cell of the dimer. Based on this ideas, it is possible to use the information the other way around: one can take the set of zig-zag paths of a given singularity to build up the dimer. In figure 2.5 I provide an example describing how to obtain the conifold dimer from its (p, q) web, and refer to [38] for further examples and details. The (p, q) web of the conifold was given in figure 2.4(b).

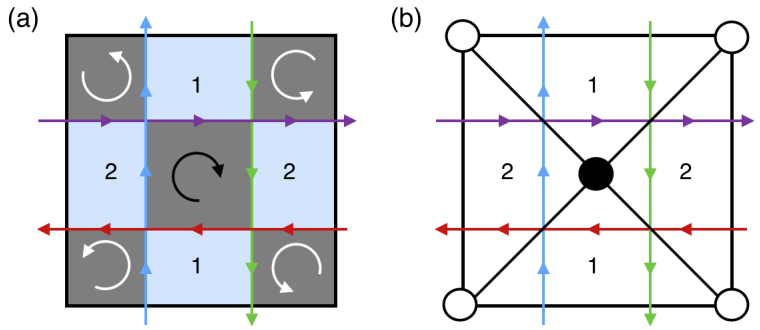

Figure 2.5: Use of the fast forward algorithm to derive the dimer diagram of the conifold from the (p, q) web. The (p, q) web for the conifold is shown in figure2.4(b). (a) The zig-zag paths placed on the unit cell. They bound faces of two types: the ones shaded in grey are bound by zig-zag paths whose orientation always goes on the clockwise direction (black arrow) or counter-clockwise direction (white arrow); and the ones in light blue, bound by zig-zags that have *opposite directions* at the points where they cross each other. (b) From the previous setup, one obtains the dimer by replacing faces in black by black and white nodes depending on the orientation of the zig-zags on the face, and zig-zag crossings map to edges bounding by a white and a black node. This dimer is the same as the one in figure 2.3 but with a different choice of unit cell.

2.3.3. The mirror perspective

The mirror dual of a toric CY singularity was shown in [43] to live in a threefold given by a double fibration over the complex plane

$$\begin{aligned} z &= uv \\ z &= P(x,y) = \sum_{m,n \in Q} c_{mn} x^m y^n \end{aligned} \tag{2.11}$$

where $u, v, z \in \mathbb{C}$ and $x, y \in \mathbb{C}^*$ are the coordinates defining the threefold and $P(x, y)$ is the Newton polynomial of the toric diagram of the singularity. In this picture[4], the gauge groups of the dimer translate to D6-branes wrapping 3-cycles on the geometry, bifundamental fields arise from open strings on the intersections between these branes and superpotential terms come from worldsheet instantons in discs bound by three or more branes. All intersections between branes, and thus all worldsheet instantons, were shown to meet at the Riemann surface Σ given by $P(x, y) = 0$, that I will focus on in this section. For other aspects of the mirror dual see [43].

The surface Σ, defined by $P(x, y) = 0$, is a Riemann surface with handles and punctures. This surface was shown in [43] to be a thickening of the web diagram [46–48], such that the amount of punctures of Σ is the same as the external legs of the web diagram, and its genus g is the same as the amount of internal points of the toric diagram, which as said before is graph dual to the web diagram. In figures 2.6(a) and (b) I show the web diagram and the curve Σ corresponding to the conifold. The D6-branes giving rise to gauge groups wrap 1-cycles in Σ surrounding some of its punctures and intersecting each other. Open strings on these intersections give the bifundamental chiral fields and worldsheet instantons on the discs bound by several D6-branes and their intersections are responsible for superpotential terms. The way D6-branes are wrapping 1-cycles in

[4] It actually corresponds to an intersecting brane configuration, in the sense of [44, 45].

Σ so that they give rise to the same chiral fields and superpotential terms as those in the dimer was described in [43]. The outcome is that D6-branes are wrapped such that each puncture in Σ is surrounded by a series of D6-brane intersections and worldsheet instantons, or equivalently fields and superpotential terms.

It is thus possible to define a bipartite graph tiling Σ, where each face represents a puncture of Σ, or equivalently an external leg of a web diagram or zig-zag of the dimer. Edges of this tiling are the fields in the intersection(s) between zig-zag paths in the dimer, and their vertices correspond to the worldsheet instantons (superpotential terms), which can be coloured as in the dimer, since each edge must have a white and a black node on each side. Finally, the 1-cycles wrapped by D6-branes are zig-zag paths of this tiling of Σ, i.e. turning maximally when they are next to a black node and maximally to the left when the node is white. Therefore, the toric theory can be described by two tilings, the original dimer and the one just described, which are strongly related via the so called untwisting procedure in [43] and with two main differences: on the one hand, the dimer is defined on a torus, whereas the tiling in the mirror has genus g. On the other hand, in the original dimer faces represented gauge groups while zig-zag paths corresponded to external legs of the web diagram, whereas in the mirror, faces are the external legs and zig-zags are D6-branes corresponding to gauge groups. In order to avoid possible confusions, from here on I will use the term dimer only describe the tiling of the torus where faces represent gauge groups, and zig-zag paths will be the paths defined on the dimer, I will not use these terms for the tiling of the mirror curve Σ.

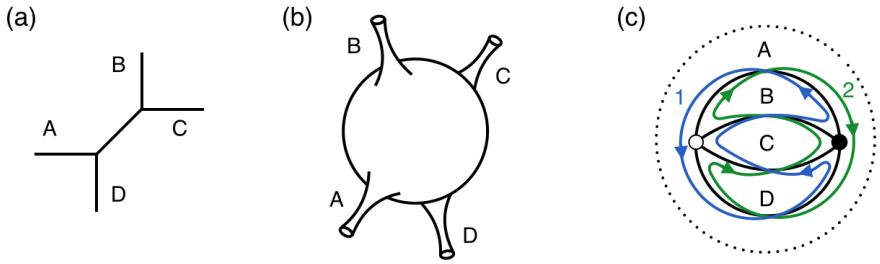

Figure 2.6: (a) Web diagram of the conifold on the resolved phase. Labels correspond to external legs of the diagram. (b) The curve $P(x, y) = 0$ of the conifold is a thickening of its web diagram. (c) The tiling of Σ for the conifold. The dotted line corresponds to a unique point, since Σ is a sphere with punctures as shown in (b), corresponding to faces in (c). Also, comparing with figure 2.4(a) it can be see that it has four edges and one vertex of each color. The paths in green and blue are the D6-branes giving rise to the two gauge groups.

2.3.4. Complex deformations

One of the main motivations to be interested on toric CY singularities is that they provide the perfect scenario to create hierarchies by complex deformations of the singularities hold by fluxes. These have been widely studied and applied for several applications on the literature, see e.g. [40, 49–51].

Among the different descriptions of this phenomenon, here I will focus on the web diagram, gauge theory and the mirror geometry descriptions.

As already mentioned, the gauge theory description of complex deformations can be easily carried out using dimer diagrams [22]. By placing fractional branes on some gauge groups (I will shortly give a criterion to determine which) their ranks increase and break conformal invariance. This triggers a duality cascade that periodically reduces the rank of all gauge groups by a unique amount that depends on how many fractional branes were put [5, 40]. At certain point on the RG flow the theory reaches a point where the groups with fractional branes number of colors and flavours satisfying $N_f \leq N_c$, so their strong dynamics leads to a modification of the moduli space and thus modification of the dimer. The resulting gauge theory and dimer have less gauge factors and correspond to the left-over (possibly singular) geometry after the complex deformation. Therefore, the singularity and thus the gauge theory are different before the complex deformation (UV of the gauge theory) and after it (IR of the gauge theory). The confinement/deformation process can be diagrammatically carried out in term of the dimer. An example of this process is shown in figure 2.7.

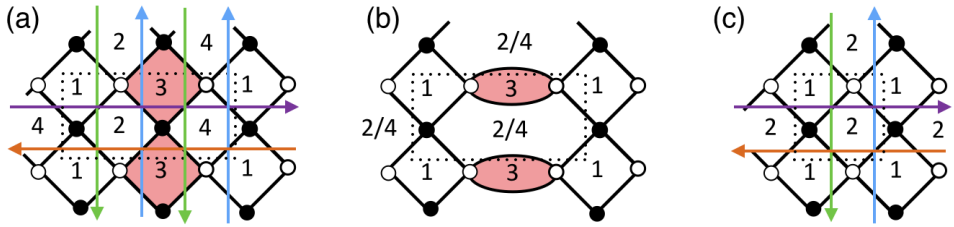

Figure 2.7: (a) Dimer diagram of the $\mathbb{Z}_2$ orbifold of the conifold describing the UV physics. Gauge group with label 3 is taken to have $N_f \leq N_c$ and thus confines. (b) An intermediate step in the confinement/deformation process following the recipe in [40]. (c) The resulting dimer after the deformation process, that describes the IR physics of the gauge theory. This dimer corresponds to the conifold.

The difference between the UV and the IR theories is also reflected on the web diagram, where the deformation process corresponds to the removal of a sub-web in equilibrium. By this removal one is left with a new web diagram also in equilibrium and a smaller toric diagram of smaller area. This is illustrated in figure 2.8.

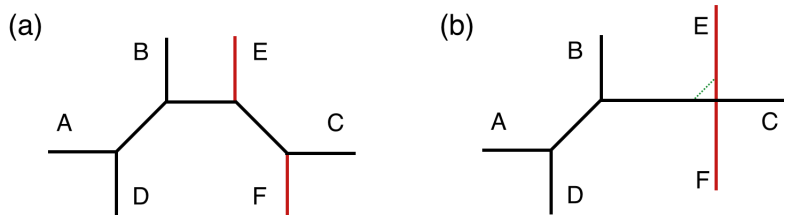

Figure 2.8: (a) Web diagram for the $\mathbb{Z}_2$ orbifold of the conifold on the resolved phase. (b) Web diagram representation of the complex deformation from the $\mathbb{Z}_2$ orbifold of the conifold to the conifold. The dashed green line represents the separation between the conifold web diagram and the removed subweb in equilibrium. The dashed line also represents pictorially the 3-cycle grown in the deformation process.

Finally, since the surface Σ is a thickening of the web diagram, the deformation process must necessarily change this surface as explained in [41]. In the mirror surface Σ

the D6-branes corresponding to the confining gauge groups wrap certain punctures, which correspond to the external legs of the web diagram to be removed. The removal of the external legs corresponds to cutting out these faces from Σ and then gluing together the boundaries of the surface left after cutting them. This process involves a recombination of the remaining D6-branes on the mirror, corresponding to the higgsing in the gauge theory due to mesons that get a *vev*. The new surface one is left with is the one describing the IR physics. Figure 2.9 shows an example of this kind.

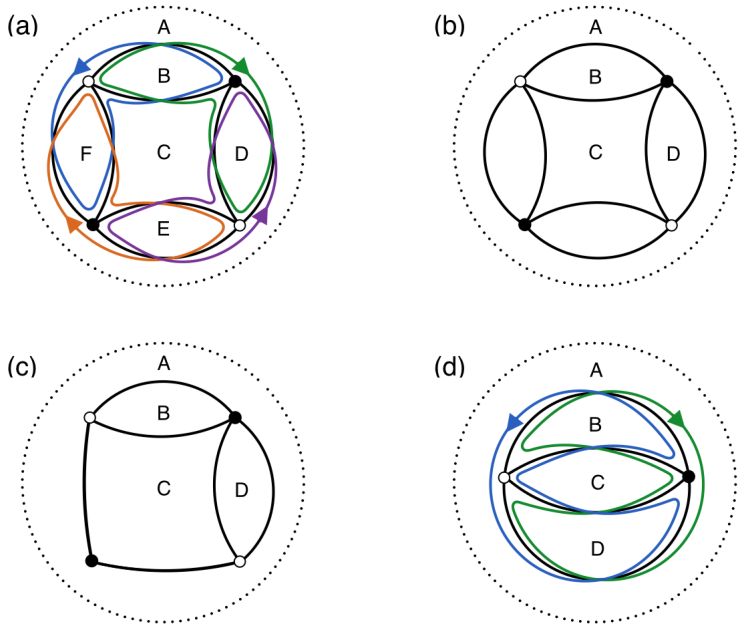

Figure 2.9: (a) Tiling of the mirror surface Σ of the $\mathbb{Z}_2$ orbifold of the conifold. The paths in colours represent the four D6-branes giving rise to the gauge groups in the gauge theory. The confining group is represented by the D6-brane in orange. (b) Tiling of Σ after cutting out the tiles corresponding to external legs E & F. (c) Tiling of Σ after gluing together the boundaries left after cutting out the tiles. The black node touching only two edges represents a mass term for the two fields. (d) The tiling of Σ after integrating out the massive fields together with the D6-branes left after the deformation. See that the D6-branes in blue and purple in (a) now recombined to the one drawn in blue. This Σ corresponds to the conifold.

2.3.5. Orientifolds of dimer models

The last object to be discussed in this chapter are orientifolds of dimers. These were widely studied in [42] and here I will summarize the relevant features for the thesis.

Orientifolds are the key ingredient to eliminate some degrees of freedom of certain theory such that the outcome is a theory with different gauge factors and matter representations. Regular dimers only have gauge groups of the $SU(N)$ type and matter in bifundamental and adjoint representations. When an orientifold action is implemented on a toric CY singularity, the theory can also have $SO(N)$ and $USp(N)$ types of gauge groups depending on the orientifold charges, and also matter in the two index symmetric

and antisymmetric representations. The way to obtain these new degrees of freedom in dimers was described in [42].

Since dimer theories live on tori, they can accept two different types of orientifolds: the ones leaving fixed lines, also known as orientifold lines, and the ones leaving fixed points, known as orientifold points. The geometric action of the two types of orientifolds is different, and thus they act in a different manner on the mesonic operators (gauge invariant operators from field products of the theory). In particular, they act in a different way on superpotential terms, which will be specially relevant in chapter 5, so I will discuss them separately.

I will start with orientifold lines. These can be of two types as shown in figures 2.10(a) and (b) depending on their geometric action: they can either invert one coordinate or exchange the two coordinates. In what follows I will refer to these orientifold lines as parallel and diagonal orientifold lines respectively, for reasons obvious in the figure. Nevertheless, recall that the fixed line crossing e.g. the diagonal on the second case depends on the choice of unit cell, so these labels must not be taken seriously and are just a simple way of referring to both cases. These kinds of orientifolds were shown to relate superpotential terms corresponding to vertices with same color, as can be seen in the examples of figures 2.10(a) and (b).

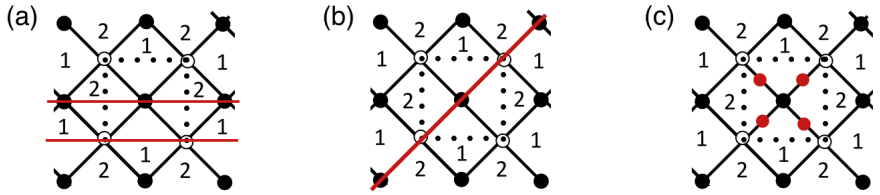

Figure 2.10: (a) Dimer of the conifold with orientifold lines inverting one of the coordinates. (b) Dimer of the conifold with an orientifold line exchanging the coordinates. (c) Dimer of the conifold with orientifold points.

In the case of orientifold points the geometric action inverts both coordinates of the $\mathbb{T}^2$, with four fixed points, as shown in figure 2.10(c). This time the orientifold relates vertices with different color. This sets some restrictions, since this is only possible if orientifold points fall on top of edges of the dimer or in the middle of hexagonal faces.

2.4. Applications of warped throats

The review in this chapter shows the enormous amount of work in previous years in order to develop the warped throat technology from toric CY singularities. The use of these singularities so far mostly focused on particle physics model building to e.g. embed (MS)SM-like field theories in ST provinding an explanation for the hierarchy problem [52–55] or to slightly break supersymmetry [22, 56–60].

Nonetheless, there are also some well known cosmology related topics where these throats were proven to be useful, probably the most famous one being the KKLT uplift of the cosmological constant by placing anti D3-branes on a fluxed warped throat [61]. This time, the effect of warping was to explain the tunability of the cosmological constant Λ.

Another approach to obtain a positive cosmological constant will be presented in chapter 6, this time using a sector where supersmmetry is dynamically broken on a D3-brane worldvolume. Following the KKLT approach, by placing this D3-brane on the bottom of a warped throat, the breaking of supersymmetry can be parametrically small and thus Λ is parametrically tunable.

This suppression mechanism can be useful in many more scenarios in physics, and in particular in their ST embeddings. In the next two chapters I will use this technology to address several issues about Inflation and its ST description. This embedding is specially interesting if the measurements to come tell that Inflation requires transplanckian field excursions for the inflaton, demanding a UV completion in a theory of quantum gravity such as ST. The ST constructions to describe inflation will be shown to require of warping effects on the internal manifold for consistency, which will be achieved by using warped throats.

3

Bifid throats for axion monodromy inflation

As mentioned in chapter 1, we are starting an era of precision B-mode observations in cosmology, especially since the recent results from BICEP2 and Planck (see [62] for their combined analysis). Future observations [63] will either detect or put stringent constraints on primordial B-modes from gravitational waves during inflation, therefore sharpening our picture of the very early universe, and providing new tools to discriminate among the plethora of present inflationary models/scenarios (see [64] for a recent string-motivated review). Indeed, in single field inflation models, the Lyth bound [65] correlates the tensor to scalar ratio r with the inflaton field range. Interestingly, the present observational bound $r < 0.12$ [62] is still compatible with large field inflation models, in which the field range is trans-Planckian and the inflation scale is very high. Large-field inflation models are sensitive to an infinite number of corrections to the inflaton potential which are suppressed by the Planck mass scale. The construction of viable models in a concrete framework of quantum gravity, such as string theory, is proving an interesting adventure.

A natural way to suppress the couplings of the inflaton to the heavy degrees of freedom is through axions, i.e. periodic scalars with an approximate continuous shift symmetry. In ST, there are two broad proposals to realize large-field inflation with axions [64]. The first involves multiple axions [66–71]. These models seem to be in trouble due to recent developments on the Weak Gravity Conjecture [72–85]. The second utilizes a single axion with a non-trivial monodromy in field space (either arising via brane couplings [86,87] or via potentials from flux backgrounds [88–91]) and so far seem to be free from the constrains coming from the weak gravity conjecture. The monodromy idea was proposed in [92–94] for a 4 dimensional phenomenological approach. Both the multiple axion and the axion monodromy scenario were developed to achieve a trans-Planckian inflaton range for an axion with a sub-Planckian decay constant, the later being what is expected from ST [95].

The axion monodromy idea is particularly interesting in that the ingredients involved (shift symmetries, branes, maybe antibranes, and fluxes) are rather common in ST. However, the construction of concrete string theoretical models is non-trivial. The original models, based on supersymmetry breaking brane configurations [86, 87] (see also [96]), require complicated geometries with multiple warped throats [97], which have not been amenable to detailed study until recent developments [49] presented in this chapter.

In more detail, the configurations in [87,97] take the inflaton to be an axion coming from the type IIB RR 2-form integrated over a 2-cycle. Actually, the geometry must contain two 2-cycles in the same homology class but located at the bottom of two different warped throats. Wrapping an NS5-brane and an NS-antibrane on these two 2-cycles, their charges cancel but their couplings to the RR axion add up, endowing it with a

monodromic potential suitable to host large field inflation. The energy increase in these systems is associated to the appearance of induced D3 brane-antibrane charge due to the axion shift. Finally, in order to suppress the backreaction of the NS brane-antibrane pair on modes localized on a complex dimension one region [98], the configuration must be located at the bottom of a common throat [97]. Such a geometry, which is nowadays known as *bifid throat*, is illustrated in figure 3.1.

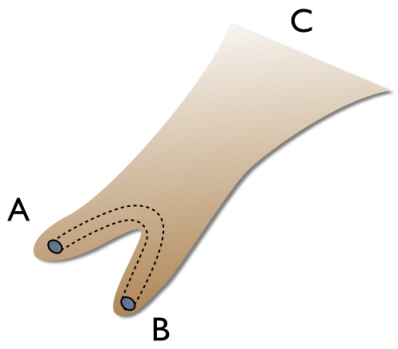

Figure 3.1: Sketch of the bifid throat. The dashed line denotes the 3-chain showing that the two 2-cycles are homologous.

The potential appeal of these models is concealed by the naive complexity of the underlying geometry. Actually, relatively simple geometries can enjoy the right topological properties to host such systems. In this chapter I provide the simplest such explicit example, based on a orbifold of the conifold. Similar more involved examples could be worked out with the same techniques. The main motivation of this chapter is to moreover provide a new handle on the bifid throat geometries required for brane-antibrane axion monodromy inflation. This is done by providing a holographic dual field theory for the throat geometry (and to some extent, of the brane-antibrane system), generalizing the KS throat [5]. This holographic description allows to study the backreaction of the brane-antibrane system, and its suppression due to the warping.

The chapter is organized as follows. In section 3.1 I provide the holographic field theory description of a simplified bifid throat, which contains all ingredients except the homologous 2-cycles at the infrared ends of the geometry. Once the necessary ideas are presented with the simple example, in section 3.2 a similar analysis is performed for a bifid throat with the required homologous 2-cycles. Finally, in section 3.3 the holographic view of introducing D5 brane-antibrane pairs is described, and their backreaction in field theory language, assessing it is localized at the energies of the neck connecting the IR throats. A similar result is plausible for the S-dual configuration with NS branes.

3.1. A simple bifid throat

In this section I describe a simple geometry with the right ingredients to support two small throats (denoted the IR throats) at the bottom of a common one (the UV throat), and provide its holographic dual gauge theory. It arises as the worldvolume theory on a stack of D3-branes at the tip of a toric CY singularity, in the presence of fractional

branes. As in [5], the throats are dual to energy regimes in which the theory experiences cascades of Seiberg dualities, whereas the end of the throat is mapped to confining gauge dynamics and quantum deformations of the moduli space. In addition, the separation between the two IR throats is dual to a Higgs mechanism induced by *classical* mesonic vevs (i.e. not arising from strong dynamics). The ordering (or relative geometry) of the throats is associated to the scales of confining dynamics and of the Higgsing.

The simple model in this section has all ingredients, except for the requirement of having a homologous 2-cycle on the two IR throats, recall figure 3.1. This latter property will be achieved in section 3.2, by simply adding an extra $\mathbb{Z}_2$ orbifold to the model in this section, which is therefore an optimal warmup exercise.

3.1.1. The geometry and dual gauge theory

As just mentioned, in this section I skip the requirement of having the 2-cycle at the end of the throat. The local geometry required to build a bifid throat requires of the possibility to perform three independent complex deformations, so that it contains three independent 3-cycles which support the fluxes producing the UV and the two IR throats. Finding a geometry with these properties is in general not a simple task, but can be more easily carried out for toric CY singularities, as explained in section 2.3. The criterion for a toric singularity to admit a complex deformation was discussed in [40]: the web diagram must admit a split into subwebs in equilibrium. Therefore, the singularity must admit the removal of three independent subwebs to account for the three throats. The question of why two are inside a common one is a question of scales, as will be clear later on.

The explicit model I provide here is based on the simplest toric singularity with the desired properties; it is straightforward to construct other toric examples. The web diagram of the singularity is shown in figure 3.2(a), its dual toric diagram in (b) and the result of complex deformation is shown in (c). Each complex deformation is locally identical to a conifold transition, hence the 3-cycles are non-intersecting 3-spheres, which I denote by $A_{\rm UV}$, $A_{\rm IR,1}$, $A_{\rm IR,2}$. Their (non-compact) dual 3-cycles are denoted by B's.

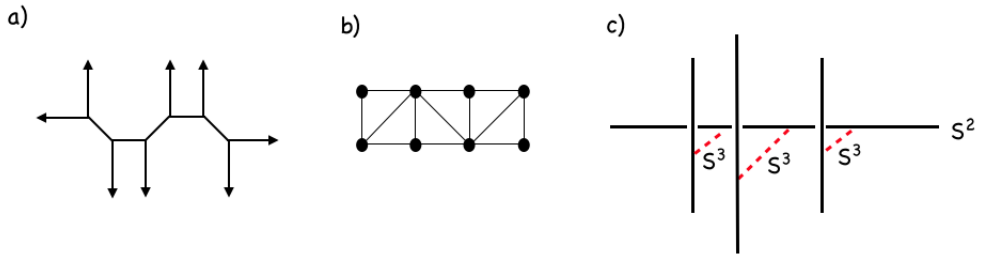

Figure 3.2: (a) Web diagram of the singularity of interest; for the sake of clarity I depicted the collapsed 2-cycles of finite size. (b) Toric diagram, where the initiated easily recognizes an orbifold of the conifold. (c) Splitting of the web diagram displaying the three complex deformations of the geometry, and the three corresponding 3-cycles.

The physics of the throat can be very explicitly discussed in terms of the holographic dual gauge theory (with fractional branes). The gauge theory is that corresponding to

D3-branes at the singularity of figure 3.2(a), in the limit of collapsed 2-cycles. Since the singularity is toric, dimer diagrams can be used to construct the gauge theory.

In fact, this geometry is easily recognized as a $\mathbb{Z}_3$ orbifold of the conifold. For completeness I provide its description. Describing the conifold by $xy - zw = 0$, the $\mathbb{Z}_3$ orbifold is given by the action

$$x \to e^{2\pi i/3}x \quad ; \quad y \to e^{-2\pi i/3}y \quad ; \quad x, y \text{ invariant.} \tag{3.1}$$

Defining the invariant coordinates $x' = x^3$, $y' = y^3$, the resulting space can be described by

$$x'y' - z^3w^3 = 0. \tag{3.2}$$

It is easy to describe the three complex deformations. To do so, rewrite (3.2) as $xy - t^3 = 0$, $zw = t$, and deform with three complex parameteres ϵ_i, $i = 1, 2, 3$ to

$$\begin{aligned} xy &= (t - \epsilon_1)(t - \epsilon_2)(t - \epsilon_3) \\ zw &= t. \end{aligned} \tag{3.3}$$

The dimer describing the field theory on a probe D3-brane on this throat is just that of the conifold with an order-3 enlargement of the unit cell, as shown in figure 3.3(a). The dimer is shown together with its zig-zag paths, which can be seen to reproduce the external legs of the web diagram for the geometry, shown in figure 3.3(b).

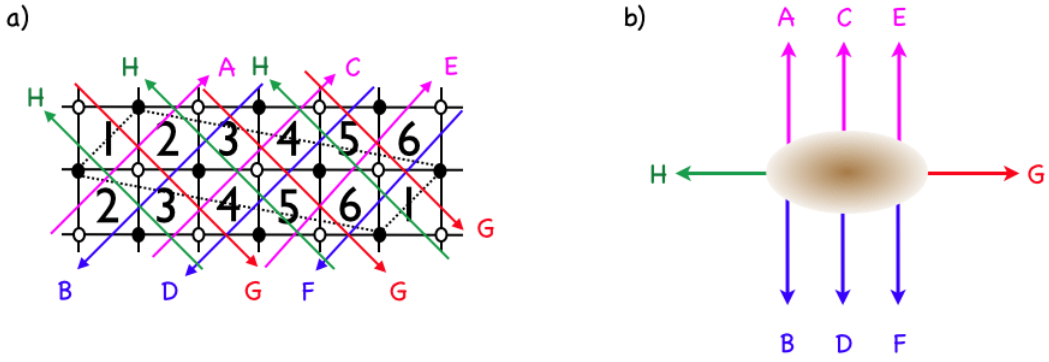

Figure 3.3: (a) Dimer describing the gauge theory for the underlying system of D3-branes at the singular geometry in figure 3.2. It corresponds to enlarging the unit cell in the infinite periodic array corresponding to the conifold dimer. The dimer is shown together with the zig-zag paths. (b) (p, q) homology charge of the zig-zags as external legs of the web diagram after a $SL(2, \mathbb{Z})$ transformation. The diagram can be seen to agree with that of figure 3.2(a).

3.1.2. The holographic flow

On the geometry side, RR 3-form fluxes are introduced in the 3-cycles obtained upon complex deformation of the geometry, and NSNS 3-form fluxes on their dual (non-compact) 3-cycles. The RR 3-form flux quanta over $A_{\rm UV}$, $A_{\rm IR,1}$, $A_{\rm IR,2}$ are denoted M, P_1, P_2; in addition, N is the D3-brane charge at some radial position. In the dual gauge

theory, they correspond to the introduction of fractional D-branes in the above singular CY. They just correspond to anomaly-free rank assignments in the dimer gauge theory in figure 3.3. The theory is non-chiral, so any assignment is allowed. As will be clear from the analysis below, the following rank assignment for the different gauge groups matches the holographic dual.

$$n_2 = N + P_1 \quad , \quad n_4 = N + M \quad , \quad n_6 = N + P_2 \quad , \quad n_1 = n_3 = n_5 = N \tag{3.4}$$

(clearly, due to the cyclic symmetry of the gauge theory, any cyclic permutation of the above rank assignment leads to the same results, up to relabeling). Assume that $N \gg M \gg P_1, P_2 \gg 1$, in order to produce long throats in the dual, describable in the geometric regime, and such that M corresponds to the UV throat and P_1, P_2 to the IR throats.

In addition to the above rank assignments, it is necessary to specify some vevs to trigger the symmetry breaking effects, to split the bottom of the UV throat into two IR throats, which are easier to specify later on.

The UV cascade

The dynamics starts at some UV scale with the above rank assignment. The RG flow takes the theory through a duality cascade, which reduces the effective value of N as one runs to lower energies. The discussion of the Seiberg dualities involved in this cascade is easily carried out in terms of a T-dual HW configuration [99], which for the present singularity was discussed in [18]. Concretely, the T-duality (3.2) is done along the $\mathbb{S}^1$ parametrized by α in the orbit of

$$x \to e^{i\alpha} x \quad , \quad y \to e^{-i\alpha} y. \tag{3.5}$$

The degeneration locus of the $\mathbb{S}^1$ (namely, when $x = y = 0$) corresponds to $z^3 w^3 = 0$, and describes 3 NS branes at $z = 0$ and 3 NS-branes at $w = 0$. Changing to more standard HW brane configuration conventions, the outcome is a set of three NS-branes and three NS'-branes, and D4-branes suspended between them. The presence of the M fractional branes triggers a set of dualities detailed in figure 3.4, which essentially corresponds to a triple unfolding of the KS duality cascade. It is however modulated by the presence of the P_1, P_2 fractional branes in the gauge factors 2, 6, such that the reduction in the number of regular D3-branes upon three steps in the duality cascade is $\Delta N = -(M + P_1 + P_2)$.

First complex deformation

Starting with a configuration such that $N = k(M + P_1 + P_2) + M$, after k periods of the duality cascade the gauge theory runs out of D3-branes and reaches the confinement regime dual to the complex deformation supporting the UV throat. Taking the last step, the ranks are as in (3.4) with an effective value $N = M$, i.e.

$$\begin{aligned} &n_2 = M + P_1 \quad , \quad n_4 = 2M \quad , \quad n_6 = M + P_2 \\ &n_1 = n_3 = n_5 = M. \end{aligned} \tag{3.6}$$

For the gauge factor 4, at this point $N_f = 2N_c$ and there is a complex deformation of the moduli space, as in KS [5]. Accounting for the full non-perturbative dynamics of the gauge factors is easily done in terms of the dimer diagram [40]. Following this

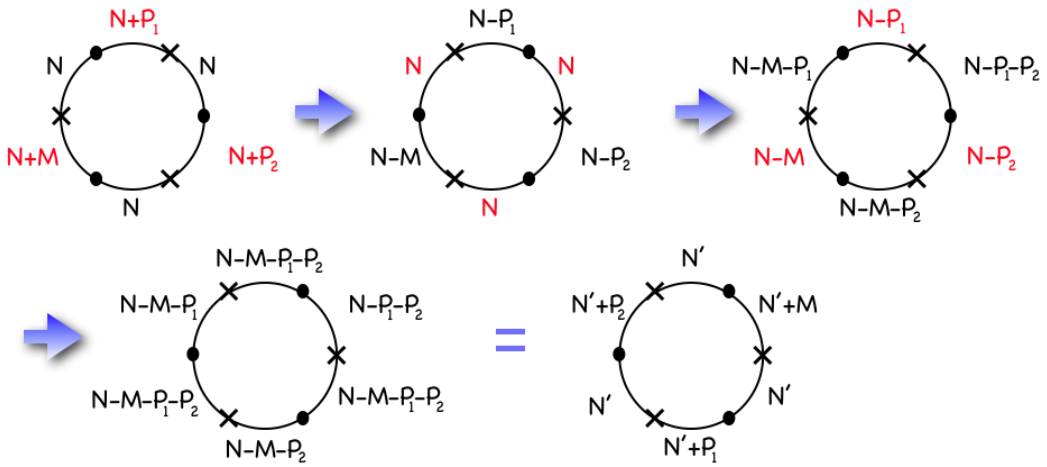

Figure 3.4: Basic period of the UV cascade, in terms of a HW T-dual configuration of branes. Dots and crosses denote NS and NS'-branes localized on a periodic direction (denoted as the circle), with D4-branes suspended among them. The red labels denote the gauge factors experiencing Seiberg duality in going to the next step. Upon three such steps, one recovers a configuration identical to the original with the number of regular branes effectively decreased by $M + P_1 + P_2$ (and a shift of the circle by 3 intervals).

reference, the fractional brane corresponding to node 4 is a deformation brane associated to the removal of the legs C, D from the web diagram. The dimer diagram corresponding (or holographically dual) to the left-over geometry after the deformation is obtained by removing the zig-zag paths C, D from the picture, and zipping together the unpaired remaining paths. This has the effect of recombining some of the faces, concretely 3 & 5, that from now I will refer to as 3 (3 & 5 $\to$ 3). Physically, this is because the mesons of the confined groups get vevs and this breaks part of the flavor symmetry. The result of this operation is shown in figure 3.5.

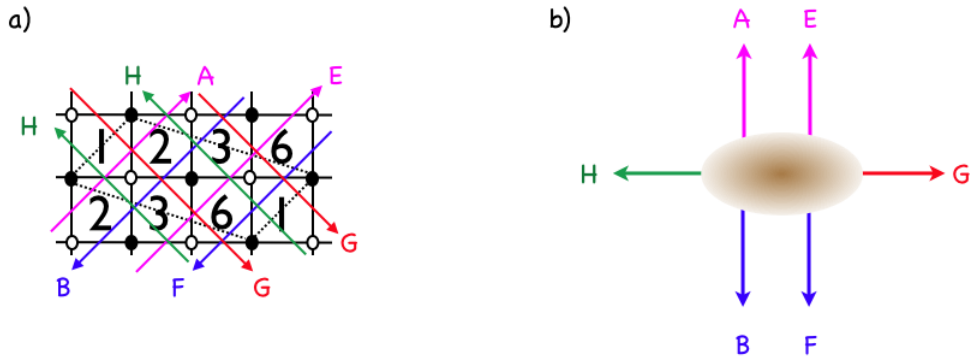

Figure 3.5: (a) Dimer resulting from the complex deformation of the initial geometry. it corresponds to a $\mathbb{Z}_2$ orbifold of the conifold. Zig-zags of the dimer are drawn as well. (b) Zig-zag paths as external legs of the web diagram. It can be seen that they correspond to the leftover geometry after removing the first subweb in equilibrium from figure 3.2(c).

The deformation is also easy to follow in the HW picture. It corresponds to the simultaneous removal of the NS and NS'-brane bounding interval 4, together with M of the suspended D4-branes, hence recombining the intervals 3 and 5.

In either picture, one is left with a $\mathbb{Z}_2$ quotient of the conifold, with nodes 1,2,3,6 and rank assignments

$$n_2 = M + P_1 \quad , \quad n_1 = n_3 = M \quad , \quad n_6 = M + P_2. \tag{3.7}$$

It is possible to achieve a more general rank assignment, with the number of regular branes differing from M (the fractional branes of the UV throat), by starting with $N = k(M + P_1 + P_2) + M + Q$. The strong dynamics is trickier, and I simply quote that it leads to the same quantum deformation and Q additional regular branes, in analogy with the appendix in [5] for the conifold. In these cases, the strong dynamics typically corresponds to the appearance of a non-perturbative Affleck-Dine-Seiberg superpotential, whose F-term conditions enforce the quantum deformation of the moduli space of the left-over regular D-branes.

Splitting the throat

Once the first cascade has taken place, the geometry reaches a lower energy scale at which the gauge theory must split into two, corresponding to the two theories to become the duals of the two IR throats. Geometrically, the process is a splitting of the singularity into two remaining singularities, by a small resolution in which the web diagram is elongated (keeping it in the same plane) by separating the legs A,B,H from E,F,G. The result is a factorization of the diagram into two, one per left-over singularity, see figure 3.6. At the level of the gauge theory, blowing up the singularity corresponds to turning on FI terms, whose contribution to the D-term potential must be cancelled by turning on suitable vevs, triggering a Higgs mechanism. Geometrically, fractional branes of the original singularity combine together to form fractional branes of the left-over singularities.

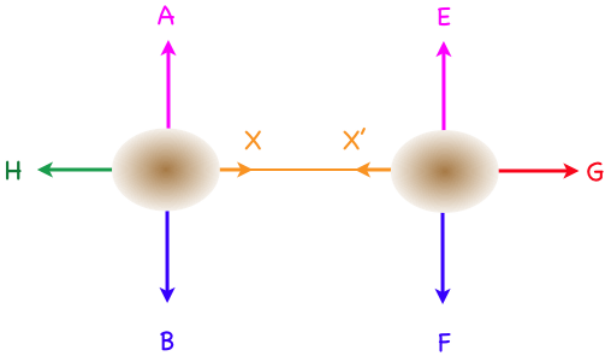

Figure 3.6: Elongation of the web diagram into two subwebs.

This can be easily reproduced using the HW brane configurations, as shown in figure 3.7.

The same result can be recovered using the techniques in [41]. Basically, the gauge theory splits into two, associated to the subsets (A,B,H) and (E,F,G). To get the first gauge theory sector, first draw the dimer diagram with only the zig-zag paths A,B,H and complete the unpaired paths by introducing a new one, labeled X. The edges not touched by A,B, H are precisely those bifundamentals getting a vev in the Higgssing. This breaks some of the gauge factors to their diagonal, specifically, 1,3,6 are combined together (and

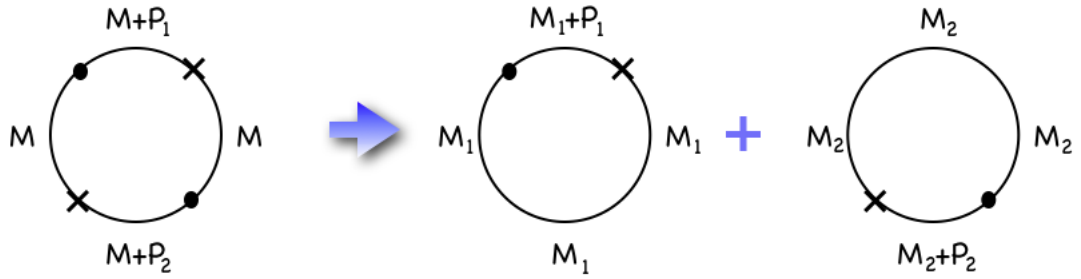

Figure 3.7: Higgs mechanism in the gauge theory in terms of a T-dual HW brane configuration. The partial blowup of the geometry, equivalent to the field theory FI terms, corresponds to the motion of one NS-NS' brane pair with respect to the other in the transverse direction 7, which enforces partitioning the stacks of D4-branes and recombining them across some intervals. The resulting two diagrams on the right-hand side are separated in the direction 7, and describe two decoupled conifold theories.

subsequently denoted by 1). The result of the operation is shown in figure 3.8(a), and simplified in (b), by a contraction of the diagram that corresponds to integrating out some massive fields. The resulting theory is simply a conifold theory.

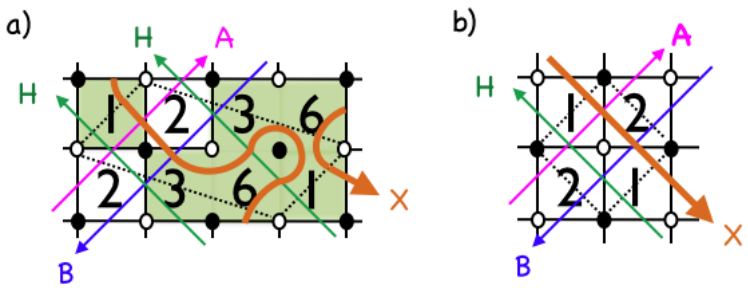

Figure 3.8: Dimer of the first gauge theory resulting from the elongation of the web diagram.

In the same way, to get the second gauge theory, I draw the dimer diagram with only the zig-zag paths E, F & G, and complete them with a new path denoted X′. The process is a Higgs mechanism in which the gauge factors 1, 2, 3 are broken to the diagonal, subsequently denoted by 3. The resulting theory is shown in figure 3.9 and corresponds to a second conifold theory.

In purely field theoretical terms, the above operations in either brane picture correspond to turning on vevs of the form

$$\Phi_{23} = \Phi_{12}^T = \begin{pmatrix} 0_{(M_1+P_1)\times M_1} & \\ & v_2\,\mathbf{1}_{M_2\times M_2} \end{pmatrix}$$
$$\Phi_{61} = \Phi_{36}^T = \begin{pmatrix} v_1\mathbf{1}_{M_1\times M_1} & \\ & 0_{(M_2+P_2)\times M_2} \end{pmatrix}. \tag{3.8}$$

In words, the first matrix takes the $SU(M+P_1)$ theory at node 2, and breaks it with vevs for M_2 of its flavours $Q = \Phi_{23}$, $\tilde{Q} = \Phi_{12}$, breaking also the $SU(M)^2$ flavour symmetry.

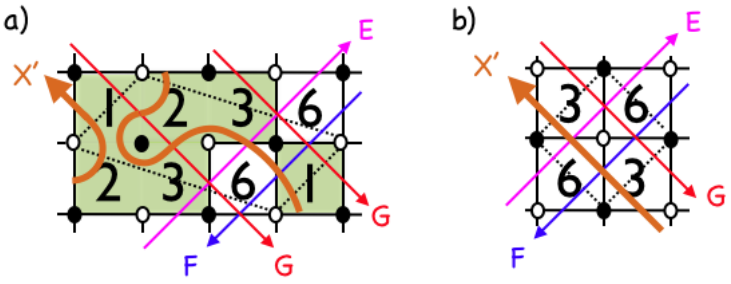

Figure 3.9: Dimer of the second gauge theory resulting from the elongation of the web diagram.

The surviving group is $SU(M_1+P_1)_2 \times SU(M_2)_{123} \times SU(M_1)_1 \times SU(M_1)_3$ [1]. The second matrix corresponds to taking the $SU(M+P_2)$ theory at node 6, and giving mesonic vevs to M_1 of its flavours $Q = \Phi_{61}$, $\tilde{Q} = \Phi_{36}$, breaking the $SU(M)^2$ symmetry. The surviving group is $SU(M_1)_{136} \times SU(M_2+P_2)_6 \times SU(M_2)_1 \times SU(M_2)_3$. The actual symmetry surviving both Higgsings is $SU(M_1+P_1)_2 \times SU(M_1)_{136}$ and $SU(M_2+P_2)_6 \times SU(M_2)_{123}$, that is denoted $SU(M_1+P_1)_2 \times SU(M_1)_1$ and $SU(M_2+P_2)_6 \times SU(M_2)_3$ in the dimers of figure 3.8 and figure 3.9. It is simple but tedious to check that the field theory Higgsing leads to two decoupled conifold gauge theory sectors, in agreement with the geometric splitting of the D3-branes on the two left over conifold singularities.

Smaller throats

Below the scale of the symmetry breaking, the massive fields can be integrated out to recover two decoupled conifold theories. Each independent conifold theory has fractional branes which can trigger standard Klebanov-Strassler throats [5], providing the holographic dual of the two smaller throats. This part of the discussion is standard and requires no further comment.

One last remark concerns the ordering of scales. The geometry of the throats corresponds to a precise ordering of the scales of strong dynamics for the UV gauge theory, Λ, the scale of symmetry breaking vevs v, and the strong dynamics scales of the final conifold theories Λ_1, Λ_2. Concretely, one needs

$$\Lambda \gg v \gg \Lambda_1, \Lambda_2. \tag{3.9}$$

It is possible, but uninteresting for the purposes of this thesis to consider other orderings, which would lead to different throat geometries.

[1] $SU(M_2)_{123}$ stands for the $SU(M_2)$ diagonal subgroup coming from gauge groups 1, 2 & 3 after the Higgsing by (3.8).

3.2. Bifid throat with homologous 2-cycles

In this section, I construct a bifid throat similar to that in the previous section, but including homologous 2-cycles at the tip of the IR throats. The simplest way to achieve this is to consider a $\mathbb{Z}_2$ orbifold of the geometry in the previous section (hence a $\mathbb{Z}_3 \times \mathbb{Z}_2$ orbifold of the conifold). To be concrete, quotient (3.2) by the action $z \to -z$, $w \to -w$; defining the invariants $z' = z^2$, $w' = w^2$, $t' = zw$ so that

$$x'y' = t'^3 \quad , \quad z'w' = t'^2. \tag{3.10}$$

This produces a (complex) curve of $\mathbb{C}^2/\mathbb{Z}_2$ singularities (manifest in the second equation above), which I will show to fall inside both IR throats, and whose blown-up 2-cycle provides the (common) homology class where the brane-antibrane pair will ultimately wrap. In this section I focus on the construction of the geometry, and postpone the introduction of the branes to section 3.3.

The construction, even after the inclusion of fractional branes dual triggering the complex deformations supporting the fluxes in the dual geometry, is simply a $\mathbb{Z}_2$ quotient of that in the last section. Although it does not admit a simple T-dual HW brane configuration, it remains toric and can be easily described using dimer diagrams, which are just given by a two-fold extension of the dimers in the previous section. Therefore, I will keep the discussion sketchy, as most ideas already appeared on the previous case.

The web diagram for the geometry is shown in figure 3.10 (a), its toric diagram in (b) and the result of the complex deformations is shown in (c). The existence of a curve of $\mathbb{C}^2/\mathbb{Z}_2$ singularities, even after the complex deformations, is manifest in the presence of two sets of parallel horizontal legs in the web diagram.

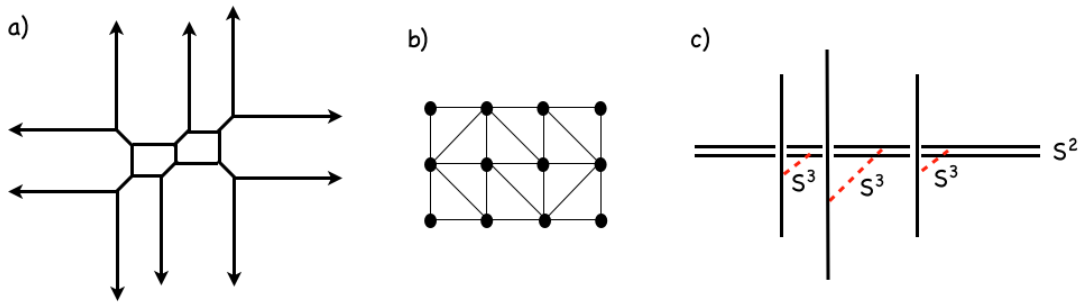

Figure 3.10: (a) Web diagram of the singularity of interest. (b) Its toric diagram. (c) Complex deformations of the geometry, showing the 3-cycles and the left-over curve of collapsed 2-spheres.

3.2.1. The dimer

As previously done for the $\mathbb{Z}_3$ orbifold of the conifold, the dynamics of a D3-brane probing the geometry can be nicely encoded by using dimer diagrams. The dimer is shown in figure 3.11(a). To show that it corresponds to the geometry of interest, the zig-zag paths are also shown together with their (p, q) homology class in the $\mathbb{T}^2$ unit cell of the dimer, corresponding to the geometry, see figure 3.11(b).

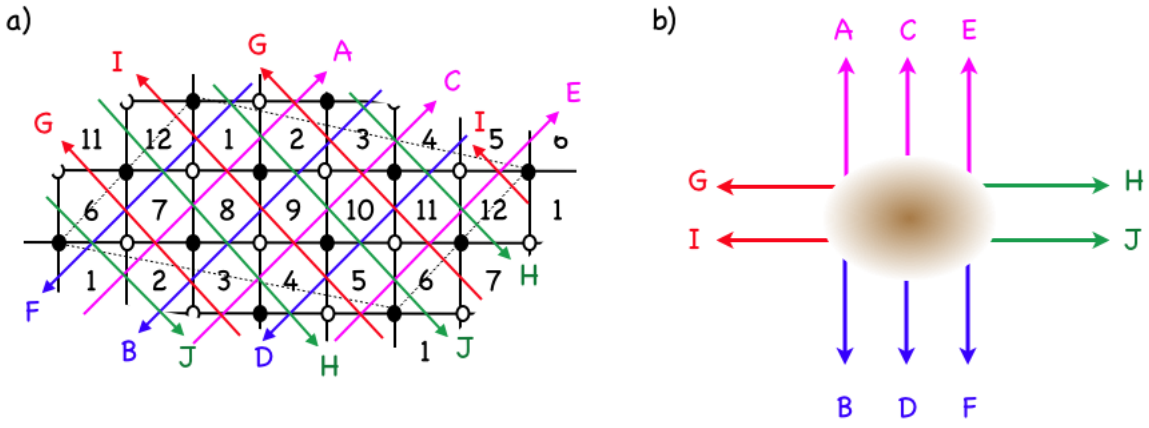

Figure 3.11: (a) Dimer corresponding to the $\mathbb{Z}_3 \times \mathbb{Z}_2$ orbifold of the conifold together with its zig-zag paths. (b) External legs in the web diagram as obtained from their (p, q)-classes.

According to the structure of the system, which is a $\mathbb{Z}_2$ orbifold of the construction in the previous section, the choice of fractional branes is $n_{i+6} = n_i$ with n_i as in (3.4), namely

$$\begin{gathered} n_2 = n_8 = N + P_1 \quad , \quad n_4 = n_{10} = N + M \quad , \quad n_6 = n_{12} = N + P_2 \\ n_1 = n_3 = n_5 = n_7 = n_9 = n_{11} = N. \end{gathered} \tag{3.11}$$

The UV cascade proceeds as in section 3.1.2, by simply operating on nodes i and $i + 6$ simultaneously. This preserves the $\mathbb{Z}_2$ symmetry throughout the process, so the dimer remains the two-fold extension of the dimers in the previous section, with the $n_{i+6} = n_i$ rank assignment rule.

3.2.2. First complex deformation: the common throat

As in section 3.1.2, the throat eventually runs out of regular D3-branes and encounters the first complex deformation. This corresponds to the removal of the legs C, D from the web diagram, and is triggered by the M fractional branes on faces 4, 10 in the dimer (precisely those bounded by the paths C, D), see figure 3.11. The gauge theory dynamics is (a two-fold extension) of that in the previous section, and the remaining field theory after the complex deformation is obtained by similar diagrammatics. Namely, remove the paths C, D, and zip up unpaired paths. The gauge groups 5 and 9 are combined together (I label the result by 5), and so are 3 and 11 (labeled 3 henceforth). The result of this operation is shown in figure 3.12. It corresponds to a $\mathbb{Z}_2 \times \mathbb{Z}_2$ orbifold of the conifold. The remaining rank assignment is

$$\begin{gathered} n_2 = n_8 = M + P_1 \quad , \quad n_6 = n_{12} = M + P_2 \\ n_1 = n_3 = n_5 = n_7 = M. \end{gathered} \tag{3.12}$$

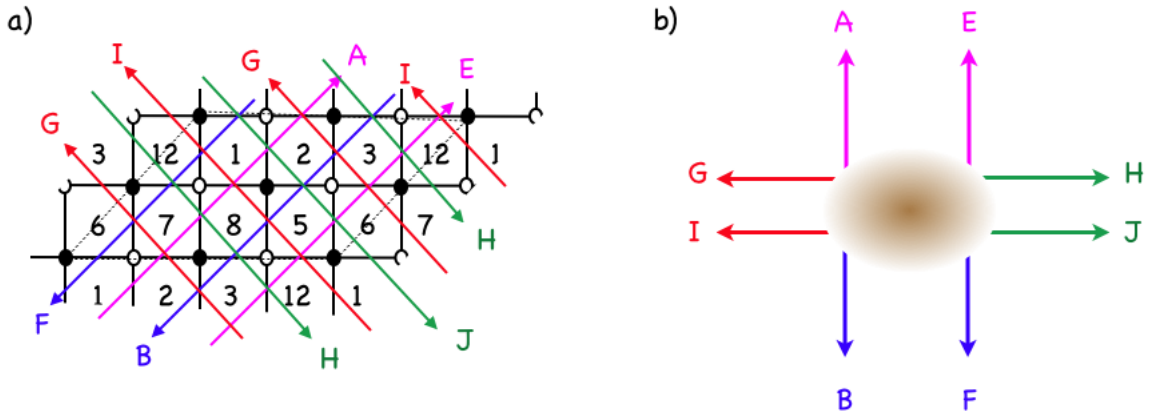

Figure 3.12: (a) Dimer resulting of the complex deformation of the initial geometry, together with its zig-zag paths. It corresponds to a $\mathbb{Z}_2 \times \mathbb{Z}_2$ orbifold of the conifold. (b) External legs in the web diagram as obtained from their (p, q)-classes.

3.2.3. Separating the stacks

After the deformation/strong dynamics at the IR of the first throat/cascade, this reaches a lower energy scale at which the gauge theory must split into two. Geometrically, this is a resolution of the singularity in which the web diagram is elongated (keeping it in the same plane) by separating the legs A,B,G,I from E, F, H, J. The end result is a factorization of the diagram into two, see figure 3.13.

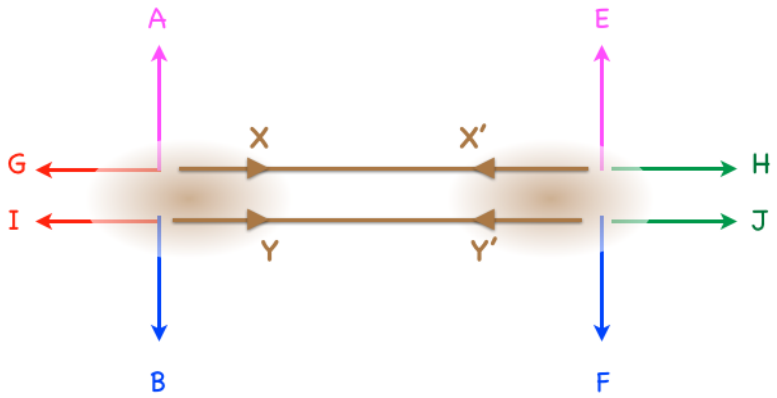

Figure 3.13: Elongating the web diagram into two effective sub-singularities.

At the level of the gauge theory, this corresponds to the introduction of FI terms, whose D-terms are cancelled by suitable bifundamental vevs, which Higgs down the gauge theory and split it in two sectors. The field theory analysis is enormously simplified in terms of the dimer diagrams [41], as follows. To get the first gauge theory sector, draw the dimer diagram with only the zig-zag paths A,B,G,I, and complete the unpaired paths with new ones, in this case two, labeled X,Y. The edges not touched by A,B, G,I are precisely

those bifundamentals getting a vev in the Higgsing.

The diagrammatic process breaks some of the gauge factors to their diagonal, specifically, 3,7,12 are combined together (and subsequently denoted by 3), and so are 1,5,6 (herefrom denoted by 1). The result of the operation is shown in figure 3.14 (a), and simplified in (b), by a contraction of the diagram that corresponds to integrating out some massive fields. It corresponds to the dimer of a $\mathbb{Z}_2$ orbifold of the conifold (in agreement with the fact that its zig-zag paths reproduce, by construction, those of the web for such geometry). For concreteness, the orbifold action on $xy - zw = 0$ is $z \to -z$, $w \to -w$, as inherited from the $\mathbb{Z}_2$ action at the beginning of section 3.2. The rank assignments in this gauge theory sector are

$$n_3 = n_1 = M_1 \quad , \quad n_2 = n_8 = M_1 + P_1. \tag{3.13}$$

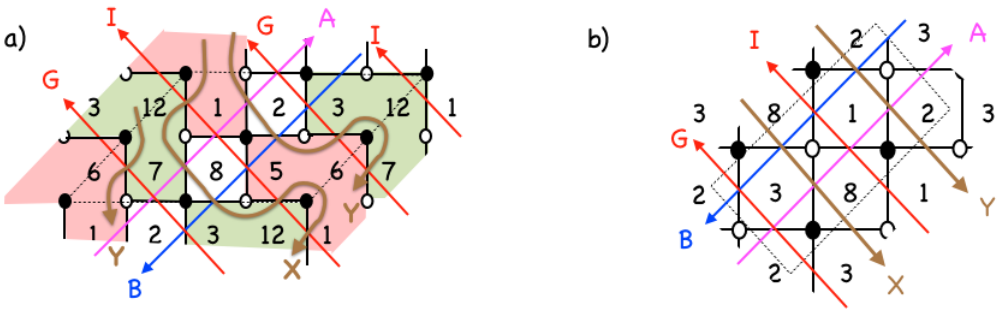

Figure 3.14: Dimer of the first gauge theory resulting from the elongation of the web diagram.

The second gauge theory sector is obtained by drawing the dimer diagram with only the zig-zag paths E, F, H, J, and then completing the unpaired paths by two new ones, labeled X',Y'. The factors 2,3,7 are broken to the diagonal (denoted by 2), and so are 1,5,8 (denoted by 1 from now on). The operation is shown in figure 3.15. The rank assignments in this gauge theory sector are

$$n_2 = n_1 = M_2 \quad , \quad n_6 = n_{12} = M_2 + P_2. \tag{3.14}$$

The resulting geometries are two copies of a $\mathbb{Z}_2$ orbifold of the conifold. It is important to point out that both small throats pass through the same curve of $\mathbb{C}^2/\mathbb{Z}_2$ singularities, so both singularities share a common homology class for one of their 2-cycles. This is manifest from the web diagram, where the two parallel legs responsible for the $\mathbb{C}^2/\mathbb{Z}_2$ are common to both sub-diagrams.

At the field theory level, the explicit expression for the vevs can be simply obtained from the above dimer analysis, following [41], or by taking a two-fold extension of the

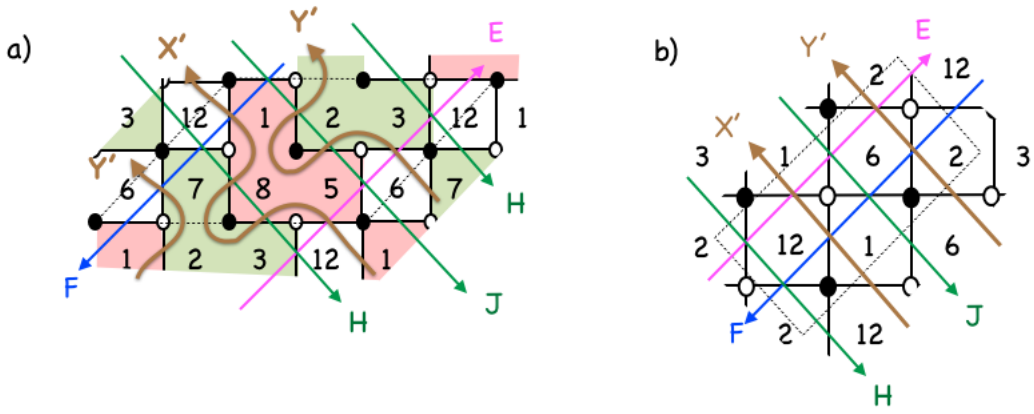

Figure 3.15: Dimer of the second gauge theory resulting from the elongation of the web diagram.

result for the simpler construction in section 3.1. For completeness I quote the result:

$$\Phi_{81} = \Phi_{58}^T = \Phi_{27} = \Phi_{32}^T = \begin{pmatrix} 0_{(M_1+P_1)\times M_1} \\ v_2\, \mathbf{1}_{M_2\times M_2} \end{pmatrix}$$
$$\Phi_{12,7} = \Phi_{3,12}^T = \Phi_{61} = \Phi_{56}^T = \begin{pmatrix} v_1 \mathbf{1}_{M_1\times M_1} \\ 0_{(M_2+P_2)\times M_2} \end{pmatrix}. \tag{3.15}$$

3.2.4. Last complex deformations: the small throats

The rank assignments (3.13), (3.13) show that the two gauge theories are the holographic duals of configurations with P_1 and P_2 fractional branes, and hence define the UV of the subsequent duality cascades. Since the two sectors are very similar, I just discuss one of them. The cascade for this orbifold of the conifold has already been discussed in [40], and merely corresponds to a two-fold extension of the KS conifold cascade. The IR physics is also similar, and leads to a quantum deformation of the moduli scape, dual to a complex deformation of the geometry, see below.

The geometry is simple enough to be described explicitly. As advanced in the previous section, the $\mathbb{Z}_2$ orbifold action on the conifold

$$xy - zw = 0 \tag{3.16}$$

is defined by $x \to -x$, $y \to -y$. Introducing $x' = x^2$, $y' = y^2$, the orbifold of the conifold is

$$x'y' - z^2w^2 = 0. \tag{3.17}$$

There are two curves of $\mathbb{C}^2/\mathbb{Z}_2$ singularities at $x' = y' = z = 0$ and $x' = y' = w = 0$; in other words, at $x' = y' = 0$ and $zw = 0$. The complex deformation is explicitly described by considering the same quotient but for the deformed conifold $xy - zw = \epsilon$, namely

$$x'y' = (zw - \epsilon)^2, \tag{3.18}$$

which clearly contains $\mathbb{C}^2/\mathbb{Z}_2$ singularities (of the form $x'y' = t^2$) along the curve $x' = y' = 0$ and $t \equiv zw - \epsilon = 0$.

In the theory shown in figure 3.14 (b), the effect of the complex deformation corresponding to removing the legs A, B. Following [41], this is done by removing the paths A, B from the dimer, and zipping together the unpaired paths. The gauge factors 2 and 8, corresponding to the fractional branes, disappear (due to confinement), and in this case nodes 1 and 3 remain independent. The remaining picture is shown in figure 3.16(a), and corresponds to a dimer associated to $\mathbb{C}^2/\mathbb{Z}_2$, as expected. A similar operation in the second gauge theory produces the picture in figure 3.16(b).

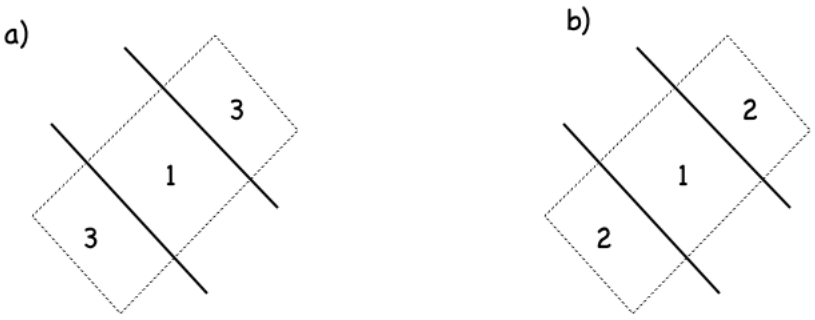

Figure 3.16: Dimer of the gauge theories after the complex deformation at the bottom of the small throats.

Notice that even though the two gauge theories are $\mathbb{C}^2/\mathbb{Z}_2$, by construction they belong to the same curve of singularities. Therefore, the 2-cycle in the blowup of this singularity falls inside both throats. This can be seen in the gauge theory language, because the fractional branes of the $\mathbb{C}^2/\mathbb{Z}_2$ in the first gauge theory are the same as those in the second (modulo gauge factors which have confined, i.e. whose homology 2-class has become trivial in the geometry). More explicitly, in the first $\mathbb{C}^2/\mathbb{Z}_2$ gauge theory, the final fractional branes correspond to labels 1, and 3. Now each of these came from the recombination of the original faces, specifically 1 comes from the set (1,5,6,9) and 3 comes from (3,7,11,12). Similarly, in the second gauge theory, the fractional branes carry labels 1 and 2, and actually correspond to the faces (1,5,8,9) and (2,3,7,11) of the original gauge theory. Since the faces 2,8,6,12 of the original theory have actually disappeared by confinement, they do not define non-trivial homologly classes in the dual throat. Hence, the two fractional branes carry charges corresponding to the sets (1,5,9) and (3,7,11) in either of the two theories, consistently with the fact that they belong to the same curve of singularities.

3.3. Inclusion of fivebrane-antibrane pair and axion monodromy

In this section the above holographic picture is used as a framework to study the brane-antibrane system wrapped on the homologous 2-cycle at the tip of the two final throats. As explained, these systems provide a realization of axion monodromy inflation [87, 97].

In this discussion, I consider the simpler setup of D5 brane-antibrane pairs wrapped on the 2-cycle. In applications to inflation, an NS5 brane-antibrane pair was proposed; this is because such branes couple to an axion coming from integrating the RR 2-form over the 2-cycle, and such axion scalar was argued not to appear in the Kähler potential in type IIB compactifications with O3/O7-planes. However, many local features of the system can be analyzed by considering the realization in terms of D5-branes (and performing S-duality if necessary). Moreover, D5-brane realizations may be interesting in their own right in global setups beyond O3/O7 CY compactifications. Hence, I stick to the D5-brane picture in what follows.

The description of D5 branes (antibranes) wrapped on the 2-cycle corresponds to the inclusion of suitable fractional branes (antibranes) with respect to the $\mathbb{C}^2/\mathbb{Z}_2$, and is hence very simple. The 2-cycle is visible in the web diagram in figure 3.13 as the segment stretching between the legs X, Y. Then, adding Q extra wrapped branes corresponds to increasing the ranks on the faces of the dimer enclosed by the corresponding zig-zag paths, for instance 1, 8, see figure 3.14(b). The rank assignments change from (3.13) to

$$\begin{aligned} n_1 = M_1 + Q \quad , \quad n_8 = M_1 + P_1 + Q \\ n_3 = M_1 \quad , \quad n_2 = M_1 + P_1. \end{aligned} \tag{3.19}$$

The addition of the extra Q branes has a small backreaction on the RG cascade, which will be described in some more detail in section 3.3.2.

It is convenient to trace this rank change up in the UV to the theory before the Higgsing. The addition of the Q fractional branes corresponds to a modification of the ranks on faces bound by paths X, Y, see figure 3.14(a), namely 1,5,6,8. The rank assignments change from (3.12) by

$$\Delta n_1 = \Delta n_5 = \Delta n_6 = \Delta n_8 = Q. \tag{3.20}$$

Clearly, there is a second choice of fractional brane bounded by X, Y, which corresponds to 2, 3, 7, 12 in figure 3.14(a), corresponding to 2, 3 in figure 3.14(b). This corresponds to a fractional D3-branes with opposite 2-cycle homology charge. To keep track of this charge, take into account the orientation of the paths, so the fractional branes used in (3.20) correspond to increasing the ranks of the faces in the strip bounded by $X - Y$ (i.e. by X and the orientation-reversed Y).

Consider now the addition of Q fractional antibranes on the second throat. At the level of the charges, this is equivalent to decreasing some of the ranks of suitable faces, especifically those bounded by $Y' - X'$ (keeping track of orientation, as explained above) in figure 3.15. Namely, the rank assignments in the gauge theory corresponding to the second IR throat are

$$\begin{aligned} n_1 = M_2 - Q \quad , \quad n_6 = M_2 + P_2 - Q \\ n_2 = M_2 \quad , \quad n_{12} = M_2 + P_2. \end{aligned} \tag{3.21}$$

Moving up in the UV to the level of the theory before the Higgsing, the rank assignments change from (3.12) by

$$\Delta n_1 = \Delta n_5 = \Delta n_6 = \Delta n_8 = -Q. \tag{3.22}$$

The fact that this variation is precisely opposite to that in (3.20) means that the combined set of two objects carries no charge.

At the level of the charges, the above description amounts to imposing a different split of ranks in the Higgs mechanism, changing the vevs (3.15) to

$$\begin{aligned}
\Phi_{81} = \Phi_{58}^T &= \begin{pmatrix} 0_{(M_1+P_1+Q)\times(M_1+Q)} & \\ & v_2\,\mathbf{1}_{(M_2-Q)\times(M_2-Q)} \end{pmatrix} \\
\Phi_{27} = \Phi_{32}^T &= \begin{pmatrix} 0_{(M_1+P_1)\times M_1} & \\ & v_2\,\mathbf{1}_{M_2\times M_2} \end{pmatrix} \\
\Phi_{61} = \Phi_{56}^T &= \begin{pmatrix} v_1\mathbf{1}_{(M_1+Q)\times(M_1+Q)} & \\ & 0_{(M_2+P_2-Q)\times(M_2-Q)} \end{pmatrix} \\
\Phi_{12,7} = \Phi_{3,12}^T &= \begin{pmatrix} v_1\mathbf{1}_{M_1\times M_1} & \\ & 0_{(M_2+P_2)\times M_2} \end{pmatrix}.
\end{aligned} \tag{3.23}$$

The Higgsing by these vevs reproduces two decoupled gauge sectors corresponding to the UV of the two throats, with ranks modified by $\mathbb{Z}_2$ fractional brane charge. This reproduces the first throat with K extra fractional branes, and the second throat with reduced rank groups

$$SU(M_2-Q)_1 \times SU(M_2)_2 \times SU(M_2+P_2-Q)_6 \times SU(M_2+P_2)_{12}\ . \tag{3.24}$$

Actually, in analogy with [100] (see also [59, 60]), this gauge sector should be regarded as providing a supersymmetric groundstate in a field theory in which the antibrane configuration should correspond to a metastable state (especifically, Q fractional antibranes in the throat defined by the $SU(M_2)^2 \times SU(M_2+P_2)^2$ theory, so that the total charges match). The energy associated to the susy breaking is suppressed by the RG cascade, compared with the energies at which the splitting of the throat occurs, so this justifies the approximation of describing the splitting as a mere Higgs mechanism at those scales.

3.3.1. Hanany-Witten T-dual of axion monodromy

The appearance of axion monodromy upon the introduction of the D5-brane admits a simple intuitive description in terms of a T-dual HW brane configuration [99], which directly connects with a picture developed in [87].

Recall the description of the singularity (3.10), namely (removing the primes)

$$\begin{aligned} xy &= t^3 \\ zw &= t^2 \end{aligned} \tag{3.25}$$

This equations describe the geometry as the superimposition of a $\mathbb{Z}_3$ and a $\mathbb{Z}_2$ orbifolds. A T-duality along the $\mathbb{S}^1$ in (x, y), defined by the orbit (3.5) would lead to a configuration given by a $\mathbb{Z}_2$ orbifold of figure 3.4, i.e. with the $\mathbb{Z}_3$ orbifold T-dualized into three NS

and NS' branes, but with an explicit $\mathbb{Z}_2$ orbifold geometry (the $\mathbb{Z}_2$ acting as a sign flip in the directions 4589), similar to those considered in [101]. Hence this T-duality does not geometrize the B-field on the 2-cycle collapsed at the $\mathbb{Z}_2$. So I instead T-dualize along the $\mathbb{S}^1$ parametrized by β in the orbit

$$z \to e^{i\beta} z \quad , \quad w \to e^{-i\beta} w. \tag{3.26}$$

In this picture, the $\mathbb{Z}_2$ orbifold is geometrized in the T-dual into two NS- and two NS'-branes, in a $\mathbb{Z}_3$ orbifold geometry. The structure of NS5-branes is manifest in the fact that the locus of degeneration of the $\mathbb{S}^1$ in (z, w) is $t = 0$ (with multiplicity 2), which corresponds by the first equation to $xy = 0$ (with multiplicity 2). This describes two kinds of objects, i.e. along $x = 0$ or along $y = 0$.

The B-field of the 2-cycle collapsed at the $\mathbb{Z}_2$ orbifold singularity is geometrized as the relative distance between the two (NS, NS') pairs. The other relative brane separations correspond to B-fields on 2-cycles which actually disappear due to the complex deformations of the singularity. This can be seen explicitly, by following the action of the deformations in the HW T-dual deforming the singularity (3.25) to (c.f. (3.3))

$$\begin{aligned} xy &= (t - \epsilon_1)(t - \epsilon_2)(t - \epsilon_3) \\ zw &= t^2. \end{aligned} \tag{3.27}$$

Performing the T-duality in this deformed geometry, the degeneration locus of the $\mathbb{S}^1$ is $t = 0$ (with multiplicity 2), which now corresponds to $xy = \text{const}$ (with multiplicity 2); describes two copies of a unique kind of object, which is a recombination of the NS and NS'-brane. In other words, the complex deformation corresponds to shrinking the intervals within each (NS,NS') pair and combining the branes in the pair into a bound state. In the following I refer to this combined object as an NS5-brane (along the $t = 0$).

The B-field of the 2-cycle collapsed at the $\mathbb{Z}_2$ orbifold singularity corresponds to the surviving distance between the two NS5-branes. Also, the fractional D5-brane wrapping the collapsed 2-cycle corresponds to a D4-brane suspended along the interval between the NS5-branes. In this picture, the axion monodromy is manifest, and corresponds to the additional winding of the D4-branes when dragged by the relative motion of the two NS5-branes, see figure 3.17, as described in [87].

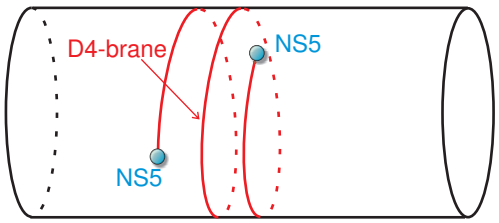

Figure 3.17: T-dual configuration of the fractional D5-brane at the deformed singularity. The picture is precisely as in [87].

Actually, because the singularity contains a D5/anti-D5 pair located at different points of the curve of $\mathbb{C}^2/\mathbb{Z}_2$ singularities, the HW T-dual contains one anti-D4-brane

stretched between the NS5-branes, in addition to the above mentioned D4-branes. The D4- and anti-D4-branes are located at different positions along the NS5-branes.

3.3.2. Brane-antibrane backreaction

The holographic dual description can be used to address questions like the backreaction of the brane-antibrane system in the throat geometry.

There are two kinds of backreaction that can be considered in this setup. The first is due to the presence of anti-D3-brane charge in the second throat. This bulk antibrane charge, in an otherwise supersymmetric throat, is completely similar to the anti-D3-branes in KS throats. These have been used in several applications [61], and are the subject of heated controversy concerning its backreacted solution in supergravity (see e.g. [102–111]). I will not add anything this debate in this thesis.

The novel feature about fivebrane-antibrane pairs in bifid throats is the existence of a backreaction on closed string fields associated to the homologous 2-cycle [98]. In the just presented geometry these fields correspond to closed string twisted states at the $\mathbb{C}^2/\mathbb{Z}_2$ curve of singularities. On the geometrical side, one stack of fractional branes sources this field and lead to a log profile for it (see e.g. [112]), so it does not decrease as one moves away from the stack (the analysis in [98] dealt with flat space or weakly curved geometries, the logs are still present in warp geometries [113]).

This behaviour is easily reproduced in the holographic field theory describing the two IR throats. In fact, what follows is a simple generalization of what happens for fractional D3-branes at a $\mathbb{C}^2/\mathbb{Z}_2$ singularity (see e.g. [112]): the closed string twisted fields couple to the fractional brane by contributing to their gauge coupling constant, and the log dependence on the 2-plane transverse to the D3-branes is just the log dependence of the gauge coupling with the Coulomb branch parameter, controlled (at long distance / vev large compared with the strong dynamics scale) by the perturbative beta function of the corresponding $\mathcal{N}=2$ gauge theory.

The same analysis for the backreaction of the fractional branes can be reproduced in e.g. the first IR throat. Consider the theory with ranks (3.19) at the scale corresponding to the next-to-last step in the cascade. It has gauge group

$$SU(P_1+Q)_1 \times SU(2P_1)_2 \times SU(P_1)_3 \times SU(2P_1+Q)_8 \tag{3.28}$$

and chiral bifundamentals X_{12}, X_{21}, X_{23}, X_{32}, X_{38}, X_{83}, X_{81}, X_{18} and a superpotential clear from the dimer, that can be ignored at the moment. The non-perturbative dynamics of this theory can be analyzed directly, and reproduces (a number of fractional branes in) the deformed geometry. The result of interest can be obtained more easily as follows. There is a flat direction corresponding to giving vevs to X_{81}, X_{18}, which corresponds to moving the Q $\mathbb{Z}_2$ fractional branes away from the singular point, along the curve of $\mathbb{C}^2/\mathbb{Z}_2$ singularities, while the left-over $SU(P_1)^2 \times SU(2P_1)^2$ theory generates the deformation of the throat as usual. The flat direction is actually the Coulomb branch of the $\mathbb{Z}_2$ fractional branes. Denoting by Λ_i the dynamical scales of the gauge factors before taking the flat direction, and Λ'_i the scales after integrating out the modes made massive by the vev z, the matching of scales gives

$$\begin{aligned} \Lambda_1'^{-P_1} &= \Lambda_1^{-P_1+2Q} z^{-2Q} \quad , \quad \Lambda_2'^{4P_1} = \Lambda_2^{4P_1-Q} z^{Q} \\ \Lambda_3'^{-P_1} &= \Lambda_3^{-P_1-Q} z^{Q} \quad , \quad \Lambda_8'^{4P_1} = \Lambda_8^{4P_1+2Q} z^{-2Q}. \end{aligned}$$

Relating the dynamical scales and the gauge couplings at some scale μ

$$\Lambda^{3N_c-N_f} = \mu^{3N_c-N_f} \exp\Big(\frac{1}{g^2_{\rm YM}(\mu)} + i\theta \Big), \tag{3.29}$$

one has the following parametric dependence of the different gauge couplings (for gauge factors labelled by i)

$$\frac{1}{g^2_{{\rm YM},i}(\mu)} + i\theta_i \sim Q \log z. \tag{3.30}$$

This is the field theory description of the log dependence in the backreaction of fractional branes. The effect of these modifications in the RG flow that describes the throat is amenable to quantitative study, but on general grounds it does not spoil the geometric picture: the log is comparable to that generated by the fractional branes associated to the fluxes, but its coefficient is suppressed by the factor $Q/P_i \ll 1$.

Moreover, the backreactions due to the brane-antibrane pair disappear as soon as both throats are combined into a single one, namely at the scale corresponding to the Higgsing separating the two IR throats. This is manifest in the field theory description of the introduction of the $\mathbb{Z}_2$ fractional branes in terms of a specific choice of vevs. Above such scale, the vevs are negligible and fractional branes can be ignored.

Moreover, extending the discussion above it is possible to estimate the backreaction effect in the holographic gauge theory description. For simplicity, I set the daughter throats symmetrical, and hence work with a hierarchy of scales $\Lambda \gg v \gg \Lambda' \equiv \Lambda_1 = \Lambda_2$. In the singular limit of the original $\mathbb{Z}_3$ singularity, this corresponds to a hierarchy $N > M > P_i \equiv P_1 = P_2$, where N denotes effective D3-brane at the UV end of the parent throat, and I put M and P_i units of RR 3-form flux on the deformation A-cycles at the IR end of the parent throat which forms the UV of the daughter throats, and at the IR end of the daughter throats, respectively. Furthermore, I put K units of NSNS 3-form flux at the dual B-cycle of the parent throat and K' units of NSNS 3-form flux on the dual B-cycles of the daughter throats. this gives the warp factors $\Lambda/M_p = e^A$ and $\Lambda'/M_p = e^{A'}$ at the bottom of the parent throat (and thus top of the daughter throats) and the bottom of the daughter throats, respectively, expressions reading [4]

$$\Lambda \sim e^{-\frac{2\pi}{3}\frac{K}{Mg_s}} \quad , \quad \Lambda' \sim e^{-\frac{2\pi}{3}\frac{K'}{Pg_s}}. \tag{3.31}$$

In order to estimate for the scales Λ, Λ', I use the results of the original geometric description of 5-brane axion monodromy [87]. Axion monodromy inflation arises now from the tension and the action of an NS5-brane wrapping a small resolution 2-cycle Σ at the end of the curves of $\mathbb{C}^2/\mathbb{Z}_2$ singularities at the bottom (IR) of the daughter throats. Consider first the DBI action of a D5-brane

$$S_{D5} = \underbrace{\frac{1}{(2\pi)^5 g_s \alpha'^3}}_{T_{\rm D5}} \int_{M_4\times\Sigma} d^6\xi \sqrt{-\det(G+B_2)} \quad . \tag{3.32}$$

By S-duality the corresponding part the NS5-brane action reads

$$S_{NS5} = \underbrace{\frac{1}{(2\pi)^5 g_s^2 \alpha'^3}}_{T_{\rm NS5}} \int_{M_4\times\Sigma} d^6\xi \sqrt{-\det(G+g_s^2 C_2)} \quad . \tag{3.33}$$

If the volume of the 2-cyle Σ is denoted $r^2 \equiv vol(\Sigma)$, then in terms of the RR-axion $c \equiv \int_\Sigma C_2$

$$\int_\Sigma d^2y \sqrt{-\det(G + g_s^2 C_2)} = \sqrt{r^4 + g_s^2 c^2} \quad . \tag{3.34}$$

Hence, for large fields the inflationary axion potential is linear. The overall warping of the NS5-brane energy density at the bottom of the daughter throat is included here

$$\begin{aligned} V = e^{4A_{IR}^{daughter}} \frac{1}{(2\pi)^5 g_s^2 \alpha'^3} g_s \int_\Sigma C_2 &\sim M_p^4 \left(\frac{\Lambda'}{M_p}\right)^4 \frac{g_s c}{4(2\pi)^3 g_s \mathcal{V}_E^2} \\ &\sim M_p^4 \frac{1}{8\pi\sqrt{g_s} vol_E^{5/3}} \frac{\Lambda'^4}{\Lambda M_p^3} \frac{\phi_c}{M_p} \equiv \mu^4 \frac{\phi_c}{M_p} \quad . \end{aligned} \tag{3.35}$$

After using that $\alpha' M_p^2 = \frac{2}{(2\pi)^7} \mathcal{V}/g_s^2 = \mathcal{V}_E/(\pi\sqrt{g_s})$ and $\mathcal{V}_E = g_s^{-3/2}/(2\pi)^6 \mathcal{V}$, $\mathcal{V} = L^6$ denotes the 4D Einstein frame Calabi-Yau volume (in a suitably global version of the construction).

Moreover, the curves of $\mathbb{C}^2/\mathbb{Z}_2$ singularities on which the C_2-axion is supported only reach up to the IR scale Λ of the parent throat, which affects the definition of the canonically normalized inflaton field as in

$$\frac{\phi_c}{M_p} = \frac{\Lambda}{M_p} \frac{g_s c}{\sqrt{g_s}(2\pi)^2 \mathcal{V}_E^{1/3}} \quad . \tag{3.36}$$

Altogether, this produces the Λ, Λ' dependence above. Imposing COBE normalization of the curvature perturbation power spectrum at the value $\phi_c = 11 M_p$ corresponding to 60 e-folds of slow-roll inflation yields the condition

$$\frac{\mu^4}{M_p^4} \simeq 2.2 \times 10^{-10}. \tag{3.37}$$

The resulting condition on the throat scales reads

$$\frac{\Lambda'^4}{\Lambda M_p^3} \sim 3.8 \times 10^{-6} \sqrt{\frac{g_s}{0.1}} \left(\frac{\mathcal{V}_E}{100}\right)^{5/3} \quad . \tag{3.38}$$

Requiring the desired hierarchy $\Lambda > \Lambda'$ implies a lower bound on Λ given by

$$\Lambda \gtrsim 0.016 \left(\frac{g_s}{0.1}\right)^{1/6} \left(\frac{\mathcal{V}_E}{100}\right)^{5/9} . \tag{3.39}$$

For equality the daughter throats would vanish into the parent throat as then $\Lambda = \Lambda'$.

It is useful to give an example to get a feeling of the typical hierarchies achievable. By taking typical values $g_s \sim 0.1$ and $\mathcal{V}_E \sim 100$ then this condition can be satisfied e.g. by choosing $\Lambda \sim 0.3$ and $\Lambda' \sim 0.03$. This can be realized taking (3.31) and turning on (non-compact) B-cycle NSNS flux quanta $K = K'$ and A-cycle RR flux quanta $M = 17K$, $P_i = 6K$ which satisfies the above constraint $M > P_i$.

If the axion inflaton potential above arises from Q NS5-branes and anti-NS5-branes wrapped on the small 2-cycles at the bottom of the daughter throats, then the backreaction estimate expressed as ratio over the P_i background fractional branes becomes

$$\frac{\Delta g_{\mathrm{YM},i}^{-2}(\mu)}{g_{\mathrm{YM}}^{-2}(\mu)} \sim \frac{Q}{P_i} \log \frac{z}{\Lambda'} < \frac{Q}{6K} \log \frac{\Lambda}{\Lambda'} \simeq 2.3 \times \frac{Q}{6K} \ll 1 \quad . \tag{3.40}$$

Here I used that the top-to-bottom radial distance in the daughter throats z is bounded by throat splitting VEV v which in turn must sit below the IR scale of the parent throat $z < v < \Lambda$. In conclusion, the fractional size of the backreaction can be almost arbitrarily small, given that one can choose the NSNS flux K large subject only to tadpole bounds.

The above results also clearly tell that for regimes with realistic scales the 5-brane-anti-brane backreaction is clearly subdominant to the backreaction driven by the 3-brane charge induced on the 5-branes by the wound-up axion [86, 97]. The induced 3-brane charge is proportional to the axion winding number corresponding to a given canonical inflaton field displacement. This number of axion windings in turn scales inversely with the axion decay constant f_a. The decay constant arises from an integral over the homologous 2-cycle family reaching from one daughter throat into the other. This will suppress f_a by the warp factor at the top of the daughter throats, that is, the scale Λ at the bottom of the parent throat [86]. For a parametric estimate of this effect, see section 4.4, where the increased winding number is also shown to have a negligible impact on the tunnelling rate despite the enhanced number of monodromy branches [114]. Hence, warping the whole 2-cycle family setup as in the present bifid throat does increase the amount of 3-brane charge build-up and its backreaction compared to the unwarped 'snake' of [86]. However, imposing realistic scale constrains $\Lambda \gtrsim 0.02$, while for the presented bifid throat one finds $\Lambda \sim 0.3$. This serves to demonstrate that in phenomenologically viable setups the warping reduction of f_a usually constitutes a rather mild effect.

4

Fluxed axion monodromy inflation on warped throats

As explained in the previous chapter, the underlying shift symmetry of axions makes these fields good candidates for the inflaton, once a controllable potential is introduced. Axions are ubiquitous in string theory, as they arise in the KK compactification of higher dimensional p-form gauge potentials. The continuous shift symmetry is inherited from the higher dimensional gauge invariance, and although it is broken by non-perturbative effects from euclidean string or brane instantons, charge quantization of the latter allows a discrete periodicity to survive.

In order for axions with sub-Planckian periods to achieve super-Planckian field ranges, it is natural consider a monodromic potential. The first type of axion monodromy inflation models in string theory [86, 87] were presented on the previous chapter. On these type of models, the axion arises from e.g. the RR 2-form on 2-cycles, and the monodromy is achieved by introducing NS5 brane-antibrane pairs, such that the shift of the axion produces an energy increase due to the induced D3-brane charge. In order to suppress brane-antibrane annihilation, and to keep backreaction under control [97,98], the brane anti-brane pair is proposed to be on the bottom of a bifid throat [49], as described in the previous chapter. One of the problems of these systems is that they are inherently strongly coupled, and are actually constructed as the S-duals of models with an axion from the NSNS 2-form and monodromy from D5-branes.

A new and better monodromy inflation framework was proposed in [88] (see also [89–91, 115, 116] for subsequent work), in particular in flux compactifications, based on a topological effect of fluxes anticipated in [117]. For the purposes of this chapter, the key ingredient in fluxed axion monodromy arises from the 4d couplings in the KK reduction of the Chern-Simons (CS) terms in the 10d action, in the presence of fluxes. For instance, consider the 10d coupling in type II strings (IIA/B for p even/odd)

$$\int_{10d} B_2 \wedge F_p \wedge F_{8-p} \tag{4.1}$$

and compactify to 4d on a (not necessarily Calabi-Yau) space $\mathbf{X}_6$, with a 2-cycle Σ_2 and a p-cycle Π_p. Defining the flux and 4d fields

$$\int_{\Pi_p} F_p = M \quad , \quad \phi = \int_{\Sigma_2} B_2 \quad , \quad F_4 = \int_{\Pi'_{4-p}} F_{8-p} \tag{4.2}$$

where Π'_{4-p} is transverse to Σ_2 and Π_p in $\mathbf{X}_6$ (concretely, the dual of $\Sigma_2 \times \Pi_p$). As explained in [88], the 4d axion ϕ has a monodromy induced by the flux F_p. Due to the

10d CS term, the physical RR $(p+2)$-form field strength is

$$\tilde{F}_{p+2} = F_{p+2} + F_p \wedge B_2 \tag{4.3}$$

with $F_{p+2} = dC_{p+1}$. Hence, a change in ϕ away from its minimum increases the physical $(p+2)$-form flux on $\Sigma_2 \times \Pi_p$. This leads to an inflaton potential, arising from the kinetic term for $\tilde{F}_{p+2}$, and is hence quadratic at lowest order. Despite the monodromy, the system has an underlying periodic structure because the theory contains 4d domain walls, given by D$(6-p)$-branes wrapped on Π'_{4-p}, which can change the F_{p+2} background (and thus $\tilde{F}_{p+2}$) by an integer amount, thereby interpolating among the different branches.

In the 4d theory, by doing dimensional reduction of the CS term (4.1) one gets a coupling

$$M \int_{4d} \phi\, F_4. \tag{4.4}$$

This 4d description is the one proposed in [92–94] as an effective action for axion monodromy. As emphasized there, and in [88], the axion shift symmetry is related to gauge invariance of a dual 3-form, in a generalization of the Stückelberg mechanism for 3-forms (see [118] for related discussions).

In this framework, the appearance of the monodromy is related to the fluxes stabilizing moduli in the model. The intricate relation between the inflationary potential and the moduli stabilization potential is an interesting feature of these models, as emphasized in [88, 91]. However, realistic large field inflation models demand a hierarchy between the moduli stabilization scale and the inflation scale in in order to have a unique light scalar at the scale of inflation. Although this point has been recognized in the literature, it has not been properly addressed hitherto. In this chapter I consider the explanation of this hierarchy by using warped throats.

The local warped throats I present can be used to describe fluxed axion monodromy inflation in type IIB ST and come from toric CY singularities, so they can be built using the tools in section 2.3. The IR region of these throats supports an axion (arising from a 2-cycle at the tip of the throat) with a monodromy from the dimensional reduction of a 10d CS term of the type (4.1). As usual, the geometry of the throats is based on performing a geometric transition in a system of fractional branes at a toric singularity, in which some 2- and 4-cycles shrink and are replaced by 3-cycles which support RR 3-form flux.

In this chapter I will first give the requirements that a warped throat must fulfill in order to describe fluxed axion monodromy in section 4.1, including techniques to construct fairly general classes of such throats in type IIB in section 4.1.1. Then, I provide an explicit example based on the cone over the del Pezzo 3 (dP$_3$) surface in section 4.1.2. Afterwards I present an analogous construction for type IIA throats in section 4.2. Then, the implications of the warping for the hierarchy between the moduli stabilization and the inflation scale are discussed in section 4.3. Finally, in section 4.4 I provide an analysis of the risk of tunneling through different branches of the multi-valued potential of the inflaton, which could spoil inflation via bubble nucleation, and check how the warping affects these transitions. T

The warped throats in this chapter are amenable to embedding in global compactifications (fairly easily in the case of type IIA models, and in type IIB if one allows for global non-trivial 1-cycles), although such global embedding are not explicitly discussed.

4.1. Warped fluxed axion monodromy

The warped throats of interest where axion monodromy inflation can happen in type IIB string theory are based on a complex deformation of a CY singularity given by real cones over a Sasaki-Einstein 5-manifold $\mathbf{X}_5$. The geometry of the throat must contain a unique non-trivial 2-cycle Σ_2, for simplicity an $\mathbb{S}^2$, at its bottom, which gives rise to the inflaton. The throats are supported by a 3-cycle Π_3, with M units of RR 3-form flux. Application of (4.1) and (4.2) to this case leads to

$$\int_{10d} F_3 \wedge B_2 \wedge F_5 \quad \rightarrow \quad M \int_{4d} \phi\, F_4 \tag{4.5}$$

with ϕ the integral of the NSNS 2-form over Σ_2, and F_4 the integral of F_5 along the radial direction. This is a bit ill-defined in the non-compact setup, and should be more properly regarded by cutting off the throat at some scale (or including a compactification). For the above KK reduction to produce the 4d topological term, a non-trivial wedge product of F_3 and B_2 is necessary. Equivalently, there must be a non-trivial intersection $q = [\Pi_3] \cdot [\Sigma_2]$ in $\mathbf{X}_5$.

This system has an axion monodromy for ϕ, which increases the flux $\tilde{F}_5 \sim F_3 \wedge B_2$ along $\mathbf{X}_5$ (by qM units). The associated domain wall is given by a D3-brane stretching in the radial direction. As in [117], the domain wall is $\mathbb{Z}_M$ valued, as M such domain walls can decay (by ending on a string, given by a NS5-brane on the $\mathbb{S}^3$ times the radial direction, which has a Freed-Witten anomaly and therefore must spit off D3-brane domain walls). Note that these domains walls are different from those in the literature e.g. [10].

Clearly, there are many other similar systems that can be constructed. For instance, the S-dual configurations of the above systems provide a realization of axion monodromy in which the axion arises from the RR 2-form, rather than the NSNS 2-form. This may be useful for applications to inflation in compactifications in which the NSNS axion suffers from η problems. In fact, these throats can be regarded as holographic duals of NS5-brane models similar to those considered in [86, 87]; namely, the NS5-branes on 2-cycles are replaced by NSNS H_3 fluxes on the 3-cycle after the geometric transition. This representation has the advantage of admitting a description in string perturbation theory. For concreteness I stick to the original realization in terms of an NSNS axion and RR fluxes (and the RR axion models can be obtained by a mere S-duality).

4.1.1. The geometry of general throats

Geometrizing monodromy inflation in terms of warped throats provides an efficient framework for generating a wide class of generalizations of the simplest models. While exhibiting the same basic behavior at the bottom of the throat, it is natural to expect that the distinctive features of such generalizations might be relevant in concrete applications. For example, they might be important when completing the geometry into a compactification along the lines of [119].

In order to illustrate the flexibility of the throat approach to monodromy inflation, in this section I provide a series of geometries that result on a singularity with a unique 2-cycle after a complex deformation. The important issue of the intersection between the 2- and 3-cycles which, as mentioned in section 4.1 is crucial for axion monodromy

to work, is not taken into account in this section but will be addressed shortly for many of the models presented in this section. In order to find the parent geometry, one can start from the (p, q) web for a singularity with a single 2-cycle (the IR web) and add to it different webs. A key fact at this point is that only two toric CY singularities have a single 2-cycle: the conifold and $\mathbb{C}^2/\mathbb{Z}_2 \times \mathbb{C}$. In this chapter I will focus on the former. For the application of interest, the problem is strongly constrained and easy to study in full generality. Since the additional webs represent other pieces of the geometry at the IR bottom of the throat, it is important that they do not contain additional 2-cycles. This severely limits the possible webs one can add to the IR web, namely either a line with label (p, q), or the web associated to $\mathbb{C}^3$, i.e. a set of three semi-infinite lines joining at a vertex. I refrain from a general description of infinite classes of models arising from the second alternative, and just provide an example of this type corresponding to the complex cone over the non-generic del Pezzo surface PdP_4, whose web diagram is shown in 4.1.

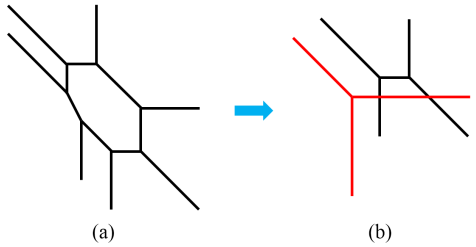

Figure 4.1: (a)The (p, q) webs for PdP_4 (b) Its complex deformation to the conifold.

For concreteness, I focus on adding a line with slope $(p, q) = (1, p)$. In more detail, I add to the web two external legs with (p, q) charges $(1, p)$ and $(-1, -p)$. This apparently simple setup will turn out to be extremely rich and exhibit interesting dynamics. The general configuration of the (p, q) web is shown in figure 4.2. The first two members of this infinite family of geometries, $p = 0, 1$, correspond to a $\mathbb{Z}_2$ orbifold of the conifold and the complex cone over dP_3, to be studied in the following sections.

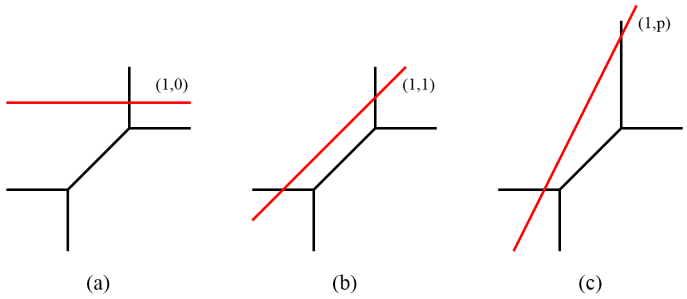

Figure 4.2: Addition of a line with slope $(1, p)$ to the (p, q) web of the conifold. (a) $p = 0$ gives rise to the $\mathbb{Z}_2$ orbifold of the conifold. (b) $p = 1$ corresponds to the complex cone over dP_3. (c) Additional line with general p.

Turning to the gauge dynamics by which the conifold theory emerges from the corresponding quivers at low energies from some new angles, I first consider the dP_3 and $\mathbb{Z}_2$ orbifold of the conifold. When going from the IR conifold to the UV dP_3, the numbers

of 2-cycles and 4-cyles are increased by three and one, respectively. This implies that there are four new independent ways of wrapping D-branes in the singularity. As a result, the parent UV theory has four more gauge groups than the conifold. The confinement plus higgsing process by which the these four additional gauge groups disappear at low energies will be explained in detail in section 4.1.2.2. As will be shown, the two gauge groups of the conifold are precisely the two diagonal subgroups surviving the Higgs mechanism. In this theory, the higgsings associated to the two confining nodes are actually not independent: the vevs of mesons coming from different nodes trigger the same higgsings.

The situation is rather similar for the $\mathbb{Z}_2$ orbifold of the conifold. When going from the IR conifold to the UV $\mathbb{Z}_2$ orbifold of the conifold, the geometry gets two additional 2-cycles and no new 4-cycle. This implies that the parent theory has two more gauge groups than the conifold one. The disappearance of this pair of gauge groups at low energies is easy to understand: one gauge group confines and another one is lost when two gauge groups are higgsed to the diagonal subgroup by the non-zero vevs in the quantum moduli space. The loss of gauge groups in pairs at low energies by a combination of confinement and higgsing leaving behind a diagonal gauge group, as in the previous two theories, is a common feature of many of the explicit examples considered so far in the literature, such as in e.g. [40]. However, this behavior is not the only possibility and the pattern of higgsings in the IR can be much more elaborate.

For theories with $p > 1$ the transformation of the geometry when going to the UV becomes more interesting. In this case, the fact that the (p, q) charges of internal branes in the web must be coprime requires an increase in the genus of the web beyond the one that follows from intersecting the new line with the external legs of the conifold. The parent (p, q) web can always be put in the canonical form shown in figure 4.3.

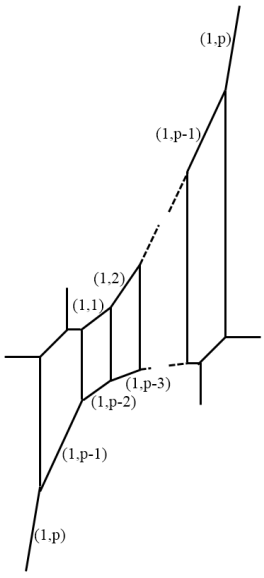

Figure 4.3: The general form of the (p, q) web after adding a line with slope $(1, p)$ to the conifold. Pairs of integers indicate the slopes of internal lines (signs are not important), which have not be drawn to scale.

It is also illustrative to look at the corresponding toric diagram, which is presented in figure 4.4. This general toric diagram clearly becomes the ones for the $\mathbb{Z}_2$ orbifold of

the conifold and the complex cone over dP_3 for $p = 0$ and 1, respectively.

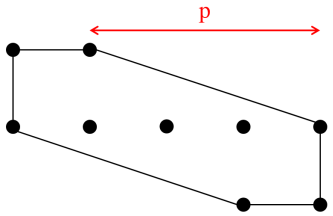

Figure 4.4: Toric diagram for the UV geometry for general values of p.

From figure 4.4, one can conclude that the parent geometry has $p+2$ 2-cycles and p 4-cycles more than the conifold, accounting for a total of $2p+4$ gauge groups. How does such a large number of gauge groups reduce to two? A more dramatic process than the one for the simple examples mentioned earlier is necessary in order to reduce the number of gauge groups from $2p+4$ down to just two. For illustration, in figure 4.5 the dimer model for the gauge theory associate to $p = 2$ is given, together with the fractional branes responsible for the desired deformation.

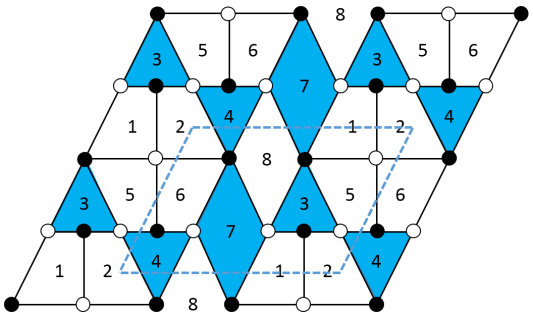

Figure 4.5: Dimer model encoding the gauge theory for $p = 2$. It contains 8 gauge groups, 16 chiral fields and 8 superpotential terms. The gauge groups associated to the fractional brane giving rise to the deformation are shown in blue.

4.1.2. An explicit example based on del Pezzo 3

In this section I will introduce an explicit realization of the warped monodromy scenario based on the complex cone over dP_3, whose geometry can be nicely encoded in the (p, q) web diagram shown in figure 4.6. Over the next couple of sections, I will discuss it from both a geometric and field theoretic perspectives.

Complex cones over del Pezzo surfaces have been extensively studied in the context of the gauge/gravity correspondence for D3-branes at singularities [28,120]. The del Pezzo surface dP_n can be constructed as $\mathbb{P}_2$ blown up at n generic points. It contains $n+1$ 2-cycles inherited from the $\mathbb{P}_1 \subset \mathbb{P}_2$. One can build a 5-manifold admitting a Sasaki-Einstein metric by fibering an $\mathbb{S}^1$ over dP_n. Finally, one can construct a conical CY singularity $\mathbf{X}_6$ as a real cone over $\mathbf{X}_5$; this has the structure of a complex cone over dP_n.

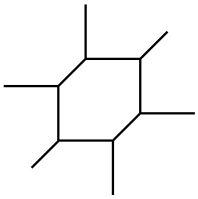

Figure 4.6: (p, q) web diagram for the complex cone over dP_3. For clarity the 4- and 2-cycles are shown as slightly blown up.

The 4d $\mathcal{N} = 1$ gauge theory on D3-brane probing the cone over dP_3 is nicely encoded by the dimer diagram in figure 4.7(a). The quiver diagram for this theory is given in figure 4.7(b). In fact, this theory is only one of four so-called *toric phases* interconnected by Seiberg duality, which is often referred to as phase 1 [30, 120].

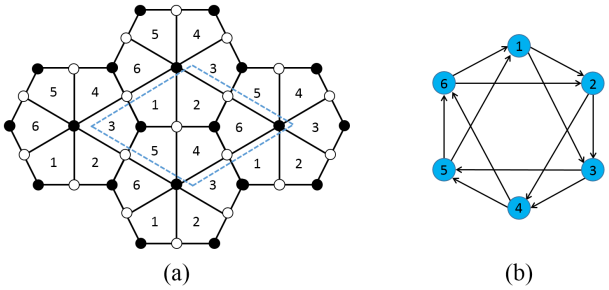

Figure 4.7: (a) Dimer model for phase 1 of dP_3. (b) The corresponding quiver diagram.

4.1.2.1. The RG cascade

I first consider throats in the KT regime, i.e. far from their IR bottom. On the dual field theory, when all nodes in the quiver in figure 4.7 have equal ranks the field theory is superconformal and its gravitational dual is the space $\mathrm{AdS}_5 \times \mathbf{X}_5$, with N units of RR 5-form flux on $\mathbf{X}_5$. This theory has marginal operators corresponding to modifications of the gauge couplings. Their gravity duals are the type IIB axio-dilaton (fixing the overall gauge coupling), and the integrals of the NSNS 2-form field B_2 over different 2-cycles in $\mathbf{X}_5$, which are all moduli with no potential. The interest of this chapter goes to the field theory dual to warped throats with fluxes. As mentioned above, this is achieved by introducing fractional branes. For concreteness, consider a type of fractional branes corresponding to the rank vector $\vec{n} = N(1,1,1,1,1,1) + M(1,0,0,1,0,0)$, with N and M the number of regular and fractional branes, respectively. The effect of the fractional branes is to break conformal invariance. As in [5], this theory has a non-trivial RG flow that takes the form of a duality cascade, in which gauge groups are Seiberg dualized every time they reach infinite coupling. In the example at hand, the RG cascade iterates the following sequence of dualization of antipodal pairs of nodes: (1,4), (2,5), (3,6) [40]. As shown in figure 4.8, after six dualizations one obtains the original quiver, but with ranks $\vec{n} = (N - M)(1,1,1,1,1,1) - M(0,0,1,0,0,1)$. Up to a trivial permutation of the nodes,

the number of regular D3-branes decreases according to $N \to N - M$ and the number of fractional branes transforms as $M \to -M$. In fact after an additional six dualizations the sign flip in the number of fractional branes is reversed, and thus their number remains constant throughout the cascade.

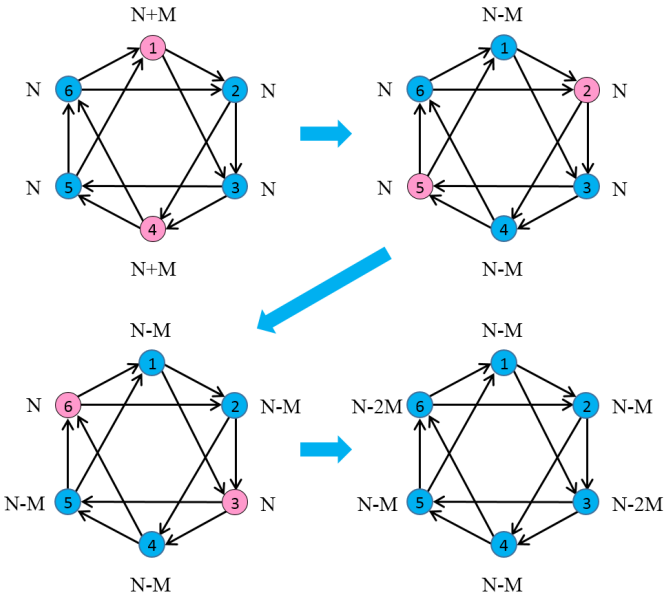

Figure 4.8: A few steps in the RG cascade for dP_3 starting with ranks $\vec{n} = N(1,1,1,1,1,1) + M(1,0,0,1,0,0)$. The pair of nodes dualized at each time is shown in pink.

4.1.2.2. Bottom of the throat: complex deformation from strong dynamics

As already explained, complex deformations of toric singularities can be efficiently described in terms of (p,q) webs. Figure 4.9 presents the particular deformation of the dP_3 singularity of interest. As desired for axion monodromy applications, the geometry grows a finite size $\mathbb{S}^3$, and in contrast with [5], the deformed space is not completely smooth but possesses a conifold singularity, which contains a vanishing $\mathbb{S}^2$.[1] This geometry is the one at the bottom of the throat generated by the fractional branes considered in section 4.1.2.1.

The RG cascade discussed in the previous section progressively reduces the number of regular D3-branes until reaching a point in the IR at which the ranks of the quiver become $\vec{n} = (2M, M, M, 2M, M, M)$. Nodes 1 and 4 have $N_f = N_c = 2M$ and hence lead to a *quantum modified moduli space*.

Every $N_f = N_c$ gauge group confines and gives rise to gauge invariant (from the point of view of the node under consideration) mesons $\mathcal{M}$ and baryons $\mathcal{B}$ and $\tilde{\mathcal{B}}$. The

[1] It is in principle possible to consider the blow-up of the 2-cycle, along the lines of [121], although this usually complicates the supergravity solution beyond tractability. Nevertheless, string theory is perfectly well-defined even in the limit of collapsed 2-cycle, since the non-trivial NSNS 2-form on it makes the physics smooth.

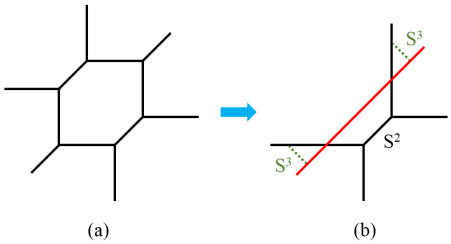

Figure 4.9: (a) Web diagram of the complex cone over dP_3. (b) Complex deformation showing the 2- and 3-cycles in the resulting geometry. The two $\mathbb{S}^3$, indicated by dashed lines, are actually homologous.

quantum moduli space corresponds to the constraint

$$\det \mathcal{M} - \mathcal{B}\tilde{\mathcal{B}} = \Lambda^{4M}, \tag{4.6}$$

with Λ the dynamical scale of the node under consideration. This equation clearly forces non-zero vevs for the mesons and baryons. The quantum constraint can be efficiently incorporated by introducing a Lagrange multiplier chiral field X and extending the original superpotential W_0 to

$$W = W_0 + X(\det \mathcal{M} - \mathcal{B}\tilde{\mathcal{B}} - \Lambda^{4M}). \tag{4.7}$$

Focusing on the dimer in figure 4.10(a), nodes 1 and 4 give rise to mesons $\mathcal{M}$ and $\mathcal{N}$, which can be put in matrix form as follows

$$\begin{aligned} \mathcal{M} &= \begin{pmatrix} M_{63} & M_{62} \\ M_{53} & M_{52} \end{pmatrix} = \begin{pmatrix} X_{61}X_{13} & X_{61}X_{12} \\ X_{51}X_{13} & X_{51}X_{12} \end{pmatrix} \\ \mathcal{N} &= \begin{pmatrix} N_{36} & N_{26} \\ N_{35} & N_{25} \end{pmatrix} = \begin{pmatrix} X_{34}X_{46} & X_{24}X_{46} \\ X_{34}X_{45} & X_{24}X_{45} \end{pmatrix} \end{aligned} \tag{4.8}$$

In addition, there are also baryons $\mathcal{B}$, $\tilde{\mathcal{B}}$, $\mathcal{C}$ and $\tilde{\mathcal{C}}$ for these two nodes.

Motivated by the structure of the RG cascade, by taking $\Lambda_1 = \Lambda_4 \equiv \Lambda$, the deformed geometry is easily recovered along the mesonic branch of the gauge theory, saturating the quantum constraint with meson vevs

$$\det \mathcal{M} = \det \mathcal{N} = \Lambda^{4M}. \tag{4.9}$$

For simplicity, consider diagonal vevs for the mesons, i.e. non-zero vevs for M_{63}, M_{52}, N_{36} and N_{25}, while all the others vanish. As a result, nodes 3 and 6 are higgsed down to the diagonal subgroup, which I call 3/6. The same happens for nodes 2 and 5, which are higgsed to a single node 2/5. Carefully studying the gauge theory, it is possible to determine that at low energies it is reduced to the conifold one [8], a process that can be captured graphically by a transformation of the dimer [22, 41], as shown in figure 4.10. Shaded faces correspond to the gauge factors whose ranks are changed to account for the introduction of the deformation fractional brane providing the field theory dual of the RR 3-form flux in the warped throat. The remnant dimer diagram describes the gauge theory of D3-branes at the surviving conifold singularity. This analysis reproduces via a field theoretic calculation, the results of the geometric analysis.

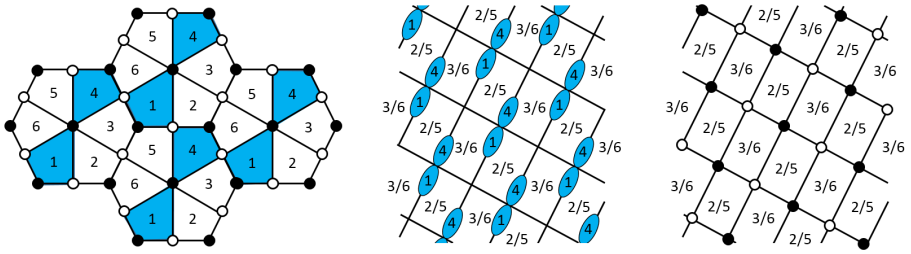

Figure 4.10: (a) Dimer for phase 1 of dP_3. The steps (b) and (c) describe the gauge dynamics of the system, resulting in a complex deformation of the moduli space, c.f. [22, 41].

4.1.2.3. Axion monodromy as Seiberg duality

This is a good point to provide a field theory interpretation of axion monodromy. Anticipating the main conclusion, the bottom line is that the axion monodromy corresponds to a periodic chain of Seiberg dualities whose net effect is to increase the total D3-brane charge in the system. This is triggered by a brane creation effect, in a concrete realization of the mechanism proposed in appendix A.1 of [88]. Although this is very similar to an RG cascade, it must be emphasized that it is not driven by an RG flow, but rather by the change of a scalar field vev (a would-be modulus, were it not for the monodromy). In order to distinguish it from the RG cascade, I refer to the new sequence of dualities induced by rolling of the ϕ vev as a *monodromy cascade*.

This can be shown using the dP_3 example. The deformation branes triggering the RG cascade discussed in section 4.1.2.1 correspond to adding M units to the ranks of nodes 1 and 4. As discussed in section 4.1.2.2, the RG cascade terminates in a complex deformation generating the finite 3-cycle and is responsible for the exponential suppression of its size. The strong dynamics associated to the deformation is such that the remaining four nodes are higgsed in pairs, 2/5 and 3/6, giving rise to the two gauge groups of the leftover conifold theory. Therefore, the B_2 field on the surviving $\mathbb{S}^2$ is associated to the relative gauge coupling of these gauge groups.

It is convenient to organize the six nodes of the dP_3 quiver into three pairs: (14), (25) and (36).The deformation branes correspond to giving them ranks $(N+M, N, N)$. The non-trivial intersection of the 2-cycle associated to ϕ and the 3-cycle associated to the flux/fractional branes manifests in the fact that the deformation fractional branes contribute M additional flavors to the node (25) associated to the B-field. Following the analysis in section 4.1, the expectation is a non-trivial monodromy for ϕ related to the value of M. Its realization in the field theory dual is as follows. Changing the B_2 field will bring e.g. the node 2/5 past infinite gauge coupling, so it must be Seiberg dualized (i.e. dualize both 2 and 5 in the dP_3 quiver), and the ranks become $(N+M, N+M, N)$. Next, for similar reasons, dualize 3 and 6, which takes the ranks to $(N+M, N+M, N+2M)$. The next step involves a dualizations of 1 and 4. This is trickier to justify, because the corresponding 2-cycle disappears in the geometric transition, but it is natural to expect that there is a contribution of the B_2 field to the gauge couplings of 1 and 4 in the parent geometry. Assuming that this is the case, the appearance of the effect of monodromy will turn out to be the right one, which justifies the step. The ranks now become $(N+2M, N+M, N+2M)$.

These steps in the monodromy cascade are shown in figure 4.11. Repeating the same sequence of dualizations on nodes (25), (36) and (14), one obtains the original quiver, but with ranks $(N+4M, N+3M, N+3M)$. A period of the monodromy cascade thus involves twelve dualizations and increases the number of D3-branes by $3M$.[2]

The structure of the monodromy cascade is almost identical to the RG cascade discussed in section 4.1.2.1. The main difference is that the dualizations are not driven by beta functions. In particular, it is not the gauge groups with higher ranks which are dualized at each step. In fact, the symmetry of this theory is such that the sequence of dualizations in the monodromy cascade is simply related to the RG cascade in figure 4.8 by a 60° rotation in the quiver.

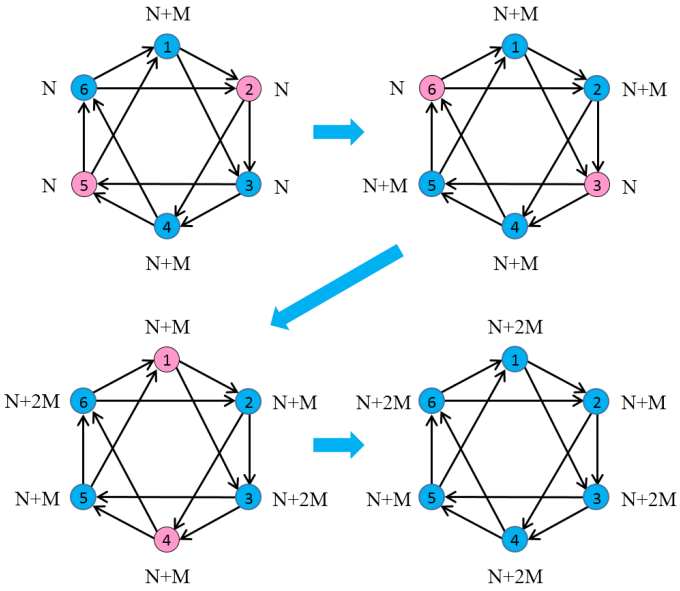

Figure 4.11: A few steps in the monodromy cascade for dP_3. The pair of nodes dualized at each time is shown in pink. This monodromy cascade is simply related to RG cascade in figure 4.8 by a 60° rotation in the quiver.

4.1.3. No 5d intersection in an orbifold of the conifold

In the general discussion in section 4.1, I showed that the existence of a non-trivial monodromy in the warped throat requires a non-trivial intersecting number between the 2-cycle Σ_2 and the 3-cycle Π_3 in the 5d horizon $\mathbf{X}_5$. As discussed in the dP_3 example, this corresponds to the requirement that the fractional branes contribute to the number of flavors of the nodes associated to the 2-cycle yielding ϕ. This requirement is generically satisfied, and in particular holds for the infinite class of models in section 4.1.1, except for the case $p = 0$. I now describe this case, as an illustration of a warped throat which contains 2- and 3-cycles but does not lead to axion monodromy.

[2] A non-trivial numerical factor, in this case 3, multiplying the number of fractional branes in the change in the number of D3-branes in a cascade period is a generic feature and has been observed in several examples of RG cascades in the literature, see e.g. [40, 122].

Consider the orbifold of the singular conifold $xy - zw = 0$ by the $\mathbb{Z}_2$ action $x, y \to -x, -y$. By defining invariant monomials $x' = x^2$, $y' = y^2$, the quotient space is described by the geometry $x'y' - z^2w^2 = 0$. This $\mathbb{Z}_2$ orbifold of the conifold was discussed in [18] and admits a complex deformation given by

$$x'y' - z^2w^2 = \epsilon\, zw. \tag{4.10}$$

It is possible to see that the 3-cycle has $\mathbb{S}^3$ topology. The deformed geometry still contains a singularity at $x' = y' = z = w = 0$, which is a singular conifold. This is manifest when neglecting the higher order z^2w^2 term, or equivalently sending the deformation parameter $\epsilon \to \infty$. This can be taken as the singular limit of its small resolution phase, so that there is an $\mathbb{S}^2$ of vanishing size at that remnant singularity. The web diagram of the singularity considered in this section and its complex deformation are shown in figure 4.12.

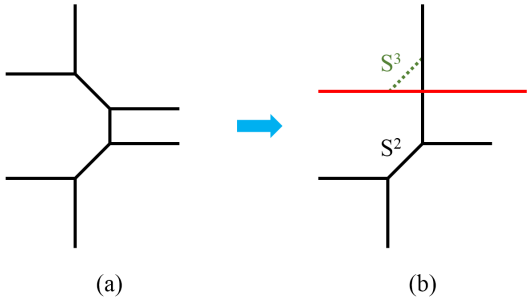

Figure 4.12: (a) Web diagram of the conifold/$\mathbb{Z}_2$. For clarity the collapsed 2-cycles are shown as slightly blown up. (b) Complex deformation showing the 2- and 3-cycles in the resulting geometry.

Now turn to the holographic dual field theory, and its description of the complex deformation. The theory is encoded by the dimer in figure 4.13(a).

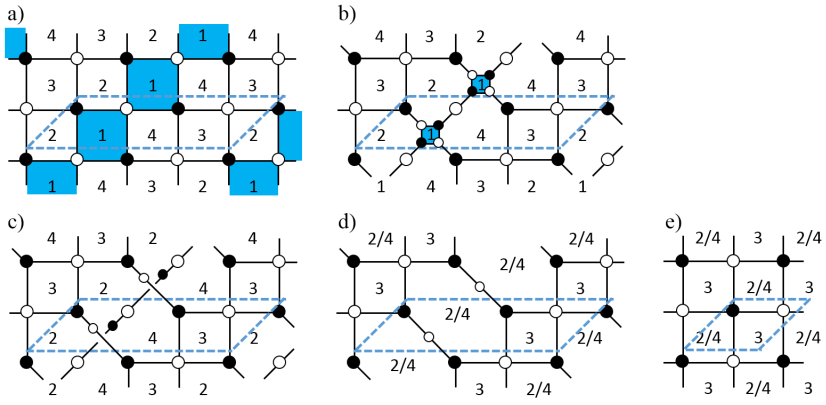

Figure 4.13: (a) Dimer of the orbifold of the conifold. The steps (b)-(e) describe the gauge dynamics of the system, resulting in a complex deformation of the moduli space, c.f. [41].

The throat of interest corresponds to introducing M D5-branes on the 2-cycle associated to e.g. node 1, namely $n_1 = N + M$, $n_2 = n_3 = n_4 = N$. As in [5], this theory

has a non-trivial RG flow along which a cascade of Seiberg dualities effectively reduces the value of N, while keeping the fractional branes intact. The IR dynamics corresponds effectively to $n_1 = 2M$, $n_2 = n_3 = n_4 = M$, so that the strong dynamics at node 1 (which has $N_f = N_c$) produces a complex deformation of the moduli space, matching that of the geometry. The field theory analysis can be mapped a to simple diagrammatic process in the dimer diagram, shown in figure 4.13. The result agrees with the fact that the deformed geometry is not completely smooth but contains a remnant conifold singularity.

A complementary description of the systems is in terms of a HW brane configuration [99], which is related to the D3-brane system by a T-duality (along the $U(1)$ orbit of the action $x' \to e^{i\alpha}x'$, $y' \to e^{-i\alpha}y'$) [18], see figure 4.14(a). It contains D4-branes along 0123 and stretched along 6 between two NS-branes and two NS'-branes. The D4-branes suspended in each of the intervals in 6 corresponds to a gauge factor, and the gauge group, matter content and superpotential can be obtained using standard rules (see [18], and [123] for a review), which agree with the above dimer.

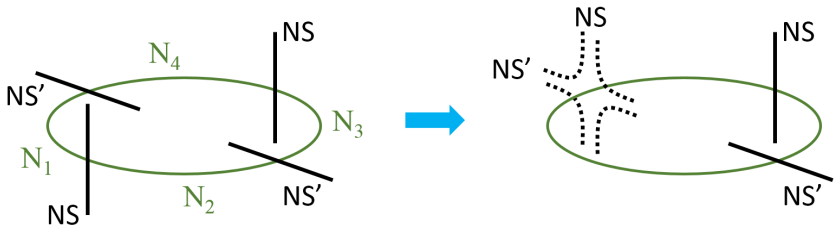

Figure 4.14: (a) Hanany-Witten T-dual picture of the system of D3-branes at the orbifold of the conifold. It involves D4-branes suspended in one direction between relatively rotated NS5-branes (denoted by NS- and NS'-branes). (b) The geometric transition is described as the recombination of one NS- and one NS'-brane, which effectively disappear from the picture. The remaining NS- and NS'-brane describe the T-dual of the remaining conifold singularity.

.

The complex deformation is attained by suspending M D4-branes on e.g. interval 1, in addition to the N D4-branes in all intervals. The RG duality cascade corresponds to the dynamical motion of the NS and NS'-branes bounding the initial interval 1, moving them across other branes, which results in an effective change in the value of N due to brane creation effects. The IR configuration only contains the M D4-branes on interval 1, while others are empty, and the strong dynamics maps to the recombination of the NS- and NS'-branes, see figure 4.14(b). This heuristic description follows from the M-theory lift of the configuration, as in [124]. The $\mathbb{S}^3$ in the complex deformation is mapped to a 1-cycle (or rather, the disk bounded by it) in the recombined 5-brane, while the remnant conifold singularity is T-dual to the remnant system of one NS and one NS'-brane.

It is possible to see that there is no axion monodromy in the present setup. The field ϕ (the B-field on the conifold 2-cycle) maps to the modulus controlling the distance between the NS- and NS'-branes in the HW picture. Moving the axion around its period corresponds to moving e.g. the NS'-brane around the circle. Even accounting for brane creation effects, it is easy to check that the resulting configuration is exactly identical to the original one, and there is no net creation of D3-branes and no monodromy. Both in the HW or the dimer pictures, the hint is that the gauge factor 3 associated to the 2-cycle gets no flavors from the fractional brane inducing the deformation. This is the field theory

counterpart of the 2-cycle Σ_2 and the 3-cycle Π_3 not having intersection in $\mathbf{X}_5$.

It is tempting to blame the failure to generate monodromy to the presence of parallel NS5-branes in the HW picture, or more precisely of parallel external legs in the two (p,q) sub-web diagrams in the complex deformation, c.f. figure 4.12. This is however not the origin of the problem, since it is easy to construct examples with such parallel external legs and with a nice monodromy. For instance, the cone over PdP_4 deformed to a conifold, c.f. figure 4.1, has parallel legs, but also monodromy (in fact, related to that of dP_3 by a simple higgssing process). Empirically, the crucial difference between the orbifold of the conifold and the examples with actual monodromy (like dP_3, PdP_4 or the models $p \neq 0$ in section 4.1.1) seems to be that the sub-webs of the former intersect only once, whereas the latter have sub-webs with multiple intersections.

4.2. Type IIA models

The Type IIB models in the previous section have the drawback of requiring non-trivial 1-cycles in the compact space, a feature not present in CY compactifications. However, many of the ideas discussed there are valid more generally. As an illustration, consider their implementation in the type IIA setup, where now the required ingredients are 2- and 3-cycles. These IIA models are therefore very amenable to embedding into CY compactifications. Interestingly, the relevant local geometries are again given by the geometric transition studied in the IIB setup, c.f. section 4.1.1.

Consider as a simplified setup a local geometry with two 2-cycles Σ_2 and Π_2, and introduce M units of RR 2-form flux F_2 on Π_2. From the general discussion around (4.1), one has the couplings

$$\int_{10d} B_2 \wedge F_2 \wedge F_6 \to M \int_{4d} \phi F_4 \tag{4.11}$$

with

$$\phi = \int_{\Sigma_2} B_2 \ , \ \int_{\Pi_2} F_2 = M \ , \ F_4 = \int_{\Pi_2'} F_6 \tag{4.12}$$

where Π_2' is such that there is a non-trivial triple intersection number among Σ_2, Π_2 and Π_2' (note that the 4d F_4 is not the 10d RR 4-form field strength). Following the general arguments in section 4.1, the physical 10d field strength $\tilde{F}_4 = dC_3 + B_2 \wedge F_2$ increases non-trivially along $\Sigma_2 \times \Pi_2$ upon shifts of ϕ. The periodicity structure, leading to the monodromy, is associated to the existence of 4d domain walls changing the value of this flux, given by D4-branes wrapped on Π_2'. As in [117], these domain walls are $\mathbb{Z}_M$-valued and can decay in sets of M by ending on a 4d string given by an NS5-brane wrapped on $\Pi_2 \times \Pi_2'$.

The above kind of local models appear naturally in the context of the holographic gauge/gravity duality, as pioneered in [125] in the conifold case. Consider a stack of M type IIA D6-branes wrapped on the $\mathbb{S}^3$ of a deformed conifold, so that below the KK compactification scale they describe pure $SU(N)$ SYM. This string embedding provides a gravity dual, given by type IIA on the resolved conifold, with no D6-branes, and with M units of RR F_2 flux over the $\mathbb{S}^2$. In other words, the gravitational throat solution can be

obtained by a geometric transition in which a system of D6-branes on 3-cycles is replaced by F_2 flux. The M-theory lift of the geometric transition has been considered in [126,127]. Notice that in the M-theory setup the F_2 flux lifts to the presence of torsion cycles in a Lens space $\mathbb{S}^3/\mathbb{Z}_M$, thereby connecting with the description of monodromy by torsion homology in [88].

Hence, the type IIA picture involves throats which can be constructed with standard toric geometry, and are described by (p,q) web diagrams. Some of the corresponding 2-cycles support RR field strength 2-form fluxes; more specifically, these are the 2-cycles that are traded for a 3-cycle in the geometric transition. Interestingly, this is precisely the reverse process of that exploited in the IIB context in earlier sections. Concretely, take a toric CY singularity with fractional D5-branes on a (total) 2-cycles class Π_2 triggering a complex deformation in which a 3-cycle Π_3 appears supporting RR 3-form flux. One can now use the same geometries in reverse order to engineer a Type IIA axion monodromy model as follows. By taking the deformed geometry and wrapping M D6-branes on Π_3, its strong dynamics triggers a geometric transition in which Π_3 disappears and there is a RR 2-form flux along the newly created 2-cycle (total class) Π_2. In the process, there may appear new 2-cycles (and 4-cycles), which support no fluxes and which can be used to produce axion candidates.

An important difference with the IIB setup is that in general, type IIA throats tend to have several flux-less 2-cycles, and therefore may produce inflation scenarios with multiple fields. This is however a question that must be addressed in specific model building, and thus I will not address it in this chapter.

Another interesting remark is that, as emphasized in [88,91], type IIA models can produce inflationary models with higher powers in the potential ϕ^p, $p>2$, for instance by introducing RR 0-form flux (i.e. the Romans mass parameter).

4.3. Implications for inflation

One often emphasized requirement of realistic inflationary models in string theory is that they properly address the question of moduli stabilization. Fluxed axion monodromy models have been applied to inflation [88] (see also [89–91,115,116] for subsequent work). In this respect, an interesting feature of these models is the intricate relation between the inflationary potential and the moduli stabilization potential, as emphasized in [88,91], since the appearance of the monodromy is related to the fluxes stabilizing moduli in the model. When these two flux-induced effects occur at comparable scales, inflation can still proceed, albeit with a flattened potential due to backreaction of the other fields [128]. A more model-independent possibility is to find natural suppression mechanisms for the inflaton sector. This is nicely achieved by the present warped throat axion monodromy models.

In the models presented in this chapter, the axion arises from the NSNS 2-form field on a 2-cycle localized at the bottom of the throat, so its associated scales are redshifted by the warp factor. As usual in fluxed axion monodromy [88], to lowest order in the canonically normalized inflaton field ϕ, the action takes this simple chaotic inflation form[3]

[3] As emphasized in [88,91], higher power potentials ϕ^p, $p>2$ can be achieved in 10d models involving additional powers of the NSNS 2-form in the CS couplings.

:

$$S = \int d^4x\sqrt{-g_4}\left(-\frac{1}{2}(\partial\phi)^2 - \frac{1}{2}\rho^2\phi^2 + \dots\right) \tag{4.13}$$

where ρ is the physical mass scale, set by the warp factor at the bottom of the throat. Since the full supergravity solution is not available for the throats required for warped axion monodromy,[4] I provide an estimate. Using the warp factor in (2.5), the mass scale at the bottom of the throat is

$$\rho^2 \sim M_{\rm UV}^2\, e^{-\frac{4\pi K}{3Mg_s}}. \tag{4.14}$$

Namely, it is fixed by the size of the complex deformation, which is exponentially suppressed with respect to some bulk/UV scale. A typical value is $M_{\rm UV} \sim \frac{1}{M\alpha'}$ (see e.g. [129, 130]). The inflation scale admits a nice interpretation in terms of the increase in the F_5 flux in the geometry, or in the number of D3-branes in the holographic dual. Therefore its contribution scales as

$$V \sim M^2 e^{-\frac{8\pi K}{3Mg_s}} T_{\rm D3}. \tag{4.15}$$

It is a simple matter to choose parameters of the throat so as to reproduce an inflaton mass of around 10^{13} GeV, and an inflation scale of 10^{16} GeV, e.g. $K/M \sim 1$, and $g_s \sim 0.1$. These models produce a UV completion of the standard chaotic inflation model, with tensor to scalar ratio of $r \sim 0.1$, compatible with the combined Planck and BICEP2 results [62] .

In order to achieve super-Planckian field ranges, the inflaton axion must wind around its basic period a sufficient number of times. A potential drawback of axions at the bottom of throats is that this period is also redshifted, as follows. An estimate of the axion period (or decay constant) f_ϕ is obtained by noticing that upon winding once, the number of flux/D3-branes increases by qM, where q is an integer (e.g. $q = 3$ in the dP_3 example). Using the above values of V, ρ, the axion period can be estimated to scale as

$$f_\phi \sim qMe^{-\frac{4\pi K}{3Mg_s}}\, M_{\rm UV}. \tag{4.16}$$

The period experiences a suppression by the warp factor[5], hence comparable with the inflaton mass suppression (e.g. by a factor in the range 100-1000). The period could be increased by considering larger values of M and q (namely, more involved monodromy cascades, such as those in section 4.1.1), but this would render the models more complicated. Therefore, it is fair to say that the period is typically shortened, and thus the models require more windings of the axion, increased by a factor which is parametrically exponential, but numerically moderate.

This reduced periodicity leads to an increased packing of the branches of the multivalued potential in a given length of Planck scale field range (by the same factor). One may worry about the stability of super-Planckian field excursions, due to a possible enhancement of the tunneling transitions among branches, unwinding the axion by jumping rather than slow-roll, considered e.g. in [93] (see also [132]). However, in section 4.4 I show that the tunneling rates are mainly controlled by the distances in field space, rather than by the branch multiplicity. The bottom line is that the exponential suppression overcomes

[4] In fact, given that the axion ϕ is the B-field on a collapsed 2-cycle, its full quantitative most likely requires features beyond the supergravity approximation.

[5] The suppression of the axion periodicity due to warping effects was also observed in [131].

the multiplicative factor from the decay channel multiplicity. Hence, the extra packing of branches does not introduce additional instabilities.

Incidentally, it is still possible to realize unsuppressed axion periodicities by realizing the axion as the NSNS 2-form on a 2-cycle collapsed at a curve of singularities, which is supported not only at the bottom of the throat, but also extends radially. These are obtained by complex deformations of singularities, whose remaining singularity is $\mathbb{C}^2/\mathbb{Z}_2$. These delocalized axions still have a suppressed mass parameter, since their potential arises from the effect of 3-form fluxes, which are localized at the bottom of the throat (specifically, the increase of the flux (4.3) is proportional to F_3, which is localized on the $\mathbb{S}^3$ at the bottom of the throat). On the other hand, their 4d kinetic term involves an integral over the zero mode wavefunction, which spreads radially along the throat and is not suppressed by the warp factor. Therefore their period is not redshifted. There may be additional issues in this scenario, regarding possible backreactions carried out of the throat along the curve of singularities (in analogy with [98]). The detailed analysis of this further class of models is however beyond the focus of this chapter.

A final comment before concluding goes to supersymmetry in this setup. The throats I have considered are supersymmetric, hence the axion is always accompanied by a second scalar partner, the saxion. Having equal mass, the latter can participate non-trivially in the inflationary dynamics and modify the properties of single field scenario. This is certainly an important question for supersymmetric setups, which needs to be addressed in future work.

4.4. Tunneling between branches

In models of axion monodromy inflation the inflaton potential is multivalued. In the warped realizations of this chapter the decay constant is suppressed and as a result the number of windings becomes equally increased. It thus becomes important to address the possibility of the axion tunneling to lower branches, which would spoil large-field inflation. Following [93], in this section I estimate the tunneling probability based on standard thin-wall approximation techniques [133–135]. The outcome will be that the tunneling probability to lower branches is indeed highly suppressed. I shall first review the necessary tools for the computation and then apply them to the type IIB setup in this chapter.

4.4.1. The thin-wall approximation

Starting from a field which is initially in a false vacuum state ϕ_i over the entire space, it is possible to nucleate a bubble by tunneling to a lower energy vacuum state ϕ_f. The region interpolating between both regions is known as the *wall* and is characterized by its tension σ. The probability for the tunneling to happen goes as

$$P \sim \exp\left(-\Delta S_E\right) \quad , \quad \Delta S_E = S_E(\phi_f) - S_E(\phi_i) \tag{4.17}$$

where S_E is the Euclidean action of the corresponding field configuration. Once the bubble has nucleated, the space is divided into three regions: the interior, the exterior and the

wall of the bubble. In the thin-wall approximation, the various contributions to ΔS_E are given by:

$$\Delta S_{E,\text{int}} \sim -\Delta V r^4 \quad , \quad \Delta S_{E,\text{wall}} \sim \sigma r^3 \quad , \quad \Delta S_{E,\text{ext}} = 0 \tag{4.18}$$

where $\Delta V \equiv V(\phi_i) - V(\phi_f) > 0$ and r is the bubble radius. The radius is fixed by maximizing the probability for the bubble to form and is such that the energy released within the bubble goes to the wall, giving rise to its tension σ.

4.4.2. Tunneling probability

In the type IIB setups on this chapter the tunneling corresponds to the generation of D3-branes that extend along the radial direction of the throat, taking the energy from the interior of the 3-sphere wall and shifting F_5 by an integer amount. Despite the more intricate details of this particular construction, such as the fact that this is a 10d theory with gravity and the tunneling happens between different branches of the potential, the thin-wall analysis can be applied to this scenario to estimate the tunneling probability. In this approximation, one finds that [93]

$$P \sim \exp\left(-\frac{27\pi^2\sigma^4}{2(\Delta V)^3}\right). \tag{4.19}$$

By assuming that the tunneling is such that $\phi_i = \phi_f$; processes for which $\phi_i \neq \phi_f$ have an additional exponential suppression. These ideas allow to tackle the tunneling to multiple branches. First, see that the most likely jumps, i.e. those with least Euclidean action, are those with a large energy difference. The dominating tunneling process will hence be from the highest-energy state, i.e. at the start of inflation, to the branch of lowest energy with the same field value. In fact, a simple estimate can be obtained by approximating the potential at this lowest branch to be zero, giving $\Delta V \simeq V_i$.

The bubble wall is a D3-brane "wrapping" the radial direction, so its tension is $\sigma \sim r_{UV} T_{D3} \sim r_{UV}/g_s(\alpha')^2$, r_{UV} being the radius where the throat is cut. This can be written in terms of the axion decay constant, that from dimensional reduction can be seen to be $f_\phi \sim r_{UV}/g_s\alpha'$, so that the tension goes as $\sigma \sim f_\phi/\alpha'$. Using this, the conclusion is that the most likely tunnelling process is heavily suppressed

$$P_{\max} \sim \exp\left(-\frac{27\pi^2\sigma^4}{2V_i^3}\right) \ll 1. \tag{4.20}$$

The lifetime for tunneling to the lowest branch is thus much longer than the time scale of inflation.

Finally, it is important to point out that there is an increase number possible tunneling channels due to the packing of multiple branches due to warping. This multiplicity turns out not to be dangerous for the model, since it is overcome by the additional exponential suppression of nearby branches.

5

Orientifolds of Warped Throats from Toric Calabi-Yau Singularities

In this chapter the topic changes. ST embeddings of Inflation will be left aside in order to study orientifolds of warped throats.

In ST compactifications including throats it is common to find setups where cancellation of RR charges carried by the fluxes supporting the throat forces the introduction of orientifold planes [4]. These are usually located away from the throat, and therefore their presence is irrelevant to the infrared physics down the throat. However, some recent applications exploit the presence of orientifold planes at the infrared tip of the throat, i.e. they involve orientifolded warped throats. This will be used to provide de Sitter uplift using a DSB sector [51] in chapter 6 (these type of ideas were also used in [136] for the same purpose), and a gauge theory description of certain D-brane instantons [50] in chapter 7 (see also [137, 138]).

The construction of orientifolds of D3-branes at toric CY singularities was systematized in [42], based on dimer diagrams [37, 139] (see also [140, 141] and references therein). However, the discussion of the deformed geometries has been carried out only for a few examples. In this chapter I will provide a systematic recipe to build complex deformations of orientifolds of toric CY singularities, in terms of dimer diagram combinatorics [142].

The strategy will be to first characterize which toric singularities admit a given orientifold quotient, this can be done using dimer diagrams and studying the effect of the orientifold on the zig-zag paths. This will be done in section 5.1.1 for orientifolds leaving fixed lines on the dimer and in section 5.1.2 for those leaving fixed points. As will be shown, the effect easily translates to the external legs of the web diagram, providing a simple recipe to tell which singularities are compatible with orientifolds. Then, the description of complex deformations in terms of the removal of a subweb in equilibrium of the web diagram, or equivalently a series of zig-zags from the dimer diagram allows to study systematically which complex deformations of the parent geometry are possible in the orientifolded theory. This analysis will be presented in section 5.2. Once again, I will deal separately with singularities compatible with orientifold lines on the dimer and those with orientifold points, which are studied in section 5.2.1 and then in section 5.2.2 respectively.

Before starting the analysis, it is important to mention that in this chapter I restrict to classical phases of dimers. Non-classical phases of dimers [143, 144] have recently shown to be compatible with more orientifold actions [145].

Also, it is important to note that the analysis includes recently found setups of toric singularities that do not accept resolutions if orientifolds are present [23]. The concrete setup of [23] involves a conifold with orientifold lines on its dimer. Throughout the chapter I will restrict to the analysis of toric CY's on singular and deformed phases, so I will not study the impossibility of having resolution phases. However, this analysis is straightforward for orientifolds leaving fixed lines on the dimer: an orientifold of a singular geometry is incompatible with its resolutions if the corresponding singular web diagram admits no desingularization compatible with the $\mathbb{Z}_2$ symmetry.

5.1. Toric singularities compatible with orientifolds

In order to find out which kind of singularities are compatible with both complex deformations and orientifold actions, I will first provide criteria to easily guess if a singularity is compatible with orientifold actions, and if so, which kind(s) of orientifold action(s) it admits.

5.1.1. Singularities compatible with orientifold lines

The strategy to explain which toric CY's can have orientifold actions leaving fixed lines on the corresponding dimer will be to start considering an example of this kind and derive the general rules from it.

As explained in section 2.3.5, dimers with orientifold lines can be of two kinds. Both cases have many common features, so it is enough to study one of these cases and then extrapolate the knowledge to the other case.

The example I will use is the dimer of the singularity known as $L^{1,3,1}$ [146,147], that was shown in [42] to accept orientifold actions with parallel fixed lines. The corresponding dimer and its zig-zag paths are shown in figure 5.1.

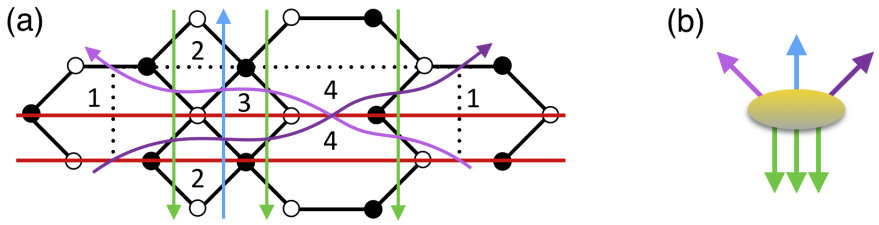

Figure 5.1: (a) Unit cell of the dimer for $L^{1,3,1}$ with orientifold lines in red, and zig-zag paths in colors; those with the same winding numbers (p,q) have the same colour. (b) Set of (p,q)'s of the zig-zag paths of $L^{1,3,1}$ as the external legs of its web diagram.

From figure 5.1(a) one can observe that the zig-zag paths of $L^{1,3,1}$ are compatible with the $\mathbb{Z}_2$ symmetry of the orientifold: after inverting the direction of any zig-zag path, it becomes the orientifold image of one of the original zig-zag paths. This symmetry can be made more explicit in a two step process. First, one must invert the (p,q) winding

numbers of all zig-zags to reverse their orientation

$$\left\{\begin{pmatrix} p_i \\ q_i \end{pmatrix}\right\}_{i=1,\ldots,Z} \rightarrow \left\{\begin{pmatrix} -p_i \\ -q_i \end{pmatrix}\right\}_{i=1,\ldots,Z} . \tag{5.1}$$

Z is the number of zig-zags of the singularity. Since the orientifold inverts the vertical component of the dimer, one must do the same with the inverted (p, q)'s:

$$\left\{\begin{pmatrix} -p_i \\ -q_i \end{pmatrix}\right\}_{i=1,\ldots,Z} \rightarrow \left\{\begin{pmatrix} -p_i \\ q_i \end{pmatrix}\right\}_{i=1,\ldots,Z} . \tag{5.2}$$

Since there exists a $\mathbb{Z}_2$ symmetry allowing for an orientifold of the singularity, the resulting set of zig-zag paths must agree with the original one:

$$\Omega : \left\{\begin{pmatrix} p_i \\ q_i \end{pmatrix}\right\}_{i=1,\ldots,Z} \rightarrow \left\{\begin{pmatrix} -p_i \\ q_i \end{pmatrix}\right\}_{i=1,\ldots,Z} = \left\{\begin{pmatrix} p_j \\ q_j \end{pmatrix}\right\}_{j=1,\ldots,Z} . \tag{5.3}$$

In this case, the paths without a horizontal component remain the same after the two steps and thus are their own orientifold images, whereas for zig-zags winding the horizontal 1-cycle the orientifold relates two different zig-zags. It is possible to follow this process diagrammatically by starting with the external legs of the web diagram and doing the same inversions. The process is shown in figure 5.2(a). Comparing the initial and final web diagrams in figure 5.2(a) one finds that zig-zags in green and blue are their own orientifold images, and the ones in light and dark purple are the image of one another, in agreement with figure 5.1(a).

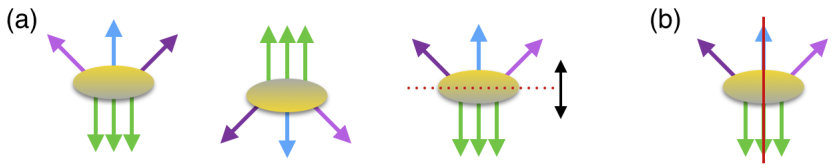

Figure 5.2: (a) Starting with the external legs of the web diagram of $L^{1,3,1}$ in 5.1(b), if one first inverts all zig-zags and then acts on them with the geometric action of the orientifold line on the dimer, i.e. invert the vertical direction, the resulting web diagram looks the same as the initial one, up to certain identifications between different zig-zag paths that agree with the identifications on the dimer of figure 5.1(a). (b) The $\mathbb{Z}_2$ action that leaves a line invariant on the web diagram of $L^{1,3,1}$ and is equivalent to doing the two previous steps. This time it corresponds to a vertical line.

In fact, since in this case I first inverted both components of the (p, q)'s and then inverted again the vertical one, the outcome is just inverting the horizontal component, and thus the set of external legs in figure 5.2(a) are related by a $\mathbb{Z}_2$ action that leaves invariant a vertical line, which is shown in figure 5.2(b). Moreover, since physics is independent of the choice of what is horizontal and what is vertical on the dimer, the important fact here is that the external legs of the web diagram are compatible with a $\mathbb{Z}_2$ action leaving a horizontal/vertical line invariant because the dimer is compatible with parallel orientifold lines. Indeed, this idea is general and works for any toric singularity. Moreover this property can be used the other way around to state that for any singularity whose external legs accept a $\mathbb{Z}_2$ action that leaves a horizontal/vertical line invariant, the corresponding dimer accepts orientifold lines.

The next case to consider is that of dimers with a single fixed line. In figure 5.3(a) I show the dimer corresponding to the Suspended Pinched Point (SPP) as well as its zig-zag paths. This time the fixed line under the orientifold action exchanges both coordinates. The corresponding (p, q)'s are shown in figure 5.3(b) together with the orientifold line action leaving the web diagram invariant.

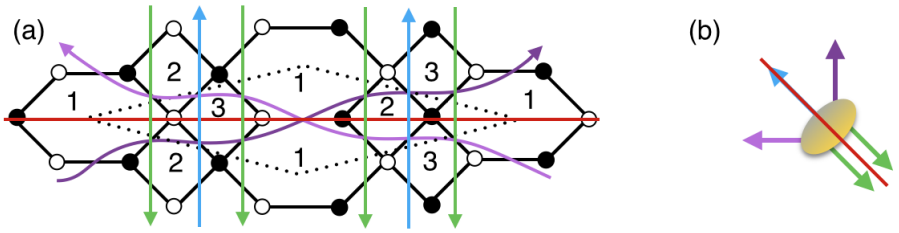

Figure 5.3: (a) The unit cell of the dimer of SPP, together with the orientifold line crossing the diagonal of the cell and the zig-zag paths. (b) External legs of the web diagram of SPP. The line in red is the fixed line left invariant under the $\mathbb{Z}_2$ action of the orientifold line. Since the orientifold line crosses the dimer in the diagonal direction of the unit cell, the red line has a diagonal direction.

Following the same procedure as before, the identification of zig-zags with their orientifold images can be done in a two step process. One must first invert all the winding numbers of zig-zag paths as in (5.1), and then, since the fixed line is diagonal and its action on the dimer is to identify the two 1-cycles, its action on the (p, q)'s leads to an exchange of the two entries. Since this $\mathbb{Z}_2$ action is a symmetry of the dimer, the resulting set of (p, q)'s is the same as the one in the beginning.

$$\Omega : \left\{ \begin{pmatrix} p_i \\ q_i \end{pmatrix} \right\}_{i=1,\ldots,Z} \rightarrow \left\{ \begin{pmatrix} -q_i \\ -p_i \end{pmatrix} \right\}_{i=1,\ldots,Z} = \left\{ \begin{pmatrix} p_j \\ q_j \end{pmatrix} \right\}_{j=1,\ldots,Z} . \tag{5.4}$$

Once again, the $\mathbb{Z}_2$ symmetry is clearly manifest on the web diagram, as can be seen on figure 5.3(b). The difference with the previous case is that for $L^{1,3,1}$ the line invariant under the $\mathbb{Z}_2$ action on the web diagram was horizontal, whereas now it is diagonal. It is a general fact that singularities compatible with diagonal orientifold lines have web diagrams that are $\mathbb{Z}_2$ symmetric with respect to a fixed line.

Knowing how to characterize the action of orientifold lines on the web diagrams, it is possible to use the criterion in the inverse direction to know which singularities are compatible with this type of action:

Criterion for toric CY singularities accepting orientifold lines: A toric CY singularity can have orientifold lines on its dimer if its web diagram has a $\mathbb{Z}_2$ symmetry that leaves a line invariant. Moreover, if the fixed line on the web diagram is horizontal/vertical, the orientifold line will invert one coordinate on the dimer; whereas for diagonal fixed lines on the web diagram, it will exchange its two coordinates.

The fact that a singularity admits a dimer with orientifold lines does not mean that all its toric phases are compatible with it. Starting from a phase compatible with this action, only the phases related to the initial one by Seiberg dualities performed in a $\mathbb{Z}_2$ symmetric way will also be compatible with the orientifold line. In general, there are also

other Seiberg dualities which are not symmetric with respect to the fixed line action and thus lead to phases where the orientifold line action is not possible.

In order to build up toric phases which are compatible with orientifold lines, one can use the *fast inverse algorithm* in [38] while taking into account the required $\mathbb{Z}_2$ symmetry. The best way to proceed seems to be starting from a square unit cell together with the fixed line(s) that cross(es) it in a direction fixed by the (p,q) web in the sense of the criterion above. Then, the easiest way to start placing zig-zag paths is usually by first putting the pairs that are paired between themselves and cross each other, since they cross each other on top of the fixed line(s) and thus they may be more difficult to place in later steps. The next convenient step is to include the zig-zags mapped to themselves, as these also cross the fixed line. Finally, the remaining paths are the ones mapped between themselves but not crossing each other, since they do not touch the orientifold line.

Finally, some comments go on the different representatives of the (p,q) web and thus the unit cell, since the $\mathbb{Z}_2$ symmetry may or may not be manifest on certain representatives.

A remark on modular invariance of the unit cell

The fact that dimers (without orientifolds) are defined on tori allows for different unit cells related via $SL(2,\mathbb{Z})$ transformations. Different choices of unit cell thus lead to changes on the (p,q) winding numbers of the zig-zag paths, and thus to different representatives of the web and toric diagrams. In the previous examples, the unit cell was chosen to make the $\mathbb{Z}_2$ symmetry obvious on the web diagram, this can be seen e.g. in figure 5.2. It is important to understand the general situation, so start by considering the $L^{1,3,1}$ theory with a different choice of unit cell, shown in figure 5.4(a). The (p,q)'s of the zig-zag paths are now different as can be seen in figure 5.4(b), where it is not manifest that the singularity is compatible with orientifold lines.

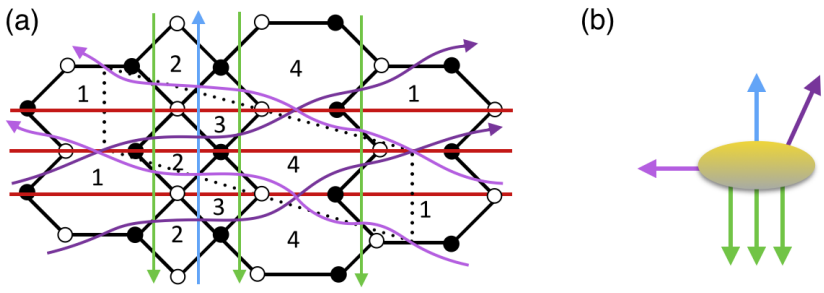

Figure 5.4: (a) Dimer for $L^{1,3,1}$ with orientifold lines and a different unit cell to the one in figure 5.1. (b) External legs of the web diagram of $L^{1,3,1}$ for the unit cell in (a). This unit cell does not make manifest on the web diagram the the $\mathbb{Z}_2$ symmetry required to have orientifold lines.

Since the change of unit cell is just a $SL(2,\mathbb{Z})$ transformation acting on the set of all (p,q)'s, it is possible to find out if a singularity allows orientifold lines just by checking if the whole set is invariant under the action of a $GL(2,\mathbb{Z})$ matrix in a way I now explain.

Start by noting that for e.g. $L^{1,3,1}$, in (5.3) the action of the orientifold on the (p,q)'s can be represented by a matrix, that in this case was given by $\mathrm{diag}(-1,1)$.

$$\Omega: \left\{\begin{pmatrix} p_i \\ q_i \end{pmatrix}\right\}_{i=1,\ldots,Z} \to \left\{\begin{pmatrix} -1 & 0 \\ 0 & 1 \end{pmatrix}\begin{pmatrix} p_i \\ q_i \end{pmatrix}\right\}_{i=1,\ldots,Z} = \left\{\begin{pmatrix} -p_i \\ q_i \end{pmatrix}\right\}_{i=1,\ldots,Z} = \left\{\begin{pmatrix} p_j \\ q_j \end{pmatrix}\right\}_{j=1,\ldots,Z} \tag{5.5}$$

A change in the unit cell changes this matrix to a more general M_Ω:

$$\begin{pmatrix} -1 & 0 \\ 0 & 1 \end{pmatrix} \quad \rightarrow \quad M_\Omega = \pm M^{-1} \begin{pmatrix} -1 & 0 \\ 0 & 1 \end{pmatrix} M \quad , \quad M \in SL(2,\mathbb{Z}) \ , \tag{5.6}$$

where the two possible signs stand for the different choices of what one considers the horizontal and the vertical axis. Therefore, the conclusion is that for a general representative of the toric/web diagram, if the set of all (p,q)'s is invariant under the action of a matrix M_Ω given by (5.6), then this singularity accepts two parallel orientifold lines.

For the case of dimers with a single diagonal orientifold line, the same can be done to find the type of matrices that leave the set of (p,q)'s for a singularity accepting such action on the dimer. The simplest matrix can be easily read from (5.1), so this time the general matrices are of the kind

$$M_\Omega = \pm M^{-1} \begin{pmatrix} 0 & 1 \\ 1 & 0 \end{pmatrix} M \quad , \quad M \in SL(2,\mathbb{Z}) \ , \tag{5.7}$$

where the sign once again depends on the choice of what is the horizontal axes, and thus is irrelevant for physics.

Even though this analysis is more general than the one based on the $\mathbb{Z}_2$ symmetry of certain representative of the web diagram, if one wants to find out if a toric CY singularity accepts orientifold lines, finding a matrix that leaves the set of (p,q)'s invariant is not a very practical approach. Instead, the best way to proceed is to look for the most symmetric representative of the toric/web diagram, where this symmetry is clearly manifest.

The mirror perspective

I now turn to explain the effect of the orientifold on the dual mirror theory. This perspective is not necessary for the following analysis, but it is quite visual and it can be helpful specially in section 5.2, since complex deformations of singularities are well understood on the mirror [41].

As explained in [42], in the mirror picture the Type IIB orientifolds map to an O6-plane in Type IIA. This O6-plane preserves the same supersymmetry as the D6-branes giving rise to the gauge groups, and it usually intersects the punctured Riemann surface Σ given by $P(x,y)=0$ in (2.11)[1]. Starting from the original surface Σ, the theory with the orientifold will have a new mirror dual that lives on a new Riemann surface Σ'. This new surface Σ' is related to the initial one as follows. In the simplest situations, the O6-plane will wind a 1-cycle in Σ that splits this surface into two surfaces Σ' with boundaries. The boundary is the 1-cycle wrapped by the O6-plane on the original surface, and the two surfaces are orientifold images of one another. Slightly more involved situations are those involving cross-caps on Σ', where the mirror of the orientifolded theory does not split Σ into two surfaces, but is given by a unique surface Σ' that may or may not have boundaries (intersections with the O6).

The starting point is a generic dimer where the numbers of gauge groups, fields, superpotential terms and zig-zag paths before the orientifold are G, F, T and Z respectively. The corresponding numbers after the orientifold identification are G', F', T' and

[1] There are cases where the O6 plane does not intersect this surface that will be studied on section 5.1.2.

Z', and the numbers of elements mapped to themselves n_G, n_F, n_T and n_Z. The relation between the numbers before and after the orientifold are

$$G' = \frac{G + n_G}{2} \quad ; \quad F' = \frac{F + n_F}{2}$$
$$T' = \frac{T + n_T}{2} \quad ; \quad Z' = \frac{Z + n_Z}{2} \ . \tag{5.8}$$

By looking at e.g. the dimer of figure 5.1(a) it is easy to see that the number n_T of superpotential terms mapped to themselves equals the sum $n_G + n_F$ of gauge groups and fields mapped to themselves. This is a general feature of orientifold lines. A similar relationship can be easily obtained on the mirror surface by observing that the fields and superpotential terms mapped to themselves must do the same on the tiling of Σ', see figure 5.5.

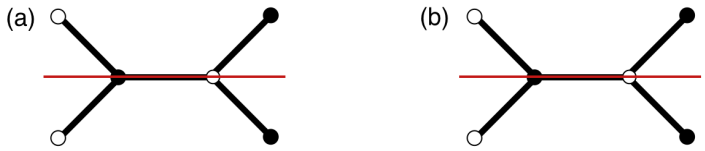

Figure 5.5: (a) Part of a dimer with an orientifold line where certain fields and superpotential terms fall on top of the orientifold. (b) In the mirror of the previous setup the same fields and superpotential terms fall on top of the boundary of Σ', this time the difference being the meaning of the adjacent tiles that are zig-zag paths instead of gauge groups.

The difference on the mirror is that the faces represent zig-zags, so in this case there is one superpotential term per each field and each zig-zag. Putting both things together one finds that

$$n_T = n_G + n_F = n_Z + n_F \quad \rightarrow \quad n_Z = n_G \ , \tag{5.9}$$

so the numbers of gauge groups n_G and zig-zags n_Z that are mapped to themselves is the same when a dimer has orientifold lines. These fields and terms falling on top of the orientifold are relevant for other things. For example, it is important not to count them when computing the Euler characteristic of the surface where the orientifold theories live. Therefore, I define the Euler characteristic of the orientifold of the dimer and the orientifold of the mirror this way:

$$\chi(\mathbb{T}^2/\Omega) = G' + T' - F' - (n_T - n_F) \ , \tag{5.10}$$
$$\chi(\Sigma') = Z' + T' - F' - (n_T - n_F) \ . \tag{5.11}$$

Using these expressions and (5.9) it is easy to check that the equation

$$\chi(\Sigma' \equiv \Sigma/\Omega) = \frac{\chi(\Sigma)}{2} \tag{5.12}$$

between the Euler characteristic of a Riemann surface and its orientifold surface holds for singularities whose dimers can have orientifold lines. This equation can be used e.g. to relate the genus g of the initial surface on the mirror to the genus g', number of boundaries b' and cross-caps c' on the orientifold of the mirror. Noting that in each case the Euler characteristic has different contributions

$$\chi(\Sigma) = 2 - 2g \quad , \quad \chi(\Sigma') = 2 - 2g' - b' - c' \ , \tag{5.13}$$

(5.12) implies

$$g = 2g' + (b' - 1) + c' \ . \tag{5.14}$$

This equation sets bounds on how the orientifold cuts the mirror surface for a given singularity.

5.1.2. Singularities compatible with orientifold points

As done for the orientifold line case, I will start with an example in order to derive a general criterion which tells what singularities accept orientifold points. The singularity I will use this time is a $\mathbb{Z}_2 \times \mathbb{Z}_3$ orbifold of the conifold, whose dimer together with the zig-zag paths and orientifold points are shown in figure 5.6(a). The (p, q)'s of the singularity are shown in figure 5.6(b).

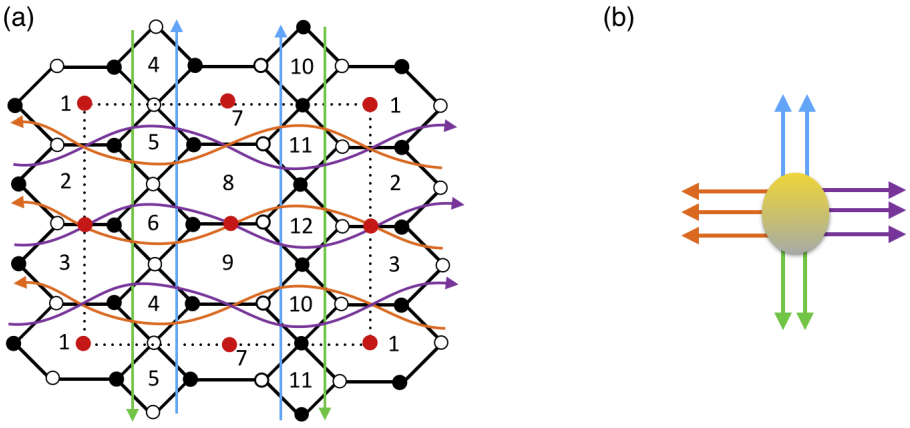

Figure 5.6: (a) Dimer for the $\mathbb{Z}_2 \times \mathbb{Z}_3$ orbifold of the conifold with orientifold points in red and its zig-zag paths. Zig-zag paths with the same winding numbers have the same colour. (b) External legs of the web diagram of the previous singularity.

The first observation to be made is that for each field mapped to itself, one has two zig-zags that pass through the field. Also, each zig-zag passes through two different fixed points. From here, one sees that the numbers of zig-zags and fields that are mapped to themselves is the same. Therefore, since dimers with orientifold points have four fixed points, the number of fields (and also zig-zags) mapped to themselves will be between zero and four.

$$n_Z = n_F \leq 4 \tag{5.15}$$

Next, I check the effect of the orientifold on the zig-zags. As happened for orientifold lines, in this case I will also separate the procedure in two steps. First, one must invert the direction of zig-zags, as in (5.1), and then use of the geometrical action on the dimer, which this time inverts both coordinates

$$\left\{ \begin{pmatrix} -p_i \\ -q_i \end{pmatrix} \right\}_{i=1,\ldots,Z} \quad \rightarrow \quad \left\{ \begin{pmatrix} p_i \\ q_i \end{pmatrix} \right\}_{i=1,\ldots,Z} . \tag{5.16}$$

The result is that the orientifold action leaves the (p,q)'s of zig-zags invariant.

$$\Omega : \left\{ \begin{pmatrix} p_i \\ q_i \end{pmatrix} \right\}_{i=1,\ldots,Z} \rightarrow \left\{ \begin{pmatrix} p_i \\ q_i \end{pmatrix} \right\}_{i=1,\ldots,Z} . \tag{5.17}$$

This trivial action on the set of all (p,q)'s does not imply that the orientifold action is in fact trivial. In figure 5.6 it is easy to see that the geometric action relates zig-zag paths among them. These relations are of two types: either a zig-zag path crosses fixed points and is mapped to itself, or two zig-zag paths of the same (p,q) are orientifold images of one another. In the example of figure 5.6 both zig-zag paths in blue and in green fall on the second category, whereas both for zig-zags in orange and in purple one zig-zag of each color is mapped to itself while the rest are mapped by pairs. The underlying reason for this are the limitations to arrange zig-zag paths of the same (p,q) in a way compatible with orientifold points.

There are two possible cases: on the one hand, when the number of zig-zags with same (p,q) is odd, one zig-zag must necessarily get mapped to itself and the rest can be arranged in pairs, as happens for the orange and purple ones in the example. On the other hand, if the number of zig-zags with same (p,q) is even two possibilities exist: one of them is arranging them in pairs as the green and blue zig-zags in figure 5.6; but it is also possible to place two of them on top of fixed points and then arrange the rest in pairs. This case is illustrated with the dimer in figure 5.7, where there are two zig-zags with the same (p,q) in green that pass through orientifold points.

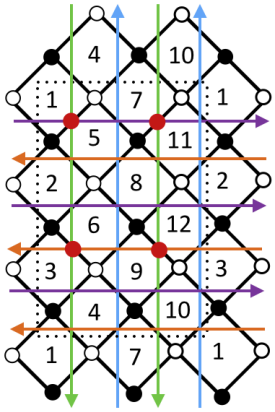

Figure 5.7: Dimer corresponding to the $\mathbb{Z}_2 \times \mathbb{Z}_3$ orbifold of the conifold in a different toric phase to the one shown in figure 5.6(a). See that in this toric phase the number of zig-zags mapped to themselves is $n_Z = 4$, whereas in figure 5.6(a) $n_Z = 2$. The difference between both cases is that in the previous toric phase the two zig-zags in green where orientifold images of one another, and this time each of them is mapped to itself. This is possible for this singularity because the number of zig-zags in green is even, and so accepts two types of zig-zag configurations compatible with the orientifold $\mathbb{Z}_2$ action.

Another important point can be obtained from the dimer in figure 5.7. Observe that it corresponds to another toric phase of the $\mathbb{Z}_2 \times \mathbb{Z}_3$ orbifold of the conifold, but now with $n_Z = 4$ zig-zags falling on top of orientifold points instead of the previous $n_Z = 2$. This means that it is possible to have different values of n_Z for a given singularity. This general property sometimes requires of different toric phases of a given singularity in order to obtain different values of n_Z, but this is not always the case, as I will show shortly.

With the information gathered from the examples, it is possible to get some general properties about toric CY singularities accepting orientifold points. I just showed that for an odd number of zig-zags with the same (p, q) one of them will be mapped to itself if the dimer has fixed points. This sets the minimum number of zig-zag paths (and so fields) mapped to themselves on a dimer with orientifold points. This can be made more precise by splitting the set of all zig-zags of a given singularity into subsets such that all zig-zags in each subset have the same winding numbers (p, q):

$$\left\{ \begin{pmatrix} p_i \\ q_i \end{pmatrix} \right\}_{i=1,\ldots,Z} = \left\{ Z_k \times \begin{pmatrix} p_k \\ q_k \end{pmatrix} \right\}_{k=1,\ldots,k_S} . \tag{5.18}$$

Here k_S is the number of subsets and Z_k is the number of elements on the subset with label k, i.e. the number of zig-zags with winding numbers (p_k, q_k). Using this splitting of the set of all zig-zag paths, one can now talk about odd (even) subsets when the subset has Z_k odd (even). The number of odd subsets was shown above to set the minimum number of zig-zags mapped to themselves n_Z^{min}, that I define as

$$n_Z^{min} = \sharp(\text{Odd } Z_k) . \tag{5.19}$$

This number, together with the fact that dimers with orientifold points have four fixed points can be used to give the following rule:

Criterion for toric CY singularities accepting orientifold points: A toric CY singularity can have orientifold points on its dimer if $n_Z^{min} \leq 4$. For singularities with more odd subsets of zig-zags, it is not possible to have orientifold points.

Furthermore, from figure 5.7 it can be seen that some singularities are compatible with orientifold points and different numbers n_Z of zig-zag paths mapped to themselves. This possibility depends on the value of n_Z^{min} of each singularity, so I now explain what the possibilities for each value of n_Z^{min} are. The n_Z^{min} odd cases will be studied first since they are more restrictive, and then the even n_Z^{min} cases.

- **There are no singularities with $n_Z^{min} = 1$.** The set of all (p, q)'s of a given singularity sums up to zero. If $n_Z = 1$ would be possible, this means that after subtracting a unique zig-zag the rest of zig-zags can be arranged in pairs, where each pair has two zig-zags with same (p, q). The sum of all these zig-zags would then have two even entries. But this sum should also be minus the (p, q) of the zig-zag that is mapped to itself. Since (p, q) are winding numbers, they must be mutually prime numbers, so this makes no sense.

- **Singularities with $n_Z^{min} = 3$ accept $n_Z = 3$.** If a singularity has odd n_Z^{min} , it means that after taking n_Z^{min} zig-zags the rest can be arranged by pairs of the same (p, q). Therefore, in these cases Z is odd. Furthermore, since the number of zig-zags Z and that of gauge groups G of a singularity are related by its toric diagram as observed in [38],

  $$G = Z + 2g - 2 , \tag{5.20}$$

  odd Z also implies odd G. And odd G can only be compatible with orientifold points if n_G (and so $n_F = n_Z$) is odd, which is the starting point. Finally, noting that $n_Z \leq 4$ and $n_Z \neq 1$, one finds that the only singularities compatible with an odd number of zig-zags mapped to themselves are those with $n_Z = n_Z^{min} = 3$. In figure 5.8 I provide an example of this kind.

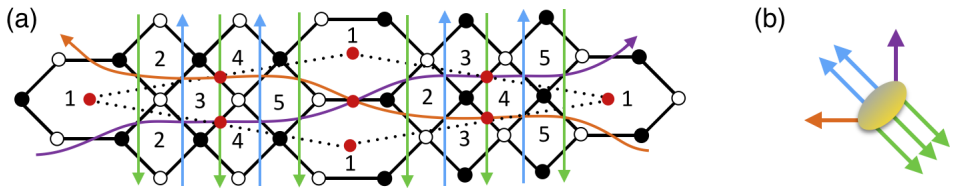

Figure 5.8: (a) Dimer of $L^{2,3,2}$ with orientifold points in red. Zig-zag paths in orange, purple and one of those in green are mapped to themselves while the rest are mapped by pairs. (b) External legs of the web diagram. It is easy to see that the subsets in orange, purple and green are the ones with an odd number of zig-zags, and thus have one element of each subset mapped to itself.

- **Singularities with $n_Z^{min} = 0$ accept both $n_Z = 0$ and $n_Z = 4$.** In this cases all subsets have an even number of elements. It is always possible to have $n_Z = 0$. No zig-zag is mapped to itself, and so no field: all fixed points fall on top of gauge groups. An example of this kind is shown in figure 5.9(a).

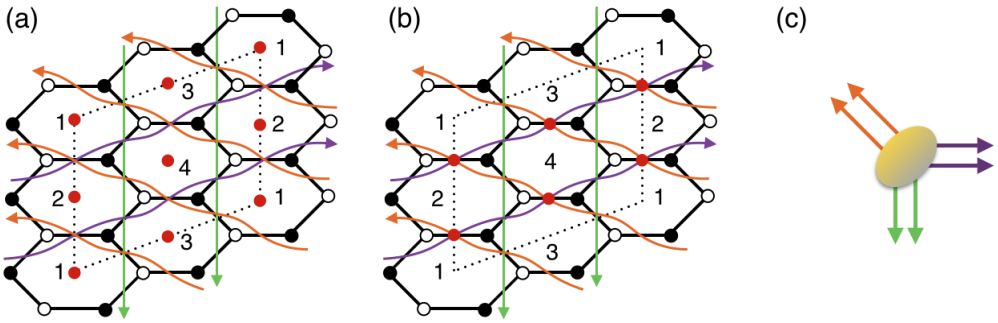

Figure 5.9: (a) Dimer of the $\mathbb{C}^3/(\mathbb{Z}_2 \times \mathbb{Z}_2)$ orbifold with orientifold points in red in a configuration where $n_Z = 0$. (b) The dimer in (a), but this time fixed points fall on top of fields so that $n_Z = 4$. (c) External legs of the web diagram. Note that all zig-zags can be arranged by pairs with same (p, q).

Following the ideas on the $n_Z^{min} = 3$ case, n_Z^{min} even implies both Z and G to be even. This leaves the possibility of even values of n_Z when $n_Z^{min} = 0$. $n_Z = 2$ turns out not be an option. For this to happen in a singularity with $n_Z^{min} = 0$, the two zig-zags that would be mapped to themselves would have the same (p, q), and would have to intersect each other. Zig-zags with the same (p, q) never intersect, so I conclude that this is not an option. $n_Z = 4$ instead is always an option, that sometimes requires the dimer to be in a different toric phase compared to the one allowing $n_Z = 0$. I illustrate this with figure 5.9(b), where the dimer of $\mathbb{C}^3/(\mathbb{Z}_2 \times \mathbb{Z}_2)$ shows to allow both $n_Z = 0$ and $n_Z = 4$ in (a) and (b) respectively. As an observation, note that unlike in the case of the $\mathbb{Z}_2 \times \mathbb{Z}_3$ orbifold of the conifold studied above, here both possibilities for n_Z are compatible with the same toric phase.

- **When $n_Z^{min} = 2$, both $n_Z = 2$ and $n_Z = 4$ are possible.** This time, there is no argument preventing that both even values of n_Z are possible for a singularity with $n_Z^{min} = 2$. As shown in the example, sometimes different toric phases are necessary for the different values of n_Z.

- **For singularities with $n_Z^{min} = 4$ one has $n_Z = 4$.** Of course, no other possibility exists in this case.

All these cases are put together on the following table:

n_Z^{min}	Possible $n_Z = n_F$
0	0 & 4
1	-
2	2 & 4
3	3
4	4
>4	-

As it happened for orientifold lines, in the case of orientifold points one finds that usually not all toric phases are compatible with orientifold points, or not all phases accept certain n_Z. The best way of obtaining a dimer compatible with orientifold points and n_Z for a given singularity, is to use the *fast inverse algorithm* [38]. This time, the best option is usually to put first the zig-zags that are mapped to themselves and thus fall on top of orientifold points, and leave the rest for the next steps.

The mirror perspective

This time I will use the mirror perspective for different purposes. I will first derive many of the properties I already obtained from the mirror perspective. Then, I will carry out a similar analysis to the one done for orientifold line case.

The constrains of the previous section can be well understood in terms of the mirror. The key feature to derive the conclusions is that two zig-zags (punctures on the mirror) with the same (p, q)'s will never cross each other on the dimer. Recall that as explained in section 2.3.3, in the tiling of the mirror surface zig-zags are faces bounding the corresponding puncture, with the boundary given by a set of edges and vertices corresponding to the fields and superpotential terms that the zig-zag path touches on the dimer. Therefore, the faces bounding two punctures with the same (p, q) on the mirror surface will never share an edge. From this fact it follows that in any boundary of Σ' it is necessary to have at least two zig-zags and two fields mapped to themselves. This fact provides a nice description in the mirror of some constrains I gave above:

- $n_Z^{min} = 0$ **implies** $n_Z \neq 2$**.** If only two punctures are mapped to themselves, the corresponding tiles in Σ must be touching each other. Therefore, it is not possible that they have the same (p, q)'s. For a singularity with $n_Z^{min} = 0$, to have $n_Z = 2$ one would need that two punctures with same (p, q)'s are mapped to themselves and thus touching each other, and this is impossible as I just explained.

- $n_Z = 1$ **is impossible.** A zig-zag never crosses itself. Equivalently, there is no edge on the tiling of Σ touching the same tile twice. Therefore, it is impossible that on the mirror of the orientifold geometry there is only one puncture that falls on top of the boundary in Σ'.

- Z **odd only accepts** n_Z **odd.** If the tiling of Σ has an odd number of punctures, once the orientifold action taken the only way of arranging the punctures on a $\mathbb{Z}_2$ invariant way is by putting an odd number of them on top of the O6-plane, giving the boundary of Σ', and then putting the rest of punctures on the *bulk* of Σ' and its orientifold image. This can also be derived from (5.8): for Z' to be an integer there is no other chance.

- Z **even only accepts** n_Z **even.** The argument is the same I just gave for Z odd, but now with even Z.

The distinction about the punctures on the boundary and the *bulk* of Σ' will be relevant when dealing with complex deformations compatible with orientifold points on section 5.2.

Now, I once again perform an analysis about some topological properties of the orientifold of the mirror surface Σ'. Start by taking the orientifold action on the dimer, so the numbers of gauge groups, fields, etc. are reduced according to (5.8). The difference this time comes on the relations between the numbers of elements mapped to themselves. From section 2.3.5 recall that no vertex is mapped to itself by orientifold points. This has consequences on the tiling of the mirror, since the only way to have a field on the boundary of Σ' in a way such that the vertices on its sides are mapped to themselves is by placing the edge perpendicular to the boundary, as in figure 5.10.

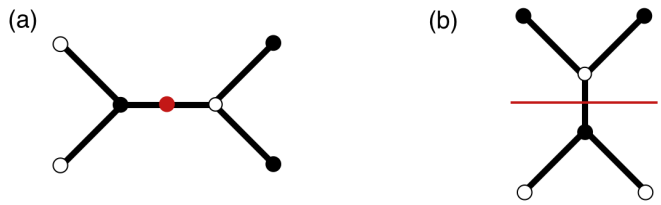

Figure 5.10: (a) Part of a dimer with orientifold points where a field that is mapped to itself and superpotential terms and other fields that are mapped by pairs under the orientifold action. (b) On the mirror of the previous part of the dimer, the only way to have the field mapped to itself as well as the right mapping between the vertices is to place the field perpendicular to the boundary.

This implies that there will be one field per each zig-zag on the boundary of Σ', in agreement with the conclusion from the dimer given in (5.15). Summing up

$$n_Z = n_F \quad ; \quad n_T = 0 \ . \tag{5.21}$$

The next step is to proof that dimers with orientifold points live on spheres. Being more concrete, they live on spheres with four punctures (the fixed points). In order to proof this, consider a case where all fixed points fall on top of faces of the dimer

$$G' = \frac{G+4}{2} \quad ; \quad T' = \frac{T}{2} \quad ; \quad F' = \frac{F}{2} \ . \tag{5.22}$$

When computing the Euler characteristic for this surface fixed points fall on top of faces that must be count normally, so

$$\chi(\mathbb{T}^2/\Omega_{\text{fixed points}}) = G' + T' - F' = \frac{G+T-F+4}{2} = 2 \ , \tag{5.23}$$

which is the Euler characteristic of the sphere.

On the mirror of the orientifold theory there is a boundary[2] that crosses the edges orthogonally, so the Euler characteristic of the orientifold of the mirror is computed in the regular way

$$\chi(\Sigma') = Z' + T' - F' \ . \tag{5.24}$$

This allows to relate the initial surface Σ and the one after taking the orientifold Σ'. Start by writing (5.20) in terms of the parameters on the orientifold of the theory

$$2G' - n_G = 2Z' - n_Z + 2g - 2 \ . \tag{5.25}$$

Summing $2(T' - F') + n_F$ on both sides and using (5.8), (5.21) and (5.24) this is

$$0 = G + T - F = 2(G' + T' - F') - (n_G - n_F) = 2\chi(\Sigma') - \chi(\Sigma) \ . \tag{5.26}$$

So for orientifold points one also has $2\chi(\Sigma') = \chi(\Sigma)$ and so (5.14) holds.

Another very important conclusion can be made from the fact that the tile corresponding to a puncture in Σ never touches itself is that for orientifold points there is an upper bound on the possible number of boundaries b'. Since each boundary involves at least two punctures, and the maximum number of punctures mapped to themselves is 4, the mirror Σ' of a dimer with orientifold points can have a maximum of 2 boundaries.

5.2. Deformations of dimers with orientifolds

Now that I found the criteria to tell if a toric CY singularity is compatible with orientifold actions and if these correspond to fixed points/lines on the dimer, I can tell which singularities are compatible both with the orientifold action and complex deformations. As reviewed in section 2.3.4, complex deformations correspond to the removal of subwebs in equilibrium from the web diagram. The physics behind this was better understood from the mirror perspective in [41]. Combining the above knowledge with this idea, I now provide criteria to tell which singularities are compatible with both orientifolds (of both kinds) and complex deformations.

5.2.1. Deformations compatible with orientifold lines

In section 5.1.1 I showed that the best way of finding out if a singularity is compatible with orientifold leaving fixed lines on the dimer was to take the most symmetric representative of the web/toric diagram of the singularity (without the orientifold) and see if it is compatible with a $\mathbb{Z}_2$ action that leaves a line invariant.

If one starts with a singularity describing the UV of a warped throat compatible with orientifold lines, the IR physics after performing the complex deformation must correspond to another singularity compatible with the same $\mathbb{Z}_2$ action both on the dimer and on the web/toric diagram. Therefore, the way to deform the singularity must respect the $\mathbb{Z}_2$ symmetry. This means that the sub-web in equilibrium that is removed from the web

[2] In the $n_Z = 0$ case there is no boundary, and in the $n_Z = 2$ case there might be two boundaries. For any case, equation (5.24) holds.

diagram on the UV must also be symmetric with respect to the $\mathbb{Z}_2$ action: this way the web diagram describing the IR preserves the same symmetry.

From the mirror perspective the deformation process corresponds to removing punctures from the tiling of Σ, or Σ' for the orientifold of the theory. For orientifold lines the deformation can happen on the bulk of Σ', on its boundary (this is the 1-cycle wrapped by the O6-plane), or in both at the same time. I illustrate these possibilities with an example of each kind.

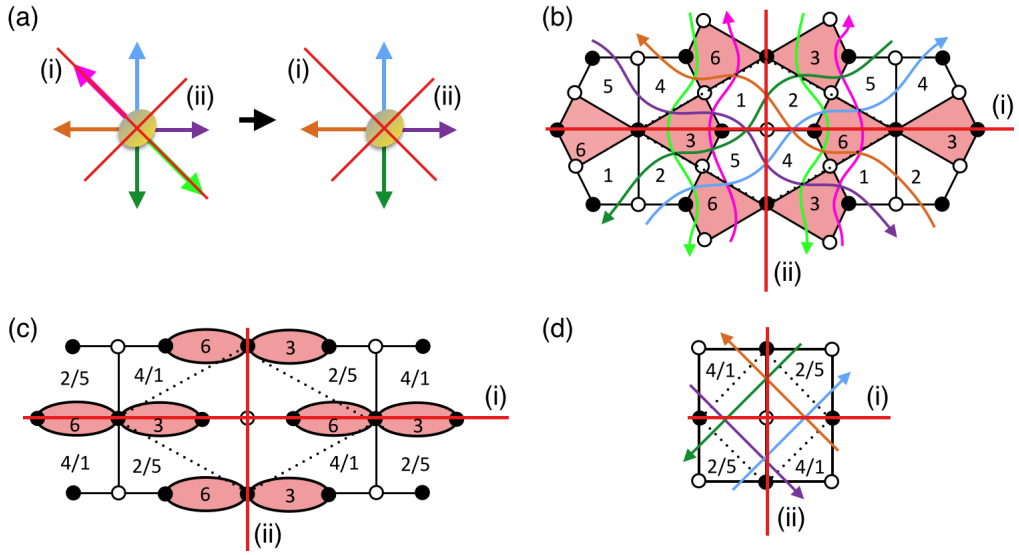

Figure 5.11: (a) External legs of the dP_3 theory and the conifold theory. It is easy to see that the complex deformation relating both corresponds to removing legs in light green and pink from the former. Two orientifold lines are compatible with both singularities, I represented their action with red lines. In case (i) the removed zig-zags are invariant under the orientifold action and so the corresponding punctures lie on the boundary of Σ'; whereas in case (ii) the removed zig-zags are mapped between themselves and thus they fall on the bulk of Σ'. (b) Dimer of the dP_3 theory with the zig-zags in different colors. The straight lines in red (i) and (ii) correspond to the two possible orientifold lines compatible I just mentioned. I am interested on the deformation involving the removal of the zig-zag paths in light green and pink, and so the confinement of gauge groups with labels 3 & 6, that I shaded in red. (c) Intermediate step in the confinement of gauge groups 3 & 6, showing that it involves higgsing groups 1 & 4 on the one hand and 2 & 5 on the other hand to their diagonals. (d) The dimer after the deformation process together with the two possible orientifold lines.

First, in figure 5.11 I consider the transition from the del Pezzo 3 (dP_3) theory to the conifold studied in [40]. This transition is compatible with two different types of orientifold lines, that correspond to removing punctures either only on the boundary of Σ' (case (i) of the figure) or only on the bulk of this surface (case (ii) of the figure).

For completeness, let me mention that these cases of deformations sometimes involve strong dynamics of gauge groups of the SO or/and USp kind [148, 149]. For example, in the case (i) of figure 5.11 one finds that both gauge groups 3 and 6 are of one of these types. Similar processes were described in [50], where it could be seen that the fixed lines do not change the diagrammatic description of the deformation process.

The last example of a deformation with orientifold lines mixes the two previous cases: it involves zig-zags both in the bulk and in the boundary of Σ'. This is shown in figure 5.12

. Also in this case one finds strong dynamics of gauge groups of he SO or/and USp kind, but this time they involve a new type of phenomenon. In the confinement of gauge group 3 note that it higgses e.g. group 1 (and its orientifold image 5) from being of the SU type to being of the SO/USp type. This happens when the massive mesons of the confining group get a vev. These transform in the (anti)symmetric representation of gauge group 1 depending on the orientifold charge. The outcome is the same diagrammatic evolution of the dimer as the one without the orientifold line, that respects the $\mathbb{Z}_2$ symmetry.

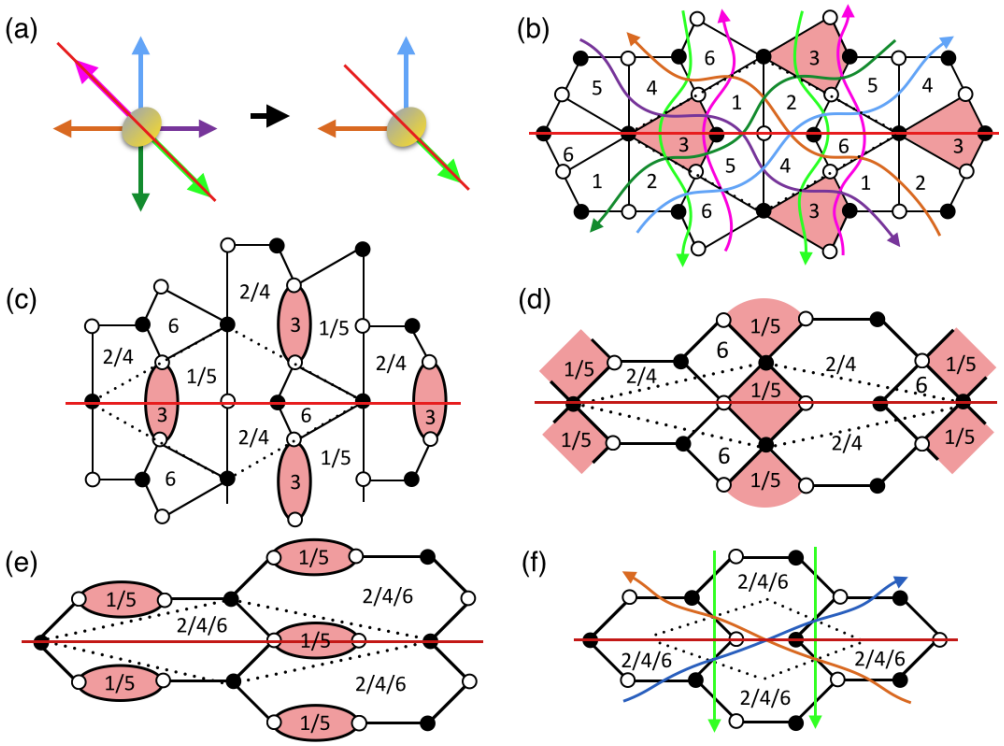

Figure 5.12: (a) External legs of the dP_3 theory and the $\mathbb{C}^3$ theory. The complex deformation relating both corresponds to removing legs in dark green, purple and pink from the former. The effect of the orientifold line is shown in red, and can be seen to be compatible with the removal of the subweb. (b) Dimer of the dP_3 theory with the zig-zags in different colors. I am interested on the deformation involving the removal of the zig-zag paths in dark green, purple and pink, and so the confinement of gauge groups with labels 1, 3 & 5. Since they touch each other, this deformation was shown in [40] to require more than one step. Start by first confining gauge group 3, shaded in red. (c) Intermediate step in the confinement of gauge group 3, showing that it involves higgsing group 1 and its orientifold image 5 from being of SU type to SO/USp type depending on the orientifold line charge. The condensation process makes the (anti)symmetric field X_{15} massive together with the (anti)symmetric meson M_{51}, so they get a (anti)symmetric *vev* leaving a SO/USp gauge factor. The same happens to gauge factor 2 and its image 4. (d) The dimer after the first confinement process. Now gauge group 1/5 confines, so I shaded it in red. (e) The next intermediate process, where gauge groups 2/4 & 6 are higgsed to the diagonal. (f) Final dimer, corresponding to $\mathbb{C}^3$ theory with its zig-zags paths.

If one intends to UV complete a singularity accepting orientifold lines on the dimer, the recipe is then pretty simple. One must first find the $\mathbb{Z}_2$ action leaving a fixed line on the web diagram and then add external legs in a symmetric way with respect to this fixed

line. Finding the toric phase of the IR dimer resulting from the deformation may not be an easy task, therefore, the best option seems to be to start from the IR theory, add the subweb in equilibrium to the IR web diagram, and then build the dimer of the UV theory using the *fast inverse algorithm* in [38] and following the recommendations above. Finally, one needs to study the duality cascade and the deformation from the UV to the IR on the dimer.

5.2.2. Deformations compatible with orientifold points

Unlike singularities compatible with orientifold lines on their dimer, those accepting orientifold points turn out to require a more careful analysis and are in a sense more restrictive with respect to complex deformations. In section 5.1.2 I showed that the possibility of having orientifold points for a given toric singularity depends on the multiplicities of zig-zag paths with the same (p, q) winding numbers: there will be one zig-zag path mapped to itself per each set of zig-zags with same (p, q) and odd multiplicity. This sets an upper bound on the number of zig-zags mapped to themselves, that can by no means be more than four.

The starting point is to note that complex deformations are described as condensation of certain gauge groups on the dimer. These gauge groups need to be rectangles in order to have at certain point $N_c \geq N_f$. As explained in section 2.3.5 rectangles do not accept orientifold points on top of them. Therefore, when orientifold points are present for every gauge group condensing there will be another one (its orientifold image) doing the same. At this point one can think of two possibilities: the groups to confine can be touching each other and thus touching a fixed point, or they can be away from the orientifold point and thus not touching each other. These correspond to D6-branes on the mirror surface Σ', that do touch the boundary in the first case, but do not touch it on the second one. This means that the first case translates to a deformation on the boundary of Σ', whereas the second case corresponds to a deformation on the bulk of Σ' and its orientifold image, or equivalently, in the first case one wants to remove punctures/zig-zags that are mapped to themselves and in the second case pairs of punctures/zig-zags away from the orientifold.

I will first deal with the case where the confining groups do touch a fixed point as well as its orientifold image on the dimer. I anticipate that this process is not possible. Since this is a D6-brane touching the boundary and confining, the dimer looks locally as shown in figure 5.13(a).

The argument against deformations in this case relies on the distribution of fractional branes (distribution of ranks of gauge groups) on the dimer. The orientifold has RR charge and thus contributes to the anomaly cancellation conditions, but its effects are $\mathcal{O}(1)$ compared to those of the N regular branes and M fractional branes that I consider. For simplicity, it is thus better to consider a dimer without the orientifold point contribution but preserving the $\mathbb{Z}_2$ symmetry, as in figure 5.13(b). I will eventually that a deformation on the boundary is not possible, which extends to the case where the orientifold point is included. As a starting point, consider the dimer with no fractional branes. Now, in roder to try to have strong dynamics in two adjacent groups I put fractional branes on them, leaving the local setup in the dimer in figure 5.13(b). In order for these groups to be anomaly-free, it is necessary to include fractional branes on other faces of the dimer.

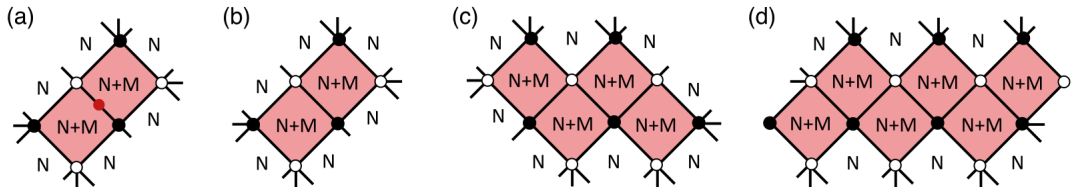

Figure 5.13: (a) In order to have a complex deformation removing punctures on the boundary of Σ' one needs gauge groups whose D6-branes on the mirror touch the orientifold. They would give a configuration like this one on the dimer, with N regular branes and M fractional branes on the confining groups. (b) In order to simplify the analysis, one can remove the orientifold point while keeping the $\mathbb{Z}_2$ symmetry. (c) The setup in (b) is anomalous and requires putting fractional branes in more gauge factors. (d) Following the same philosophy, the gauge factors with fractional branes keeps growing.

Including these fractional branes in adjacent faces while keeping the $\mathbb{Z}_2$ symmetry, see figure 5.13(c). At this point, the faces where I just put fractional branes are anomalous, and require putting new fractional branes on other gauge groups. This process follows, growing the number of gauge groups with fractional branes until one reaches the point where the bi-periodicity of the dimer makes faces with fractional branes meet other faces with fractional branes and no more steps need to be taken. This means that in the end, in the resulting anomaly-free $\mathbb{Z}_2$ configuration, one can wind at least one of the 1-cycles of the $\mathbb{T}^2$ of the dimer. An example of this kind is shown in figure 5.14. These type of fractional branes were dubbed in [22] $\mathcal{N} = 2$ branes, and it was shown that they do not lead to complex deformations. A more extreme possibility would be that the final configuration requires putting fractional branes on all faces of the dimer, which are just regular branes, and thus cannot lead to confinement. Let me emphasize here that this conclusions come just from demanding that the fractional branes fall on top of adjacent gauge groups and are distributed in a $\mathbb{Z}_2$ symmetric way. From here I conclude that it is not possible to perform a complex deformation removing zig-zags that are mapped to themselves for a singularity with orientifold points.

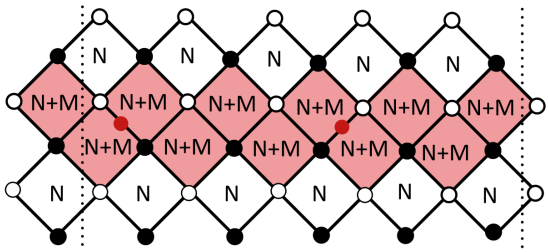

Figure 5.14: Part of a dimer describing the prototypical situation one finds when adding fractional branes until anomaly cancellation conditions are satisfied for all gauge groups on the dimer. Shaded faces are those with fractional branes, whereas the ones in white only have regular branes. For simplicity, the $\mathcal{O}(1)$ effects due to the orientifold RR charge where neglected. These type of fractional brane distribution corresponds to the so-called $\mathcal{N} = 2$ fractional branes. This figure could describe part of e.g. a $\mathbb{Z}_5 \times \mathbb{Z}_n$ orbifold of the conifold.

The other option is that the confining gauge groups and their images do not touch any fixed point. In this case, the corresponding D6-branes in the mirror dual do not touch

the orientifold, and so are wrapping a series of punctures in Σ' that are on the bulk. Therefore, the external legs removed on the deformation will be on the bulk of Σ' (and its orientifold image). This corresponds to removing a subweb in equilibrium that contains no zig-zag path that is mapped to itself under the orientifold action, i.e. the deformation requires removing two copies of a subweb in equilibrium from the web diagram of the UV theory. In figure 5.15 I show an example of this kind.

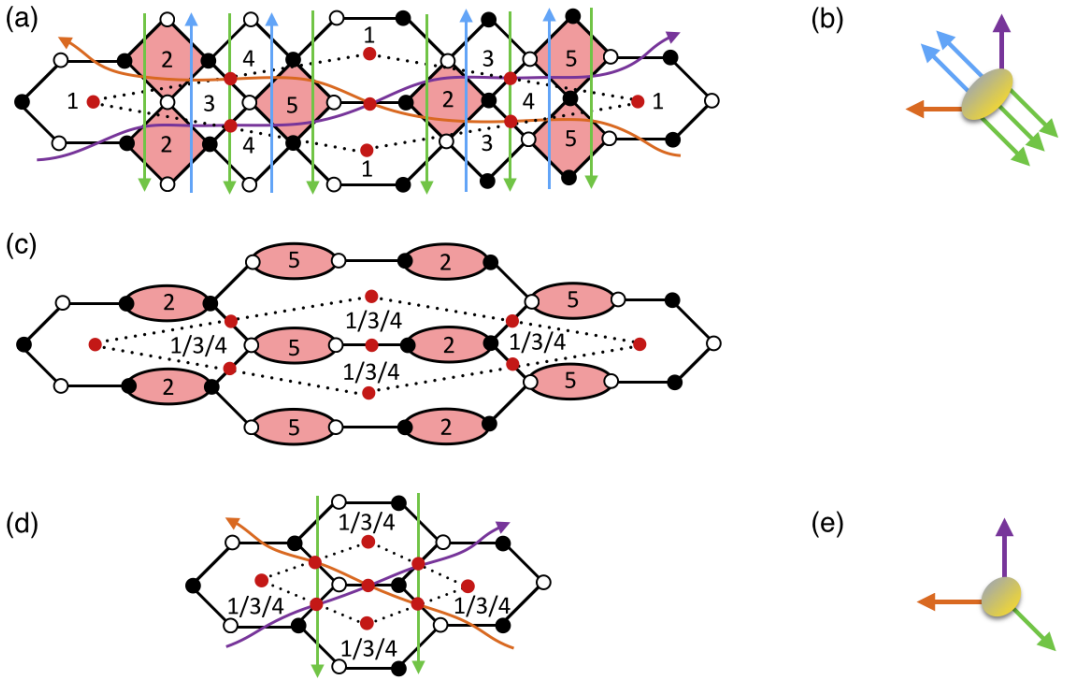

Figure 5.15: (a) Dimer diagram of $L^{2,3,2}$ with orientifold points. I am interested on the deformation process to the IR that removes zig-zags on the bulk and their orientifold images, this corresponds to studying the strong dynamics of gauge group 2 and its orientifold image 5, each bound by a zig-zag in green and one in blue. I shaded these groups in red. (b) External legs of $L^{2,3,2}$. See that one zig-zag in green plus the ones in purple and orange must be mapped to themselves ($n_Z = 3$), in agreement with the dimer. Since I want to remove external legs mapped between themselves, this corresponds to the other two external legs in green plus the two in blue. Note that without the orientifold this process could be separated into two individual deformations. (c) Intermediate step in the deformation process, when groups 2 and 5 confine their mesons acquire *vevs* that higgs gauge group $SU(n_1) \times USp(n_3) \times SU(n_5)$ to $USp(n_1/2 = n_3 = n_5/2)$ for e.g. negative orientifold charge on the fixed point on the top. (d) Dimer of the $\mathbb{C}^3$ theory with orientifold points and zig-zags after the complex deformation. (e) External legs of the $\mathbb{C}^3$ theory. By comparing it with (b) note that the external legs missing were orientifold images of one another.

A final remark goes on how to UV complete singularities with orientifold points. As done for orientifold lines, the best strategy seems to be to start with the web diagram of the IR singularity and add to it a subweb in equilibrium twice. This gives the UV singularity, whose dimer can be constructed using the *fast forward algorithm* [38]. The warped throat behaviour and following deformation can then be addressed by finding the RG cascade on the UV dimer and then the confinement process that gives the IR singularity.

6

De Sitter uplift with Dynamical Supersymetry Breaking

This chapter retakes the line of using warped throats for cosmological model building in ST, this time focusing on the source of the current accelerated expansion of the Universe. The technology in the previous chapter will be used here, providing an application of those tools.

The construction of de Sitter vacua in string theory is a most fertile industry in the field. The prototypical approach [61] is to consider string compactifications with full moduli stabilization (by fluxes [3, 4, 150], non-perturbative effects, and possibly α' corrections [151]), and add some additional sector introducing tunably small contributions to the vacuum energy, to motivate the existence of vacua with parametrically small cosmological constant. This additional sector, typically producing the 'uplift' of an originally anti de Sitter stabilized vacuum to a de Sitter one, was introduced in [61] as a sector of anti D3-branes at the bottom of a warped throat, whose redshift suppression underlies the claimed tunability. A general difficulty in approaches of this type is that the uplift is not well described within effective field theory. Fortunately, recently there were some improvements in this direction, see e.g. [23, 136, 152, 153]. Nonetheless, several alternatives have been proposed in the past years to uplift the cosmological constant [154–162].

In this chapter I present a class of models where the uplifting mechanism is built-in in the effective field theory, since it arises from the spontaneous susy breaking dynamics of strongly coupled gauge theory sectors on D3-branes (DSB sectors). Therefore, this setup is free from potential problems arising from limitations of an effective field theory description. The DSB sector is located at the bottom of a warped throat in order to achieve the tunability of the susy breaking contribution to the vacuum energy. Although this idea is very general, the discussion is particularized to a concrete explicit model, in which the DSB sector is the susy breaking 1-family $SU(5)$ theory in [163], whose D-brane embedding appeared in [42]. This particular model has the advantage of having a unique trivial vacuum that becomes non-supersymmetric due to quantum effects [163]. This ensures that the setup lies on the true vacuum of the theory, as opposed to other proposals to uplift the cosmological constant [100, 156]. The D-brane embedding and the corresponding throat geometry is described by providing an explicit holographic dual in terms of a duality cascade. Although the particular DSB model is of the 'non-calculable' kind, similar constructions can be carried out for other DSB D-brane gauge theories in the market [22, 56–60].

One interesting advantage of the proposal is that the holographic description of the strong gauge dynamics underlying the DSB and thus the uplift lies, by construction,

beyond the regime of validity of 10d supergravity. Therefore this uplift mechanism possibly circumvents problems associated to the description of antibranes and their backreaction in supergravity (for a recent discussion, see [109, 111] and references therein).

The chapter is organized as follows. In section 6.1 I describe a orientifold of toric singularity accepting a fractional brane assignment leading to DSB. Then, in section 6.2 I embed this singularity within a warped throat using the techniques in chapter 5, describing its RG cascade in section 6.2.1 and the deformation process in section 6.2.2.

6.1. DSB from D-branes at singularities

The field theory with DSB I will focus on was described in [163]. This theory can be nicely embedded in the worldvolume theory of a D3-brane at a toric CY singularity. More concretely, the model can be embedded on a orientifold of the $\mathbb{C}^3/\mathbb{Z}_6'$ geometry, which is a $\mathbb{C}^3/(\mathbb{Z}_3 \times \mathbb{Z}_2)$ orbifold generated by

$$\begin{aligned} \theta : (z_1, z_2, z_3) &\rightarrow (-z_1, z_2, -z_3) \\ \omega : (z_1, z_2, z_3) &\rightarrow (e^{2\pi i/3} z_1, e^{-2\pi i/3} z_2, z_3) \end{aligned} \tag{6.1}$$

The dimer with the orientifold action corresponding to this geometry is shown in figure 6.1.

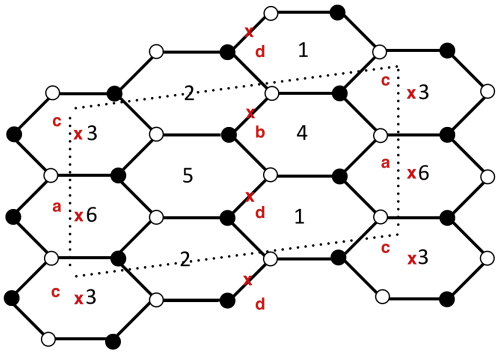

Figure 6.1: Dimer of $\mathbb{C}_3/\mathbb{Z}_6'$ with orientifold points. The labels a, b, c, d are used in the main text to list the orientifold point sign assignment.

For a suitable choice of orientifold point signs (a,b,c,d)=(+ + - -), the gauge theory for general ranks is

$$\begin{gathered} SO(n_6) \times U(n_1) \times U(n_2) \times Sp(n_3) \\ (\,\square_6,\, \overline{\square}_1) + (\,\square_1,\, \overline{\square}_2) + (\,\square_2,\, \overline{\square}_3) + \\ +(\,\square_6,\, \overline{\square}_2) + (\,\square_1,\, \square_3) + \square\!\!\square_2 + \overline{\square\!\!\square}_1 + \\ +[\,(\,\square_6,\, \square_3) + (\,\square_1,\, \square_2) + (\,\overline{\square}_1,\, \overline{\square}_2)\,] \quad . \end{gathered} \tag{6.2}$$

As discussed in [42], the orientifold group is $(1+\theta)(1+\omega+\omega^2)(1+\Omega\alpha(-1)^{F_L})$, where α acts as

$$(z_1, z_2, z_3) \rightarrow (e^{2i\pi/12}, e^{4i\pi/12}, e^{-6i\pi/12}). \tag{6.3}$$

The RR tadpole cancellation condition reads

$$-n_6 + n_2 + n_3 - n_1 - 4 = 0. \tag{6.4}$$

It can be solved by e.g. $n_1 = n_3 = 0$, $n_6 = N$, $n_2 = N + 4$. The gauge theory then becomes $SO(N) \times U(N+4)$ with matter $(\,\square\,,\,\overline{\square}\,) + (1,\,\begin{smallmatrix}\square\\\square\end{smallmatrix}\,)$ and vanishing superpotential. The rank assignment

$$n_1 = n_3 = n_5 = 0 \quad ; \quad n_6 = 1 \quad ; \quad n_2 = n_4 = 5 \tag{6.5}$$

produces a theory with gauge group $SO(1) \times U(5)$ and matter content $(\,\square\,,\,\overline{\square}\,) + (1,\,\begin{smallmatrix}\square\\\square\end{smallmatrix}\,)$. The $U(5)$ gauge factor is actually $SU(5)$ since the $U(1)$ gauge factor is anomalous and becomes massive after coupling to a RR field. Hence one gets a $SU(5)$ theory with chiral multiplets in the $10 + \overline{5}$ and no superpotential. This theory has been argued to show dynamical supersymmetry breaking [15, 163].

The argument for susy breaking is indirect, but compelling. Basically, the theory has a unique vacuum (i.e. trivial moduli space), and the anomaly matching conditions are so strong that cannot be satisfied by any reasonable supersymmetric spectrum. Therefore, susy breaking appears as the simplest option for the low-energy dynamics. The idea in this chapter is to bring this DSB system to a form usable as uplifting mechanism in attempts to realize de Sitter vacua in string theory, a la KKLT.

The indirect description of susy breaking implies that the IR theory is strongly coupled, and therefore non-calculable. This is hardly a drawback for uplifting applications, which only require information about the scaling the vacuum energy contribution with parameters. It therefore suffices to introduce a dynamical scale $\Lambda_{\rm DSB}$ to describe the scale of susy breaking strong dynamics, which also controls the vacuum energy of the susy breaking minimum in the rigid limit. The main extra input one needs is the embedding of this DSB sector in a warped throat to redshift this scale, and render the vacuum energy tunable.

6.2. Embedding DSB D-branes in a cascading host

In order to use this kind of DSB sector to uplift with a tunable cosmological constant, it is crucial that the DSB scale is tunable and hierarchically suppressed with respect to the bulk scales. This can be achieved, as in the original anti-D3-brane setup in [61], by locating the DSB brane sector at the bottom of a warped throat.

Recall that the field theory description of a warped throat corresponds to a field theory admitting a cascade of Seiberg dualities whose IR end is the DSB sector of interest. This seems problematic, because the quiver realizing the DSB theory is non-cascading by itself. However, there is a way out recently exploited in [50] (see [53, 55] for earlier implementations of this idea), which proceeds in two steps. The first, studied in this section, is to realize the DSB theory as the IR description of a suitable larger theory, which from now on I will refer to as the 'host', eventually admitting a duality cascade. The second, studied in section 6.2.1.2, is the description of the duality cascade for the host theory.

The warped throat embedding of the above orientifold of an orbifold can be easily done using web diagrams [142]. The web diagram of the orbifold is given by figure 6.2(a).

To host this theory, following the ideas in section 5.2.2, one can introduce two additional parallel lines (related by the orientifold projection) as shown in figure 6.2(b). By construction it admits a complex deformation to the $\mathbb{C}^3/\mathbb{Z}_6'$ singularity, by removal of the two lines.

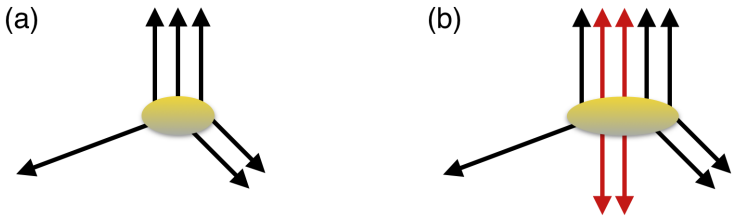

Figure 6.2: (a) External legs of the web diagram of the $\mathbb{C}_3/\mathbb{Z}_6'$ orbifold whose dimer is given by figure 6.1. (b) The addition of one line and its orientifold image provide the web diagram for a host configuration, which by construction can be deformed back to $\mathbb{C}_3/\mathbb{Z}_6'$.

The dimer corresponding to the web in figure 6.2(b) is shown in figure 6.3. The two lines added in the web diagram correspond to the new columns of rhombi that are each other's orientifold image.

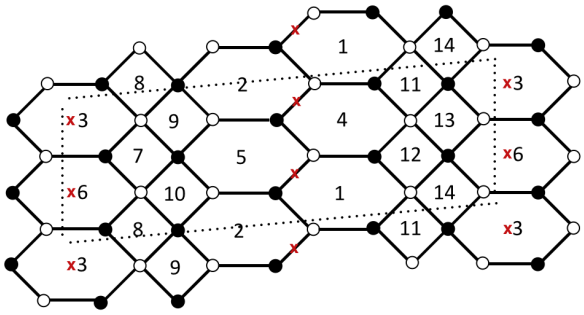

Figure 6.3: Dimer of the host theory for the DSB sector of D-branes at the $\mathbb{C}_3/\mathbb{Z}_6'$ orientifold.

6.2.1. Warped down DSB using the host cascade

The host theory described above admits a duality cascade, which provides the holographic dual of the embedding of the DSB sector in a warped throat. This cascade is described in this section.

Initially, I will first work for simplicity in the UV theory, with large numbers of branes, so ignoring the $\mathcal{O}(1)$ effects due to orientifolds, etc. This simplifies the analysis and displays the cascade structure more nicely. Later on I will consider the dualities near the IR of the cascade, where orientifold contributions will be taken into account.

The cascade involves dualities involving whole columns of hexagons/rhombi, already explored in [164–166]. This UV theory arises as a $\mathbb{Z}_2$ orbifold of parent theory that one obtains by omitting the $\mathbb{Z}_2$ orbifold action θ in (6.1) and UV completing it in a similar way to the one followed above. This parent theory admits a description in terms of HW brane configurations that I study to understand better the RG cascade.

6.2.1.1. Parent Hanany-Witten cascade

The parent singularity is described by the equation $xy = z^2w^5$, and by performing T-duality along the $\mathbb{S}^1$ direction x^6, one recovers a system of D3-branes at a singularity $xy = z^2w^5$, see [18]. It corresponds to the configuration of NS, NS' and D4-branes shown in figure 6.4.

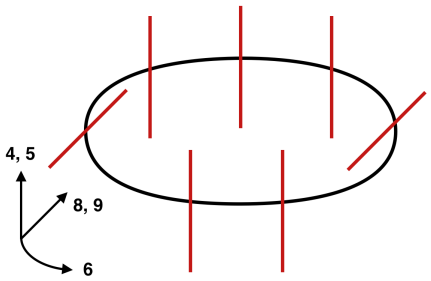

Figure 6.4: HW configuration of NS, NS' and D4-branes.

In this picture the cascade is nicely described because Seiberg dualities are brane crossings [21]. Thus, the cascade corresponds to moving the NS'-branes around the circle, crossing the NS-branes. Since the interest goes on orientifolded theories, the two NS'-branes will move in opposite directions in a $\mathbb{Z}_2$ symmetric way. The resulting picture is related to the cover space description of the eventual orientifold cascade.

The choice of ranks and the basic period of the cascade are shown in figure 6.5. At the level of the brane configuration, the changes in the numbers of D4-branes are determined by conservation of the linking number [99] for NS- and NS'-branes. Recall that the linking number for a 5-brane is given (in this simple configurations) by the difference

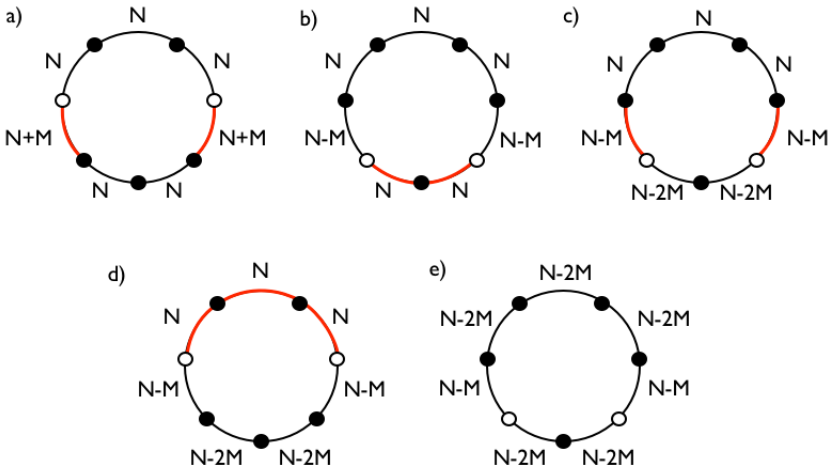

Figure 6.5: Structure of the basic period of the HW cascade. Black and white circles denote the two kinds of 5-branes. The gauge factors dualized in each step are shown as red intervals. After four steps, one recovers the original configuration with a reduced number $N' = N - 2M$ of regular D-branes, and the same number M of fractional branes.

in the numbers of D4-branes ending on it from both sides. This number corresponds to a vortex number from the viewpoint of the 5-brane worldvolume theory, and is conserved in any local deformation, including brane crossings.

From the viewpoint of the 4d field theory, the brane motions sometimes correspond to some Seiberg dualities involving $\mathcal{N} = 2$ fractional branes [22]. These are steps (b) to (c) and (d) to (e) in figure 6.5. I now provide some details about them.

Simultaneous dualization of two neighbouring gauge groups

Consider first the dualization taking from the configuration in (b) to (c) in figure 6.5. It involves the simultaneous dualization of the neighbouring intervals in red in (b), which does not directly follow from sequential application of dualities. The HW configuration describing the initial gauge theory is shown in figure 6.6(a).

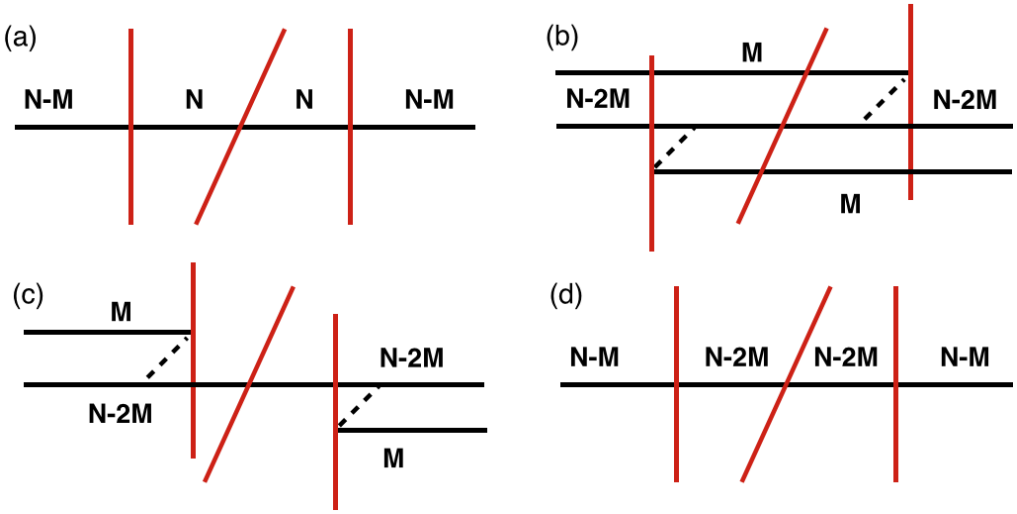

Figure 6.6: HW description of the simultaneous Seiberg duality of two neighbouring nodes. Vertical and tilted red lines represent NS- and NS'-branes, respectively, while horizontal black lines are D4-branes. Starting from the original theory in (a), move the NS-branes off along with M D4-branes (b). The NS-branes are subsequently moved across the NS'-brane (c), and brought back in line (d).

In the HW picture Seiberg duality is represented as the crossing of a NS5 and a NS5' brane. This can be achieved by moving the NS-branes off in say direction 7, together with M D4-branes as shown in figure 6.6(b). They are subsequently moved across the NS'-brane, and brought back into position. The resulting theory has the same geometry of NS- and NS'-branes, but the number of D4-branes in the middle segments is decreased.

The HW configuration easily translates into gauge theory data, allowing to read out the Seiberg dual field theories. The number of D4-branes in the dualized segments decreases by $2M$. This amount can be computed by using the amounts of colors and flavours the $\mathcal{N} = 2$ fractional branes sees. In this case one has $2(N - M)$ flavours and N colors from the $\mathcal{N} = 2$ fractional brane perspective. Following standard Seiberg duality rules, the dual theory has $\tilde{n}_c = 2(N - M) - N = N - 2M$ colors and the same amount of flavours. For the $\mathbb{Z}_2$ orbifold of this HW setup found on the singularity of interest of this

chapter, it is interesting to generalize this relation and write it as follows:

$$\tilde{n}_i = \Delta + n_i \quad ; \quad \Delta = \sum_{\text{adjacent}} n_i - \sum_{\text{dualized}} n_j \ , \tag{6.6}$$

where $\tilde{n}_i$ stands for the rank of the dualized gauge group after the dualization. The first sum goes over the ranks of gauge groups not dualized in the process (the ones with $N-M$ branes in this case) and the second sum goes over the dualized gauge groups (the ones starting with N branes). See that in this case $\Delta = 2(N-M) - 2N = -2M$, reproducing the step from figure 6.5(b) to (c).

Seiberg duality involving $\mathcal{N} = 2$ sectors

Consider now the dualization taking from the configuration in (d) to (e) in figure 6.5. It involves the simultaneous dualization of the three intervals in red in (d), including the one in the middle, which locally has $\mathcal{N} = 2$ supersymmetry. This cannot be described in terms of a usual sequence of dualities and requires similar techniques to the ones in the previous section. The HW configuration describing the initial gauge theory is now shown in figure 6.7(a).

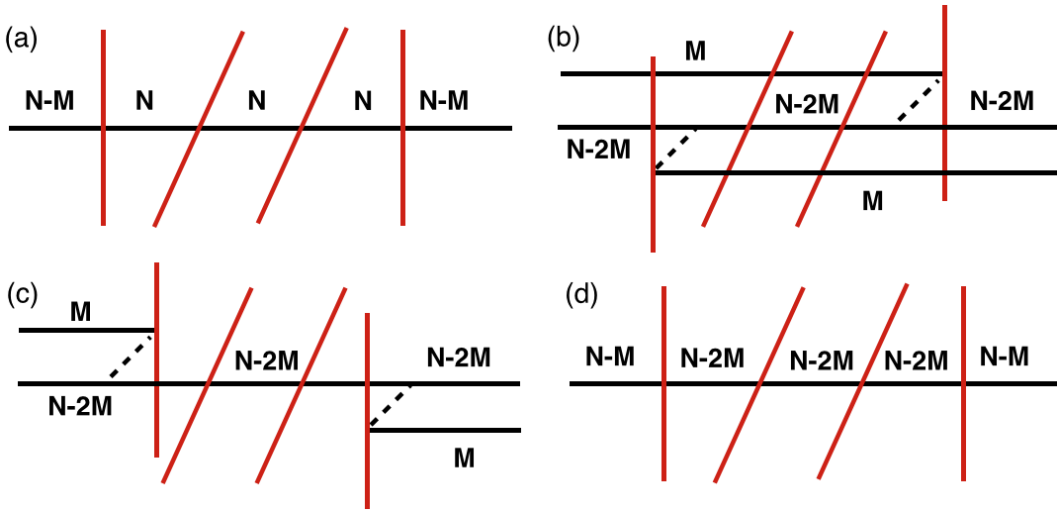

Figure 6.7: HW description of the simultaneous Seiberg duality involving an $\mathcal{N} = 2$ sector. In the original theory (a) first move the NS-branes off along with M D4-branes (b). The NS-branes are subsequently moved across the NS'-brane (c), and brought back in line (d).

The HW configuration and the brane moves corresponding to the overall Seiberg duality are shown in figure 6.7. The dualization process involves not only the gauge group arising from D4-branes between the NS'-branes, but also the adjacent ones, since in the HW picture it corresponds to moving the NS branes on both sides in opposite directions. In order to describe the dualization, one must first take the NS-branes to opposite points on direction 7 and then move them along direction 6 as shown in figure 6.7(b) and 6.7(c). Finally, putting the NS-branes back at $x^7 = 0$, one ends up with the configuration in figure 6.7(d), that looks very similar to the initial one, the only difference being the amount of D4-branes in all the intervals between both NS-branes.

Once again, the two brane configurations only differ on the amounts of D4-branes on the dualized intervals, and therefore the dual gauge theory differs only on the rank of the three dualized gauge groups. The amount of colours on the Seiberg dual gauge theory can be obtained by following the ideas in the previous section. Once again, it is interesting to provide a general formula relating the ranks of the gauge factors on the two dual theories for orbifolds of this HW setup, given by

$$\tilde{n}_i = \Delta + n_i \quad ; \quad \Delta = \sum_{\text{adjacent}} n_i - \sum_{\text{dualized, no NS'-NS'}} n_j \ . \tag{6.7}$$

The second sum goes over ranks of dualized gauge groups between a NS and a NS'-brane, which in the dimer corresponds to columns of rectangles, but not hexagons. In this case $\Delta = 2(N-M) - 2N = -2M$, in agreement with figures 6.5(d) and (e).

6.2.1.2. The cascade in the DSB host theory

With the knowledge acquired from the previous HW brane configuration it is possible to extrapolate the gauge dynamics to the RG cascade of the host theory for the DSB sector. Since this singularity is a $\mathbb{Z}_2$ orbifold of the HW brane configuration in section 6.2.1.2, the cascade pattern follows very easily from the one above. In particular, each node of the HW theory is related to a column of either hexagons or rhombi in the dimer of interest, and the dualization of a HW node by brane crossing is related to the dualization of whole columns in the dimer. This is a particular application of ideas already introduced in [165].

I will first deal with the discussion in the UV, where the numbers of regular and fractional branes are large compared with the orientifold plane charge. Hence, the effects of the orientifold are suppressed and can be neglected, save for the fact that the cascade should respect the $\mathbb{Z}_2$ symmetry. Afterwards I will deal with the IR dyanmics, where the $\mathcal{O}(1)$ effects due to the orientifold plane charge will no longer be negligible.

The far UV

Consider the theory described by figure 6.3 without the orientifold points. This is directly related to the HW configuration in figure 6.5(a) with the columns $(1,4)$, $(11,12)$, $(13,14)$, $(3,6)$, $(7,8)$, $(9,10)$ related to the HW intervals according to the following rule: columns of hexagons relate to intervals between parallel 5-branes, while columns of rhombi relate to intervals between orthogonal 5-branes.

According to this relation, consider the initial ranks at certain point in the UV of the cascade:

$$\begin{aligned} n_1 = n_2 = n_3 = n_4 = n_5 = n_6 = n_7 = n_8 = n_{13} = n_{14} = N \\ n_9 = n_{10} = n_{11} = n_{12} = N + M \end{aligned} \tag{6.8}$$

with $N \gg M$.

The next step in the cascade is to dualize nodes 9, 10, 11 & 12. As discussed in [165], such dualizations of columns change the adjacent columns from hexagons to squares (for 1,4 and 2,5) and vice-versa (for 7,8 and 13,14), resulting in the dimer shown in figure 6.8 (without the orientifold points).

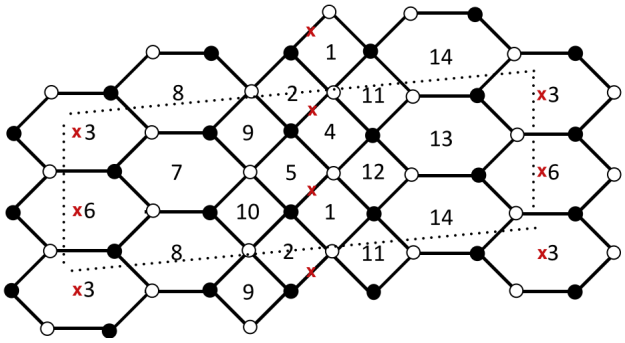

Figure 6.8: Dimer of the DSB host theory after performing Seiberg duality in nodes 9, 10, 11 & 12.

The ranks after performing the duality are

$$\begin{aligned} n_1 = n_2 = n_3 = n_4 = n_5 = n_6 = n_7 = n_8 = n_{13} = n_{14} = N \\ n_9 = n_{10} = n_{11} = n_{12} = N - M \end{aligned} \tag{6.9}$$

in agreement with the result in the parent HW configuration figure 6.5(b).

The next step is to dualize 1, 2, 4, 5, which is a generalization of the process in figure 6.6. The ranks after the dualization process can be computed using (6.6)

$$\begin{aligned} n_1 = n_2 = n_4 = n_5 = N - 2M \\ n_3 = n_6 = n_7 = n_8 = n_{13} = n_{14} = N \\ n_9 = n_{10} = n_{11} = n_{12} = N - M \end{aligned} \tag{6.10}$$

and agree with the fact that this cascade behaves as the one in the parent theory in figure 6.5. It is important to note at this point that the dualization process does not change the shape of the dimer. This can understood starting from figure 6.6, where the initial and final setups (a) and (d) only differ on the number of D4-branes between the 5-branes. This can be extrapolated to the dimer description of the HW configuration, where the two Seiberg dual theories have the same dimer but with different ranks. Finally, performing a $\mathbb{Z}_2$ orbifold will not change this structure. The same thing will happen when dealing with the dualization of gauge factors 3 and 6, together with 7, 8, 13, 14: the HW configuration only differs on the ranks and thus the orbifolds of this setup will behave the same way on the dimer picture.

A detailed discussion of the remaining steps is unnecessary, with the above explanations, since the cascading behaviour is directly inherited from the cascade in the HW brane configuration above.

The near IR regime

When approaching to the IR, the number of regular branes has decreased and eventually becomes not large enough compared with the orientifold charge. Hence, the last steps of the cascade require dealing with the latter.

Consider the near IR regime theory to be given by the by-now familiar dimer, in

figure 6.3, with this specific rank choice:

$$\begin{gathered} n_1 = n_5 = 6+2M \quad ; \quad n_7 = n_{14} = n_3 = 6+2M \quad ; \quad n_{10} = n_{12} = 12+3M \\ n_2 = n_4 = 11+2M \ ; \ n_9 = n_{11} = 11+3M \ ; \ n_8 = n_{13} = 11+2M \ ; \ n_6 = 7+2M \ , \end{gathered} \tag{6.11}$$

with $M \gg 1$. Start by dualizing nodes 9, 10, 11, 12 following the order in the HW configuration. This dualization has two consequences: on the one hand, it decreases the ranks of these gauge groups according to usual Seiberg duality rules. On the other hand, it changes the shape of the dimer to figure 6.8. The ranks after the dualization are:

$$\begin{gathered} n_1 = n_5 = 6+2M \quad ; \quad n_7 = n_{14} = n_3 = 6+2M \quad ; \quad n_{10} = n_{12} = 5+M \\ n_2 = n_4 = 11+2M \ ; \ n_9 = n_{11} = 6+M \ ; \ n_8 = n_{13} = 11+2M \ ; \ n_6 = 7+2M \ . \end{gathered} \tag{6.12}$$

At this point one can perform double Seiberg duality at nodes 1, 5, 2, 4. Following the ideas above, the dimer after performing the dualization looks the same as the one before the dualization, and the difference between both dual theories lies on the ranks of the dualized gauge groups. In the double Seiberg dualities performed so fat there was no orientifold, and this is the first time that the orientifold contribution must be considered. The effect of the orientifold on the duality is that it modifies the ranks of the gauge factors as compared to the non-orientifold case, due to its RR charge. When performing the double dualization, the orientifold effect will come on the rank assignment, but this does not require any modification the procedure of the non-orientifold case. The ranks of all these gauge groups after the duality decrease by an amount Δ, that according to (6.6) is given by

$$\Delta = n_9 + n_{10} - n_1 - n_2 = -6 - 2M \ . \tag{6.13}$$

This change on the ranks of groups 1, 5, 2, 4 leaves the ranks after the double duality

$$\begin{gathered} n_1 = n_5 = 0 \quad ; \quad n_7 = n_{14} = n_3 = 6+2M \quad ; \quad n_{10} = n_{12} = 5+M \\ n_2 = n_4 = 5 \ ; \ n_9 = n_{11} = 6+M \ ; \ n_8 = n_{13} = 11+2M \ ; \ n_6 = 7+2M \ . \end{gathered} \tag{6.14}$$

Now dualize faces 9, 10, 11, 12 again to end up with a dimer with the previous shape and ranks

$$\begin{gathered} n_1 = n_5 = 0 \quad ; \quad n_7 = n_{14} = n_3 = 6+2M \quad ; \quad n_{10} = n_{12} = 6+M \quad ; \quad n_2 = n_4 = 5 \\ n_9 = n_{11} = 5+M \quad ; \quad n_8 = n_{13} = 11+2M \quad ; \quad n_6 = 7+2M \ . \end{gathered} \tag{6.15}$$

At this point one must dualize the hexagon column formed by faces 3 and 6 together with the adjacent rhombi columns with faces 7, 8 and their orientifold images 13, 14. Once again, the dimer after the duality has the same shape and decreased ranks in the dualized gauge groups. The change in all these ranks this time is given by (6.7)

$$\Delta = n_9 + n_{10} - n_7 - n_8 = -6 - 2M \ , \tag{6.16}$$

leaving the ranks after the dualization

$$\begin{gathered} n_1 = n_3 = n_5 = n_7 = n_{14} = 0 \quad ; \quad n_{10} = n_{12} = 6+M \\ n_2 = n_4 = n_8 = n_{13} = 5 \quad ; \quad n_{11} = n_9 = 5+M \quad ; \quad n_6 = 1 \ , \end{gathered} \tag{6.17}$$

that as I will now show to produce partial confinement leading to the DSB gauge theory.

6.2.2. Confinement onto the DSB theory

For the rank choice in (6.17) with $M \gg 1$ one obtains a large deformation. At this point the host theory experiences confinement of some of its gauge factors, after which the effective field theory describing the light degrees of freedom is precisely the DSB theory.

The superpotential at this point can easily be read from the dimer after taking into account that many faces are empty:

$$W = X_{9,8}X_{8,10}X_{10,2}X_{2,9} \ . \tag{6.18}$$

At this point gauge groups 9 and 10 and their orientifold images 11 and 12 have $N_c > N_f$ and thus confine, developing ADS superpotentials. The dynamics of both groups is described in terms of their mesons. Looking at the dimer one would expect the mesons to be

$$\mathcal{M} = \begin{pmatrix} M_{82} & M_{87} \\ M_{52} & M_{57} \end{pmatrix} = \begin{pmatrix} X_{8,10}X_{10,2} & X_{8,10}X_{10,7} \\ X_{5,10}X_{10,2} & X_{5,10}X_{10,7} \end{pmatrix} \tag{6.19}$$

$$\mathcal{N} = \begin{pmatrix} N_{28} & N_{25} \\ N_{78} & N_{75} \end{pmatrix} = \begin{pmatrix} X_{29}X_{98} & X_{29}X_{95} \\ X_{79}X_{98} & X_{79}X_{95} \end{pmatrix} \tag{6.20}$$

but since several nodes have rank zero, there are no mesons charged under these gauge groups. This leaves really one meson for each confining gauge group:

$$\mathcal{M} = M_{82} = X_{8,10}X_{10,2} \quad ; \quad \mathcal{N} = N_{28} = X_{29}X_{98} \ . \tag{6.21}$$

The superpotential, taking into account the strong dynamics of these groups, becomes

$$W = \mathcal{M}\mathcal{N} + M\left(\det \mathcal{N}\right)^{-1/M} + (M+1)\left(\det \mathcal{M}\right)^{-1/(M+1)} \ . \tag{6.22}$$

Using the F-terms of $\mathcal{M}$ and $\mathcal{N}$ it is easy to see that both get a vev. This breaks gauge groups $SU(n_8) \times SU(n_2)$ and $SU(n_7) \times SU(n_5)$ to their diagonals, and the same happens with their orientifold images. The resulting theory agrees with the recombined dimer which describes the DSB theory.

This confinement pattern can be easily studied using the dimer diagram, as shown in figure 6.9. Specifically, since nodes 9, 10, 11 and 12 confine and force some of their mesons to acquire non-zero vevs, this breaks their respective flavour symmetry factors (corresponding to neighbouring faces in the dimer) to the diagonal combinations. The resulting theory is described by the dimer with recombined faces, which is easily recognized as that in figure 6.3. The fact that this confinement corresponds to the removal of lines in the web diagram, c.f. figure 6.2 can be easily shown using the techniques in [41].

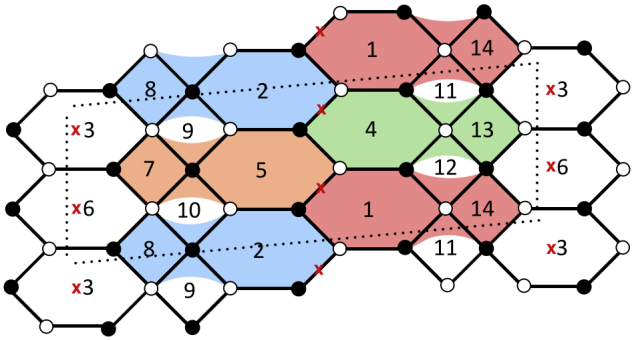

Figure 6.9: Dimer description of partial confinement in the host theory, leaving the DSB dimer theory at low energies. Confinement of nodes 9, 10, 11 and 12 triggers non-zero vevs for suitable mesons, which higgs certain gauge factors to the diagonal combinations, depicted as the recombination of dimer faces shaded with same color. The resulting theory is easily seen to agree with figure 6.3.

7

D-brane instantons as gauge instantons in orientifolds of chiral quiver theories

This last chapter before the conclusions takes yet another direction. This time the focus goes on stringy instantons on the bottom of orientifolds of warped throats, thus requiring to use the ideas in chapter 5.

D-brane instantons can generate superpotential contributions to gauge theories on D-branes, which are forbidden to all orders in perturbation theory by global symmetries [167–169], see [170,171] for reviews. These global symmetries, often anomalous, arise from the $U(1)$ factors inside the $U(n_i)$ groups associated to n_i fractional branes of a given type. The contributions of D-brane instantons are exponentially sensitive to the volume of the cycles they wrap. There is a vast list of scenarios in which such effects are crucial. Just to mention a few, they can generate neutrino masses [167, 168] (see also [172]), Yukawa couplings [173], the μ-term in SUSY extensions of the Standard Model [174, 175], or be crucial in SUSY breaking [59, 60, 176] or its mediation [177], as well as in rare processes [178–181] (see [170, 171] for reviews of these and other applications). Achieving these effects typically requires introducing orientifold projections to remove additional fermion zero modes associated to the otherwise underlying $\mathcal{N} = 2$ supersymmetry [172, 182, 183].

In some cases, when D-brane instantons sit on top of gauge D-branes, they can be interpreted as ordinary gauge instantons. In other more general situations, the D-brane instantons are a consequence of the UV completion of the theory. In other words, restricting the dynamics to the naive low-energy gauge theory one loses the information about the possible presence of these D-brane instantons. These two possibilities have led to distinction between 'gauge' and 'exotic' D-brane instantons. Interestingly, in some situations, it is also possible to derive exotic instantons from an alternative, fully gauge theoretic, UV completion [137], showing that the distinction is to some extent an artifact of the low-energy truncation. This completion involves a cascade of Seiberg dualities and some non-trivial IR dynamics of the gauge theories.

By now, there are various explicit examples in the literature for which this has been achieved [137, 184].[1] However, all these examples correspond to theories that, before orientifolding, are non-chiral. This may be problematic in certain applications when these theories are combined with extra ingredients, which may remove the non-chiral instanton fermion zero modes, and consequently the insertions of charge matter fields in the instanton amplitude evaporate. An interesting analysis of the last Seiberg duality transformations, but not the full cascades, leading to D-brane instantons in some chiral theories has appeared in [138].

[1] See also [185, 186] for similar conclusion in different approaches.

One of the main goals of this chapter is to construct similar UV completions for theories that are quiral even before orientifolding. This can be taken as a mere proof of existence, but can be relevant for the applications mentioned above, in which now the chiral nature of the theory protects the instanton fermion zero modes, and the presence of charged matter fields in the instanton induced operator is also protected. Another novel feature of some of the theories I consider, absent from previous constructions in the literature, is the presence of D-brane instanton couplings involving flavors.

As an application of the ideas introduced in this chapter, I provide a UV duality cascade completion and gauge theory derivation for the exotic D-brane instantons models considered in [187], where the instanton effects were told to break conformal invariance.

The chapter is organized as follows. Section 7.1 contains a lightning review of D-brane instantons and the field theory couplings they can generate. Section 7.2 summarizes the general approach used for finding cascading UV completions of D-brane instantons. In section 7.3 I describe chiral IR theories that can be directly completed in terms of cascades, which maintain the underlying geometry at which D3-branes are located. Then, in section 7.4 I turn to consider chiral IR theories that do not correspond directly to cascading geometries, but can be UV completed in terms of a duality cascade which, upon complex deformation produces the IR theory of interest. Since the earlier examples correspond to orientifolds line actions in the dimer, section 7.5 briefly discusses models with orientifold points. Finally, in section 7.6 I discuss the introduction of flavor D7-branes under which some of the instanton fermion zero modes are charged.

7.1. Superpotential couplings from D-brane instantons

In this section I quickly review the basic ideas on how gauge theories on stacks of space-time filling D-branes can be perturbed by superpotential couplings generated by Euclidean Dp-brane instantons [167–169].[2] More detailed techniques will be explained in later sections as needed.

Consider first the extended quiver diagram in figure 7.1(a), which encodes the relevant field content for a configuration with D-brane instantons and 4d spacetime filling gauge D-branes. In this figure, circles correspond to two $SU(N)$ gauge groups in the quiver living on 4d space-filling branes which, in principle, might contain additional nodes and chiral fields. The ranks of both nodes need to be equal for a non-vanishing instanton contribution to exist. X_{ij} can correspond to a single bifundamental field or, more generally, to a product of them of the form $X_{ij} = X_{ik_1} X_{k_1 k_2} \dots X_{k_n j}$, where intermediate color indices are contracted. The explicit form of X_{ij} is controlled by the geometry of the D-brane instanton under consideration. The D-brane instanton is represented by the triangular node in figure 7.1. There are charged fermionic zero modes α_i and β_j at the intersections between the instanton and the gauge D-branes. The instanton action contains the following term

$$\mathcal{L} = \alpha_i X_{ij} \beta_j. \tag{7.1}$$

[2] D-brane instantons can lead to other modifications of these gauge theories, by higher derivative operators, but this is beyond the focus of this chapter. For some examples, see e.g. [188].

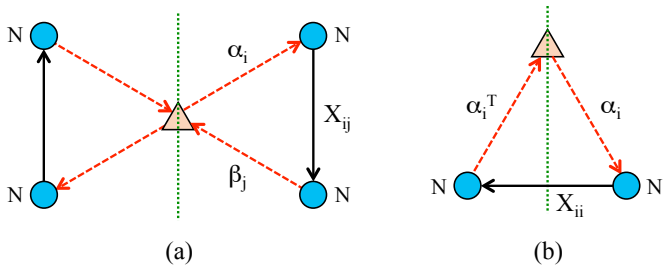

Figure 7.1: (a) Quiver for an instanton with zero modes coupling to a field not invariant under the orientifold action. The green line represents the fixed locus under the orientifold action. No D-brane instanton coupling is generated if the ranks of the nodes connected by X_{ij} differ. (b) Quiver for an instanton with zero modes coupling to a field mapped to itself under the orientifold action.

Strings with both endpoints on the instanton give rise to neutral zero modes. Instantons break 1/2 of the $\mathcal{N}=1$ supersymmetry preserved by the D-branes at the Calabi-Yau and hence there are two fermionic zero modes, the corresponding goldstinos, which are represented by Grassmann variables θ^α. However, the sector of open strings with both endpoints on the D-brane instanton sees an enhanced $\mathcal{N}=2$ supersymmetry so one should generically expect two additional fermionic zero modes. In order to generate non-vanishing superpotential couplings, it is necessary to have only two fermionic zero modes, which are used to saturate the superspace measure. It is possible to imagine various ways in which the two extra zero modes can be in principle eliminated. A particularly clean way of getting rid of them, which will be realized in the theories I consider, is by projecting them out with an orientifold plane reducing the instanton worldvolume group to $O(1)$ (these are dubbed $O(1)$ instantons). Therefore, in this chapter I consider configurations in which the D-brane instanton is on top of an orientifold plane, figure 7.1(a). Consider first the case where the orientifold is not relating the two $SU(N)$ nodes under which fermion zero modes are charged (i.e. the operator X_{ij} is not mapped to itself under the orientifold action). Integrating out the zero modes, the following contribution to the gauge theory superpotential is generated

$$W_{inst} = M_s^{3-N} e^{-V_\Sigma/g_s} \det X_{ij} \ , \tag{7.2}$$

with M_s the string scale and V_Σ the volume of the cycle Σ wrapped by the instanton in string units. I assumed that the numerical constant in front of the expression is $\mathcal{O}(1)$.

Consider now the case that the orientifold identifies the two $SU(N)$ nodes of the quiver, figure 7.1(b) For $O(1)$ instantons, the orientifold of interest is such that the operator X_{ij} is projected down to the antisymmetric representation (or its conjugate) of the surviving $SU(N)$. The orientifold also identifies the fermions zero modes $\beta_j \sim \alpha_j{}^T$, so the instanton action now contains an interaction of the form

$$\mathcal{L} = \alpha_i X_{ii} \alpha_i{}^T \ . \tag{7.3}$$

After integration over all fermionic zero modes, the superpotential picks a contribution of the following form

$$W_{inst} = M_s^{3-N/2} e^{-V_\Sigma/g_s} \mathrm{Pf}\, X_{ij} \ . \tag{7.4}$$

It is important to emphasize an important difference between non-chiral and chiral quivers. Non-chiral quivers can be regarded as a subset of the theories described above for which both $SU(N)$ nodes happen to be the same, whereas chiral examples correspond to the generic case. This has an impact on the behavior of the instantons with respect to $U(1)$ symmetries. Actually, the gauge groups on the gauge D-branes are actually $U(N) = SU(N)\times U(1)$. The $U(1)$ factors either become massive due to the Green-Schwarz anomaly cancellation mechanism [189] or become free in the IR. For non-chiral theories, the operator X_{ij} is uncharged under the $U(1)$'s, and so is the field theory operator induced by the instanton. On the other hand, chiral examples produce field theory operators violating the $U(1)$ symmetries. It is therefore in the chiral examples that $U(1)$ symmetries forbid couplings such as (7.2) and (7.4) perturbatively, and are generated by the instantons. The fact that the instanton amplitude implies some charge violation is related to the chiral nature of the charged fermion zero modes, and is robust under deformations of the theory.

7.2. General approach to field theoretic UV completions

Before presenting a detailed analysis of a cascading UV completion of the theories of interest, it is useful to present a general roadmap summarizing its key points. While this class of theories has novel features which will be emphasized as they appear, the general approach is similar to the one used in other examples [137, 138, 184].

The starting point is a gauge theory, which corresponds to the IR of a more complete UV configuration that includes extra ingredients to support the instanton generating the non-perturbative correction. In principle, it is possible to take a bottom-up approach and try to guess a UV quantum field theory that results in the desired one at low energies. This is however rather challenging, since some of the gauge groups may disappear while flowing to the IR (by confinement or other strong coupling phenomena). The strategy in this chapter is based on using ST constructions to determine the UV theory. Namely, I will describe ST configurations of D-branes at singularities to engineer the IR theory, and use toric geometry technology to construct UV completions with the appropriate IR flow. Their orientifold quotients can be constructed systematically using the tools in section 2.3.5 and in [42].

The general strategy to follow to construct such UV completions can be summarized this way:

- The first step is to engineer the geometry probed by the D-branes realizing the IR gauge theory. This typically corresponds to a quiver gauge theory, which must involve additional empty nodes to support the stringy instantons. As explained in section 7.1, the instantons need to have an $O(1)$ orientifold projection, hence the opposite orientifold action on spacefilling D-branes leads to USp gauge groups. For the cases considered in this article, the gauge group takes the form $\prod_i SU(n_i) \times \prod_a USp(n_a)$.[3]
- The next step is to construct the corresponding duality cascade. In principle, it is necessary to specify the ranks and dynamical scales of the gauge groups (even for

[3]Even restricting to D-branes at toric singularities, it is possible to have multiple USp nodes, and also to simultaneously include SO ones. Since the latter do not support interesting instantons in the IR, for notational simplicity I will ignore the SO factors in the discussions.

those empty in the IR theory) at some UV scale, since this information determines the sequence of dualizations. In practice, I will exploit examples where this analysis has already been carried out (or orbifolds thereof), and apply the dualities with the rule of thumb that the node that is dualized at each step is asymptotically free. If the IR theory does not admit a direct UV completion with a duality cascade, one must embed it as the IR result of a confinement process of a more involved theory with additional nodes, such that the latter does admit a cascade completion in its UV. Explicit examples of both kinds of behaviors will be provided.

- In some models, I will be interested in introducing additional flavors, obtained by enriching the systems of D3-branes at singularities with additional D7-branes. These extra flavors modify the strict periodicity of the cascades, by $\mathcal{O}(1/n_i)$ corrections, where n_i denotes the ranks of the gauge factors. In the gravity dual counterpart, they correspond to numbers of D3-branes, and the corrections are due to one-loop effects from the D7-brane backreaction; ignoring them corresponds to the familiar probe approximation, in which the D7-branes simply probe the geometry generated by the fractional D3-brane duality cascade and their IR deformation.
- The last step is to verify that, upon running the cascade down, one recovers the original IR gauge theory of interest (modified by the non-perturbative operator). This heuristically corresponds to the extrapolation of the cascade until the number of D3-branes reaches a lower bound. More rigorously, the procedure takes the theories beyond the range of validity of Seiberg duality; requiring to study the strong dynamics of the last steps in the cascade. This sometimes involves confinement and a complex deformation of the moduli space, reflecting geometric transitions in the underlying singularities.

All these ideas are illustrated in detail in the explicit examples considered in the next sections.

7.3. Cascading geometries

7.3.1. Cascading versus non-cascading geometries

It is convenient to classify IR theories according to whether they admit fractional branes, which trigger duality cascades, or not. These are known as *cascading* and *non-cascading* geometries, respectively. All examples in the literature in which D-brane instanton couplings have been UV completed by cascading geometries associated to non-chiral theories. Since fractional branes are related to anomaly free rank assignments for gauge groups, non-cascading geometries can only arise when considering chiral theories. The UV completion of non-cascading geometries requires additional ingredients, which will be presented in section 7.4. In this section, I consider the simpler case of chiral theories for cascading geometries.

7.3.2. D-brane instanton couplings

For concreteness I will carry out the discussion for a prototypical example, the $\mathbb{F}_0$ theory, which corresponds to a chiral $\mathbb{Z}_2$ orbifold of the conifold. The quiver diagram for

one of the two toric phases of $\mathbb{F}_0$ is given in figure 7.2[4] , where the ranks n_i of the gauge groups correspond to the numbers of (fractional) branes wrapped at the singularity and are constrained by the cancellation of non-abelian anomalies. The anomaly constraints are modified in the presence of flavor branes, which will be introduced later on, so for the moment the ranks are kept general and I will focus on the structure of the quiver theory. The superpotential is

$$W = X^1_{12}X^1_{23}X^2_{34}X^2_{41} - X^1_{12}X^2_{23}X^2_{34}X^1_{41} - X^2_{12}X^1_{23}X^1_{34}X^2_{41} + X^2_{12}X^2_{23}X^1_{34}X^1_{41}\,. \tag{7.5}$$

The theory has an $SU(2)\times SU(2)$ global symmetry under which the fields on each side of the square transform as doublets, whose components are indicated by the superindices.

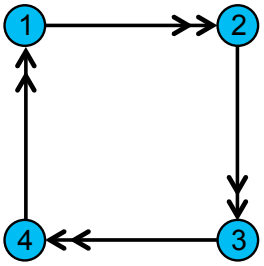

Figure 7.2: Quiver diagram for $\mathbb{F}_0$.

In order to properly study the orientifold of this theory it is better to consider the corresponding dimer, or the graph-dual periodic quiver, which are shown in figure 7.3. In the following I consider the orientifold line shown in figure 7.3. This theory also admits orientifolds associated to fixed points in the dimer, but I will not consider this possibility, see section 7.5 for orientifolds with fixed points in the dimer.

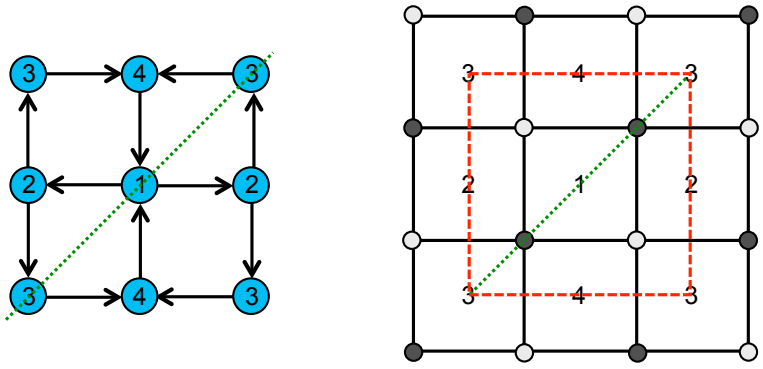

Figure 7.3: The periodic quiver and dimer diagram for the $\mathbb{F}_0$ theory.

Taking the orientifold line charge such that the instanton has a worldvolume group $O(1)$ to get rid of unwanted fermion zero modes; its action on gauge branes is of USp

[4]It was previously argued that dimers diagrams contains more information than quivers and thus are in general more useful. For the setups with flavors from D7-branes that I will present in this chapter quivers turn out to be more useful in order to keep track of the matter content of the theory. Furthermore, I will often use a diagram in 'between': the periodic quiver. This quiver is graph-dual to the dimer (so it encodes the superpotential as well) and allows to easily include the flavors.

kind. The orientifolded theory has three gauge groups [5]

$$USp(n_1) \times USp(n_3) \times U(n_2) \tag{7.6}$$

and four bifundamental chiral multiplets, since the orientifold identifies nodes $2 \leftrightarrow 4$ and relates $X^a_{41} \leftrightarrow X^{a\,T}_{12}$ and $X^a_{34} \leftrightarrow X^{a\,T}_{23}$ for $a = 1, 2$. I took the convention of preserving fields (and coupling) on the right hand side of the orientifold line in the dimer. The corresponding superpotential can be obtained by truncating (7.5) onto invariant states, and becomes

$$W = X^1_{12} X^1_{23} X^{2\,T}_{23} X^{2\,T}_{12} - X^1_{12} X^2_{23} X^{2\,T}_{23} X^{1\,T}_{12} - X^2_{12} X^1_{23} X^{1\,T}_{23} X^{2\,T}_{12} \,, \tag{7.7}$$

with appropriate contractions of the color indices.[6] Two of the original terms are identified, resulting in three terms. The transposition arises when relating fields to their orientifold images and allows the standard contraction of color indices. This is in agreement with the structure of the superpotential in the orientifolded dimer, shown in figure 7.3, as two of the nodes in the dimer are identified by the orientifold.

The configurations of interest are similar to the one in figure 7.4, where the vertical green dashed line schematically represents the effect of the orientifold projection in the quiver and two stacks of flavor branes represented by square nodes were added (actually, one stack and its orientifold image). Node 1 is taken to be empty in order to support a 'exotic' D-brane instanton. With the above choice of orientifold charge, the instanton has a worldvolume $O(1)$ group and the orientifold removes extra neutral fermion zero modes. Since the action on gauge branes is of USp kind, one must introduce at least two D3-branes at node 3. Including n_2 deformation fractional branes, these are responsible for driving the duality cascade in the UV, and additional $\mathcal{O}(1)$ D3- and D7-branes are necessary to render the structure anomaly free. The ranks of nodes 2 and 3 and the number of D7-branes are kept as general as possible, while consistent with anomaly cancellation. The D7-branes introduce D7-D3 flavors, with cubic couplings 73-33-37 to the D3-D3 chiral multiplets, described by triangles of arrows in the quiver. The detailed structure of these couplings is not necessary since the purpose of the D7-D3 flavors is to cancel anomalies and play no further role in the analysis.[7]

The structure zero modes and their couplings to D3-D3 fields are identical to those on space-filling D-branes. Hence, from (7.5) it is possible to infer the following couplings in the instanton partition function of the unorientifolded theory

$$\lambda^1_{12} X^1_{23} X^2_{34} \lambda^2_{41} - \lambda^1_{12} X^2_{23} X^2_{34} \lambda^1_{41} - \lambda^2_{12} X^1_{23} X^1_{34} \lambda^2_{41} + \lambda^2_{12} X^2_{23} X^1_{34} \lambda^1_{41} \,. \tag{7.8}$$

[5] The convention here is $USp(N_c) = Sp(N_c/2)$, where N_c is an even number. This convention has the advantage of capturing the number of branes in the configuration in a simple way: $USp(N_c)$ gauge group arises from N_c D-branes in the parent theory at the corresponding node, which is fixed under the orientifold. The number of flavors N_f is defined as the number of number of chiral multiplets in the fundamental representation (equivalently, half the chiral multiplets in the fundamental representation in the covering space), which is N_c-dimensional.

[6] Since the theory now has SU and USp groups, one must contract each kind of index in a different way. SU indices are directly contracted, while USp ones are contracted with the USp invariant tensor J.

[7] In addition, generically, mesons that are bifundamental of a pair of D7-brane nodes can be generated whenever a gauge group is dualized in a flavored quiver. Depending on the theory, such mesons can become massive after a number of steps in the cascade or accumulate. These chiral fields are neutral under all gauge symmetries and do not affect the analysis, so I will not include them in the discussion of any of the models in this chapter.

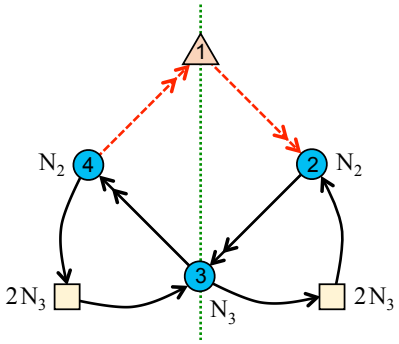

Figure 7.4: The $\mathbb{F}_0$ quiver with an empty node, supporting a D-brane instanton. Here n_3 is an even number since the group 3 is of USp kind.

In addition to the D3-D3 field identifications, the orientifold relates $\lambda^a_{12} \leftrightarrow \lambda^{a\,T}_{41}$, for $a = 1, 2$. Then, (7.8) becomes

$$\lambda^1_{12} X^1_{23} X^{2\,T}_{23} \lambda^{2\,T}_{12} - \lambda^1_{12} X^2_{23} X^{2\,T}_{23} \lambda^{1\,T}_{12} - \lambda^2_{12} X^1_{23} X^{1\,T}_{23} \lambda^{2\,T}_{12} \,, \tag{7.9}$$

which can equivalently be obtained from (7.7) by replacing some fields by zero modes.

Integrating out the charged fermionic zero modes, the following non-perturbative D-brane instanton superpotential is obtained:

$$W \sim \mathrm{Pf}\, \mathcal{N}_{22} \,, \tag{7.10}$$

where $\mathcal{N}_{22}$ is the matrix of D3-D3 mesons of node 3 (note that it does not include the D3-D7 flavors)

$$\mathcal{N}_{22} = \begin{pmatrix} \mathcal{N}^{11}_{22} & \mathcal{N}^{12}_{22} \\ \mathcal{N}^{21}_{22} & \mathcal{N}^{22}_{22} \end{pmatrix} = \begin{pmatrix} X^1_{23} X^{1\,T}_{23} & X^1_{23} X^{2\,T}_{23} \\ X^2_{23} X^{1\,T}_{23} & X^2_{23} X^{2\,T}_{23} \end{pmatrix} . \tag{7.11}$$

In constructing $\mathcal{N}_{22}$ one should take into account the appropriate contractions of color indices at node 3 I alluded to before. The subindices emphasize that the resulting $\mathcal{N}_{22}$ transforms in the adjoint representation of node 2.

Before concluding, it is important to emphasize that the origin of (7.10) is the stringy instanton sitting on node 1, and not the strong dynamics of node 3.

7.3.3. The cascade

This theory has a UV completion which accepts a periodic cascade of Seiberg dualities that I now explain.

The unorientifolded cascade

It is convenient to discuss the cascade in the unorientifolded theory first. This cascade has been investigated in detail in [40, 122, 190].

Consider starting from the quiver in figure 7.5(a), which corresponds to N regular D3-branes and M fractional branes, at some point in the UV. The periodic cascade corresponds to repeating the sequence of dualizations (1,3,2,4), i.e. sequentially dualizing pairs of diagonally opposite nodes.

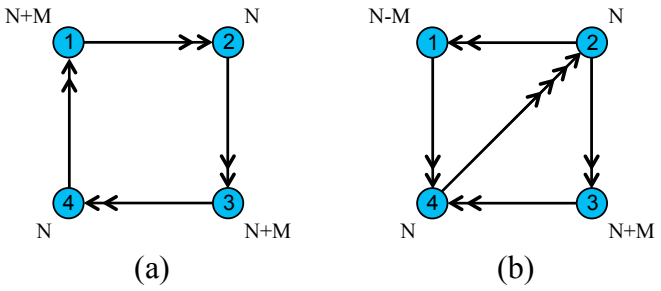

Figure 7.5: (a) Quiver diagram for one of the phases of $\mathbb{F}_0$ for N regular D3-branes and M fractional branes. (b) The quiver diagram after Seiberg dualizing node 1.

The first step is to take the setup in figure 7.5(a) and dualize node 1, to obtain the quiver shown in figure 7.5(b). The four chiral fields in the diagonal connecting nodes 4 and 2 arise as mesons of node 1. Dualizing node 3, four new mesons are generated stretching between nodes 2 and 4, in the opposite orientation. The superpotential contains mass terms for all fields in the diagonal, which disappear after integrating them out. After these two dualizations, one recovers the original theory, up to a reversal of the direction of all arrows and a reduction in the ranks of nodes 1 and 3. It is hence clear that completing a period in the cascade by further dualizing nodes 2 and 4 brings back to the original theory, where the number of D3-branes is reduced $N \to N - 2M$ and the number of fractional branes M remains constant. The effective number of D3-branes decreases logarithmically as a function of energy along the cascading RG flow. The cascade is just a $\mathbb{Z}_2$ orbifold version of the conifold cascade in [5].

The orientifolded cascade

The orientifolded cascade starts from the quiver in figure 7.6(a) and repeats the sequence of dualizations (1,3,2), alternating between the quivers shown in figure 7.6. In these quivers, arrows are oriented to keep track of the representation under the $U(N)$ gauge factor from nodes 2, 4 (but note that representations of the USp groups at nodes 1, 3 are real, so the orientation *at* those nodes is meaningless).

In general lines, the dualizations of nodes 1 and 3 work as in the parent theory, although using the USp version of Seiberg duality. Let me first recall how Seiberg duality works for a $USp(N_c)$ gauge group with N_f flavors, namely N_f chiral fields in the fundamental representation (c.f. footnote 5 for conventions). The dual theory has $USp(N_f - N_c - 4)$ gauge group, N_f flavors, and mesons with cubic superpotential couplings to the flavors. Further details can be found in [149]. In the present setup, when dualizing node 1, there appear mesons connecting nodes 4 and 2, as shown in figure 7.6(b). These mesons transform in the conjugate antisymmetric representation of node 2. They become massive by combining with the oppositely oriented mesons that appear

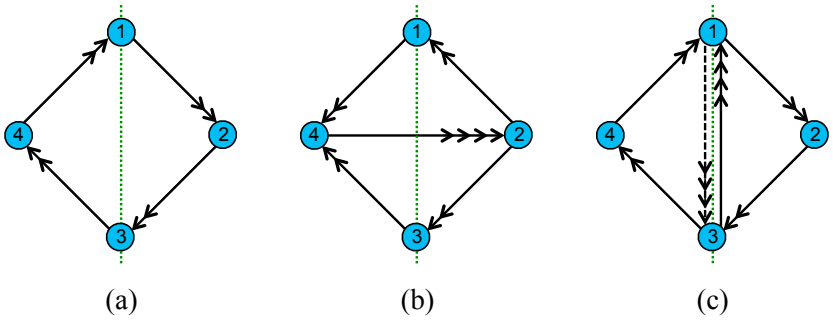

Figure 7.6: The orientifolded cascade alternates between these three quivers. As explained below, the theory (c) is actually equivalent to (a).

upon dualization of node 3. The result is a diagram similar to figure 7.6(a), up to reversal of arrows.

When subsequently dualizing node 2, one obtains the quiver shown in figure 7.6(c). This step gives rise to mesons connecting nodes 1 and 3. In terms of the parent quiver, this step actually also involves the dualization of its orientifold image, node 4, which would give rise to the dashed fields in figure 7.6(c). Moreover, the superpotential (7.7) gives rise to masses for all the mesons and the theory becomes the one in figure 7.6(a) after integrating them out. Therefore, the sequence of dualizations (1,3,2) corresponds to a period in the cascade.

7.3.4. The IR bottom of the cascade

I now explain how (7.10) can be alternatively understood as resulting from the gauge dynamics at the IR bottom of the duality cascade discussed in section 7.3.3, in which the instanton is realized in terms of a standard gauge instanton. To do so, consider the theory a couple of steps before the one in figure 7.4. One can quickly determine the corresponding quiver by Seiberg dualizing nodes 3 and 1. The latter is just a formal dualization of an empty node, but it will acquire more physical significance when I consider how the strong dynamics of the UV gauge theory indeed reproduces the properties of the empty node, as shown in section 7.3.5.

This formal Seiberg duality on nodes 1 and 3 in figure 7.4 produces the quiver shown in figure 7.7. All arrows connected to the dualized nodes have been inverted. Note that the dualization of node 3 produces several mesons. First, there are mesons connecting node 2 to its orientifold image, which become massive with mesons arising upon dualization of node 1. In addition, some of the flavors of the final theory connected to node 2 are mesons that arise when node 3 is dualized. There is an $\mathcal{O}(n_2)$ excess in the numbers of branes at nodes 1 and 3. This is the fractional brane triggering the cascade and ultimately responsible for the end of the cascade via strong dynamics (the capping of the warped throat in the gravity dual).

The perturbative superpotential is just the one that follows from (7.7) by reversing the direction of arrows and the cyclic order in the trace and adding an overall minus sign

$$W = -X^1_{32}X^1_{21}X^{2\,T}_{21}X^{2\,T}_{32} + X^2_{32}X^1_{21}X^{1\,T}_{21}X^{2\,T}_{32} + X^1_{32}X^2_{21}X^{2\,T}_{21}X^{1\,T}_{32}\,. \tag{7.12}$$

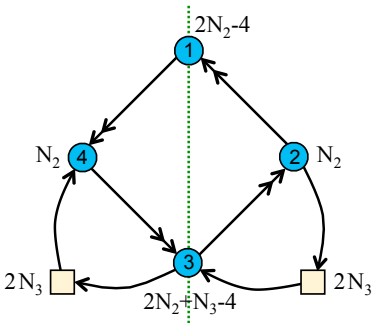

Figure 7.7: The quiver of the orientifolded $\mathbb{F}_0$ theory, two steps before the IR bottom of the cascade.

For simplicity, and since they do not participate in the dynamics I am interested in, here and in the remaining analysis of this model I will not consider the flavors.

Node 1 has $N_f = N_c + 4$ and hence confines, disappearing from the quiver, and generates a 1-instanton superpotential

$$W_{\text{gauge inst}} \sim \text{Pf}\, M_{22}\,, \tag{7.13}$$

with M_{22} the matrix of mesons for node 1

$$M_{22} = \begin{pmatrix} M_{22}^{11} & M_{22}^{12} \\ M_{22}^{21} & M_{22}^{22} \end{pmatrix} = \begin{pmatrix} X_{21}^1 X_{21}^{1\,T} & X_{21}^1 X_{21}^{2\,T} \\ X_{21}^2 X_{21}^{1\,T} & X_{21}^2 X_{21}^{2\,T} \end{pmatrix}. \tag{7.14}$$

Note that this matrix is antisymmetric due to insertions of the invariant tensor J in the USp color index contractions.

Notice that (7.13) is not the desired coupling (7.10), which instead involves mesons of node 3. For clarity, in what follows I will reserve the calligraphic font for the operators generated by D-brane instantons. Combining (7.13) and (7.12) expressed in terms of the mesons M_{22}^{ij}, one gets the following superpotential

$$W = \text{Pf}\, M_{22} - M_{22}^{12} X_{32}^{2\,T} X_{32}^1 + M_{22}^{11} X_{32}^{2\,T} X_{32}^2 + M_{22}^{22} X_{32}^{1\,T} X_{32}^1\,. \tag{7.15}$$

Next, dualizing node 3 one arrives at the theory of interest, whose quiver is shown in figure 7.4. This dualization generates the following mesons of node 3

$$N_{22} = \begin{pmatrix} N_{22}^{11} & N_{22}^{12} \\ N_{22}^{12} & N_{22}^{22} \end{pmatrix} = \begin{pmatrix} X_{32}^{1\,T} X_{32}^1 & X_{32}^{1\,T} X_{32}^2 \\ X_{32}^{2\,T} X_{32}^1 & X_{32}^{2\,T} X_{32}^2 \end{pmatrix}, \tag{7.16}$$

and inverts the direction of all arrows connected to node 3. This is not the full meson matrix since there are mesons involving the flavors. These mesons are responsible for flipping the direction of the arrows connecting the D7-branes to node 2, but do not show up in the non-perturbative term generated by the instanton, so I ignore them here. Note that N_{22} from (7.16) should not be confused with $\mathcal{N}_{22}$ from (7.11). Both of them are mesons of node 3, but in different theories: N_{22} is made out of fields in the quiver of figure 7.7 (after confining node 1), while $\mathcal{N}_{22}$ is made out of fields in figure 7.4.

In terms of these mesons, the superpotential becomes

$$\begin{aligned} W &= \mathrm{Pf}\, M_{22} - M_{22}^{12} N_{22}^{21} + M_{22}^{11} N_{22}^{22} + M_{22}^{22} N_{22}^{11} \\ &+ N_{22}^{21} X_{23}^{1} X_{23}^{2\,T} - N_{22}^{22} X_{23}^{1} X_{23}^{1\,T} - N_{22}^{11} X_{23}^{2} X_{23}^{2\,T} . \end{aligned} \tag{7.17}$$

The M_{22}^{ij} and N_{22}^{ij} mesons are massive, and can be integrated out using their equations of motion, i.e. vanishing of their F-terms. From $\partial W/\partial N_{22}^{ij} = 0$ one obtains

$$M_{22}^{11} = X_{23}^{1} X_{23}^{1\,T} \qquad M_{22}^{22} = X_{23}^{2} X_{23}^{2\,T} \qquad M_{22}^{12} = X_{23}^{1} X_{23}^{2\,T} . \tag{7.18}$$

Recalling (7.11), $M_{22}^{ij} = \mathcal{N}_{22}^{ij}$. Plugging this into (7.17), one obtains the D-brane instanton contribution (7.10).

It is straightforward to include the D7-brane flavors throughout the analysis and check that the flavor superpotential is correctly reproduced.

7.3.5. A useful trick

In the above analysis I did not have to deal with the complications of using the F-terms of fields entering the Pfaffian superpotential. However, such operations are necessary in more complicated examples. In this section I introduce a simple trick to recast Pfaffian superpotentials, which allows to perform these operations in a straightforward manner, with results which amount to combinatorial operations in the periodic quiver/dimer. This trick provides an explanation of the formal process of dualizing empty nodes.

Consider a $USp(N_c)$ theory with N_f chiral multiplets in the fundamental, and no superpotential, for $N_f = N_c + 4$. The theory confines and develops a superpotential $W \sim \mathrm{Pf} M$ for its mesons $M = QQ$. The trick is to rewrite this contribution as a path integral over a set of auxiliary Grassmann variables λ_i, transforming under the flavor group, and with a cubic coupling to the mesons $\lambda M \lambda^T$. Many field theory computations regarding F-terms can be carried out at the level of this description, and the eventual integration over the Grassmann variables reconstructs the Pfaffian at the end.

Before discussing explicit examples, I would like to mention that this description is closely related to the magnetic description of this theory: in quiver language, it contains an empty node which supports an $O(1)$ instanton, with fermion zero modes coupling as dictated by the magnetic quiver, and which agree with the properties of the above auxiliary Grassmann variables. A graphical representation of the trick, which thus amounts to a formal Seiberg duality, is shown in figure 7.8.

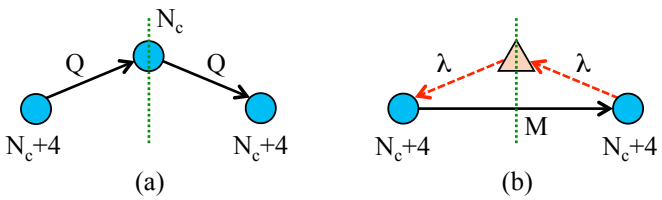

Figure 7.8: (a) Quiver diagram for a $USp(N_c)$ electric theory with $N_f = N_c + 4$. (b) The magnetic dual, with the empty node supporting an instanton, whose zero modes are shown as dashed arrows.

I will now apply the trick to the UV gauge theory of the earlier section, with the quiver shown in figure 7.7. As above, node 1 confines and generates the Pfaffian superpotential (7.13) for its mesons. This can be rewritten by introducing a set of Grassmann variables λ^1_{12} and λ^2_{12}, transforming in the antifundamental of $U(n_2)$. Their coupling to the mesons of (7.14) can be formally combined with the original tree level superpotential, leading to

$$\begin{aligned} &+\lambda^1_{12} M^{12}_{22} {\lambda^2_{12}}^T - \lambda^1_{12} M^{11}_{22} {\lambda^1_{12}}^T - \lambda^2_{12} M^{22}_{22} {\lambda^2_{12}}^T \\ &-X^1_{32} M^{12}_{22} {X^2_{32}}^T + X^1_{32} M^{11}_{22} {X^1_{32}}^T + X^2_{32} M^{22}_{22} {X^2_{32}}^T \,. \end{aligned} \tag{7.19}$$

This is just as dictated by the quiver of the Seiberg dual theory. Dualizing now node 3 and defining its mesons N as in (7.16), one has

$$\begin{aligned} &+\lambda^1_{12} M^{12}_{22} {\lambda^2_{12}}^T - \lambda^1_{12} M^{11}_{22} {\lambda^1_{12}}^T - \lambda^2_{12} M^{22}_{22} {\lambda^2_{12}}^T \\ &-M^{12}_{22} N^{21}_{22} + M^{11}_{22} N^{11}_{22} + M^{22}_{22} N^{22}_{22} + N^{21}_{22} X^1_{23} {X^2_{23}}^T - N^{11}_{22} X^1_{23} {X^1_{23}}^T - N^{22}_{22} X^2_{23} {X^2_{23}}^T \,. \end{aligned} \tag{7.20}$$

Upon integrating out the massive fields, the F-terms of N^{ij}_{22} impose $M^{ij}_{22} = X^i_{23} {X^j_{23}}^T$. The superpotential becomes precisely (7.9). It is then manifest that integration over the auxiliary Grassmann variables finally reconstructs the superpotential of the D-brane instanton (7.10).

The lesson is that confinement and the introduction of the Pfaffian superpotential for USp nodes with $N_f = N_c + 4$ is, via this trick, equivalent to performing the Seiberg duality leaving the node with the instanton and the corresponding charged zero modes. This effectively brings the duality cascade one step down towards the IR theory. This idea will be useful in the analysis of more involved examples in coming sections.

7.4. Non-cascading geometries: $\mathbb{C}^3/\mathbb{Z}_3$ examples

The second class of examples to be considered involves theories that naively do not cascade. By this I mean theories that do not cascade, even when considering the *full* quiver associated to the singularity and allow arbitrary ranks for all its nodes and the addition of flavors. Prototypical examples of this situation are provided by e.g. $\mathbb{C}^3/(\mathbb{Z}_n \times \mathbb{Z}_m)$ chiral orbifolds, and orientifolds thereof.

This problem of UV completing such systems was considered (for oriented quivers) in [53], where it was shown that such theories can emerge after partial confinement in a more complicated quiver, which can now correspond to the IR limit of a duality cascade. In the dual gravity language, the UV geometry reduces to the IR one via a complex deformation, which for toric singularities can be described very easily using dimer diagrams [41]. Hence, although the final geometry naively appears non-cascading, it can emerge from a cascade as a result of the same type of dynamics that works in more conventional examples.

7.4.1. D-brane instanton couplings

For concreteness I will focus on a prototypical example, namely gauge theories arising from orientifolds of D3-branes (and possibly D7-branes) at the $\mathbb{C}^3/\mathbb{Z}_3$ singularity. This

simple geometry gives rise to many interesting chiral theories, which have appeared in widely varied applications (see e.g. [53, 191, 192] for some of them).

The periodic quiver and dimer of the $\mathbb{C}^3/\mathbb{Z}_3$ are shown in figure 7.9. The figure also includes an orientifold line that will be used later on. The superpotential of the theory without the orientifold is given by

$$W = \epsilon_{ijk} X^i_{12} X^j_{23} X^k_{31} \,. \tag{7.21}$$

The superindices (which label the representation under an $SU(3)$ global symmetry) have a range $i = 1, 2, 3$ and are used to label the arrows going south, north-west, and north-east, respectively.

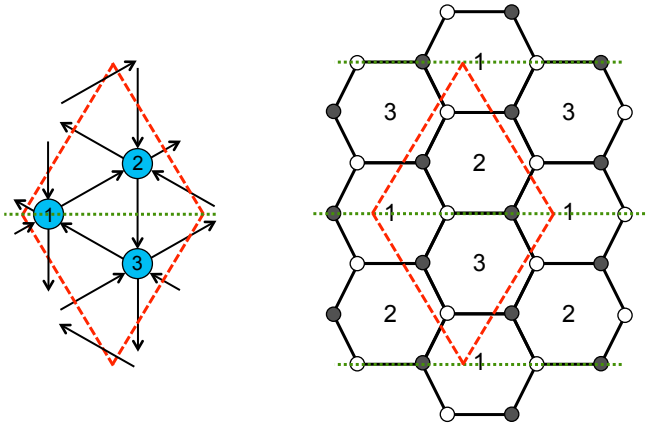

Figure 7.9: The periodic quiver and dimer diagram for the orientifold of $\mathbb{C}^3/\mathbb{Z}_3$. The theory is non-cascading and it needs a UV completion in order to embed it on a throat. This can be done by using the ideas in chapter 5 and noting that there is a single orientifold line on the dimer, crossing the diagonal of the unit cell.

Now, consider the orientifold theory defined by the line reflection in the dimer. In order to obtain non-trivial superpotentials from D-brane instantons, the orientifold charge is chosen so that the fixed gauge factor 1 is projected down to a USp factor. Using the rules in [42], this implies that the bifundamental on top of the orientifold, denoted X^1_{22}, is projected down to a two-index antisymmetric of the $U(n_2)$. In addition, the two other bifundamentals X^2_{22}, X^3_{22} are exchanged by the orientifold action, and produce one symmetric and one antisymmetric representations under $U(n_2)$. Other fields are related to their orientifold images by transposition, e.g. $X^2_{31} = X^{3\,T}_{12}$, $X^1_{31} = X^{1\,T}_{12}$, etc.

The superpotential of the orientifold theory reads (expressed it in terms of fields above the orientifold line)

$$W = X^3_{12} X^1_{22} X^{3\,T}_{12} - X^2_{12} X^1_{22} X^{2\,T}_{12} - X^3_{12} X^2_{22} X^{1\,T}_{12} + X^1_{12} X^2_{22} X^{2\,T}_{12} \,. \tag{7.22}$$

Here and in what follows X^2_{22} is understood to split into a symmetric plus an antisymmetric representation.

I am interested on the theory with node 1 empty, shown in figure 7.10. This node can support an $O(1)$ instanton (thus with two neutral fermion zero modes) and a set of charged fermion zero modes depicted as dashed arrows in the figure. Even though the

node is empty, one must cancel the Witten global anomaly of the USp node, and demand that the number of incoming arrows is even, so p is forced to be even in this model.

The fermion zero mode couplings can be obtained from the above superpotential by replacing chiral bifundamentals by zero modes, giving

$$\lambda^3_{12} X^1_{22} {\lambda^3_{12}}^T - \lambda^2_{12} X^1_{22} {\lambda^2_{12}}^T - \lambda^3_{12} X^2_{22} {\lambda^1_{12}}^T + \lambda^1_{12} X^2_{22} {\lambda^2_{12}}^T . \tag{7.23}$$

Integrating the instanton partition function over these fermion zero modes one obtains the non-perturbative superpotential

$$W_{\text{inst}} \sim \text{Pf}\mathcal{M} , \tag{7.24}$$

where $\mathcal{M}$ is a matrix built out of the fields X^i_{22}.

Since (7.22) vanishes when node 1 is empty, the full superpotential is the sum of (7.24) and the flavor superpotential. It is then given by

$$W = Q_{D7,2} A_1 {Q_{D7,2}}^T + \text{Pf}\mathcal{M} , \tag{7.25}$$

where the precise form of the flavor couplings is dictated by the embedding of the D7-branes, as explained in detail in [58], and I used the notation in figure 7.10 to emphasize I chose to couple the flavors to one of the antisymmetric fields. This theory is closely related to a model considered in [187], as explained in section 7.6.

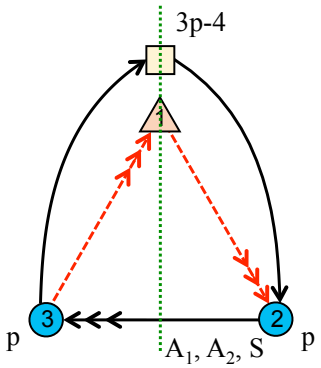

Figure 7.10: The $\mathbb{C}^3/\mathbb{Z}_3$ orientifold quiver supporting a D-brane instanton. There are p fractional branes, which cannot trigger a duality cascade, and a number of D7-branes to render the theory anomaly-free. Consistency requires p to be even.

As already mentioned, this theory cannot be directly embedded in a UV duality cascade, since the $\mathbb{C}^3/\mathbb{Z}_3$ does not admit complex deformations (conversely, the gauge theory does not admit deformation fractional branes). In the following sections I study the embedding of this model into a different quiver theory (that reduces to this one by confinement), which in turn does admit a UV completion in terms of a duality cascade.

7.4.2. The unorientifolded parent theory and its complex deformation

In order to embed the previous non-cascading field theory in a gauge theory that does cascade and thus corresponds to a warped throat on the gravitational picture, one

can note that the orientifold action on the dimer is to exchange both coordinates. This type of fixed line was studied in chapter 5, where it was argued that the tool to find the UV parent theory is the web diagram [142]. The web diagram of the $\mathbb{C}^3/\mathbb{Z}_3$ singularity is shown in 7.11(a) together with the effect of the orientifold. The parent theory can be obtained by adding a subweb in equilibrium compatible with the $\mathbb{Z}_2$ symmetry, that I will take to be a line formed by two external legs mapped to themselves by the orientifold action, as in figure 7.11(b). This singularity corresponds to a $\mathbb{Z}_3$ orbifold of the suspended pinch point (or SPP/$\mathbb{Z}_3$ for short)

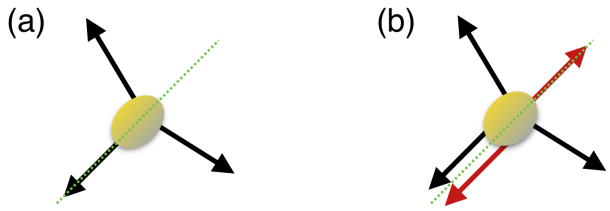

Figure 7.11: (a) External legs of $\mathbb{C}^3/\mathbb{Z}_3$ together with the orientifold fixed line in green. (b) By adding a subweb with two external legs that are invariant under the orientifold action one finds the UV completion of the singularity that accepts the same orientifold action. This is the SPP/$\mathbb{Z}_3$ singularity.

It is convenient to first consider the unorientifolded parent theory to understand the basic ingredients to be used later for the orientifold model. This construction for SPP/$\mathbb{Z}_3$ to $\mathbb{C}^3/\mathbb{Z}_3$ was extensively studied in [53,55] as a toy model in which a Standard Model-like theory emerges at the IR bottom of a throat. The possibility of a chiral theory at the end of the cascade follows from having a remnant singularity. In the following I review some aspects (and derive some new ones) that are relevant for my present purposes.

The dimer describing the gauge theory of D3-branes at SPP/$\mathbb{Z}_3$ is shown in figure 7.12. Note that although the model is fully chiral, it is related to the non-chiral SPP by orbifolding, as in [18].

Following [53,55], the duality cascade of the SPP/$\mathbb{Z}_3$ theory and its deformation to the $\mathbb{C}^3/\mathbb{Z}_3$ theory corresponds, even in the presence of extra flavors, to a $\mathbb{Z}_3$ orbifold of the cascade and complex deformation of the underlying SPP geometry to a smooth space. The cascade in SPP/$\mathbb{Z}_3$ is obtained by dualizing gauge factors in whole columns of squared faces in the dimer, which turn the squares in one of the adjacent columns into hexagons, and the hexagons in the other adjacent column into squares. A similar pattern will hold in the orientifold theory, considered in the next section.

7.4.3. The orientifolded theory and its cascade

I now describe the orientifold of the SPP/$\mathbb{Z}_3$ theory I am interested in. The orientifold is described as a line reflection in the dimer diagram, as shown in figure 7.12. The orientifold action maps gauge groups 1, 2 and 3 onto themselves, while it identifies the pairs $4 \leftrightarrow 7$, $5 \leftrightarrow 8$ and $6 \leftrightarrow 9$. The orientifold charge is negative in the notation of [42], so invariant gauge factors project onto USp groups, and invariant fields onto two-index antisymmetric representations.

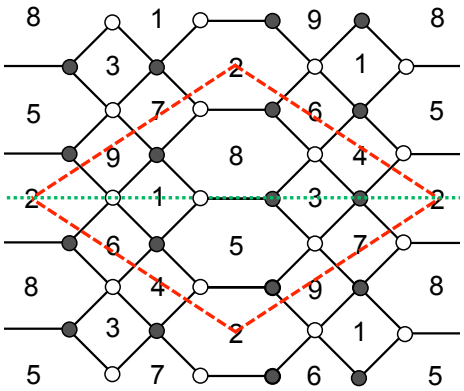

Figure 7.12: The dimer for the SPP/$\mathbb{Z}_3$ theory. The green line is included for later use to describe the orientifold projection.

At this point it is possible to introduce flavors from D7-branes. Their behavior follows very closely the unorientifolded case, and for simplicity I omit them until the study of the IR behavior of the cascade in section 7.4.4.

The resulting gauge theory thus has six gauge groups

$$USp(n_1) \times USp(n_2) \times USp(n_3) \times U(n_4) \times U(n_5) \times U(n_6) \ , \tag{7.26}$$

where to facilitate comparison, I have preserved the node labels in the parent theory. The rules to read out the spectrum and superpotential interactions are those in [42]. Let me simply mention that the bifundamental ($\overline{\square}_5$, $\square_8$), which is mapped to itself under the orientifold, turns into a two-index (conjugate) antisymmetric of $U(n_5)$, $\overline{\square\!\square}_5$. Fields not invariant under the orientifold, like e.g. ($\square_3$, $\overline{\square}_8$), combined with their image fields, e.g. ($\square_5$, $\overline{\square}_3$), descend to bifundamentals of the corresponding group in the orientifold quotient. In these operations it is important to keep in mind that the orientifold maps gauge factors by relating their representations by conjugation, e.g. $U(n_4) \leftrightarrow U(n_7)$ such that the $\square_4 \leftrightarrow \overline{\square}_7$.

The final result is shown as a quiver in figure 7.13. In order to simplify its interpretation, I color code nodes and arrows. Blue nodes are of SU type (with their images in grey), while pink nodes are their own orientifold images and hence USp. Black arrows from node a to b correspond to fields in the ($\square_a$, $\overline{\square}_b$) (with their images depicted as light color arrows). The orientation of arrows at pink nodes is irrelevant, since USp has not complex representations, but I preserve it as a useful bookkeeping device. Finally, the blue arrow transforms as $\overline{\square\!\square}_5$. It is important not to double count these fields.

It is useful to recall that the SPP theory admits a T-dual [18] in terms of a type IIA HW configuration [99] of two NS-branes and one rotated NS'-brane, with D4-branes suspended among them in the periodic coordinate x^6. In this picture, the current orientifold corresponds to the introduction of an O8-plane (along 012345689) [193]. The orbifolded theory is realized by an additional $\mathbb{Z}_3$ orbifold of the HW configuration, acting in the directions 45, 89.

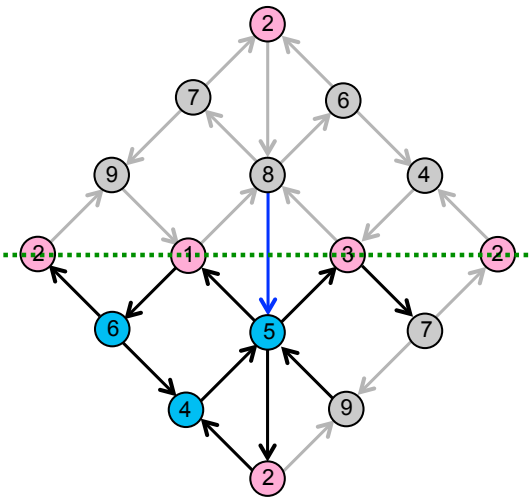

Figure 7.13: The quiver diagram for the line orientifold of the SPP/$\mathbb{Z}_3$ theory.

The discussion of the cascade is analogous to the parent SPP/$\mathbb{Z}_3$ theory without the orientifold. Namely, as each column of squares is preserved by the line orientifold, the cascade of Seiberg dualities is formally compatible with the orientifold. In a similar way to what I described in section 7.3.3, the original cascade sequentially dualizes the three nodes in each column, namely a period corresponds to the sequence (1,4,7) (2,5,8) (3,6,9). Due to the identification of nodes, in the orientifolded theory the cascade involves the two surviving nodes from each of these columns, namely: (1,4) (2,5) (3,6).

In the following I describe some details of the dualization procedure. A nice property of this particular example is that it avoids having to dualize nodes with matter in the antisymmetric representation.[8]

7.4.3.1. Basic step in the duality cascade

Here I discuss the dualization of nodes on a column of squares in the dimer in more detail. As in the unorientifolded case, I will show that its effect is to shift the line of vertical arrows sideways. For concreteness, I focus on the column consisting of nodes 1 and 4 (of type USp and SU, respectively).

Dualizing node 1

Consider dualizing the USp type node 1, as shown in figure 7.14. The rules for Seiberg duality in quivers were described in [39], and recast in terms of dimer diagram in [37]. Upon dualization, one inverts the orientation of arrows connected to node 1, effectively introducing the dual quarks, which transform in conjugate representations under the symmetries of nodes 5 and 6. In addition, one must introduce arrows corresponding to meson fields in representations ($\square_5$, $\overline{\square}_6$), $\overline{\square\!\square}_6$ and $\square\!\square_5$. The superpotential pairs up

[8] The dual of gauge theories with antisymmetric matter is only known in very few cases, see e.g. [194–197].

the latter with the original $\overline{\square}_5$ in a mass term, and the pair can be integrated out. These fields were indicated using dotted arrows to indicate that they disappear at low energies.

In figure 7.14, the dark blue arrow on the right figure represents the antisymmetric field charged under node 6, and the light blue one represents the same field at a different unit cell.

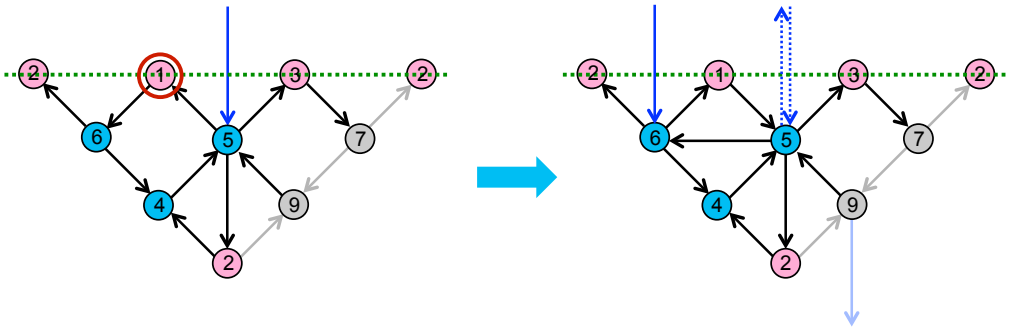

Figure 7.14: Dualization of node 1, which is a USp gauge group. In this figure and the ones that follow, it is important to keep in mind that in the orientifold, nodes 7 and 9 are identified with nodes 4 and 6, respectively.

Dualizing node 4

In the second step, I dualize node 4 (and its orientifold image in the $\mathbb{Z}_2$ covering). This is an SU gauge group and its dualization, which is rather standard, is shown in figure 7.15. As before, dotted lines indicate pairs of field that become massive and can be integrated out.

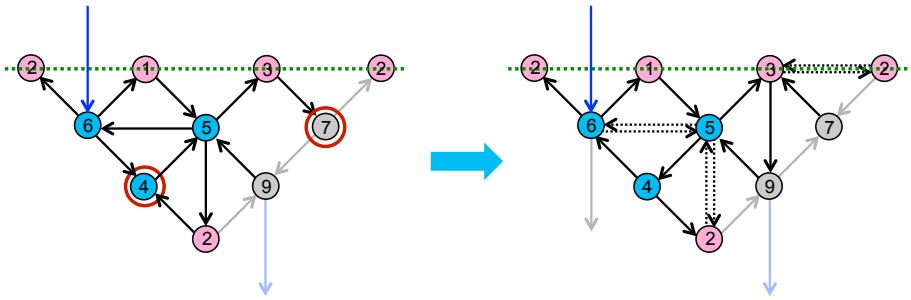

Figure 7.15: Dualization of nodes 4 and 7, which are SU gauge groups.

The final result is shown in figure 7.16. The net effect of dualizing a column of nodes is a horizontal shift of the vertical arrows. An identical analysis applies to the dualizations of nodes (2,5) and (3,6), resulting in a periodic Seiberg duality cascade. To leading order in $1/N$, the change in ranks in as in the parent oriented theory, namely the reduction in the number of D3-branes is $N \to N - 6M$. The precise numbers actually depend on the pattern of D7-brane flavors, and will be discussed in explicit examples below.

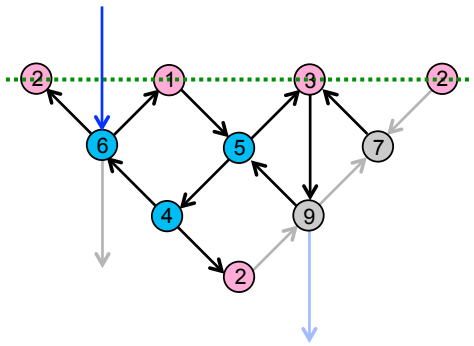

Figure 7.16: Final result after dualizing the vertical column consisting of nodes 1 and 4.

7.4.4. The instanton

I now consider a rank assignment and D7-brane content in the SPP/$\mathbb{Z}_3$ theory that relates, upon inclusion of strong dynamics, to the $\mathbb{C}^3/\mathbb{Z}_3$ orientifold theory introduced in section 7.4.1, and shown in figure 7.10. Basically, the strong dynamics of nodes 1, 4 and 7, which is responsible for the complex deformation, recombines the factors 2 and 3, and 8 and 9 (and their images 5 and 6), respectively. Hence, I set those numbers pairwise equal, and related to those of the resulting $\mathbb{C}^3/\mathbb{Z}_3$ theory, namely

$$n_2 = n_3 = 0 \quad , \quad n_5 = n_6 = n_8 = n_9 = p\,. \tag{7.27}$$

In order to verify the cancellation of anomalies, it is important to appropriately take into account the orientifold identifications of gauge groups and chiral fields. The confining nodes 1, 4 and 7 are taken to have a large number of branes, of order $M \gg p$. The precise values are obtained by demanding cancellation of anomalies, once one accounts for the D7-branes, which are located on the edge 58.[9] Thus

$$n_1 = M \quad , \quad n_4 = n_7 = M + p\,. \tag{7.28}$$

The quiver right before the SPP/$\mathbb{Z}_3 \to \mathbb{C}^3/\mathbb{Z}_3$ deformation is shown in figure 7.17, including the $O(1)$ D-brane instantons at the empty nodes 2, 3. The requirement to cancel RR K-theory charge tadpoles [199] (i.e. cancellation of Witten anomaly for the empty USp nodes) requires p even (as obtained already in the $\mathbb{C}^3/\mathbb{Z}_3$ orientifold) and M even.

I will later on derive the relation of this SPP/$\mathbb{Z}_3$ orientifold theory with the $\mathbb{C}^3/\mathbb{Z}_3$ orientifold theory in figure 7.10. Now I instead proceed to construct the UV gauge theory in which the D-brane instanton effects are realized as gauge instanton effects. This is done by moving up the cascade of SPP/$\mathbb{Z}_3$ until the empty nodes are filled. This occurs after two steps of dualization of whole columns, and the resulting quiver is shown in figure 7.18(a). The dualities are essentially as in the cascade in section 7.4.3, with the only modification that one must include the D7-brane flavors in the discussion of some dualizations.

I now study the strong gauge dynamics of the theory in figure 7.18(a). Consider node 2, which is a USp group with $N_c = 2M + p - 4$, and its number of fundamentals is

[9] For a discussion on how to describe D7-branes in terms of dimer models see [58, 198]. D7-branes are described by paths traversing edges in the dimer model, which indicate the operator made out of D3-D3 chiral fields the flavors are coupled to in the superpotential.

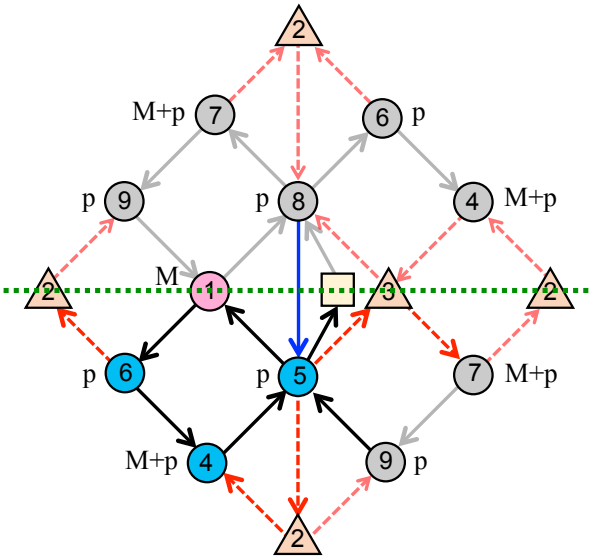

Figure 7.17: Quiver for the orientifold of SPP/$\mathbb{Z}_3$ theory with instanton. The number of D7-branes, denoted by the square, is $3p-4$. Consistency requires M and p to be even.

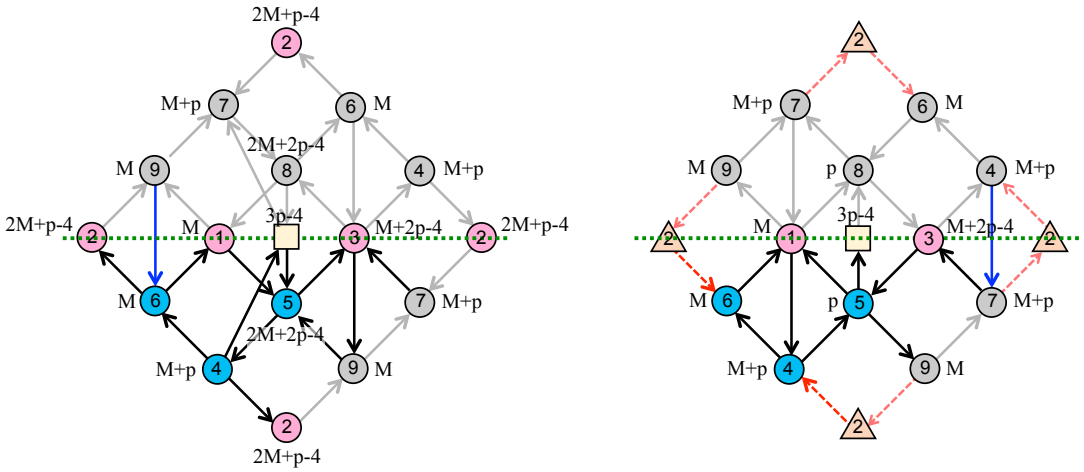

Figure 7.18: (a) Quiver for the orientifold of SPP/$\mathbb{Z}_3$ theory two steps up the duality cascade. (b) Quiver obtained after considering the strong dynamics of node 2 and dualizing nodes 5 and 8. It corresponds to the SPP/$\mathbb{Z}_3$ orientifold in the next to last setp in the cascade.

$N_f = 2M + p$. Thus it has $N_f = N_c + 4$ and generates a non-perturbative superpotential $W \sim \text{Pf}\ M$ for its mesons M. Rather than adding this superpotential to the tree level one and using the F-terms by brute force, I will take advantage of the trick in section 7.3.5, and introduce a set of auxiliary Grassmann variables as arrows of opposite orientation to the original quarks, with cubic couplings to the mesons. As shown there, this is actually equivalent to performing a formal duality on node 2, leaving it as an empty node whose

chiral multiplets are played by the Grassmann variables. In addition, one can dualize the nodes 5 and 8, to complete a duality in a whole column. This operation can be carried out very easily in the quiver, as in the discussion in section 7.4.3, and with the inclusion of D7-brane flavors in the dualization of nodes 5, 8. The resulting quiver is shown in figure 7.18(b).

In this quiver, the node 3 is a USp gauge factor with $N_c = M + 2p - 4$, and $N_f = M + 2p$, hence it has $N_f = N_c + 4$ so it confines and generates a non-perturbative superpotential $W \sim \text{Pf } M'$ for its mesons. The trick in section 7.3.5 can be used again and introduce Grassmann variables as arrows of opposite orientation to the original quarks, with cubic coupling to the mesons. In order to dualize nodes 6 and 9, some care is required since there are fermion zero modes of the instanton charged under them. The change in the fermion zero mode spectrum is given in figure 7.19. It is easily obtained by demanding conservation of the net number of fermion modes on the corresponding instanton, and results in a formal duality reversing the Grassmann arrows and introducing 'mesonic' ones. Applying this additional rule to the theory in figure 7.18(b), one gets a quiver which corresponds precisely to figure 7.17. Clearly the trick to rewrite the Pfaffian superpotentials in terms of Grassmann variables makes it trivial to recover the right IR physics, as it effectively takes the theory one step down of the duality cascade.

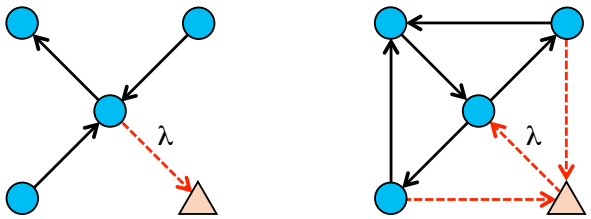

Figure 7.19: Transformation of the fermion zero mode set upon Seiberg duality of a node under which they are charged.

The next step is to consider the strong dynamics of the nodes 1, 4 and 7 in the quiver theory with two empty nodes, and show that after confinement it reduces to the $\mathbb{C}^3/\mathbb{Z}_3$ orientifold. Consider the theory in figure 7.17 in the absence of the instantons on nodes 2, 3. The superpotential in this case is

$$W = {Q_{5,\text{D7}}}^T X'_{55} Q_{5,\text{D7}} + X'_{55} X_{51} X_{51}^T - X_{51} X_{16} X_{64} X_{45} \,, \tag{7.29}$$

where the prime on X'_{55} denotes that it transforms in the conjugate antisymmetric of node 5. In the regime of interest, $M \gg p$, the groups 1 and 4 (and its image 7) generate non-perturbative Affleck-Dine-Seiberg (ADS) superpotentials. Introducing the mesons

$$N = \begin{pmatrix} N_{55} & N_{56} \\ N_{65} & N'_{66} \end{pmatrix} = \begin{pmatrix} X_{51}{X_{51}}^T & X_{51}X_{16} \\ {X_{16}}^T{X_{51}}^T & {X_{16}}^T X_{16} \end{pmatrix} \quad , \quad \tilde{N} = X_{64}X_{45} \equiv \tilde{N}_{65} \,, \tag{7.30}$$

the superpotential for the theory in terms of them is

$$\begin{aligned} W &= {Q_{5,\text{D7}}}^T X'_{55} Q_{5,\text{D7}} + X'_{55} N_{55} - N_{56}\tilde{N}_{65} \\ &+ M(\det \tilde{N})^{-\frac{1}{M}} + (M - p + 2)(\text{Pf } N)^{-\frac{2}{M-p+2}} \,, \end{aligned} \tag{7.31}$$

where the constants associated to the strong dynamics scale and some numerical prefactors were ignored.

The F-term for N_{55} fixes X'_{55} in terms of $\det N$, the F-terms for N_{56} fixes $\tilde{N}_{65}$ in terms of $\det N$ and the F-term for $\tilde{N}_{65}$ fixes N_{56} in terms of $\det \tilde{N}$. These mesonic vevs break the gauge symmetries of 5 and 6 (and those of the images 8 and 9) to their diagonal combination. Finally, the F-term for the antisymmetric X'_{55} sets $N_{55} = -Q_{5,\mathrm{D7}}{Q_{5,\mathrm{D7}}}^T$. The left over massless fields are the field X_{65} (which decomposes as a $\overline{\square\square}_5 + \overline{\square}_5$) and N'_{66} (which transforms as a $\overline{\square}_6$).

The final superpotential can be read out by restricting to the simplest case, where the meson matrix N of the USp group is 4×4, with entries N_{ij} given by 2×2 blocks. The Pfaffian in this case reads

$$\mathrm{Pf}\, N \sim N_{55}N'_{66} - N_{56}N_{65}\,, \tag{7.32}$$

which allows to write the F-term of N_{55} as

$$X'_{55} \sim (\mathrm{Pf}\, N)^{-\frac{2}{M-p+2}-1} N'_{66}\,. \tag{7.33}$$

Using this one is left with a superpotential

$$W = {Q_{5,\mathrm{D7}}}^T N'_{66} Q_{5,\mathrm{D7}}\,, \tag{7.34}$$

reproducing the perturbative piece of superpotential (7.25) for the $\mathbb{C}^3/\mathbb{Z}_3$ orientifold with flavors in figure 7.10, after the obvious map of fields.

The strong dynamics responsible for the complex deformation I just discussed can be nicely reproduced graphically in terms of the dimer as shown in figure 7.20, using a procedure developed in [22, 41]. The confinement of faces 1 and 4 (and its image 7) is represented by shrinking the corresponding faces, first into the dotted ovals and finally into a single edge. The disappearance of the faces is the dimer counterpart of the elimination of the associated gauge symmetry. In addition, as a result of these shrinking, the pairs (2,3) and (5,6) (as well as its image pair (8,9)) get recombined. This is precisely the pattern of higgsing triggered by the non-zero vevs explained above. In figure 7.20 I indicate the faces that result from this process in color. The final unit cell has three hexagonal faces and an orientifold line, which identifies the blue and pink faces. This is precisely the dimer representation of the orientifold of $\mathbb{C}^3/\mathbb{Z}_3$ presented in figure 7.9.

It is now easy to follow the fate of the instanton fermion zero modes of the complete quiver in figure 7.17 in this confinement process. The fact that the node 4 (and its image 7) confines implies that fermion zero modes charged under them have to be saturated using gauge invariant couplings. In particular, the fermion zero modes λ_{34} and λ_{24} (and their images) must be saturated using the quartic coupling $\lambda_{34}{\lambda_{24}}^T\lambda_{24}{\lambda_{34}}^T$. This pattern of saturation of fermion zero modes reflects the fact that the two instantons act simultaneously in a 2-instanton process, very much in the spirit of [188, 200]. This is in agreement with the intuition that confinement of nodes 1, 4, 7 triggers the recombination of nodes 2 and 3. Once gauge groups 1, 4 and 7 confine, and after saturating the zero modes in the quartic coupling, the remaining fermion zero modes are λ_{53}, λ_{62} and λ_{52}, with couplings[10]

$${\lambda_{53}}^T N'_{66}\lambda_{53} - {\lambda_{62}}^T N'_{66}\lambda_{62} - {\lambda_{62}}^T X_{65}\lambda_{52} + {\lambda_{52}}^T X_{65}\lambda_{53}\,, \tag{7.35}$$

[10] Until here I took the convention of representing the sets of Grassmann variables as row vectors. From here on I will change the convention since it is more convenient to write them as column vectors.

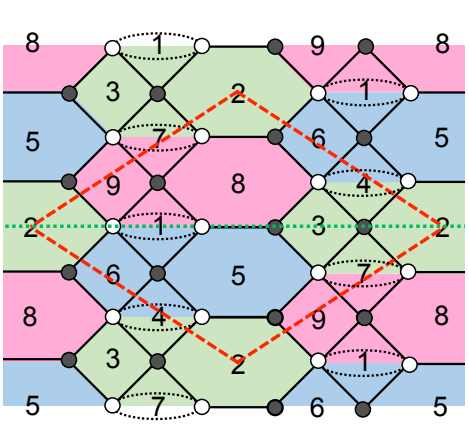

Figure 7.20: Dimer representation of the strong dynamics responsible for the complex deformation. Nodes 1 and 4 (and its image 7) confine and disappear, whereas the pairs (2,3) and (5,6) (as well as its image pair (8,9)) get recombined. The deformation is depicted as shrinking those faces as indicated by the dotted ovals. The pink, blue and green shades correspond to the faces of the resulting dimer after the complex deformation, and describe a line orientifold of $\mathbb{C}^3/\mathbb{Z}_3$.

where as usual X_{65} is understood to split into symmetric and antisymmetric parts.

This is precisely in agreement with the fermion zero modes of the instanton on the orientifold of $\mathbb{C}^3/\mathbb{Z}_3$, c.f. figure 7.10. Indeed, by comparing (7.35) with (7.23), one sees that the structure of the couplings in both cases is the same, and it is easy to map the fields and zero modes of the SPP$/\mathbb{Z}_3$ theory to the $\mathbb{C}_3/\mathbb{Z}_3$ one.

The conclusion is that the original non-perturbative gauge dynamics in the SPP$/\mathbb{Z}_3$ orientifold theory of two steps up the cascade will reproduce exactly the same non-perturbative superpotential as the stringy D-brane instanton of the infrared $\mathbb{C}^3/\mathbb{Z}_3$ orientifold theory, given by (7.24). Combining this with (7.34), the full superpotential (7.25) is recovered.

7.5. Models with orientifold points

The examples in the previous sections are based on orientifold quotients that have fixed lines in their action on the dimer diagram. It is also easy to find chiral examples with orientifolds leaving fixed points on the dimer and with duality cascades and deformations, providing a UV completion where D-brane instantons are realized as standard gauge instantons up in the cascade. Since the analysis of these questions is very similar to our earlier explicit examples, I restrict the discussion to the construction of the basic dimer models.

A UV completion of this non-cascading geometry compatible with orientifold points can easily found by using the ideas in chapter 5. This time, since the interest goes on a configuration with orientifold points, the UV completion can be obtained by enlarging the singularity adding two copies of the same subweb in equilibrium [142]. This is shown in figure 7.21.

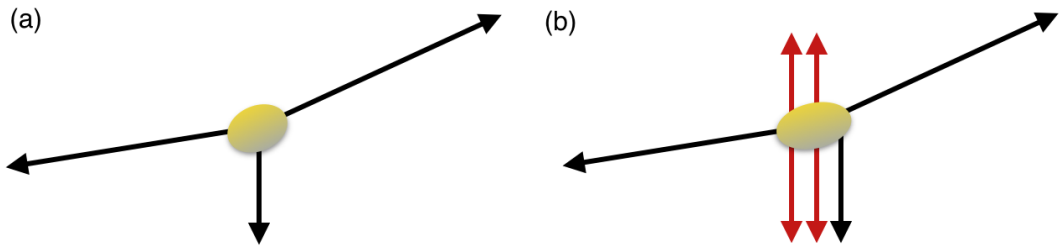

Figure 7.21: (a) External legs of $\mathbb{C}^3/\mathbb{Z}_3$ in a rather different representative. This representative was chosen since having a leg with $(p,q) = (0,-1)$ will make the corresponding dimer nicer. (b) External legs of the parent diagram after adding a web in equilibium (a line with an external leg pointing upwards and another one pointing downwards) twice.

This web diagram corresponds to a singularity known as $L^{2,3,2}$ [139], which is a $\mathbb{Z}_3$ orbifold of $xy = z^3w^2$. The dimer diagram describing the gauge theory can be constructed using the *fast inverse algorith* in [38], which is shown in figure 7.22. The picture also displays the fixed points of the orientifold action, which is clearly compatible with the complex deformation to the $\mathbb{C}^3/\mathbb{Z}_3$ theory, because the fractional branes (corresponding to faces 21, 22, 23, 41, 42, 43) form an invariant set under the orientifold action. The final dimer faces after complex deformation are depicted as three hexagons with different background colors).

In agreement with chapter 5, this singularity as well as $\mathbb{C}^3/\mathbb{Z}_3$ have $n_Z^{min} = n_Z = n_F = 3$, and so there is one face of the original dimer that is mapped to itself under the orientifold action. If empty, and for suitable choice of orientifold charges, it can support instantons that contribute to the superpotential. Up in the cascade, when the corresponding face is filled, the effect should be generated by a standard gauge instanton. In the infrared, some nodes confine and force non-trivial mesonic vevs which recombine certain faces and reconstruct the dimer for $\mathbb{C}^3/\mathbb{Z}_3$. By an analysis similar to that in earlier sections, it is easy to show that the gauge non-perturbative effects of the UV theory flow to the D-brane instanton effects of the infrared $\mathbb{C}^3/\mathbb{Z}_3$ theory. I refrain from a more detailed discussion of these and other similar examples, which can easily constructed with the techniques presented above.

7.6. Flavoring the non-perturbative superpotential

In this section I consider an alternative flavor configuration for the class of models studied in section 7.4. An interesting application of D-brane instantons has been proposed in [187], where it was argued that certain 4d $\mathcal{N} = 1$ superconformal gauge theories arising from D3-branes at orientifold singularities actually suffer a non-perturbative breaking of superconformal invariance by D-brane instanton effects. This occurs because the gauge theories are realized in terms of quivers that contain empty nodes with formally 'non-trivial beta-functions'; these do not produce gauge factors, but can support D-brane instantons whose contribution to the effective action is weighted by a non-trivial scale. The example I consider is one of the simplest theories that have been argued to realize this scenario. Independently of this application, this theory is also interesting because it exhibits a novel

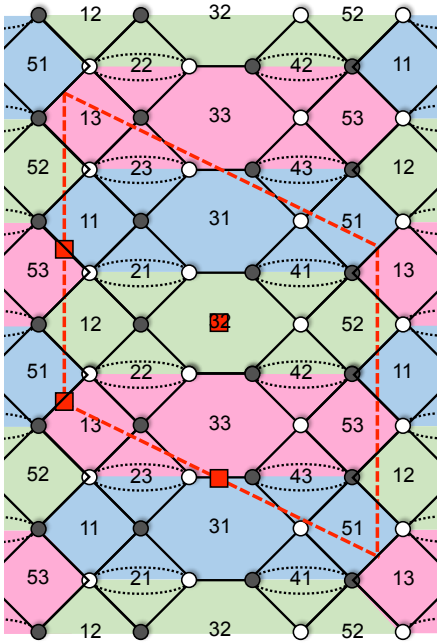

Figure 7.22: The dimer for a fixed point orientifold of the $\mathbb{Z}_3$ quotient of $xy = z^3w^2$. The faces 21, 22, 23, 41, 42 and 43 correspond to the deformation fractional brane, and form an invariant set under the orientifold action. The deformation is depicted as shrinking those faces as indicated by the dotted ovals. The pink, blue and green shades correspond to the faces of the resulting dimer after the complex deformation, and describe a point orientifold of $\mathbb{C}^3/\mathbb{Z}_3$.

feature: a D-brane instantons generates a non-perturbative superpotential involving the flavors.

In this section, I provide a UV embedding of one such example in [187], based on an orientifold of $\mathbb{C}^3/\mathbb{Z}_3$, using a duality cascade of an orientifold of the SPP$/\mathbb{Z}_3$ theory, in which the IR D-brane instanton is realized as a standard gauge instanton at some higher step up in the cascade.

The example to be considered is the orientifold of $\mathbb{C}^3/\mathbb{Z}_3$. This is the last model in Table 3 of [187], whose quiver is shown in figure 7.23. The gauge group is $SU(p)$, the D7-brane $SU(3) \times SO(3p-1)$ behaves as a global symmetry, and the fields transform as

$$\begin{gathered} SU(p)_{\text{D3}} \times SU(3)_{\text{D7}} \times SO(3p-1)_{\text{D7}} \\ (\,\square\!\square\,;1,1) + 2(\,\begin{smallmatrix}\square\\\square\end{smallmatrix}\,;1,1) + (\,\square\,;\,\square\,,1) + (\,\overline{\square}\,;1,\,\square\,) \quad . \end{gathered} \tag{7.36}$$

This model can be realized using the orientifold of $\mathbb{C}^3/\mathbb{Z}_3$ in section 7.4. Notice that in this case the RR K-theory charge cancellation conditions require odd p instead. The dimer diagram for this theory is the one in figure 7.9, and the SPP$/\mathbb{Z}_3$ orientifold theory providing its UV completion is shown in figure 7.12.

The setup in figure 7.23 is very similar to the one presented in section 7.4.1, figure 7.10, with the only difference being the inclusion of extra stacks of three flavor branes in

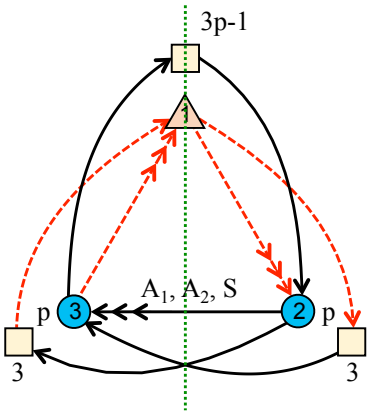

Figure 7.23: The quiver for the orientifold of $\mathbb{C}^3/\mathbb{Z}_3$ theory with flavors. Consistency requires p odd in this case.

the regular representation of the orbifold (thereby neither contributing to the net anomaly nor to the RR tadpoles). Using this relation, it is easy to find a UV completion of this theory by following the analysis in section 7.4. I keep the discussion brief and omit some of the details that were already given in the previous analysis.

Note from figure 7.23 that the 3 additional D7-branes can couple to any of the three types of charged zero modes discussed in the end of section 7.4.4, that I dubbed λ_{53}, λ_{62} and λ_{52}. In what follows I focus on one of these cases, namely coupling the flavor branes to λ_{52}. The other cases can easily be analyzed by following the same ideas explained in this section, and give rise to different non-perturbative terms that I quote by the end of this section.

Given that the IR theory only differs from figure 7.10 by the introduction of three regular D7-branes, it is natural to construct the UV theory as the SPP/$\mathbb{Z}_3$ orientifold therein, with three additional regular D7-branes. The corresponding quiver for the case of interest is shown in figure 7.24. There is a stack of $(3p-1)$ D7-branes on top of the orientifold plane (as compared with $(3p-4)$ in figure 7.17), and three D7-branes coupled to nodes 5 and 2 (and their image D7-branes). Note that the D3-brane numbers remain as in figure 7.10. Cancellation of K-theory RR charge requires p odd (as already obtained for the $\mathbb{C}^3/\mathbb{Z}_3$ orientifold) and M even.

In order to find a UV theory in which the D-brane instanton effects arise from standard gauge dynamics, one must move up the duality cascade until the nodes 2 and 3 are filled. This is done by applying Seiberg duality to whole columns, as described in section 7.4.3. Since the new regular D7-branes do not introduce flavors for the nodes 3, 6 and 9, the result of the first duality up the cascade is given by figure 7.25(b), with the addition of 3 regular D7-branes. The next step up the cascade requires dualizing the nodes 2, 5 and 8, which receive new flavors from the D7-branes. The resulting theory is given by figure 7.25(a), with the 3 additional regular D7-branes, and with the numbers of D3-branes on the dual nodes increased by 3 units for nodes 5, 8 and 2 when compared to figure 7.18.

It is straightforward to continue dualizing up to the UV to reconstruct a duality cascade where the inclusion of the flavor branes only produce $\mathcal{O}(p/N)$ corrections, with

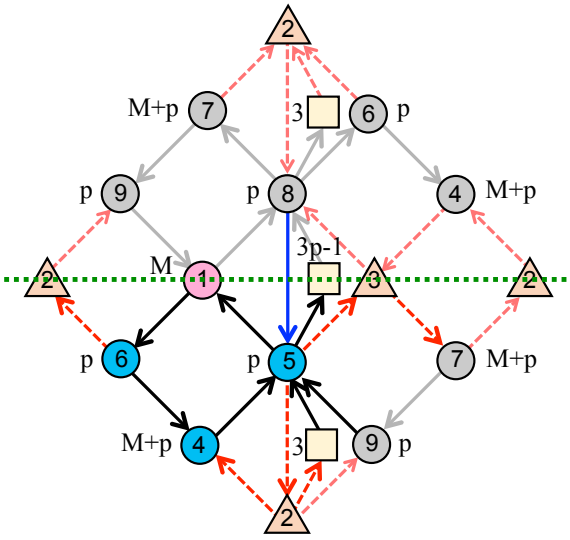

Figure 7.24: Periodic quiver for the orientifold of the SPP/$\mathbb{Z}_3$ theory with extra flavor branes and D-brane instantons sitting on nodes 2 and 3. Consistency requires p odd and M even.

N the number of regular D3-branes.

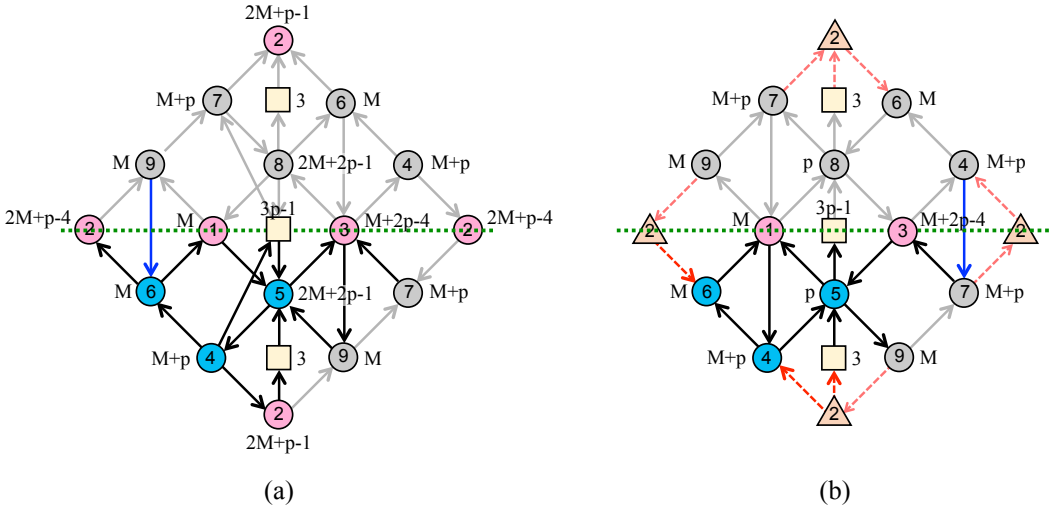

Figure 7.25: (a) Periodic quiver for the orientifold of SPP/$\mathbb{Z}_3$ theory with the extra flavor brane stacks that leads to the setup in figure 7.23 in the IR. (b) The same periodic quiver obtained after considering the strong dynamics of node 2 and dualizing node 5 and its image 8. The triangle on node 2 represents the stringy instanton.

I now use the by now familiar arguments to show that the strong gauge dynamics of the theory in figure 7.25(a) reproduces the D-brane instanton effect in the final $\mathbb{C}^3/\mathbb{Z}_3$ orientifold. First, node 2 is a USp gauge group with $N_f = N_c + 4$ that confines and generates a Pfaffian non-perturbative term in the superpotential. By using the trick in

section 7.3.5, the inclusion of this term is equivalent to performing a Seiberg duality on node 2. Dualizing also nodes 5 and 8, one gets the quiver diagram of figure 7.25(b).

At this point, node 3 is a USp group with $N_f = N_c + 4$, so it confines. Using again the trick in section 7.3.5, one ends up dualizing node 3. Then dualizing nodes 6 and 9 and taking into account the transformation of fermion zero modes in figure 7.19, the resulting theory is precisely figure 7.24.

Finally, the last step in the RG flow is the strong dynamics of nodes 1 and 4 (and its image 7). This process triggers the complex deformation that takes the theory from the orientifold of SPP/$\mathbb{Z}_3$ to the orientifold of $\mathbb{C}^3/\mathbb{Z}_3$. Since the D7-branes do not introduce flavors for these nodes, this process is as described at the end of section 7.4.4. At this point it is important to note that the only difference between the quivers in figure 7.24 and figure 7.17 is that the former contains extra flavor branes that give rise to the new coupling

$$\lambda_{2,\mathrm{D7'}} Q_{\mathrm{D7'},5} \lambda_{52} \,, \tag{7.37}$$

where the prime in the D7 flavor index represents that this stack of D7 branes is different from the one in the setup of section 7.4, which gave rise to the superpotential term (7.34). This coupling was not present in the theory in section 7.4. Fortunately, since this coupling contains no field or zero mode charged under groups 1 and 4 (and its image 7), it is a mere spectator of the deformation process. Therefore, one can just borrow the analysis in section 7.4 and add the extra coupling in the end. This leaves a final superpotential given by (7.34) and the couplings

$$\lambda_{53}{}^T N'_{66} \lambda_{53} - \lambda_{62}{}^T N'_{66} \lambda_{62} - \lambda_{62}{}^T X_{65} \lambda_{52} + \lambda_{52}{}^T X_{65} \lambda_{53} + \lambda_{52} \lambda_{2,D7'} Q_{D7',5} \,. \tag{7.38}$$

This is precisely one of the possible sets of couplings described by the quiver in figure 7.23. The other possibilities arising from that quiver differ from this one in coupling the new stack of three D7-branes to λ_{53} or λ_{62} instead of λ_{52}. In these cases the effect of this new stack on the IR is generating a new coupling of the shape of (7.37), involving the desired charged zero mode. This leaves a series of couplings for e.g. λ_{53}:

$$\lambda_{53}{}^T N'_{66} \lambda_{53} - \lambda_{62}{}^T N'_{66} \lambda_{62} - \lambda_{62}{}^T X_{65} \lambda_{52} + \lambda_{52}{}^T X_{65} \lambda_{53} + \lambda_{53} \lambda_{3,D7'} Q_{D7',5} \,. \tag{7.39}$$

This series of couplings leads to a different non-perturbative terms compared to (7.38) once the zero mode integral is saturated over the instanton partition function. Noting that the non-perturbative term will be of the form (7.4), this means that the matrices on the Pfaffian arising from (7.38) and (7.39) will be different and will have different Pfaffians. For completeness, I just mention that coupling the three D7-branes to λ_{62} leads to the same non-perturbative term as the one obtained from (7.39). These two cases generate different matrices, but their Pfaffians are the same. This is a consequence of the dimer in figure 7.9 being left-right symmetric, which implies that coupling the D7-branes to a zero mode on the left (i.e. λ_{62}) has the same effect as coupling them to the zero mode on the right (i.e. λ_{53}).

8

Conclusions - Conclusiones

In this thesis I described different applications of toric CY singularities that enable a type IIB ST embedding of many cosmology related phenomena. These type of geometries were used to engineer stable warped throats providing a natural explanation to hierarchies in the 4 dimensional effective field theories of D3-branes probing the geometry, in a ST realization of the Randal-Sundrum idea. The stability of the throats was obtained by ISD fluxes from deformation fractional branes, which lead to complex deformations of the conical singularities. The point of using this type of singularities is that many of their properties can be encoded on the so-called web diagrams, which provide a rather simple way of engineering warped throats with certain desired properties, making them very interesting for ST model building. Also, the dimer diagram description of the holographic dual gauge theory enables an alternative and very useful description of many phenomena that take place at these geometries. In the thesis I also provided some new technology that will enable future developments in this direction as I will shortly explain.

The first issue I addressed was providing a geometry where to describe 5-brane axion monodromy inflation. This was done in chapter 3. Axion monodromy scenarios are of particular interest nowadays because they provide a nice way of describing large field inflation in a controlled way: axions are protected by a shift symmetry that highly restricts the possible quantum corrections to their effective potential, and the monodromy allows for superplanckian field ranges that are otherwise very complicated (if not impossible) for a ST axion. In this scenario, the monodromy is achieved by wrapping a NS5-brane in a 2-cycle of the compactification space. Tadpole cancellation then requires to include also an anti NS5-brane wrapping a 2-cycle in the same homology class. For a controlled backreaction of the brane-antibrane pair, these need to be located on the bottom of two daughter warped throats such that the gravitational redshift can cancel the attraction between them. Moreover, control of the backreaction required this geometric structure to arise at the bottom of a larger warped parent throat that splits on the daughter throats forming a 'bifid' throat.

In chapter 3 I provided the technology to build throats with these properties and built up the first explicit realization of a geometry of this kind. This example was based in a very tractable geometry: a $\mathbb{Z}_3 \times \mathbb{Z}_2$ orbifold of the conifold. Moreover, using the holographic description of the explicit example I found the logarithmic backreaction due to the brane-antibrane pair, which is parametrically small compared to the effect of fluxes holding the 3-cycles of the bifid throat. In fact, the backreaction is not only small compared to the warping due to the fluxes, but is of order $\mathcal{O}(1)$ once the warp factors of the different throats are fixed so that they agree with the COBE normalization of the curvature perturbation power spectrum.

The next issue I addressed was the hierarchy between the moduli stabilization scale and the scale of inflation. This was carried out in chapter 4. For inflation to be driven by a single field it is important to set a hierarchy between the inflation scale and the mass of the other moduli, such that the inflaton is the only light scalar field in the effective field theory describing the inflation process. The hierarchy between these scales can be achieved by using warped throats: the moduli stabilization scale is associated to the bulk of a global CY and inflation happens on the throat region, where the energy scale is redshifted.

A difference with the previous chapter goes on the fact that this time I focused on the more recent and more controllable setup of *fluxed* axion monodromy inflation, instead of the 5-brane monodromy scenario. This time the monodromy was induced from the ISD 3-form fluxes supporting the geometry. In order to obtain a monodromic potential for the axion, it is important to have certain intersections on the internal space giving rise to a topological coupling of fluxes that leads to the well known Kaloper-Sorbo 4d term in the Lagrangian after performing dimensional reduction. By using web diagrams, I provided a general prescription to construct warped throats with this topological coupling in section 4.1.1, and focused in the most simple of this type: a cone over the *del Pezzo 3* surface leading to a conifold after performing a complex deformation. In this particular example, I showed that the effect of the monodromy in the holographic description of these systems is to trigger a series of Seiberg dualities that result in a increase of the D3-brane charge. This Seiberg dualities must not be confused with the ones triggered by the RG flow. In this chapter I also provided an estimate of the warping required to create hierarchies such that the scale of inflation agrees with the most recent observations by the combined analysis of Planck and BICEP2 (in the most optimistic limit). More suppressed inflation scales can be easily achieved simply by making the throat deeper. Finally, I provided an analysis of the risk of tunnelling for an axion with a monodromic potential in a warped region using standard thin wall approximation technology. I found that even though the multiplicity of possible decaying routes gets enhanced due to the warping, this is not very risky since the most likely decaying process is highly suppressed and all other processes are exponentially suppressed when compared to this one. A final remark goes on the fact that the whole analysis was performed for type IIB setups, but I also provided a discussion showing how to implement these ideas in type IIA scenarios in section 4.2.

For the rest of the thesis the focus changed to orientifolds of warped throats and applications thereof. The effect of orientifolds on toric CY singularities by their effects on the corresponding dimer diagrams were studied long ago. Still, the inclusion of orientifolds in this type of warped throats had many open questions. In chapter 5 I addressed some of these questions. The first thing I showed was which types of such singularities are compatible with orientifolds, noting that those with fixed lines and fixed points on the dimer have a different geometric action and thus need to be treated separately. The outcome was that singularities whose web diagram is compatible with $\mathbb{Z}_2$ actions leaving a line invariant accept orientifold lines on the dimer, whereas those with four or less odd subsets (odd in the sense of section 5.1.2) of zig-zags accept orientifold points. Using these ideas, I then studied which singularities compatible with orientifold actions accept also complex deformations leading to warped throats. The condition for singularities accepting orientifold lines is that the IR and UV singularities accept the same orientifold line action on the web diagram. For orientifold points instead, the deformation process can only be carried out by the removal of two equal subwebs from the web diagram. These ideas have been applied in the next chapters and provide the technology that will certainly allow for

other applications such as embedding of the nilpotent goldstino in ST constructions.

The previous technology was first used in chapter 6 to build up a geometry that uplifts the cosmological constant to a positive value via a sector with Dynamical Supersymmetry Breaking (DSB) in its effective field theory. The DSB sector I focused on is based on a ST embedding of a particular field theory which was known to lead to DSB since long ago. This explicit model, known as the $SU(5)$ model was described in [163] and first embedded in a ST configuration of D3-branes on an orientifold of a toric CY singularity in [42]. In order to achieve a parametrically small cosmological constant, this DSB sector can be put on the bottom of a warped throat. Since the embedding geometry is an orbifold of $\mathbb{C}^3$, it is a non-cascading geometry and it requires a UV completion of the gauge theory which can be achieved by adding subwebs in equilibrium to the web diagram of this orbifold. These subwebs need to be parallel lines since the effect of the orientifold on the dimer is to invert both coordinates and thus has fixed points. This stringy embedding required of new technology to describe the RG cascade equivalent to the warping of the throat, since it involved Seiberg dualities of sectors with $\mathcal{N} = 2$ fractional branes. The cascade with this technology and subsequent deformation to the DSB field theory were studied in detail throughout section 6.2.

The final topic addressed in the thesis, in chapter 7, is the first UV completion in terms of duality cascades and gauge dynamics of D-brane instanton effects in chiral gauge theories arising on D-branes at singularities. Moreover, the examples also include the first gauge theory completions of D-brane instantons couplings involving flavors. The configurations studied in this chapter had the instanton on top of a orientifold plane, which resulted in a contribution to the superpotential.

The analysis was carried out both for cascading and non-cascading IR geometries, which for the latter required of a UV completion by embedding it in a larger singularity admitting cascades and eventually leading to the IR singularity after a complex deformation. An interesting aspect was that, since the UV and IR theories are related by recombination of gauge factors, the IR instanton was reproduced by a multi-instanton process in the UV theory.

Finally, a trick was introduced in 7.3.5 recasting Pfaffian contributions from D-brane instantons as path integrals over auxiliary Grassmann variables, which precisely correspond to the fermionic zero modes in the D-brane construction. With this rewriting all necessary manipulations of the gauge theories reduce to the standard ones on the dimer or the periodic quiver and allow to integrate out the fermionic zero modes at the most convenient moment.

All in all, it is clear that warped throats from toric CY singularities provide a very nice scenario to embed many Cosmology related phenomena into ST. This goes from large field Inflation to providing a natural explanation to a small positive cosmological constant. Moreover, the criterion presented on this thesis telling which geometries of this type are compatible with orientifolds provides the tools to develop models describing other phenomena.

Conclusiones

En esta tesis he descrito diferentes aplicaciones de singularidades Calabi-Yau tóricas para embeber varios fenómenos cosmológicos en Teoría de Cuerdas tipo IIB. Este tipo de geometrías se han utilizado para diseñar gargantas con factores de deformadas estables en la geometría interna (a partir de aquí me referiré a ellas simplemente como gargantas), proporcionando una explicación natural a las jerarquías en las teorías efectivas en 4 dimensiones correspondientes a D3-branas en la geometría, en una realización de Teoría de Cuerdas de la propuesta de Randal-Sundrum. La estabilidad de las gargantas se obtiene por flujos imaginarios auto-duales (ISD por las siglas en inglés) debidos a branas fraccionarias de deformación, que provocan deformaciones complejas de las singularidades cónicas. El hecho de usar este tipo de singularidades se debe a que muchas de sus propiedades se pueden codificar en los denominados diagramas web, que proporcionan una receta sencilla para diseñar gargantas con las propiedades deseadas, haciéndolas muy interesantes para la construcción de modelos en Teoría de Cuerdas. Además, la descripción de la teoría dual holográfica de las cuerdas abiertas en la D3-brana se puede decodificar en un diagrama conocido como *dimer*, que hace posible una descripción alternativa muy útil de muchos fenómenos que tienen lugar en estas geometrías. Cabe recalcar además que en esta tesis desarrollo nueva tecnología sobre orientifolds de gargantas que será útil en futuros trabajos en esta dirección.

El primer problema que abordé fue proporcionar una geometría para describir inflación cósmica por monodromía (debida a una 5-brana) de un axión, descrita en el capítulo 3. Los modelos de monodromía de axiones son especialmente interesantes hoy en día, ya que proporcionan una buena forma de describir inflación *large field* (caracterizada por recorridos trans-Planckianos del inflatón) de una manera controlada: los axiones están protegidos por una simetría de traslación que restringe mucho las posibles correcciones cuánticas a su potencial efectivo, y la monodromía permite rangos de campo trans-Planckianos, que son muy difíciles (o quizá hasta imposibles) de obtener para axiones en Teoría de Cuerdas. En este tipo de escenario, la monodromía se consigue enrollando una NS5-brana en un 2-ciclo del espacio compacto. La cancelación de *tadpoles* requiere incluir también una anti NS5-brana enrollando otro 2-ciclo en la misma clase de homología. Para una autointeracción controlada del par brana-antibrana, el par necesita estar localizado en el fondo de dos gargantas, de tal manera que el campo gravitatorio es capaz de evitar que decaigan a pesar de la atracción entre ambas branas. Además, el control de la autointeracción requiere que esta estructura geométrica se sitúe al fondo de una garganta mayor, que en la parte de abajo se divide en las pequeñas gargantas antes mencionadas, formando lo que denominamos una garganta 'bífida'.

En el capítulo 3 proporciono la tecnología para construir gargantas con estas propiedades y construyo la primera realización explícita de una geometría de este tipo. Este ejemplo está basado en una geometría conocida: un órbifold $\mathbb{Z}_3 \times \mathbb{Z}_2$ del conifold. Además, usando la descripción holográfica de este ejemplo explícito, se puede describir la autointeracción logarítmica debido al par brana-antibrana, que es paramétricamente pequeño comparado con el efecto de los flujos que sostienen el 3-ciclo de la garganta bífida en tamaño no nulo. De hecho, la autointeracción no es sólo pequeña en comparación con la deformación debida a los flujos, sino que es de orden $\mathcal{O}(1)$ una vez que los factores de deformación de las diferentes gargantas están fijados, acuerdo con la normalización COBE del espectro de potencia de la curvatura de perturbación.

El siguiente problema que he abordado es la jerarquía entre la escala de estabilización de módulos y la escala de inflación, descrita en el capítulo 4. Esta jerarquía es importante para que inflación sea producida por un único campo en Teoría de Cuerdas, y requiere separar las escalas de Inflación y la masa del resto de módulos, para que el inflatón sea el único campo escalar ligero en la teoría efectiva que describe el proceso de inflación. La jerarquía entre estas escalas se puede lograr usando gargantas: la escala de estabilización de módulos está asociada al *bulk* del CY global, y el proceso de inflación se localiza en la garganta, donde la escala de energía está suprimida por el factor de deformación del espacio interno.

Una diferencia con el capítulo anterior reside en que esta vez la monodromía del axión se obtiene mediante el uso de flujos en vez de 5-branas, lo que permite un mejor control de la configuración. La monodromía proviene de los flujos de 3-forma ISD que sostienen la geometría. Para obtener un potencial monodrómico para el axión es importante tener ciertas intersecciones en el espacio interno, dando lugar a un acoplo topológico de flujos que da lugar, tras hacer reducción dimensional, al término del Lagrangiano que supone el orígen de la monodromía en los trabajos de Kaloper-Sorbo. Mediante el uso de diagramas web he proporcionado una prescripción general para construir gargantas deformadas con este acoplo topológico en la sección 4.1.1. Después me he centrado en el caso más simple de este tipo: un cono sobre la superficie *del Pezzo 3*, que tras una deformación compleja se convierte en el conifold. En este ejemplo muestro que el efecto de la monodromía en la descripción holográfica corresponde a una serie de dualidades de Seiberg que incrementan la carga de D3-brana. Estas dualidades de Seiberg no deben confundirse con las provocadas por el grupo de renormalización. En este capítulo también proporciono una estimación de la deformación requerida para crear jerarquías que dan una escala de inflación que concuerda con las observaciones más recientes del análisis combinado de Planck y BICEP2 en el caso más optimista. Escalas de inflación más suprimidas con respecto a la escala de estabilización de módulos pueden conseguirse incrementando la longitud de la garganta. Finalmente, proporciono un análisis del riesgo de decaimiento del axión con potencial monodrómico dentro de una garganta mediante nucleación de burbujas, utilizando tecnología estándar de la aproximación de muro fino. El resultado es que a pesar de que la multiplicidad de rutas de decaimiento aumenta debido al factor de deformación, esto no es peligroso, ya que el proceso más probable de decaimiento está altamente suprimido y el resto de procesos están exponecialmente suprimidos con respecto a éste. Una última observación: el análisis anterior describe configuraciones de Teoría de Cuerdas tipo IIB, pero en la sección 4.2 también se incluye un análisis explicando cómo implementar estas ideas en configuraciones de tipo IIA.

En el resto de la tesis el tema cambia a orientifolds de gargantas y algunas aplicaciones de este tipo de geometrías. El efecto de orientifolds en singularidades CY tóricas mediante su efecto en los diagramas dimer se conocían desde hace tiempo. No en vano, quedaban muchas preguntas abiertas sobre la inclusión de orientifolds en gargantas a partir de singularidades de este tipo. Algunas de estas preguntas se estudiaron en el capítulo 5. La primera cosa que mostré fue qué tipos de singularidades son compatibles con orientifolds, observando que los que tienen líneas fijas y puntos fijos en el dimer tienen acción geométrica diferente y por lo tanto necesitan ser tratadas por separado. El resultado es que las singularidades cuyos diagramas web son compatibles con acciones $\mathbb{Z}_2$ que dejan una línea invariante aceptan orientifolds con líneas fijas en el dimer, mientras que aquellos con cuatro o menos subconjuntos impares (impar en el sentido de la sección 5.1.2) de zig-zags

aceptan orientifolds con puntos fijos en el dimer. Usando estas ideas, he estudiado qué singularidades compatibles con acciones orientifold aceptan también deformaciones complejas que dan pie a gargantas deformadas. La condición para singularidades que aceptan orientifolds con líneas fijas es que las singularidades IR y UV aceptan la misma línea de acción orientifold en el diagrama web. Para puntos orientifold, en cambio, el proceso de deformación debe implicar la eliminación de dos subwebs iguales del diagrama web. Estas ideas han sido aplicadas en los siguientes capítulos y proporcionan la tecnología que seguramente permitirá otras aplicaciones, tales como el embebimiento del goldstino nilpotente en construcciones de Teoría de Cuerdas.

La tecnología anterior se ha usado primero en el capítulo6 para construir una geometría que incrementa la constante cosmológica para que tenga un valor positivo a través de un sector con Ruptura Dinámica de Supersimetría (DSB por las siglas en inglés) en su teoría efectiva. El sector DSB en el que me he centrado es un embebimiento cuerdoso basado en una teoría de campos particular que se sabía que llevaba a DSB. Esta teoría o modelo, conocido como modelo $SU(5)$, fue descrito en [163] e integrado por primera vez en una cofiguración de Teoría de Cuerdas en términos de D3-branas en un orientifold de una singularidad CY tórica en [42]. Con el fin de lograr una constante cosmológica paramétricamente pequeña, se puede colocar este sector DSB en el fondo de una garganta deformada. Dado que la geometría donde se embebe es un órbifold de $\mathbb{C}^3$, es una geometría que no-*cascadea* y requiere una compleción al ultravioleta de la teoría gauge dual. Esta compleción se puede conseguir añadiendo subwebs en equilibrio al diagrama web de este orientifold de un órbifold. Estas subwebs deben ser líneas paralelas ya que el efecto del orientifold deja puntos fijos en el dimer. Este embebimiento cuerdoso requiere de nueva tecnología para describir el equivalente de la garganta en términos de una cascada de dualidades de Sieberg. Esto se debe a que la cascada implica dualidades de Seiberg de sectores con branas fraccionarias $\mathcal{N} = 2$. La cascada (usando esta nueva tecnología) y la posterior deformación a la teoría con DSB fueron estudiados en detalle en la sección 6.2.

El último tema abordado en la tesis, en el capítulo 7, es la primera compleción al ultravioleta en términos de cascadas de dualidades y dinámica gauge de los efectos de instantón de D-brana en teorías gauge quirales provenientes de D3-branas en singularidades. Los ejemplos tratados en este capítulo también incluyen la primera compleción ultravioleta en teoría gauge de instantones de D-brana dando pie acoplos que implican sabores. Las configuraciones estudiadas en este capítulo tienen el instantón localizado sobre un orientifold, lo que produce un término no perturbativo en el superpotencial.

El análisis fue llevado a cabo para geometrías infrarrojas que aceptan una cascada de dualidades de Seiberg y también para aquellas que *a priori* no la aceptan. Para estas últimas es necesario embebeberlas en singularidades mayores que sí que aceptan una cascada de dualidades, y que tras una deformación compleja dan pie a la singularidad sin cascada en el infrarrojo. Estas últimas singularidades tienen la peculiaridad de que en el instantón infrarrojo se traduce en un proceso de multi-instantón en el ultravioleta, ya que los grupos gauge del infrarrojo provienen de la recombinación de varios grupos del ultravioleta.

Finalmente, cabe recalcar el desarrollo de una técnica que permite reescribir los términos no perturbativos provenientes del instantón con forma de Pfaffiano en términos de integrales sobre campos de Grassmann auxiliares. Estos campos de Grassmann corresponden precisamente a los modos zero fermiónicos del instantón. Usando esta idea es

posible manipular de forma estándar el dimer para realizar las operaciones necesarias en la teoría gauge y hacer la integral sobre estos modos zero fermiónicos en el momento que más convenga.

En conclusión, está claro que las gargantas deformes a partir de singularidades CY tóricas son una herramienta muy útil para embeber en Teoría de Cuerdas varios fenómenos relacionados con Cosmología. Esto incluye desde inflación *large field* o dar una explicación natural para una constante cosmológica positiva y pequeña. Además, en esta tesis se han presentado una serie de herramientas para decir qué gargantas de este tipo son compatibles con acciones de orientifold, una técnica que seguro que será útil en la construcción de modelos en Teoría de Cuerdas en el futuro.

Bibliography

[1] L. Randall and R. Sundrum, "A Large mass hierarchy from a small extra dimension," *Phys. Rev. Lett.*, vol. 83, pp. 3370–3373, 1999.

[2] H. L. Verlinde, "Holography and compactification," *Nucl. Phys.*, vol. B580, pp. 264–274, 2000.

[3] K. Dasgupta, G. Rajesh, and S. Sethi, "M theory, orientifolds and G - flux," *JHEP*, vol. 08, p. 023, 1999.

[4] S. B. Giddings, S. Kachru, and J. Polchinski, "Hierarchies from fluxes in string compactifications," *Phys. Rev.*, vol. D66, p. 106006, 2002.

[5] I. R. Klebanov and M. J. Strassler, "Supergravity and a confining gauge theory: Duality cascades and chi SB resolution of naked singularities," *JHEP*, vol. 0008, p. 052, 2000.

[6] A. Hanany and K. D. Kennaway, "Dimer models and toric diagrams," 2005.

[7] J. M. Maldacena, "The Large N limit of superconformal field theories and supergravity," *Int. J. Theor. Phys.*, vol. 38, pp. 1113–1133, 1999. [Adv. Theor. Math. Phys.2,231(1998)].

[8] I. R. Klebanov and E. Witten, "Superconformal field theory on three-branes at a Calabi-Yau singularity," *Nucl. Phys.*, vol. B536, pp. 199–218, 1998.

[9] P. Candelas and X. C. de la Ossa, "Comments on Conifolds," *Nucl. Phys.*, vol. B342, pp. 246–268, 1990.

[10] S. S. Gubser and I. R. Klebanov, "Baryons and domain walls in an N=1 superconformal gauge theory," *Phys. Rev.*, vol. D58, p. 125025, 1998.

[11] I. R. Klebanov and N. A. Nekrasov, "Gravity duals of fractional branes and logarithmic RG flow," *Nucl. Phys.*, vol. B574, pp. 263–274, 2000.

[12] I. R. Klebanov and A. A. Tseytlin, "Gravity duals of supersymmetric SU(N) x SU(N+M) gauge theories," *Nucl. Phys.*, vol. B578, pp. 123–138, 2000.

[13] N. Seiberg, "Electric - magnetic duality in supersymmetric nonAbelian gauge theories," *Nucl. Phys.*, vol. B435, pp. 129–146, 1995.

[14] S. Gukov, C. Vafa, and E. Witten, "CFT's from Calabi-Yau four folds," *Nucl. Phys.*, vol. B584, pp. 69–108, 2000. [Erratum: Nucl. Phys.B608,477(2001)].

[15] I. Affleck, M. Dine, and N. Seiberg, "Dynamical Supersymmetry Breaking in Supersymmetric QCD," *Nucl. Phys.*, vol. B241, pp. 493–534, 1984.

[16] M. Grana and J. Polchinski, "Supersymmetric three form flux perturbations on AdS(5)," *Phys. Rev.*, vol. D63, p. 026001, 2001.

[17] A. Hanany and I. R. Klebanov, "On tensionless strings in (3+1)-dimensions," *Nucl. Phys.*, vol. B482, pp. 105–118, 1996.

[18] A. M. Uranga, "Brane configurations for branes at conifolds," *JHEP*, vol. 9901, p. 022, 1999.

[19] K. Dasgupta and S. Mukhi, "Brane constructions, conifolds and M theory," *Nucl. Phys.*, vol. B551, pp. 204–228, 1999.

[20] M. Bershadsky, C. Vafa, and V. Sadov, "D strings on D manifolds," *Nucl. Phys.*, vol. B463, pp. 398–414, 1996.

[21] S. Elitzur, A. Giveon, and D. Kutasov, "Branes and N=1 duality in string theory," *Phys.Lett.*, vol. B400, pp. 269–274, 1997.

[22] S. Franco, A. Hanany, F. Saad, and A. M. Uranga, "Fractional branes and dynamical supersymmetry breaking," *JHEP*, vol. 0601, p. 011, 2006.

[23] I. García-Etxebarria, F. Quevedo, and R. Valandro, "Global String Embeddings for the Nilpotent Goldstino," *JHEP*, vol. 02, p. 148, 2016.

[24] R. G. Leigh and M. Rozali, "Brane boxes, anomalies, bending and tadpoles," *Phys. Rev.*, vol. D59, p. 026004, 1999.

[25] A. E. Lawrence, N. Nekrasov, and C. Vafa, "On conformal field theories in four-dimensions," *Nucl. Phys.*, vol. B533, pp. 199–209, 1998.

[26] A. Hanany and Y.-H. He, "NonAbelian finite gauge theories," *JHEP*, vol. 02, p. 013, 1999.

[27] M. R. Douglas, B. R. Greene, and D. R. Morrison, "Orbifold resolution by D-branes," *Nucl. Phys.*, vol. B506, pp. 84–106, 1997.

[28] C. Beasley, B. R. Greene, C. I. Lazaroiu, and M. R. Plesser, "D3-branes on partial resolutions of Abelian quotient singularities of Calabi-Yau threefolds," *Nucl. Phys.*, vol. B566, pp. 599–640, 2000.

[29] B. Feng, A. Hanany, and Y.-H. He, "D-brane gauge theories from toric singularities and toric duality," *Nucl. Phys.*, vol. B595, pp. 165–200, 2001.

[30] B. Feng, A. Hanany, and Y.-H. He, "Phase structure of D-brane gauge theories and toric duality," *JHEP*, vol. 08, p. 040, 2001.

[31] C. E. Beasley and M. R. Plesser, "Toric duality is Seiberg duality," *JHEP*, vol. 12, p. 001, 2001.

[32] V. Bouchard, "Lectures on complex geometry, Calabi-Yau manifolds and toric geometry," 2007.

[33] M. Aganagic and C. Vafa, "G(2) manifolds, mirror symmetry and geometric engineering," 2001.

[34] R. Kenyon, A. Okounkov, and S. Sheffield, "Dimers and amoebae," 2003.

[35] A. Okounkov, N. Reshetikhin, and C. Vafa, "Quantum Calabi-Yau and classical crystals," *Prog. Math.*, vol. 244, p. 597, 2006.

[36] A. Iqbal, N. Nekrasov, A. Okounkov, and C. Vafa, "Quantum foam and topological strings," *JHEP*, vol. 04, p. 011, 2008.

[37] S. Franco, A. Hanany, K. D. Kennaway, D. Vegh, and B. Wecht, "Brane dimers and quiver gauge theories," *JHEP*, vol. 0601, p. 096, 2006.

[38] A. Hanany and D. Vegh, "Quivers, tilings, branes and rhombi," *JHEP*, vol. 10, p. 029, 2007.

[39] B. Feng, A. Hanany, Y.-H. He, and A. M. Uranga, "Toric duality as Seiberg duality and brane diamonds," *JHEP*, vol. 12, p. 035, 2001.

[40] S. Franco, A. Hanany, and A. M. Uranga, "Multi-flux warped throats and cascading gauge theories," *JHEP*, vol. 0509, p. 028, 2005.

[41] I. Garcia-Etxebarria, F. Saad, and A. M. Uranga, "Quiver gauge theories at resolved and deformed singularities using dimers," *JHEP*, vol. 0606, p. 055, 2006.

[42] S. Franco, A. Hanany, D. Krefl, J. Park, A. M. Uranga, and D. Vegh, "Dimers and orientifolds," *JHEP*, vol. 0709, p. 075, 2007.

[43] B. Feng, Y.-H. He, K. D. Kennaway, and C. Vafa, "Dimer models from mirror symmetry and quivering amoebae," *Adv. Theor. Math. Phys.*, vol. 12, no. 3, pp. 489–545, 2008.

[44] G. Aldazabal, S. Franco, L. E. Ibanez, R. Rabadan, and A. M. Uranga, "Intersecting brane worlds," *JHEP*, vol. 02, p. 047, 2001.

[45] G. Aldazabal, S. Franco, L. E. Ibanez, R. Rabadan, and A. M. Uranga, "D = 4 chiral string compactifications from intersecting branes," *J. Math. Phys.*, vol. 42, pp. 3103–3126, 2001.

[46] O. Aharony, A. Hanany, and B. Kol, "Webs of (p,q) five-branes, five-dimensional field theories and grid diagrams," *JHEP*, vol. 01, p. 002, 1998.

[47] O. Aharony and A. Hanany, "Branes, superpotentials and superconformal fixed points," *Nucl. Phys.*, vol. B504, pp. 239–271, 1997.

[48] N. C. Leung and C. Vafa, "Branes and toric geometry," *Adv. Theor. Math. Phys.*, vol. 2, pp. 91–118, 1998.

[49] A. Retolaza, A. M. Uranga, and A. Westphal, "Bifid Throats for Axion Monodromy Inflation," *JHEP*, vol. 07, p. 099, 2015.

[50] S. Franco, A. Retolaza, and A. Uranga, "D-brane Instantons as Gauge Instantons in Orientifolds of Chiral Quiver Theories," *JHEP*, vol. 11, p. 165, 2015.

[51] A. Retolaza and A. Uranga, "De Sitter Uplift with Dynamical Susy Breaking," *JHEP*, vol. 04, p. 137, 2016.

[52] J. F. G. Cascales, M. P. Garcia del Moral, F. Quevedo, and A. M. Uranga, "Realistic D-brane models on warped throats: Fluxes, hierarchies and moduli stabilization," *JHEP*, vol. 02, p. 031, 2004.

[53] J. F. Cascales, F. Saad, and A. M. Uranga, "Holographic dual of the standard model on the throat," *JHEP*, vol. 0511, p. 047, 2005.

[54] J. J. Heckman, C. Vafa, H. Verlinde, and M. Wijnholt, "Cascading to the MSSM," *JHEP*, vol. 06, p. 016, 2008.

[55] S. Franco, D. Rodriguez-Gomez, and H. Verlinde, "N-ification of Forces: A Holographic Perspective on D-brane Model Building," *JHEP*, vol. 0906, p. 030, 2009.

[56] D. Berenstein, C. P. Herzog, P. Ouyang, and S. Pinansky, "Supersymmetry breaking from a Calabi-Yau singularity," *JHEP*, vol. 09, p. 084, 2005.

[57] M. Bertolini, F. Bigazzi, and A. L. Cotrone, "Supersymmetry breaking at the end of a cascade of Seiberg dualities," *Phys. Rev.*, vol. D72, p. 061902, 2005.

[58] S. Franco and A. M. . Uranga, "Dynamical SUSY breaking at meta-stable minima from D-branes at obstructed geometries," *JHEP*, vol. 06, p. 031, 2006.

[59] R. Argurio, M. Bertolini, S. Franco, and S. Kachru, "Gauge/gravity duality and meta-stable dynamical supersymmetry breaking," *JHEP*, vol. 0701, p. 083, 2007.

[60] R. Argurio, M. Bertolini, S. Franco, and S. Kachru, "Meta-stable vacua and D-branes at the conifold," *JHEP*, vol. 0706, p. 017, 2007.

[61] S. Kachru, R. Kallosh, A. D. Linde, and S. P. Trivedi, "De Sitter vacua in string theory," *Phys. Rev.*, vol. D68, p. 046005, 2003.

[62] P. Ade *et al.*, "Joint Analysis of BICEP2/*Keck?Array* and *Planck* Data," *Phys. Rev. Lett.*, vol. 114, p. 101301, 2015.

[63] P. Creminelli, D. L. López Nacir, M. Simonovi?, G. Trevisan, and M. Zaldarriaga, "Detecting Primordial B-Modes after Planck," *JCAP*, vol. 1511, no. 11, p. 031, 2015.

[64] D. Baumann and L. McAllister, *Inflation and String Theory*. Cambridge University Press, 2015.

[65] D. H. Lyth, "What would we learn by detecting a gravitational wave signal in the cosmic microwave background anisotropy?," *Phys. Rev. Lett.*, vol. 78, pp. 1861–1863, 1997.

[66] J. E. Kim, H. P. Nilles, and M. Peloso, "Completing natural inflation," *JCAP*, vol. 0501, p. 005, 2005.

[67] S. Dimopoulos, S. Kachru, J. McGreevy, and J. G. Wacker, "N-flation," *JCAP*, vol. 0808, p. 003, 2008.

[68] T. W. Grimm, "Axion inflation in type II string theory," *Phys. Rev.*, vol. D77, p. 126007, 2008.

[69] M. Berg, E. Pajer, and S. Sjors, "Dante's Inferno," *Phys. Rev.*, vol. D81, p. 103535, 2010.

[70] I. Ben-Dayan, F. G. Pedro, and A. Westphal, "Towards Natural Inflation in String Theory," *Phys. Rev.*, vol. D92, no. 2, p. 023515, 2015.

[71] I. Ben-Dayan, F. G. Pedro, and A. Westphal, "Hierarchical Axion Inflation," *Phys. Rev. Lett.*, vol. 113, p. 261301, 2014.

[72] N. Arkani-Hamed, L. Motl, A. Nicolis, and C. Vafa, "The String landscape, black holes and gravity as the weakest force," *JHEP*, vol. 06, p. 060, 2007.

[73] T. Rudelius, "On the Possibility of Large Axion Moduli Spaces," *JCAP*, vol. 1504, no. 04, p. 049, 2015.

[74] T. Rudelius, "Constraints on Axion Inflation from the Weak Gravity Conjecture," *JCAP*, vol. 1509, no. 09, p. 020, 2015.

[75] M. Montero, A. M. Uranga, and I. Valenzuela, "Transplanckian axions!?," *JHEP*, vol. 08, p. 032, 2015.

[76] J. Brown, W. Cottrell, G. Shiu, and P. Soler, "Fencing in the Swampland: Quantum Gravity Constraints on Large Field Inflation," *JHEP*, vol. 10, p. 023, 2015.

[77] T. C. Bachlechner, C. Long, and L. McAllister, "Planckian Axions and the Weak Gravity Conjecture," *JHEP*, vol. 01, p. 091, 2016.

[78] A. Hebecker, P. Mangat, F. Rompineve, and L. T. Witkowski, "Winding out of the Swamp: Evading the Weak Gravity Conjecture with F-term Winding Inflation?," *Phys. Lett.*, vol. B748, pp. 455–462, 2015.

[79] J. Brown, W. Cottrell, G. Shiu, and P. Soler, "On Axionic Field Ranges, Loopholes and the Weak Gravity Conjecture," *JHEP*, vol. 04, p. 017, 2016.

[80] D. Junghans, "Large-Field Inflation with Multiple Axions and the Weak Gravity Conjecture," *JHEP*, vol. 02, p. 128, 2016.

[81] B. Heidenreich, M. Reece, and T. Rudelius, "Weak Gravity Strongly Constrains Large-Field Axion Inflation," *JHEP*, vol. 12, p. 108, 2015.

[82] E. Palti, "On Natural Inflation and Moduli Stabilisation in String Theory," *JHEP*, vol. 10, p. 188, 2015.

[83] B. Heidenreich, M. Reece, and T. Rudelius, "Sharpening the Weak Gravity Conjecture with Dimensional Reduction," *JHEP*, vol. 02, p. 140, 2016.

[84] K. Kooner, S. Parameswaran, and I. Zavala, "Warping the Weak Gravity Conjecture," 2015.

[85] L. E. Ibanez, M. Montero, A. Uranga, and I. Valenzuela, "Relaxion Monodromy and the Weak Gravity Conjecture," *JHEP*, vol. 04, p. 020, 2016.

[86] E. Silverstein and A. Westphal, "Monodromy in the CMB: Gravity Waves and String Inflation," *Phys. Rev.*, vol. D78, p. 106003, 2008.

[87] L. McAllister, E. Silverstein, and A. Westphal, "Gravity Waves and Linear Inflation from Axion Monodromy," *Phys. Rev.*, vol. D82, p. 046003, 2010.

[88] F. Marchesano, G. Shiu, and A. M. Uranga, "F-term Axion Monodromy Inflation," *JHEP*, vol. 09, p. 184, 2014.

[89] R. Blumenhagen and E. Plauschinn, "Towards Universal Axion Inflation and Reheating in String Theory," *Phys. Lett.*, vol. B736, pp. 482–487, 2014.

[90] A. Hebecker, S. C. Kraus, and L. T. Witkowski, "D7-Brane Chaotic Inflation," *Phys. Lett.*, vol. B737, pp. 16–22, 2014.

[91] L. McAllister, E. Silverstein, A. Westphal, and T. Wrase, "The Powers of Monodromy," *JHEP*, vol. 09, p. 123, 2014.

[92] N. Kaloper and L. Sorbo, "A Natural Framework for Chaotic Inflation," *Phys. Rev. Lett.*, vol. 102, p. 121301, 2009.

[93] N. Kaloper, A. Lawrence, and L. Sorbo, "An Ignoble Approach to Large Field Inflation," *JCAP*, vol. 1103, p. 023, 2011.

[94] N. Kaloper and A. Lawrence, "Natural chaotic inflation and ultraviolet sensitivity," *Phys. Rev.*, vol. D90, no. 2, p. 023506, 2014.

[95] T. Banks, M. Dine, P. J. Fox, and E. Gorbatov, "On the possibility of large axion decay constants," *JCAP*, vol. 0306, p. 001, 2003.

[96] E. Palti and T. Weigand, "Towards large r from [p, q]-inflation," *JHEP*, vol. 04, p. 155, 2014.

[97] R. Flauger, L. McAllister, E. Pajer, A. Westphal, and G. Xu, "Oscillations in the CMB from Axion Monodromy Inflation," *JCAP*, vol. 1006, p. 009, 2010.

[98] J. P. Conlon, "Brane-Antibrane Backreaction in Axion Monodromy Inflation," *JCAP*, vol. 1201, p. 033, 2012.

[99] A. Hanany and E. Witten, "Type IIB superstrings, BPS monopoles, and three-dimensional gauge dynamics," *Nucl.Phys.*, vol. B492, pp. 152–190, 1997.

[100] S. Kachru, J. Pearson, and H. L. Verlinde, "Brane / flux annihilation and the string dual of a nonsupersymmetric field theory," *JHEP*, vol. 06, p. 021, 2002.

[101] J. D. Lykken, E. Poppitz, and S. P. Trivedi, "Chiral gauge theories from D-branes," *Phys.Lett.*, vol. B416, pp. 286–294, 1998.

[102] I. Bena, M. Grana, and N. Halmagyi, "On the Existence of Meta-stable Vacua in Klebanov-Strassler," *JHEP*, vol. 09, p. 087, 2010.

[103] I. Bena, G. Giecold, M. Grana, N. Halmagyi, and S. Massai, "On Metastable Vacua and the Warped Deformed Conifold: Analytic Results," *Class. Quant. Grav.*, vol. 30, p. 015003, 2013.

[104] I. Bena, G. Giecold, M. Grana, N. Halmagyi, and S. Massai, "The backreaction of anti-D3 branes on the Klebanov-Strassler geometry," *JHEP*, vol. 06, p. 060, 2013.

[105] J. Blaback, U. H. Danielsson, and T. Van Riet, "Resolving anti-brane singularities through time-dependence," *JHEP*, vol. 02, p. 061, 2013.

[106] I. Bena, M. Grana, S. Kuperstein, and S. Massai, "Anti-D3 Branes: Singular to the bitter end," *Phys. Rev.*, vol. D87, no. 10, p. 106010, 2013.

[107] I. Bena, J. Blaback, U. H. Danielsson, and T. Van Riet, "Antibranes cannot become black," *Phys. Rev.*, vol. D87, no. 10, p. 104023, 2013.

[108] J. Blĺbäck, U. H. Danielsson, D. Junghans, T. Van Riet, and S. C. Vargas, "Localised anti-branes in non-compact throats at zero and finite T," *JHEP*, vol. 02, p. 018, 2015.

[109] I. Bena, M. Grańa, S. Kuperstein, and S. Massai, "Giant Tachyons in the Landscape," *JHEP*, vol. 02, p. 146, 2015.

[110] U. H. Danielsson and T. Van Riet, "Fatal attraction: more on decaying anti-branes," *JHEP*, vol. 03, p. 087, 2015.

[111] I. Bena and S. Kuperstein, "Brane polarization is no cure for tachyons," *JHEP*, vol. 09, p. 112, 2015.

[112] A. Karch, D. Lust, and D. J. Smith, "Equivalence of geometric engineering and Hanany-Witten via fractional branes," *Nucl. Phys.*, vol. B533, pp. 348–372, 1998.

[113] M. Grana and J. Polchinski, "Gauge / gravity duals with holomorphic dilaton," *Phys. Rev.*, vol. D65, p. 126005, 2002.

[114] S. Franco, D. Galloni, A. Retolaza, and A. Uranga, "On axion monodromy inflation in warped throats," *JHEP*, vol. 02, p. 086, 2015.

[115] L. E. Ibáñez and I. Valenzuela, "The inflaton as an MSSM Higgs and open string modulus monodromy inflation," *Phys. Lett.*, vol. B736, pp. 226–230, 2014.

[116] M. Arends, A. Hebecker, K. Heimpel, S. C. Kraus, D. Lust, C. Mayrhofer, C. Schick, and T. Weigand, "D7-Brane Moduli Space in Axion Monodromy and Fluxbrane Inflation," *Fortsch. Phys.*, vol. 62, pp. 647–702, 2014.

[117] M. Berasaluce-Gonzalez, P. G. Camara, F. Marchesano, and A. M. Uranga, "Zp charged branes in flux compactifications," *JHEP*, vol. 04, p. 138, 2013.

[118] M. Berasaluce-González, G. Ramírez, and A. M. Uranga, "Antisymmetric tensor Z_p gauge symmetries in field theory and string theory," *JHEP*, vol. 01, p. 059, 2014.

[119] V. Balasubramanian, P. Berglund, V. Braun, and I. Garcia-Etxebarria, "Global embeddings for branes at toric singularities," *JHEP*, vol. 10, p. 132, 2012.

[120] B. Feng, S. Franco, A. Hanany, and Y.-H. He, "Symmetries of toric duality," *JHEP*, vol. 0212, p. 076, 2002.

[121] I. R. Klebanov and A. Murugan, "Gauge/Gravity Duality and Warped Resolved Conifold," *JHEP*, vol. 03, p. 042, 2007.

[122] S. Franco, Y.-H. He, C. Herzog, and J. Walcher, "Chaotic duality in string theory," *Phys.Rev.*, vol. D70, p. 046006, 2004.

[123] A. Giveon and D. Kutasov, "Brane dynamics and gauge theory," *Rev. Mod. Phys.*, vol. 71, pp. 983–1084, 1999.

[124] E. Witten, "Branes and the dynamics of QCD," *Nucl. Phys.*, vol. B507, pp. 658–690, 1997.

[125] C. Vafa, "Superstrings and topological strings at large N," *J. Math. Phys.*, vol. 42, pp. 2798–2817, 2001.

[126] M. Atiyah, J. M. Maldacena, and C. Vafa, "An M theory flop as a large N duality," *J. Math. Phys.*, vol. 42, pp. 3209–3220, 2001.

[127] M. Atiyah and E. Witten, "M theory dynamics on a manifold of G(2) holonomy," *Adv. Theor. Math. Phys.*, vol. 6, pp. 1–106, 2003.

[128] X. Dong, B. Horn, E. Silverstein, and A. Westphal, "Simple exercises to flatten your potential," *Phys. Rev.*, vol. D84, p. 026011, 2011.

[129] S. Kuperstein, "Non-supersymmetric deformation of the Klebanov-Strassler model and the related plane wave theory," *Subnucl. Ser.*, vol. 41, pp. 498–507, 2005.

[130] A. R. Frey and A. Maharana, "Warped spectroscopy: Localization of frozen bulk modes," *JHEP*, vol. 08, p. 021, 2006.

[131] K. Dasgupta, H. Firouzjahi, and R. Gwyn, "On The Warped Heterotic Axion," *JHEP*, vol. 06, p. 056, 2008.

[132] S. Dubovsky, A. Lawrence, and M. M. Roberts, "Axion monodromy in a model of holographic gluodynamics," *JHEP*, vol. 02, p. 053, 2012.

[133] I. Yu. Kobzarev, L. B. Okun, and M. B. Voloshin, "Bubbles in Metastable Vacuum," *Sov. J. Nucl. Phys.*, vol. 20, pp. 644–646, 1975. [Yad. Fiz.20,1229(1974)].

[134] S. R. Coleman, "The Fate of the False Vacuum. 1. Semiclassical Theory," *Phys. Rev.*, vol. D15, pp. 2929–2936, 1977. [Erratum: Phys. Rev.D16,1248(1977)].

[135] C. G. Callan, Jr. and S. R. Coleman, "The Fate of the False Vacuum. 2. First Quantum Corrections," *Phys. Rev.*, vol. D16, pp. 1762–1768, 1977.

[136] R. Kallosh, F. Quevedo, and A. M. Uranga, "String Theory Realizations of the Nilpotent Goldstino," 2015.

[137] O. Aharony and S. Kachru, "Stringy Instantons and Cascading Quivers," *JHEP*, vol. 0709, p. 060, 2007.

[138] A. Amariti, L. Girardello, and A. Mariotti, "Stringy Instantons as Strong Dynamics," *JHEP*, vol. 0811, p. 041, 2008.

[139] S. Franco, A. Hanany, D. Martelli, J. Sparks, D. Vegh, *et al.*, "Gauge theories from toric geometry and brane tilings," *JHEP*, vol. 0601, p. 128, 2006.

[140] K. D. Kennaway, "Brane Tilings," *Int. J. Mod. Phys.*, vol. A22, pp. 2977–3038, 2007.

[141] M. Yamazaki, "Brane Tilings and Their Applications," *Fortsch. Phys.*, vol. 56, pp. 555–686, 2008.

[142] A. Retolaza and A. Uranga, "Orientifolds of Warped Throats from Toric Calabi-Yau Singularities," 2016.

[143] I. Garcia-Etxebarria, B. Heidenreich, and T. Wrase, "New N=1 dualities from orientifold transitions. Part I. Field Theory," *JHEP*, vol. 10, p. 007, 2013.

[144] I. García-Etxebarria, B. Heidenreich, and T. Wrase, "New N=1 dualities from orientifold transitions - Part II: String Theory," *JHEP*, vol. 10, p. 006, 2013.

[145] I. García-Etxebarria and B. Heidenreich, "Strongly coupled phases of $\mathcal{N} = 1$ S-duality," *JHEP*, vol. 09, p. 032, 2015.

[146] S. Benvenuti and M. Kruczenski, "From Sasaki-Einstein spaces to quivers via BPS geodesics: L**p,q—r," *JHEP*, vol. 04, p. 033, 2006.

[147] A. Butti, D. Forcella, and A. Zaffaroni, "The Dual superconformal theory for L**pqr manifolds," *JHEP*, vol. 09, p. 018, 2005.

[148] K. A. Intriligator and N. Seiberg, "Duality, monopoles, dyons, confinement and oblique confinement in supersymmetric SO(N(c)) gauge theories," *Nucl. Phys.*, vol. B444, pp. 125–160, 1995.

[149] K. A. Intriligator and P. Pouliot, "Exact superpotentials, quantum vacua and duality in supersymmetric SP(N(c)) gauge theories," *Phys.Lett.*, vol. B353, pp. 471–476, 1995.

[150] K. Becker and M. Becker, "Supersymmetry breaking, M theory and fluxes," *JHEP*, vol. 07, p. 038, 2001.

[151] V. Balasubramanian, P. Berglund, J. P. Conlon, and F. Quevedo, "Systematics of moduli stabilisation in Calabi-Yau flux compactifications," *JHEP*, vol. 03, p. 007, 2005.

[152] E. A. Bergshoeff, K. Dasgupta, R. Kallosh, A. Van Proeyen, and T. Wrase, "$\overline{\text{D3}}$ and dS," *JHEP*, vol. 05, p. 058, 2015.

[153] R. Kallosh and T. Wrase, "De Sitter Supergravity Model Building," *Phys. Rev.*, vol. D92, no. 10, p. 105010, 2015.

[154] C. P. Burgess, R. Kallosh, and F. Quevedo, "De Sitter string vacua from supersymmetric D terms," *JHEP*, vol. 10, p. 056, 2003.

[155] M. Cicoli, F. Quevedo, and R. Valandro, "De Sitter from T-branes," 2015.

[156] A. Saltman and E. Silverstein, "A New handle on de Sitter compactifications," *JHEP*, vol. 01, p. 139, 2006.

[157] A. Westphal, "de Sitter string vacua from Kahler uplifting," *JHEP*, vol. 03, p. 102, 2007.

[158] M. Cicoli, A. Maharana, F. Quevedo, and C. P. Burgess, "De Sitter String Vacua from Dilaton-dependent Non-perturbative Effects," *JHEP*, vol. 06, p. 011, 2012.

[159] J. Louis, M. Rummel, R. Valandro, and A. Westphal, "Building an explicit de Sitter," *JHEP*, vol. 10, p. 163, 2012.

[160] M. Rummel and Y. Sumitomo, "De Sitter Vacua from a D-term Generated Racetrack Uplift," *JHEP*, vol. 01, p. 015, 2015.

[161] A. P. Braun, M. Rummel, Y. Sumitomo, and R. Valandro, "De Sitter vacua from a D-term generated racetrack potential in hypersurface Calabi-Yau compactifications," *JHEP*, vol. 12, p. 033, 2015.

[162] I. Ben-Dayan, S. Jing, A. Westphal, and C. Wieck, "Accidental inflation from Kähler uplifting," *JCAP*, vol. 1403, p. 054, 2014.

[163] I. Affleck, M. Dine, and N. Seiberg, "Dynamical Supersymmetry Breaking in Chiral Theories," *Phys. Lett.*, vol. B137, p. 187, 1984.

[164] D. Gaiotto and S. S. Razamat, "N=1 theories of class S_k," 2015.

[165] S. Franco, H. Hayashi, and A. Uranga, "Charting Class $\mathcal{S}_k$ Territory," 2015.

[166] A. Hanany and K. Maruyoshi, "Chiral theories of class S," 2015.

[167] R. Blumenhagen, M. Cvetic, and T. Weigand, "Spacetime instanton corrections in 4D string vacua: The Seesaw mechanism for D-Brane models," *Nucl.Phys.*, vol. B771, pp. 113–142, 2007.

[168] L. Ibanez and A. Uranga, "Neutrino Majorana Masses from String Theory Instanton Effects," *JHEP*, vol. 0703, p. 052, 2007.

[169] B. Florea, S. Kachru, J. McGreevy, and N. Saulina, "Stringy Instantons and Quiver Gauge Theories," *JHEP*, vol. 0705, p. 024, 2007.

[170] R. Blumenhagen, M. Cvetic, S. Kachru, and T. Weigand, "D-Brane Instantons in Type II Orientifolds," *Ann.Rev.Nucl.Part.Sci.*, vol. 59, pp. 269–296, 2009.

[171] L. E. Ibanez and A. M. Uranga, "String theory and particle physics: An introduction to string phenomenology," 2012.

[172] L. Ibanez, A. Schellekens, and A. Uranga, "Instanton Induced Neutrino Majorana Masses in CFT Orientifolds with MSSM-like spectra," *JHEP*, vol. 0706, p. 011, 2007.

[173] R. Blumenhagen, M. Cvetic, D. Lust, R. Richter, and T. Weigand, "Non-perturbative Yukawa Couplings from String Instantons," *Phys.Rev.Lett.*, vol. 100, p. 061602, 2008.

[174] M. Cvetic, J. Halverson, and P. Langacker, "Singlet Extensions of the MSSM in the Quiver Landscape," *JHEP*, vol. 1009, p. 076, 2010.

[175] M. Cvetic, J. Halverson, P. Langacker, and R. Richter, "The Weinberg Operator and a Lower String Scale in Orientifold Compactifications," *JHEP*, vol. 1010, p. 094, 2010.

[176] M. Cvetic and T. Weigand, "A String theoretic model of gauge mediated supersymmetry beaking," 2008.

[177] M. Buican and S. Franco, "SUSY breaking mediation by D-brane instantons," *JHEP*, vol. 0812, p. 030, 2008.

[178] R. Blumenhagen, A. Deser, and D. Lust, "FCNC Processes from D-brane Instantons," *JHEP*, vol. 1102, p. 079, 2011.

[179] A. Addazi and M. Bianchi, "Neutron Majorana mass from exotic instantons," *JHEP*, vol. 1412, p. 089, 2014.

[180] A. Addazi and M. Bianchi, "Un-oriented Quiver Theories for Majorana Neutrons," 2015.

[181] A. Addazi and M. Bianchi, "Neutron Majorana mass from Exotic Instantons in a Pati-Salam model," 2015.

[182] R. Argurio, M. Bertolini, G. Ferretti, A. Lerda, and C. Petersson, "Stringy instantons at orbifold singularities," *JHEP*, vol. 0706, p. 067, 2007.

[183] M. Bianchi, F. Fucito, and J. F. Morales, "D-brane instantons on the T**6 / Z(3) orientifold," *JHEP*, vol. 0707, p. 038, 2007.

[184] R. Argurio, D. Forcella, A. Mariotti, D. Musso, and C. Petersson, "Field Theory Interpretation of N=2 Stringy Instantons," *JHEP*, vol. 1302, p. 002, 2013.

[185] I. Garcia-Etxebarria, "D-brane instantons and matrix models," *JHEP*, vol. 0907, p. 017, 2009.

[186] D. Krefl, "A Gauge theory analog of some 'stringy' D-instantons," *Phys.Rev.*, vol. D78, p. 066004, 2008.

[187] M. Bianchi, G. Inverso, J. F. Morales, and D. R. Pacifici, "Unoriented Quivers with Flavour," *JHEP*, vol. 1401, p. 128, 2014.

[188] I. Garcia-Etxebarria and A. M. Uranga, "Non-perturbative superpotentials across lines of marginal stability," *JHEP*, vol. 0801, p. 033, 2008.

[189] L. E. Ibanez, R. Rabadan, and A. Uranga, "Anomalous U(1)'s in type I and type IIB D = 4, N=1 string vacua," *Nucl.Phys.*, vol. B542, pp. 112–138, 1999.

[190] S. Franco, A. Hanany, Y.-H. He, and P. Kazakopoulos, "Duality walls, duality trees and fractional branes," 2003.

[191] J. D. Lykken, E. Poppitz, and S. P. Trivedi, "Branes with GUTs and supersymmetry breaking," *Nucl.Phys.*, vol. B543, pp. 105–121, 1999.

[192] G. Aldazabal, L. E. Ibanez, F. Quevedo, and A. Uranga, "D-branes at singularities: A Bottom up approach to the string embedding of the standard model," *JHEP*, vol. 0008, p. 002, 2000.

[193] B. Feng, Y.-H. He, A. Karch, and A. M. Uranga, "Orientifold dual for stuck NS5-branes," *JHEP*, vol. 0106, p. 065, 2001.

[194] M. Berkooz, "The Dual of supersymmetric SU(2k) with an antisymmetric tensor and composite dualities," *Nucl. Phys.*, vol. B452, pp. 513–525, 1995.

[195] P. Pouliot, "Duality in SUSY SU(N) with an antisymmetric tensor," *Phys. Lett.*, vol. B367, pp. 151–156, 1996.

[196] J. H. Brodie and M. J. Strassler, "Patterns of duality in N=1 SUSY gauge theories, or: Seating preferences of theater going nonAbelian dualities," *Nucl. Phys.*, vol. B524, pp. 224–250, 1998.

[197] J. Terning, "Duals for SU(N) SUSY gauge theories with an antisymmetric tensor: Five easy flavors," *Phys. Lett.*, vol. B422, pp. 149–157, 1998.

[198] S. Franco and A. Uranga, "Bipartite Field Theories from D-Branes," *JHEP*, vol. 1404, p. 161, 2014.

[199] A. M. Uranga, "D-brane probes, RR tadpole cancellation and K theory charge," *Nucl.Phys.*, vol. B598, pp. 225–246, 2001.

[200] I. Garcia-Etxebarria, F. Marchesano, and A. M. Uranga, "Non-perturbative F-terms across lines of BPS stability," *JHEP*, vol. 0807, p. 028, 2008.